

*Bioinspired oxidation reactions  
of phenols with dinuclear  
copper complexes*



*Angelina Prokofieva  
Göttingen  
19th September 2007*



# **Bioinspired oxidation reactions of phenols with dinuclear copper complexes**

Dissertation  
zur Erlangung des Doktorgrades  
der Mathematisch-Naturwissenschaftlichen Fakultäten  
der Georg-August-Universität zu Göttingen  
vorgelegt von

Diplom-Chemikerin  
Angelina Prokofieva  
aus Kiev, Ukraine

Göttingen, den 19.09.07



D7

Referent: Prof. Dr. Franc Meyer

Korreferent: Prof. Dr. George M. Sheldrick

Tag der mündlichen Prüfung: 01.11.2007



Ich erkläre hiermit an Eides statt, daß ich diese Arbeit selbständig und ohne unerlaubte Hilfsmittel angefertigt habe.

1	Introduction .....	1
2	Current state of research.....	5
2.1	Metalloenzymes with a copper containing active site.....	5
2.2	Biomimetic model systems .....	11
3	Homogeneous copper catalyzed reactions .....	15
3.1	Hydroxylation and oxidation of phenols.....	15
3.2	Oxidative polymerization and coupling of phenols .....	19
3.3	C-H bond activation .....	21
3.4	Goals of the work .....	26
4	Ligand synthesis .....	28
4.1	Properties of pyrazole-based compartmental ligands.....	28
4.2	Synthesis of ligands.....	30
5	Synthesis and characterization of complexes.....	34
5.1	Complex synthesis: general procedure.....	34
5.1.1	Purification of complexes.....	35
5.2	Copper(II) complexes of ligands <b>HL</b> <sup>1</sup> and <b>HL</b> <sup>2</sup> .....	36
5.2.1	Structural characterization of copper complex with <b>HL</b> <sup>1</sup> .....	36
5.2.2	Previously studied catalytic activity of dicopper complexes .....	38
5.2.3	Equilibria in solution and structural characterization of complexes with <b>HL</b> <sup>2</sup> : unusual copper-dioxygen mediated amine to <i>N</i> -oxide transformation of <b>HL</b> <sup>2</sup> .....	40
5.3	Characterization of a dicopper complex with the new ligand <b>HL</b> <sup>3</sup> .....	47
5.4	Copper complexes of the new bioinspired ligand <b>HL</b> <sup>4</sup> .....	49
5.4.1	Elucidation of species distribution at different pH values .....	49
5.4.2	Structural characterization of complexes .....	53
5.4.3	Spectroscopic properties of the complexes and equilibria in solution .....	59
5.4.4	Magnetic properties.....	63
5.4.5	Cyclovoltammetry.....	66
5.5	Characterization of a copper complex with the new ligand <b>HL</b> <sup>5</sup> .....	68
5.6	Comparison of the spectroscopic and structural features of the copper complexes... .....	71
6	Bioinspired oxidation reactions of phenols.....	73
6.1	Screening of the phenol substrates .....	73
6.2	Oxidative C-C coupling of 2,6-dimethylphenol.....	74
6.3	Oxidative C-C coupling of 2,4,6-trimethylphenol .....	76



7	Investigations of the mechanism of C-C coupling of TMP .....	79
7.1	Determination of the optimal reaction conditions for C-C-coupling of TMP .....	79
7.2	Investigations with deuterated TMP substrate .....	80
7.3	Discussion of the nature of the UV/vis Charge Transfer band of dicopper phenolate complexes .....	83
7.4	Determination of the nature of the adduct formed upon the addition of TMP .....	85
7.4.1	Raman spectroscopy .....	86
7.4.2	EPR studies .....	90
7.5	Determination of the amount of coordinated phenol .....	92
7.5.1	General .....	92
7.5.2	Job plot of TMP with dicopper complex <b>5a</b> .....	94
7.5.3	Job plot of 4-methylphenol and 4- <i>tert</i> -butylphenol with dicopper complex <b>5a</b> ....	97
7.5.4	Job plot of 4-hydroxybenzamide and pentafluorophenol with dicopper complex <b>5a</b> .....	99
7.6	Mechanistic studies of C-C coupling of TMP under anaerobic conditions .....	101
7.6.1	UV/vis studies under N <sub>2</sub> -atmosphere .....	102
7.6.2	Job plot of TMP with <b>5a</b> under anaerobic conditions .....	103
7.6.3	Trapping of the intermediates under anaerobic conditions .....	104
7.6.4	Evidence for the formation of a mixed-valence Cu <sup>I</sup> Cu <sup>II</sup> species .....	106
7.7	Coordination behaviour of the new ligand <b>HL</b> <sup>5</sup> towards copper(I) .....	111
7.8	Time-dependent concentration profiles of TMP, TMBB and TMSQ during catalysis with <b>5a</b> .....	113
7.9	Determination of the O <sub>2</sub> derived by-product in the C-C coupling reaction .....	114
8	Adducts with model substrate molecules .....	116
8.1	Copper(II)-phenolate complexes .....	116
8.2	Characterization of the adducts with 4-hydroxybenzamide and pentafluorophenol.. .....	119
8.3	4,4'-isopropylidene-bis(2,6-dimethylphenol) and 4,4'-(hexafluoroisopropylidene) diphenol as model substrates for TMBB .....	126
8.4	A tetrachlorocatechol-adduct of dicopper(II) complex <b>5a</b> .....	132
9	Oxidative <i>ortho</i> -C-C coupling of 4-ethylphenol catalyzed by <b>8</b> .....	139
10	Nucleophilic 1,6-addition of MeOH to 2,4,6-trimethylphenol .....	146
11	Oxidative C-O coupling of 4-bromo-2,6-dimethylphenol catalyzed by <b>5a</b> .....	149
12	Discussion of the proposed mechanism for C-C coupling of TMP .....	153

13	Conclusions .....	158
14	Experimental section .....	161
14.1	General .....	161
14.2	Synthesis of ligands <b>HL</b> <sup>1</sup> - <b>HL</b> <sup>5</sup> .....	164
14.3	Synthesis of complexes .....	170
14.4	Synthesis of 3,3',5,5'-tetramethylstilbene-4,4'-quinone (TMSQ) .....	189
14.5	Synthesis of 4,4'-dihydroxy-3,3',5,5'-tetramethylbibenzyl (TMBB).....	190
14.6	Potentiometric titrations .....	192
14.7	X-ray crystallography .....	193
14.8	Crystal data and refinement details .....	195
15	Literature .....	203





*The world is all that is encased here: life, death, people, and everything else that surrounds us. The world is incomprehensible. We won't ever understand it. We won't ever unravel its secrets. Thus we must treat the world as it is: a sheer mystery.*

*The Wheel of Time*

*Carlos Castaneda*

*...to my dear parents...  
19 September 2007*





Ar	aromatic ring	HMQC	Heteronuclear Multiple Quantum Correlation
4-AP	4-hydroxybenzamide	IR	infra red
Bz	1-methyl benzimidazole	<i>J</i>	coupling constant
CT	Charge Transfer	KOtBu	potassium- <i>tert</i> -butylate
CV	Cyclovoltammetry	<i>K<sub>d</sub></i>	dissociation constant
CH <sub>2</sub> Cl <sub>2</sub>	Dichloromethane	L	Ligand
calcd.	Calculated	LMCT	Ligand-Metal-Charge-Transfer
CN	coordination number	L-Dopa	4-(2-aminoethyl)benzene-1,2-diol
CD <sub>3</sub> -TMP	deuterated 2,4,6-trimethylphenol	$\lambda$	wavelength
<i>d</i>	Distance	$\lambda_{\text{ex}}$	wavelength of laser excitation
DMF	<i>N,N</i> -dimethylformamide	<i>m</i>	Meta
DMP	2,6-dimethylphenol	M	Molar
DMPBrP	4-bromo-2,6-dimethylphenol	max	Maximum
MDP	4-methoxy-2,6-dimethylphenol	Me	Methyl
DTBC	3,5-di- <i>tert</i> -butylcatechol	MeCN	Acetonitrile
DPQ	3,3',5,5'-tetramethyl-4,4'-diphenoquinone	MeOH	Methanol
EtOH	Ethanol	MS	Mass Spectrometry
Et <sub>2</sub> O	Diethylether	4-MeP	4-methylphenol
$\epsilon$	extinction coefficient	MtBuP	2-methyl-4- <i>tert</i> -butylphenol
<i>E</i>	electrochemical potential	3-NBA	4-nitrobenzylalcohol
EI	Electron Impact	NMR	Nuclear Magnetic Resonance
ESI	Electron Spray Ionisation	<i>o</i>	Ortho
EPR	Electron Paramagnetic Resonance	PPE	poly(2,6-dimethylphenylene ether)
Et	Ethyl	<i>p</i>	Para
4-EtP	4-ethylphenol	py	Pyridyl
FAB	Fast Atom Bombardment	PFP	Pentafluorophenol
HOCF <sub>3</sub> BP	4,4'-(hexafluoroisopropylidene)diphenol	Red	Reduction
HOCH <sub>3</sub> BP	4,4'-isopropylidene-bis(2,6-dimethylphenol)	$\rho$	paramagnetic impurities
HMBC	Heteronuclear Multiple Bond Correlation	S/C	substrate/catalyst ratio

sh	shoulder
TCC	tetrachlorocatechol
TMP	2,4,6-trimethylphenol
2,5,6-TMP	2,5,6-trimethylphenol
2,3,5-TMP	2,3,5-trimethylphenol
<i>t</i> BuP	4- <i>tert</i> -butylphenol
<i>TIP</i>	temperature-independent paramagnetism
TMBD	3,3',5,5'-tetramethylbiphenyl-4,4'- diol
TMSQ	3,3',5,5'-tetramethylstilbene-4,4'- quinone
T	temperature
TON	turnover numbers
TACN	triazocyclononane
TMBB	4,4'-dihydroxy-3,3',5,5'- tetramethylbibenzyl
$\chi_M$	magnetic susceptibility
$\chi_M T$	product of magnetic susceptibility
$\nu$	wavenumber

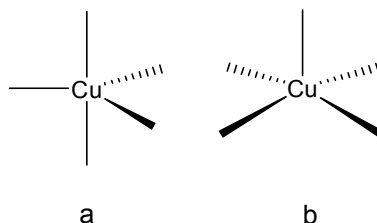
## 1 Introduction

Copper has been known as one of the important raw materials for a long time, although the content of copper in the earth's crust is only 0.003 %. Copper has played a significant part in the history of mankind, which has used the easily accessible uncompound metal for nearly 10.000 years. Civilizations in places like Egypt and Greece showed early evidence of using copper. During the Roman Empire copper was principally mined on Cyprus, hence the origin of the name of the metal as Cyprium, "metal of Cyprus", later shortened to Cuprum. It is a ductile metal with an excellent electrical conductivity, and it finds extensive use as an electrical as well as thermal conductor, as building material and as a component of various alloys (e.g. brass (Cu/Zn), bronzes (Cu/Al/Si), precious metal alloys).

In modern chemistry copper compounds play a vital role in organic synthesis as (co-)catalysts for a whole plethora of reactions. For example, copper(I) salts catalyze the decomposition of the diazonium salts, an important step in the Sandmeyer reaction. Organometallic copper complexes, such as cupric and cuprous chlorides, are known to be active in the oxychlorination of ethylene to yield 1,2-dichloroethane.<sup>1,2</sup> Other well-known catalytic applications of organometallic copper complexes include the ring-opening of epoxides and the addition to alkynes.<sup>3,4</sup> The most prominent example of copper acting as co-catalyst is in Pd-catalyzed Wacker-type oxidations of alkenes, where copper salts mediate the reduction of palladium(II) by molecular oxygen.<sup>5,6,7</sup>

The fundamental coordination chemistry of copper with respect to the role that coordination effects play in both synthetic and biological systems has been reviewed.<sup>8,9,10</sup> A large set of copper complexes are known to exist, wherein the oxidation state of the copper ion(s) can range from 0 to +4.<sup>8</sup> The most important and common for both biological and synthetic systems are the +1 and especially the +2 oxidation states. Both the coordination number (CN) and the geometry of a copper ion are highly dependent on the metal-oxidation state. Thus, for a  $d^{10}$  Cu<sup>I</sup> ion, coordination numbers from 2 to 5 are observed, with 4 being most common (CN 2: [CuCl<sub>2</sub>], CN 3: [Cu(CN)<sub>3</sub>]<sup>-</sup>). The most common coordination environments are linear (CN = 2), trigonal planar (CN = 3) and tetrahedral (CN = 4) geometries. In contrast, a copper(II)  $d^9$  ion usually prefers a coordination number of 5 or 6, resulting in a trigonal bipyramidal geometry (Figure 1 (a)) or a tetragonal pyramidal coordination environment (Figure 1 (b)) for

the former and an octahedral geometry for the latter; usually a strong Jahn-Teller effect (four ligands are strongly bound in the equatorial plane, with one (or two) additional ligand(s) less strongly coordinated in the axial position(s)) is observed.



**Figure 1.** Trigonal bipyramidal (a) or tetragonal-pyramidal (b) coordination environment of the copper ion (CN = 5).

These differences in preferred geometry (and the related coordination numbers) for  $\text{Cu}^{\text{I}}$  vs.  $\text{Cu}^{\text{II}}$  lead to drastic coordination changes in the case of a redox reaction between these two above-mentioned oxidation states. The standard aqueous reduction potentials show that copper(I) is unstable in aqueous solution due to a disproportionation reaction to form metallic copper and copper(II) ( $2 \text{Cu}^+ \rightarrow \text{Cu}^0 + \text{Cu}^{2+}$ ,  $E^0 = +0.37 \text{ V}$ ).

Copper is essential for various biological processes occurring in all higher plant and animal species and it is the third most abundant trace element found in the human body, after iron and zinc. When copper is taken up by the body, it is first absorbed in the gut, and from there transported to the liver as an albumin-bound complex. Copper is found in a wide variety of metalloenzymes, including the active sites of cytochrome *c* oxidase and the enzyme superoxide dismutase (containing copper and zinc). The main biological role of copper is centered on redox-chemistry (electron transfer or oxidation/oxygenation of organic substrates). The functions of the active sites of copper metalloproteins can be divided in four different types: (i) metal ion uptake, storage and transport, (ii) dioxygen activation, storage and transport, (iii) electron transfer, and (iv) catalytic conversion of organic molecules. Originally, copper centers in biological systems were classified in three groups on the basis of their spectroscopic features; however the immense advances in protein crystallography have led to an expansion of the classification system for the currently known biological copper-containing systems. There are now seven different classes of copper systems, within which copper is involved in completely different chemical processes, from catalytic oxidation of organic substrates (*type 3*) to the reduction of organic substrate molecules ( $\text{Cu}_\text{B}$  type).<sup>11</sup>



Recent discoveries of various novel copper containing proteins pushed the area of bioinorganic chemistry even further into the design of small-molecule models (structural and functional) for the active sites of copper metalloenzymes. Such bioinspired and biomimetic copper complexes serve two different goals. Design and synthetic use of accurate model complexes will lead to a deeper understanding of the functioning or characteristics (e.g. spectroscopic features) of the enzyme active site and in the meantime will provide a great opportunity to apply these principles and copper complexes for the selective transformation of substrate molecules in homogeneous catalysis.

The work described in this thesis was born out of inspiration fuelled by the versatile possibilities in the design and practical use of model copper complexes.

Preorganized dinuclear transition metal complexes have received a lot of attention over the past several years, mainly due to the increasing interest in cooperative effects between individual metal centers.<sup>12</sup> The body of work detailed in the following chapters is based on pyrazole-based ligands with chelating side arms in the 3- and 5-positions of the heterocyclic core, which have been developed as valuable scaffolds for further studies: the anionic pyrazolate has a high tendency to span two metal ions in a bridging fashion, while the individual coordination spheres as well as the intramolecular metal-metal separation can be tuned by appropriate alterations of the appended chelate substituents.<sup>13,14,15,16,17</sup>

New bioinspired pyrazole ligands have been designed, synthesized and fully characterized. The coordination chemistry of oligonuclear copper complexes with these different pyrazole-based ligands was thoroughly investigated, which has led to detailed insight into the apparently high flexibility of the ligand system whilst coordinating copper and has enabled a systematic determination of the spectroscopic properties of a range of different Cu-complexes. By varying the number of additional donor-functionalities, the geometry of the copper ions in the complexes could be manipulated, whereas modification of the spacer length between the pyrazolate core and the chelating side-arm substituents provided great opportunities for control over the intramolecular metal-metal distance.

Alongside these investigations into the coordination chemistry, studies were performed on the catalytic activity of these novel copper complexes. Particular attention was given to the oxidative C-C coupling of 2,6-dimethylphenol (DMP) and 2,4,6-trimethylphenol (TMP), as

well as on the 1,6-nucleophilic addition of several small molecules to TMP. Furthermore, dicopper complexes with suitable derivatives of the general class of phenolic substrates that showed no tendency for any Cu-mediated transformation were prepared and characterized in order to determine possible (structural) intermediates of the catalytic reactions studied.

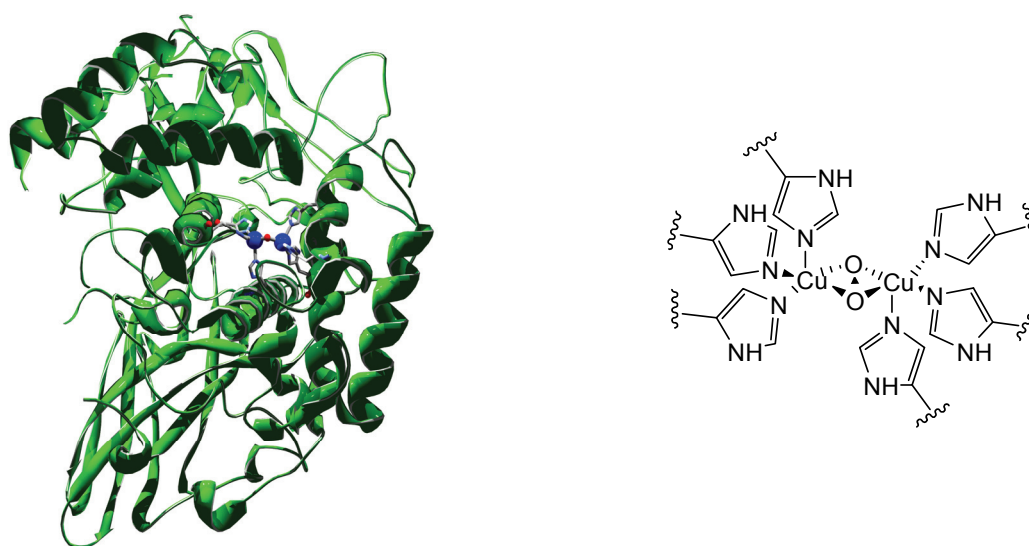
All in all, the results obtained in this work have provided a better understanding of the reaction mechanism behind, in particular for the C-C oxidative coupling of TMP.

## 2 Current state of research

### 2.1 Metalloenzymes with a copper containing active site

One of the important functions performed by metalloproteins is respiration. There are three known classes of dioxygen transport proteins: the hemoglobin-myoglobin family (containing a mononuclear heme center), hemocyanins (which feature a dinuclear copper active site), and hemerythrins (with a dinuclear non-heme iron active site).<sup>18,19,20</sup> In these proteins, a diatomic O<sub>2</sub> molecule binds to an iron or copper ion present in the active site of the metalloenzyme, without the occurrence of any irreversible electron transfer or redox reactions. In hemoglobin and myoglobin the dioxygen binding site is an iron-porphyrin complex. In the *oxy* form the Fe ion adopts a square bipyramidal geometry – four N-atoms of the porphyrin ring are coordinated in the equatorial plane, while a histidine residue and *end-on* bound dioxygen molecule occupy the apical positions. The other two classes of respiratory metalloproteins employ dinuclear active sites for the dioxygen-binding reactions. In hemerythrin the O<sub>2</sub> molecule is bound at a terminal site in the Fe<sub>2</sub> unit, concomitant with oxidation of the bimetallic center (generation of hydroperoxide).

In hemocyanin (a *type 3* copper active site found in molluscs and arthropods), reversible binding of dioxygen is performed by a pair of copper ions (Figure 2).

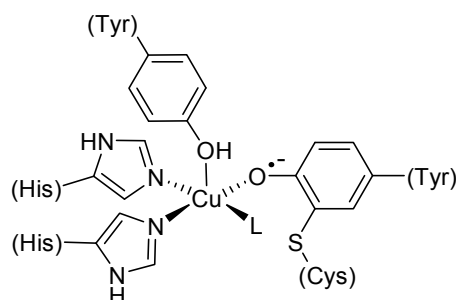


**Figure 2.** Molecular structure of hemocyanin (left) and the corresponding active site in the *oxy* form (right).

The assumption that binding of dioxygen is reversible and concomitant with reversible transformation of dicopper(I) (*deoxy* form) into the dicopper(II) (*oxy* form) species is in good agreement with the  $\text{Cu}^{\text{II}}/\text{Cu}^{\text{I}}$  reduction potential ( $E^0(\text{Cu}^{\text{II}}/\text{Cu}^{\text{I}}) = +0.15 \text{ V}$ ). Both the *oxy* and the *deoxy* form of the hemocyanin active site have been structurally characterized.<sup>21,22,23,24</sup> Dioxygen is coordinated as a side-on ( $\mu\text{-}\eta^2\text{:}\eta^2$ ) peroxo ligand, with the two copper ions being 3.60 Å apart while each Cu is ligated by three histidine residues.

The currently known biological copper systems that are involved in oxidation catalysis can be categorized in three classes: *type 2*, *type 3* and *type 4*.

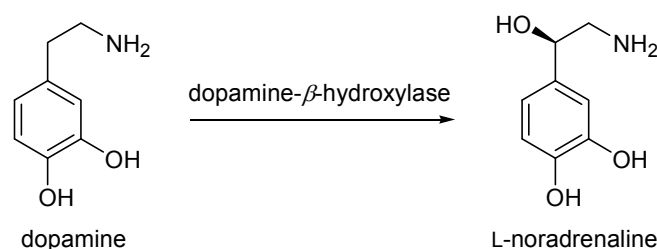
*Type 2* copper active sites are found in different oxidases (e.g. galactose oxidase (Figure.3): oxidation of primary alcohols)<sup>25</sup> and oxygenases (dopamine- $\beta$ -hydroxylase: C-H bond activation of benzylic substrates,<sup>26</sup> and phenylalanine hydroxylase: hydroxylation of aromatic substrates<sup>27</sup>) as well as in CuZn superoxide dismutase (disproportionation of  $\text{O}_2^-$  superoxide anion).<sup>28</sup>



**Figure 3.** Structure of the active site of galactose oxidase (active form),  $\text{L} = \text{H}_2\text{O}$ .

A *type 2* or normal  $\text{Cu}^{2+}$  site shows no detectable absorption features in the UV/vis region and an EPR line shape reminiscent of common low-molecular weight mononuclear copper complexes ( $A_{\text{H}} > 140 \cdot 10^{-4} \text{ cm}^{-1}$ ). In the oxidized state, their colour is light blue because of weak *d-d* transitions within the single  $\text{Cu}^{\text{II}}$  ion. The coordination sphere around Cu, which has either square planar or distorted tetrahedral geometry, contains four ligands with N and/or O donor atoms.<sup>29</sup> Galactose oxidase represents an example of a free radical metalloenzyme active site and it catalyzes the oxidation of galactose and other primary alcohols under two-electron reduction of  $\text{O}_2$  to  $\text{H}_2\text{O}_2$ , whereas dopamine- $\beta$ -hydroxylase catalyses the hydroxylation of 4-(2-aminoethyl)benzene-1,2-diol (L-Dopa) into the neurotransmitter

noradrenaline (Scheme 1) by selective benzylic C-H bond activation, thereby installing an OH-group at the  $\alpha$ -carbon. The latter system is therefore classified as an oxygenase enzyme.

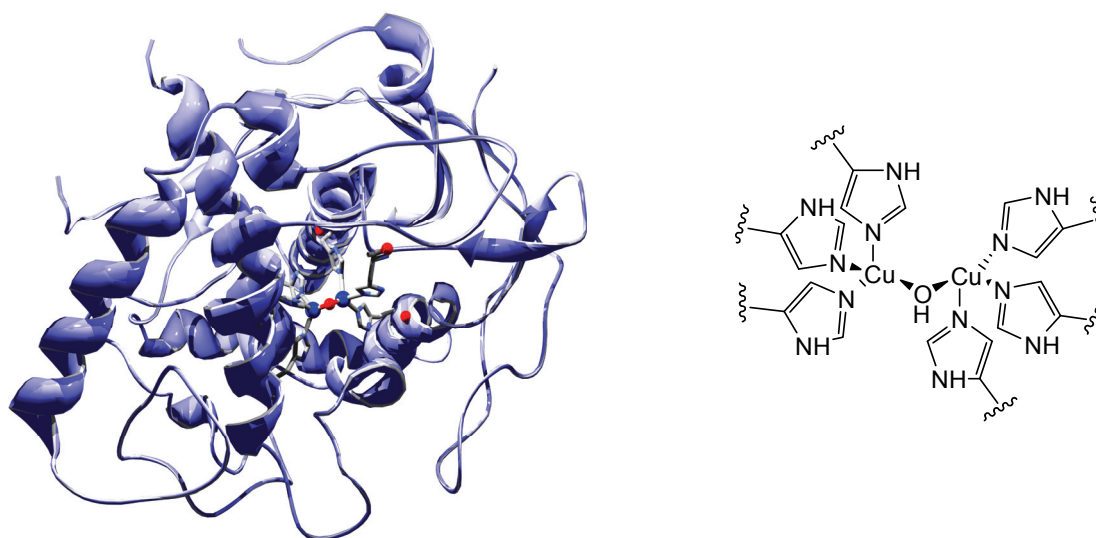


**Scheme 1.** Hydroxylation of dopamine into noradrenaline.

*Type 3* copper sites in their *oxy* form are characterized by a strong absorption band in the near UV region ( $\lambda_{\text{max}} = 330$  nm). These *type 3* copper centers are believed to consist of two copper ions that are antiferromagnetically coupled. The *type 3* class of proteins comprises hemocyanin,<sup>30</sup> tyrosinase<sup>31</sup> and catechol oxidase.<sup>32</sup> Their active sites are very similar, containing a dicopper core in which both Cu ions are ligated by three N-bound histidine residues. All three metalloproteins are capable of binding dioxygen reversibly at ambient conditions. Structural insight from X-ray crystallography is now available for all three metalloproteins.<sup>33,34,35</sup> Antiferromagnetic coupling of the two  $\text{Cu}^{\text{II}}$  ions in the *oxy* state of these metalloproteins leads to EPR-silent behaviour.

Catechol oxidase (Figure 4) performs the oxidation of catechols to *o*-quinones with  $\text{O}_2$  as the oxidant. This two-electron substrate oxidation is coupled to the reduction of  $\text{O}_2$  to water, i.e. no oxygen atom(s) stemming from  $\text{O}_2$  are incorporated in the substrate. During the catalytic cycle, each copper ion switches between the +1 and +2 oxidation states and thus provides only a single electron, but the cooperative effect of two adjacent copper ions enables two-electron redox reactions to occur at such *type 3* active sites.



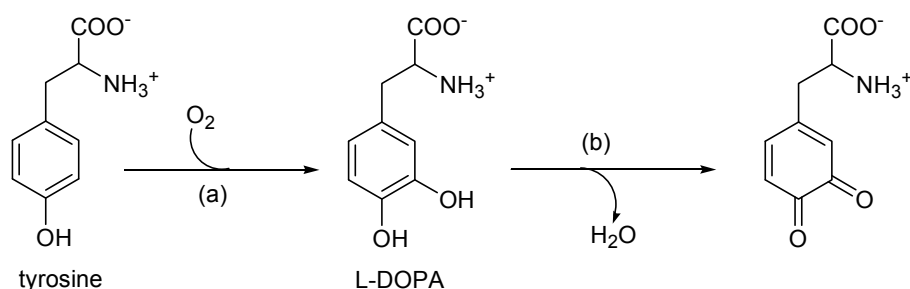


**Figure 4.** Molecular structure of catechol oxidase (left) and the corresponding active site in the *met* form (right).

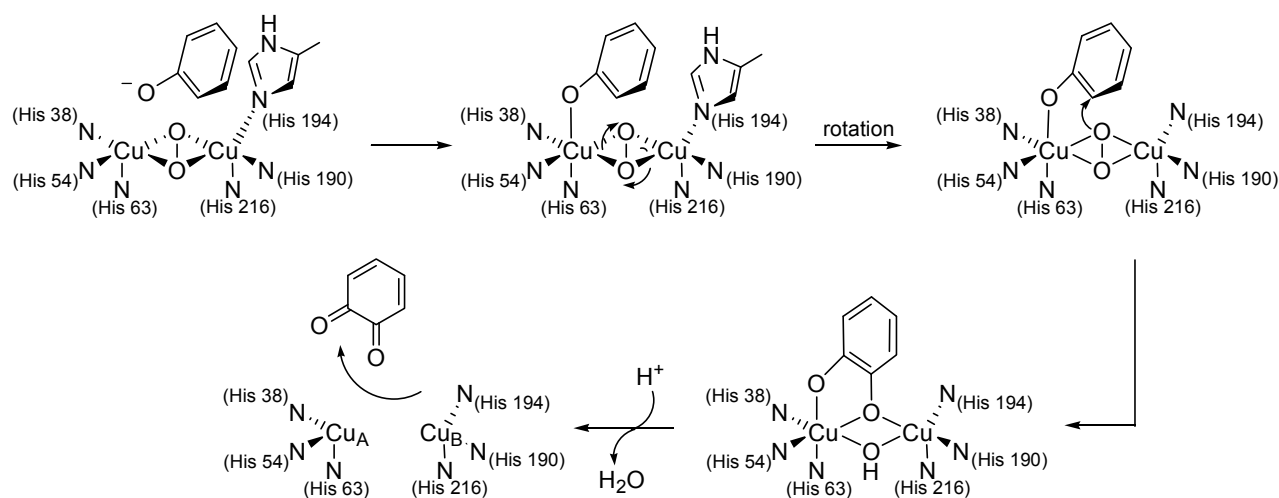
In the *deoxy* form both copper ions are in the +1 oxidation state and the metal-metal distance is around 4.40 Å, while in the oxidized *met* form the Cu ions are ligated by three N-bound histidine residues with a copper-copper distance equal to 2.90 Å and an additional bridging OH-ligand. The third representative of *type 3* copper proteins is tyrosinase (Figure 5), which functions as a catalyst in the oxidation of phenolic substrates to catechols (*cresolase* activity) as well as in the (subsequent) oxidation of catechols to *o*-quinones (*catecholase* activity).



**Figure 5.** Molecular structure of tyrosinase.

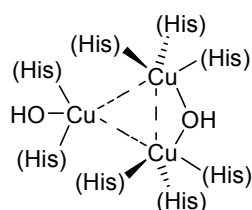


The recent elucidation at high resolution of the solid-state structure of tyrosinase by X-ray crystallographic methods has provided much information and allowed for a detailed mechanistic picture of the catalytic cycle to be proposed.<sup>31,35</sup> It starts with a  $\text{Cu}^{\text{I}}\text{Cu}^{\text{I}}$  species (the *deoxy* form) – the two Cu centers are denoted  $\text{Cu}^{\text{A}}$  and  $\text{Cu}^{\text{B}}$  – which reversibly binds  $\text{O}_2$  to form the common  $\text{Cu}^{\text{II}}(\mu\text{-}\eta^2\text{:}\eta^2\text{-peroxo})\text{Cu}^{\text{II}}$  species (*oxy* form) that is pivotal to all *type 3* dicopper sites. The substrate then docks to one of the metal ions of the *oxy* state (most likely  $\text{Cu}^{\text{A}}$ ) and is properly oriented through interactions with histidine residues to enable hydroxylation of the aromatic ring. To this end, the O-O axis of the peroxo ligand has been suggested to rotate in order to point towards the phenolic ring, leading to electrophilic attack of the  $\text{Cu}(\mu\text{-O}_2)\text{Cu}$  moiety on the ring with concomitant cleavage of the O-O bond.<sup>35</sup> The diphenolic intermediate ends up bound in a bidentate fashion and is subsequently released as the *o*-chinone to regenerate the *deoxy* form of the dicopper center. It should be noted though that alternative mechanistic proposals are being discussed,<sup>36</sup> and even the site of substrate binding ( $\text{Cu}^{\text{A}}$  or  $\text{Cu}^{\text{B}}$ ) is not yet fully clarified. Similar considerations apply to the mechanism of action in catechol oxidase, where important open questions comprise the exact mode of substrate and product binding (either to one or two Cu ions), and where several scenarios have been proposed for the catalytic cycle.<sup>33,35</sup>



**Scheme 3.** Proposed catalytic cycle for the oxidation of phenol to catechol by the tyrosinase active site.<sup>35</sup>

*Type 4* copper sites are metalloproteins that contain both *type 2* and *type 3* copper centers. Together, they form a triangular-shaped trinuclear active site, such as found in laccase (polyphenol oxidase)<sup>37,38</sup> and ascorbate oxidase (Figure 6).<sup>39</sup>



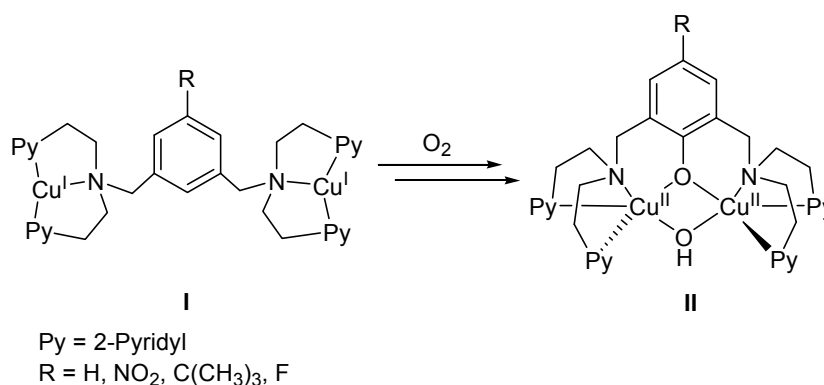
**Figure 6.** Structure of the active site of ascorbate oxidase.

The blue protein ascorbate oxidase belongs to the group of “blue” oxidases together with laccase and ceruloplasmin. These are multi-copper enzymes that catalyze the one-electron oxidation of specific substrates (no oxygen atom(s) from  $O_2$  are incorporated into the substrate) concomitant with the (overall) four-electron reduction of molecular oxygen to water.

## 2.2. Biomimetic model systems

Many of today's studies are focussed on the design of small model complexes that can aid in understanding the principle mechanisms behind the catalytic activity displayed by metalloenzyme active sites. These model biomimetic and/or bioinspired copper complexes assist in the development of new catalysts for selective oxidations of organic substrates, preferably under mild and environmentally benign conditions. Considerable attention has been given to the development of useful catalytic systems for oxidations with dioxygen, which is also very attractive from an industrial and economical point of view. The feasibility of such  $O_2$ -based oxidation catalysis has recently been demonstrated with different dinuclear model compounds for the galactose oxidase active site. In the presence of these complexes and with  $O_2$ , a range of alcohols were catalytically oxidized to the corresponding aldehydes.<sup>40,41</sup>

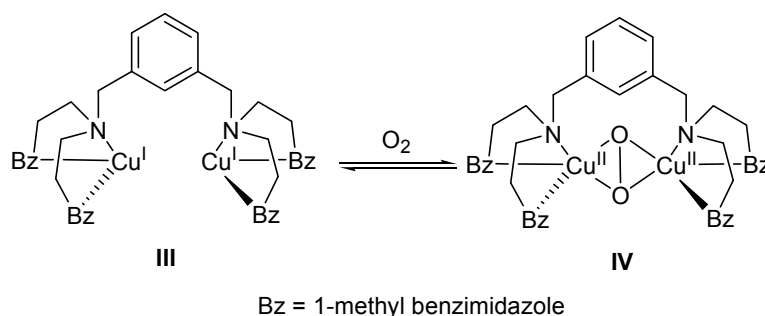
One of the first examples of a functional model complex for the tyrosinase active site was prepared by Karlin et al., wherein intramolecular hydroxylation of the phenyl group, acting as a bridgehead between two tridentate binding pockets, was observed (Scheme 4). In general, complexes derived from these dinucleating ligands feature symmetrically arranged, three-coordinate copper centers with nitrogen donors, because this arrangement simulates the coordination environment present in hemocyanin and tyrosinase.



**Scheme 4.** Intramolecular hydroxylation of the phenyl group.

After addition of dioxygen to dicopper(I) complex **I** at low temperature, a dicopper(II)( $\mu$ - $\eta^2:\eta^2$ -peroxo) species was detected by UV/vis spectroscopy. Further reaction by electrophilic attack of the bridged peroxide to the phenyl spacer led to the formation of complex **II**.<sup>42,43</sup>

Shortly thereafter, Casella reported on a modification of the ligands employing *m*-xylyl spacer. This generation of ligands contained 1-methylbenzimidazole-groups as side arms. Formation of the stable dicopper(II)( $\mu$ - $\eta^2$ : $\eta^2$ -peroxo) species **IV** only at  $-80^\circ\text{C}$  by reaction of complex **III** with dioxygen was proven by UV/vis and Raman spectroscopy, and the most interesting property of these species was the observation of tyrosinase activity (Scheme 5).



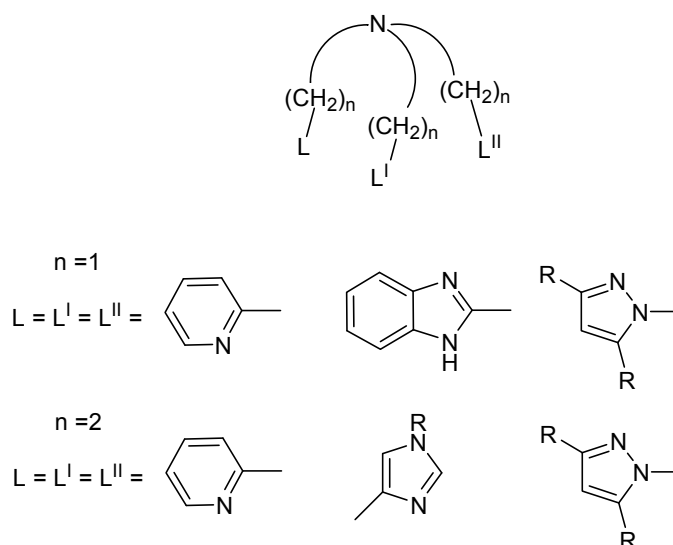
**Scheme 5.** The reversible oxygenation of the complex **III**, as reported by Casella.

The regiospecific *ortho*-hydroxylation of an exogenous, electron-poor phenol (4-carbomethoxyphenol) to catechol and oxidation of an electron-rich catechol (3,5-di-*tert*-butylcatechol) to quinone was performed by **III** in the presence of dioxygen after formation of dicopper(II)( $\mu$ - $\eta^2$ : $\eta^2$ -peroxo) complex **IV** at  $-60^\circ\text{C}$ , as detected by UV/vis spectroscopy.<sup>44,45,46,47</sup>

The most important method for modulating the reaction behaviour of copper complexes is modification of their ligands, either by introducing different donor atoms, changing the chelate ring sizes, or using substituents that can influence the steric or electronic properties of the ligand.

A prominent class of ligands used for preparation of copper complexes is comprised of tripodal tetradentate  $\{\text{N}_4\}$  ligands (Figure 7). In general, copper(II) complexes of this type of ligands feature five-coordinate copper centers. Sterically restricting tripodal ligands, forming five-membered chelate rings, stabilize trigonal bipyramidal complexes.<sup>48,49,50</sup>

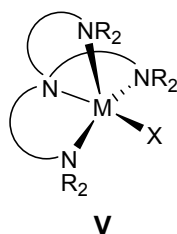




**Figure 7.** Tripodal tetradentate nitrogen-based ligands reported in the literature.

When more flexible ligands are applied (with  $n = 2$ , see Figure 7), six-membered chelate rings are formed preferentially, leading to a square pyramidal environment of the Cu ion.<sup>49,51,52</sup> As a result of their greater flexibility, ligands forming six-membered chelate rings when coordinated to Cu favor the stabilization of  $\text{Cu}^{\text{I}}$  over  $\text{Cu}^{\text{II}}$ , relative to five-membered ring forming ligand systems.

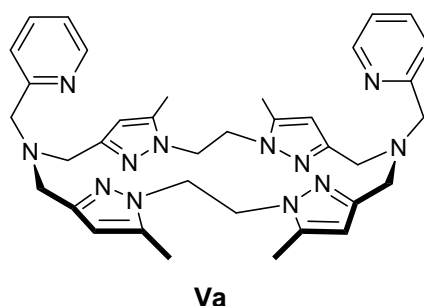
Mononuclear complexes of tripodal tetradentate  $\{\text{N}_4\}$  ligands of the general form **V** (Figure 8) have proven highly successful for emulating the properties and reactivities of monometallic N-ligated metalloproteins.<sup>53</sup> This is particularly true in biomimetic copper-dioxygen chemistry where manifold variations of the motif **V** have been employed, most prominently ligands of the tris(pyridylmethyl)amine type.<sup>54,55</sup>



**Figure 8.** Schematic representation of the complex based on the tripodal tetradentate  $\{\text{N}_4\}$  ligand.

In order to mimic the active sites of tyrosinase and hemocyanin, tripodal ligands were modified using different kinds of spacers in-between the two tripodal units. It was found that

different bridging groups could be introduced, e.g. using a xylyl linker between two tripodal ligands significantly stabilized the formation of the corresponding copper-peroxo complexes. Connecting the tripodal amines with two linkers leads to macrocyclic ligands. The potential of this approach has been highlighted by Bol with the preparation of a macrocyclic ligand **Va** where the tripodal units are connected through a pyrazolyl/ethyl bridge (Figure 9).<sup>56,57</sup> With this ligand the dinuclear copper(I) complex forms an extremely stable peroxo complex after reaction with dioxygen.<sup>56</sup>



**Figure 9.** Schematic representation of the macrocyclic ligand **Va** with the tripodal units connected through a pyrazolyl/ethyl bridge.

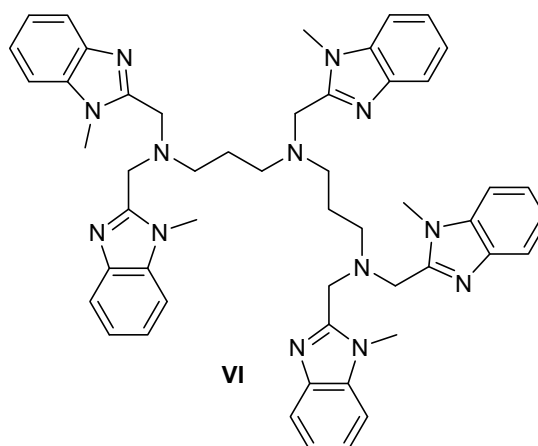
These studies on  $\text{Cu}^{\text{I}}$  and  $\text{Cu}^{\text{II}}$  species with a range of similar ligands show that small changes in the ligand architecture can have a strong influence on the observed reactivity, in particular with  $\text{O}_2$ . In the active sites of a variety of copper enzymes the nature of the ligand donors plays a pivotal role in forcing the metal ions to participate in the desired biochemical reactions. Thus further studies that focus on ligand modifications in synthetic complexes should provide deep insight into the fundamental principles of biologically relevant coordination chemistry.

### 3 Homogeneous copper catalyzed reactions

#### 3.1 Hydroxylation and oxidation of phenols

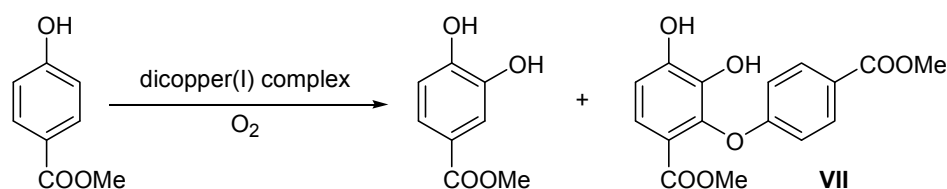
A lot of studies today focus not only on understanding the design rules in the biological systems involving Cu-dioxygen chemistry, but also on the factors governing the modes of reactivity observed with such systems as well as on the use of model bioinspired copper complexes for the catalytic oxidation or oxygenation of organic substrate molecules in homogeneous catalysis.<sup>58</sup>

As was already mentioned before, the selective *ortho*-hydroxylation of a phenolic substrate to yield the catechol derivative is catalyzed by the metalloenzyme tyrosinase. Few synthetic model systems exist that selectively perform the same monooxygenase reaction with exogenous substrates.<sup>59,60,61,62</sup> The group of Casella has studied a series of dicopper complexes based on a *m*-xylyl bridgehead with 1-methylbenzimidazole side arms **III**, as well as an amine based asymmetric tripodal ligand **VI** (Figure 10).<sup>63</sup>



**Figure 10.** Asymmetric tripodal amine based ligand.

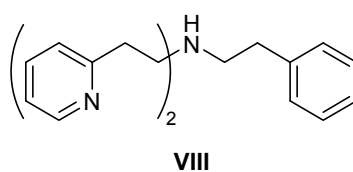
Methyl 4-hydroxybenzoate, as its *tetra-n*-butylammonium salt, was used to test the cresolase activity of two different dicopper(I) complexes, formed with the above-mentioned ligands (Scheme 6). Presence of the electron withdrawing ester-group leads to the stabilization of the dicopper(II)-catecholate product; thereby effectively increasing the selectivity of the catalytic reaction by preventing further redox and condensation reactivity of the product formed.



**Scheme 6.** Hydroxylation of the methyl 4-hydroxybenzoate.

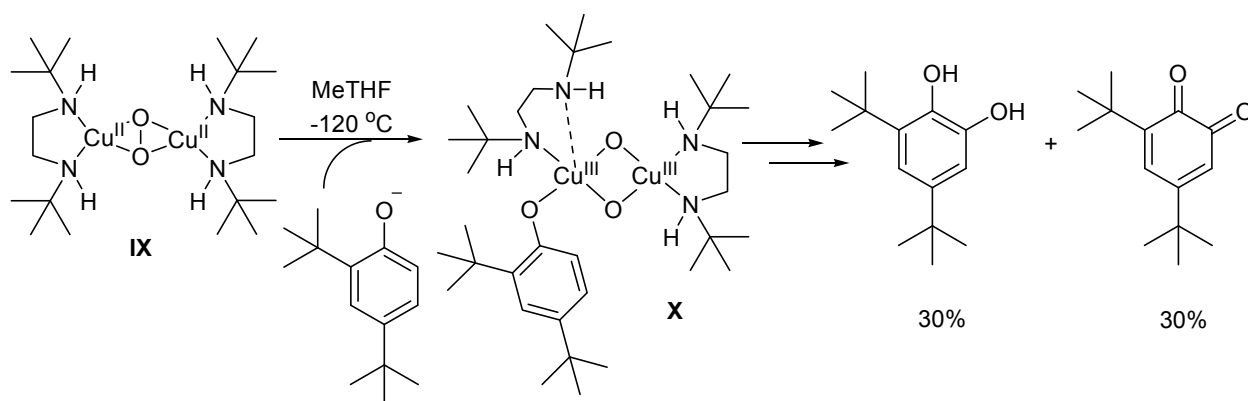
Formation of **VII** was observed only in the case of complex **III** with the *m*-xylyl spacer, unless the reaction was carried out at low temperatures. Conversions were moderate however, with a maximum of 50%. With the tripodal amine-based ligand **VI** no such undesired consecutive reactivity for the formed catechol was observed (i.e. no formation of methyl 2-[4-(methoxycarbonyl)phenoxy]-3,4-dihydroxybenzoate **VII**), even at room temperature, and the product methyl 3,4-dihydroxybenzoate was formed as the sole product. Also with neutral 4-hydroxybenzoic acid some reactivity was observed for the amine-based ligand.

A  $\mu$ - $\eta^2$ : $\eta^2$ -peroxo dicopper(II) complex based on the tridentate amine ligand **VIII** (Figure 11) was also found to act as a functional model for the *cresolase* activity of tyrosinase. Lithium salts of *para*-substituted phenols were used as substrates to react with the dicopper(II) peroxo complex in acetone at  $-94^\circ\text{C}$ , reaching yields between 60 and 90% with only the catechol product formed.<sup>62</sup> Isotope labeling experiments using  $^{18}\text{O}_2$  confirmed that the origin of one of the O atoms of the catechol product is molecular oxygen.



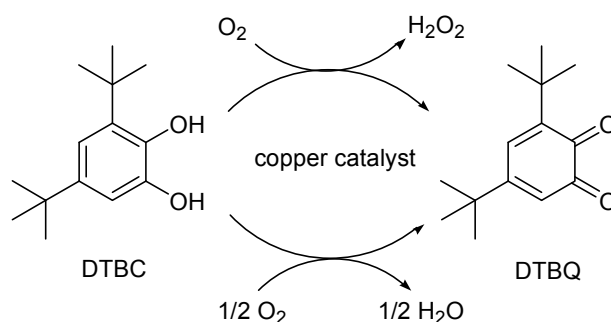
**Figure 11.** Tridentate amine ligand.

$\mu$ - $\eta^2$ : $\eta^2$ -Peroxodicopper(II) complex **IX** with a simple, bulky bidentate amine ligand was found to be active as well in the hydroxylation of phenolates at  $-80^\circ\text{C}$  (in particular for 2,4-di-*tert*-butylphenolate). Stack et al. were able to spectroscopically detect the formation of the bis( $\mu$ -oxo)dicopper(III) phenolate complex **X** with a fully cleaved O-O bond (Scheme 7).<sup>64</sup> These observations can be considered as an alternative mechanism for the catalytic hydroxylation of phenols, as carried out by the tyrosinase metalloenzyme.



**Scheme 7.** Oxidation of 2,4-di-*tert*-butylphenolate to the corresponding catechol and quinone.

Catechols formed after *ortho*-hydroxylation of a phenolic substrate can be further transformed into the corresponding *o*-quinones. This selective oxidation reaction is catalyzed by both tyrosinase and catechol oxidase. Various mono- and dinuclear copper coordination compounds have been investigated as biomimetic catalysts for the catechol oxidation,<sup>11,65</sup> in most cases using 3,5-di-*tert*-butylcatechol (DTBC) as the model substrate (Scheme 8). The bulky *tert*-butyl groups prevent undesirable side reactions such as polymerization of the resulting quinone to yield brown melanin. Depending on the copper catalyst used, either H<sub>2</sub>O<sub>2</sub> or H<sub>2</sub>O may be formed as the reduction product.

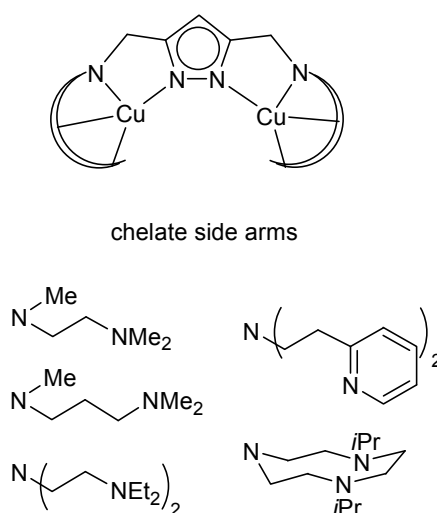


**Scheme 8.** Oxidation of DTBC by copper catalyst.

Casella and co-workers were successful in determining the reaction rates for the two proposed steps of the catalytic cycle (fast binding of catechol to the dicopper(II) complex and slow oxygenation of the dicopper(I) species with a further binding of a second catechol to the dicopper(II) peroxo intermediate, followed by electron transfer from the catechol anion to the dicopper intermediate), but detailed mechanistic studies are still under debate.<sup>66,67,68,69,70</sup>



It was found that dinuclear copper complexes are more reactive than mononuclear compounds in this particular kind of oxidation catalysis.<sup>71,72,73</sup> The activity of synthetic dicopper model complexes can be tuned by different parameters, such as the intramolecular metal-metal separation,<sup>71,74,75,76</sup> the redox properties of the two Cu ions (in a fine interplay with the properties of the ligand donor-groups),<sup>74,77,78</sup> and by the structure of the dinucleating ligands.<sup>71,78,79,80</sup> For example, well-known dicopper complexes derived from pyrazolate-based dinucleating ligands that differ only by the length of the chelate side arms (which allows to control the metal-metal distance), the number of donor atoms (which determines the number of accessible coordination sites), and the type of donor atom (e.g. aromatic versus aliphatic N, which changes the redox properties)<sup>71,81</sup> (Scheme 9) were found to be active in the oxidation of catechols to the corresponding quinones.

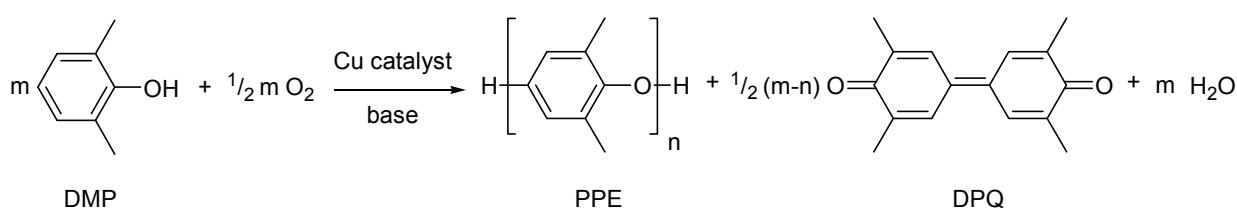


**Scheme 9.** Schematic representation of a family of dinucleating compartmental pyrazole ligands and the general dicopper(II) complex derived from them.

Such kind of ligand modification leads to a distinct activity in the catalytic oxidation of DTBC mediated by those dicopper complexes.<sup>71,74</sup> One of the important factors that determine the catalytic activity of these complexes is the Cu...Cu distance. The shortest accessible separation with the available set of systems ( $\sim 3.50$  Å) is clearly advantageous for high activity.

### 3.2 Oxidative polymerization and coupling of phenols

Several bioinspired model copper complexes were also found to be good catalysts for the oxidative polymerization and coupling of various phenols. It was first discovered in 1959 that a Cu<sup>I</sup>-pyridine complex, in the presence of dioxygen as an oxidant, was able to catalyze the oxidative coupling of phenols. Many studies were carried out to optimize the reaction conditions, in particular the factors that influence the reactivity and selectivity of the product formation. It was established that the presence of two small *ortho*-groups on the phenol ring guides the reaction in the direction of polymerization. In the meantime, larger substituents shift the selectivity towards the formation of undesirable diphenoquinone (DPQ) during the polymerization.<sup>82</sup> Considering these results, 2,6-dimethylphenol was chosen as a monomer, to yield poly(2,6-dimethylphenylene ether) (PPE) as the product after polymerization (Scheme 10).



**Scheme 10.** Copper catalyzed oxidative polymerization of DMP.

PPE is an important ingredient of high-performance engineering plastics. It is a thermoplastic polymer that exhibits unusually low moisture absorption, leading to good electrical insulating properties over a wide humidity- and temperature range. It is also very resistant to a variety of chemicals, water, most salt solutions, acids and bases. Main applications for this material include computer and television housing, keyboard frames and interface boxes.

This polymerization reaction has been extensively studied but the mechanism has not yet been well clarified.<sup>83</sup> Reedijk and co-workers were able to selectively obtain PPE with a molecular weight  $M_w$  of up to ~86000 Da, using a biphasic toluene/water emulsion, with an *in situ* prepared Cu(MeIm)-catalyst (MeIm = 1-methylimidazole). The catalytic results were highly dependent on the ligand:metal ratio used.<sup>84</sup> Different imidazole derivatives were used as ligands and it was found that monodentate ligands led to more active catalysts in comparison

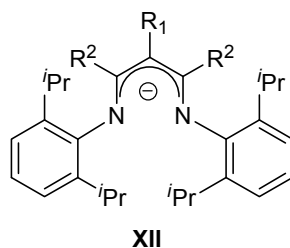


At the same time, use of phenolic substrates without substitution at the *para*-position led to oxidative coupling in the *para*-position, resulting in the formation of diphenoquinone derivatives (e.g. in case of 2,6-dimethylphenol, DPQ is formed as the main product).<sup>88</sup> Similar reactivity is observed for various other dicopper systems.<sup>89</sup>

### 3.3. C-H bond activation

Oxidation of alkanes and alkenes under aerobic conditions is of great importance from both a bioinorganic and a synthetic organic point of view.<sup>90</sup> Nowadays the selective functionalization of, *inter alia*, the family of alkanes via C-H bond activation receives much attention, as this would open up new feedstocks and routes for organic synthesis for laboratory and industrial scale applications.

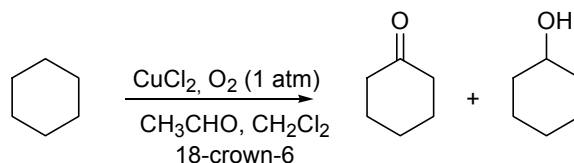
It was found by Itoh and co-workers that  $\beta$ -diketiminato ligands with the general formula **XII** (Figure 12) were able to form complexes with copper(I) or copper(II) ions, yielding the selective formation of different species, depending on the specific conditions employed.<sup>91</sup> Bis( $\mu$ -oxo) $\text{Cu}^{\text{III}}_2$  species were obtained after reaction of either  $\text{Cu}^{\text{I}}$  and  $\text{Cu}^{\text{II}}$  complexes with  $\text{O}_2$  and  $\text{H}_2\text{O}_2$ , respectively. In addition to the formation of such copper(III)-oxo species, the copper(II) complexes were also employed as pre-catalysts for the oxidation of alkanes (cyclohexane and adamantane) in the presence of  $\text{H}_2\text{O}_2$ . These complexes have therefore been described as functional models for pMMO (particulate methane monooxygenase).<sup>92</sup>



**Figure 12.** Schematic representation of  $\beta$ -diketiminato ligands used by Itoh.

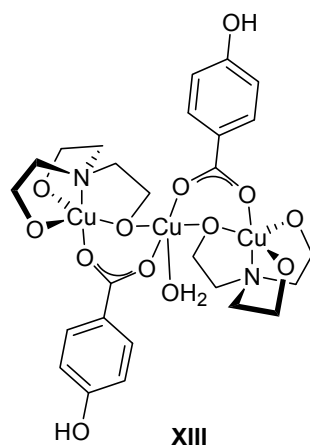
Copper-containing mono-oxygenases such as peptidylglycine- $\alpha$ -hydroxylating monooxygenase (PHM) catalyze the oxidation of aliphatic C-H bonds. Recent studies on the reactivity observed with model complexes for this particular type of metalloenzymes were carried out by Murahashi and co-workers, who have reported that with  $\text{CuCl}_2$  and acetaldehyde and in the

presence of 18-crown-6, cyclohexane could be oxidized to the corresponding cyclohexanone under relatively mild conditions (70 °C). Cyclohexanol was formed as the major side product.<sup>93</sup> The achieved yield of cyclohexanone was 61%, with turnover numbers of up to 1600 (Scheme 13).



**Scheme 13.** Oxidation of cyclohexane.

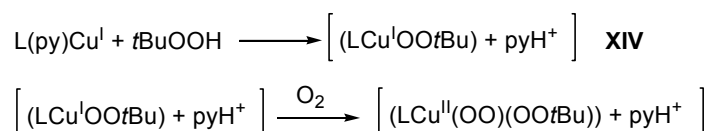
It was recently reported that reaction of  $\text{Cu}(\text{NO}_3)_2$  with triethanolamine in the presence of sodium hydroxide and different types of aromatic carboxylates, and  $\text{NaN}_3$  or  $\text{NaBF}_4$  as additional reagent, yielded multinuclear copper(II) complexes with different structural characteristics, e.g. trinuclear complex **XIII** (Figure 13). These complexes were found to be active systems for the copper catalyzed oxidation of cyclohexane in MeCN, using  $\text{H}_2\text{O}_2$  as oxidant.<sup>94</sup>



**Figure 13.** Trinuclear copper complex used for the oxidation of cyclohexane.

The optimal molar ratio of peroxide to catalyst was found to be in the range from 200:1 to 400:1 with total conversions (cyclohexanol and cyclohexanone combined) of up to 32% after 72 h at room temperature.

Moreover, copper(I) systems based on various N-donor ligands such as pyridine, bipyridine, tris(pyrazolyl)borate (tpb), and tris(pyrazolyl)methane (tpm) have been reported as catalysts for the oxidation of alkanes, alkenes, and alcohols using *t*BuOOH and 1 atm of dioxygen pressure. These mononuclear copper(I) complexes were inactive with regard to oxygen activation. However, reaction of these complexes with *t*BuOOH produced an intermediate **XIV**, which reacted further to form the superoxide species [LCu<sup>II</sup>(OO*t*Bu)(OO)] (Scheme 14).<sup>95</sup>



**Scheme 14.** Formation of the superoxide species from mononuclear pyridine base copper(I) complex.

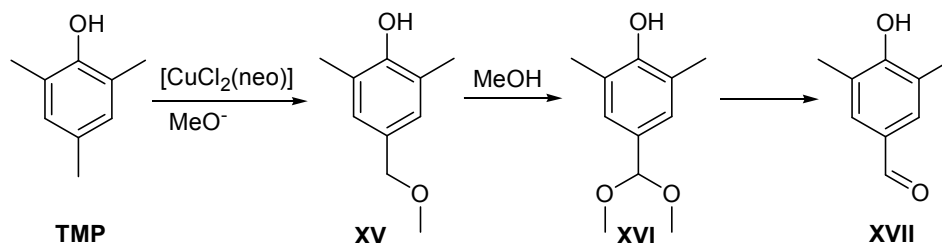
Reaction of 1 M ethylbenzene under 1 atm of O<sub>2</sub>, and in the presence of copper(I)(tpb) complex and *t*BuOOH led to the formation of acetophenone as basically the only product in almost 60% conversion.

The catalytic oxidation of benzylic C-H bonds is also feasible in the presence of copper complexes. One of the frequently used model substrates to probe the catalytic activity of a given Cu-complex in the oxidation of benzylic C-H bonds is 2,4,6-dimethylphenol (TMP), which can not undergo C-O polymerization.

Combination of CuCl<sub>2</sub> in the presence of amine or oxime ligands and alcohol (in particular MeOH)<sup>96</sup> leads to the formation of copper systems that show activity in the selective oxidation of the *para*-methyl group by molecular oxygen to yield 3,5-dimethyl-4-hydroxybenzaldehyde **XVII** (Scheme 15). This transformation bears some similarity to the oxygenation of aromatic CH<sub>3</sub>-groups to the corresponding aldehyde, as catalyzed by laccase or vanillyl alcohol oxidase.<sup>97</sup>

Reedijk and co-workers recently reported another copper system that is able to catalyze this kind of benzylic C-H oxidation.<sup>98</sup> Since the oxidation of TMP to a corresponding aldehyde is an overall four-electron process, four equivalents of a Cu<sup>II</sup>-based system [CuCl<sub>2</sub>(neo)/NaOMe] (neo = 2,9-dimethylphenanthroline) were used to stoichiometrically

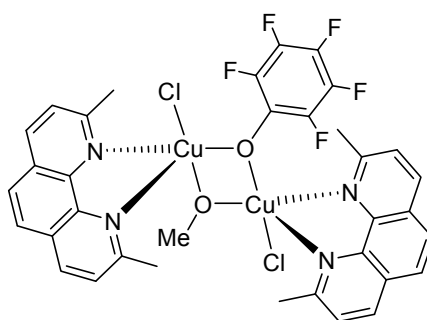
oxidize TMP selectively to 3,5-dimethyl-4-hydroxybenzaldehyde (**XVII**) at room temperature in MeOH. This reaction could also be conducted in a catalytic fashion, using  $\text{H}_2\text{O}_2$  as oxidant in refluxing MeOH.



**Scheme 15.** Sequential oxidation of TMP to **XVII**, catalyzed by the  $[\text{CuCl}_2/\text{neo}/\text{NaOMe}]$  system.

A decrease in the stoichiometry  $\text{NaOMe}:\text{TMP}$  led to selective isolation of the intermediate product 4-(methoxymethyl)-2,6-dimethylphenol **XV** (MDP). However, the catalytic activity of the  $\text{CuCl}_2(\text{neocuproine})$  system is rather low with a turnover frequency of  $\sim 1.4 \text{ h}^{-1}$ . It has been proposed that the reaction proceeds through formation of a Cu-bound phenoxyl radical (that reacts with  $\text{O}_2$ ) and a benzoquinone methide intermediate, followed by repeated 1,6-addition of alcohol to sequentially form 4-(methoxymethyl)-2,6-dimethylphenol **XV** and 3,5-dimethyl-4-hydroxybenzaldehyde dialkyl acetal **XVI**, which is further hydrolyzed to yield 3,5-dimethyl-4-hydroxybenzaldehyde **XVII**.

In order to get some insight into a possible reaction pathway or active Cu-species involved in the observed catalysis, pentafluorophenol ( $\text{C}_6\text{F}_5\text{OH}$ ) was applied as a model substrate. Together with the ligand (neo) and in the presence of  $\text{NaOMe}$  and  $\text{CuCl}_2$ , formation of a dinuclear copper(II) core, bridged by a methoxide and a phenoxide, was observed (Figure 14).



**Figure 14.** Model dinuclear copper(II) complex with a methoxide and a phenoxide bridge.

The  $[\text{CuCl}_2(\text{neocuproine})/\text{NaOMe}]$  system mentioned above has also been reported as a catalyst for the 1,6-nucleophilic addition of either 1,2-ethanediol, 2,2'-dipyridylamine or 2,4-pentanedione to TMP. These oxidative coupling reactions of TMP with various nucleophiles proposedly proceed via the *in situ* formation of a benzoquinone methide.<sup>99</sup> Reactions were carried out in DMF as non-nucleophilic solvent, and with NaOMe as base to deprotonate the *para*  $\text{CH}_3$ -group of TMP to form the proposed reactive benzoquinone methide intermediate. No oxidative coupling was observed without neocuproine present in the system, which can be considered as evidence for the necessary stabilization of the  $\text{Cu}^{\text{I}}$ -oxidation state with a bulky bidentate ligand. It was assumed that reduction of  $\text{Cu}^{\text{II}}$  to  $\text{Cu}^{\text{I}}$  takes place together with formation of the benzoquinone methide fragment.



### 3.4 Goals of the work

The framework of the thesis is provided by newly developed pyrazole-based ligands with bio-inspired chelating side arms in the 3- and 5-positions of the heterocyclic core. The synthesis of these compounds will be described and they will be applied as valuable scaffolds for further studies. The design-concept for these ligands makes use of the fact that the anionic pyrazolate unit has a high tendency to span two metal ions in a  $\mu$ - $\eta^1:\eta^1$  *exo*-bidentate fashion, while appropriate modification of the side-arms of such ligand systems makes it possible to tune the properties of the copper complexes derived from them. The coordination spheres of the individual copper ions as well as the intramolecular metal-metal separation are the most important factors when synthesizing models for biologically relevant dicopper complexes; for pyrazolate-bridged complexes, these parameters can be altered by appropriate modifications of the appended chelate substituents.

New bioinspired dinucleating ligand scaffolds that have binding compartments composed of imidazolyl groups will be reported. These ligands form very stable copper complexes, and initial studies will be performed to determine the different species formed in solution, depending on the pH (in particular for complexes based on a ligand with appended bis[2-(1-methylimidazolyl)methyl]aminomethyl chelate arms).

It is necessary to obtain a comprehensive picture of the copper coordination chemistry of the new ligand systems for any further (reactivity) studies to be performed. This will require a full characterization of the various copper complexes obtained, both in solution and in the solid state (e.g. by spectroscopic methods and X-ray crystallography).

Properly characterized copper complexes with carefully tuned and desired properties (nature of the chelate arms, metal-metal separation, nuclearity) will be further applied as catalysts in different types of oxidation of phenolic substrates. In particular, attention will be given to the oxidative C-C coupling of 2,6-dimethylphenol (DMP) and 2,4,6-trimethylphenol (TMP), as well as to the 1,6-nucleophilic addition of several small molecules to TMP, such as MeOH. In order to gain mechanistic insight, specifically for the oxidative C-C coupling of TMP, the reactions (both catalytic and stoichiometric with regard to the phenols used) will be monitored with a variety of spectroscopic methods and organic intermediates formed during the reaction will be identified.

Moreover, to shed light on the formation and structure of possible intermediates in the catalytic reactions studied, the coordination chemistry of these dicopper complexes with phenolic substrates that display no Cu-mediated transformation will be a subject of research.

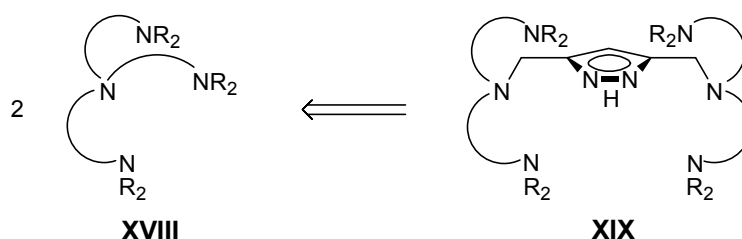
All these above-mentioned studies have to provide a better understanding of the principles/factors that govern the catalytic oxidation activity of pyrazolate-based bimetallic model complexes towards phenols. Various kinds of correlations (e.g. metal-metal separation and effective cooperativity of two adjacent copper ions; behaviour of new copper complexes in solution and catalytic activity in the C-H bond activation) will be discussed.

Furthermore, some specific examples of unprecedented C-C and C-O bond forming reactions with 4-ethylphenol and 4-bromo-2,6-dimethylphenol are described.

## 4 Ligand synthesis

### 4.1 Properties of pyrazole-based compartmental ligands

As was already described before, tripodal tetradentate  $\{N_4\}$  ligands (such as the tris(pyridylmethyl)amine type)<sup>54,55</sup> were successfully applied to emulate the properties and reactivities of mononuclear N-ligated metalloenzymes. From this point of view, the pyrazole-bridging ligands used in the present work can be described as two tripodal tetradentate  $\{N_4\}$  subunits **XVIII** bridged by a heterocyclic pyrazole core to give the overall ligand system **XIX** (Scheme 16). This general ligand architecture allows the direct and selective formation of dinuclear complexes with highly tunable properties (e.g. metal-metal separations can range from 3.40 to 4.50 Å).<sup>13,15,16</sup>

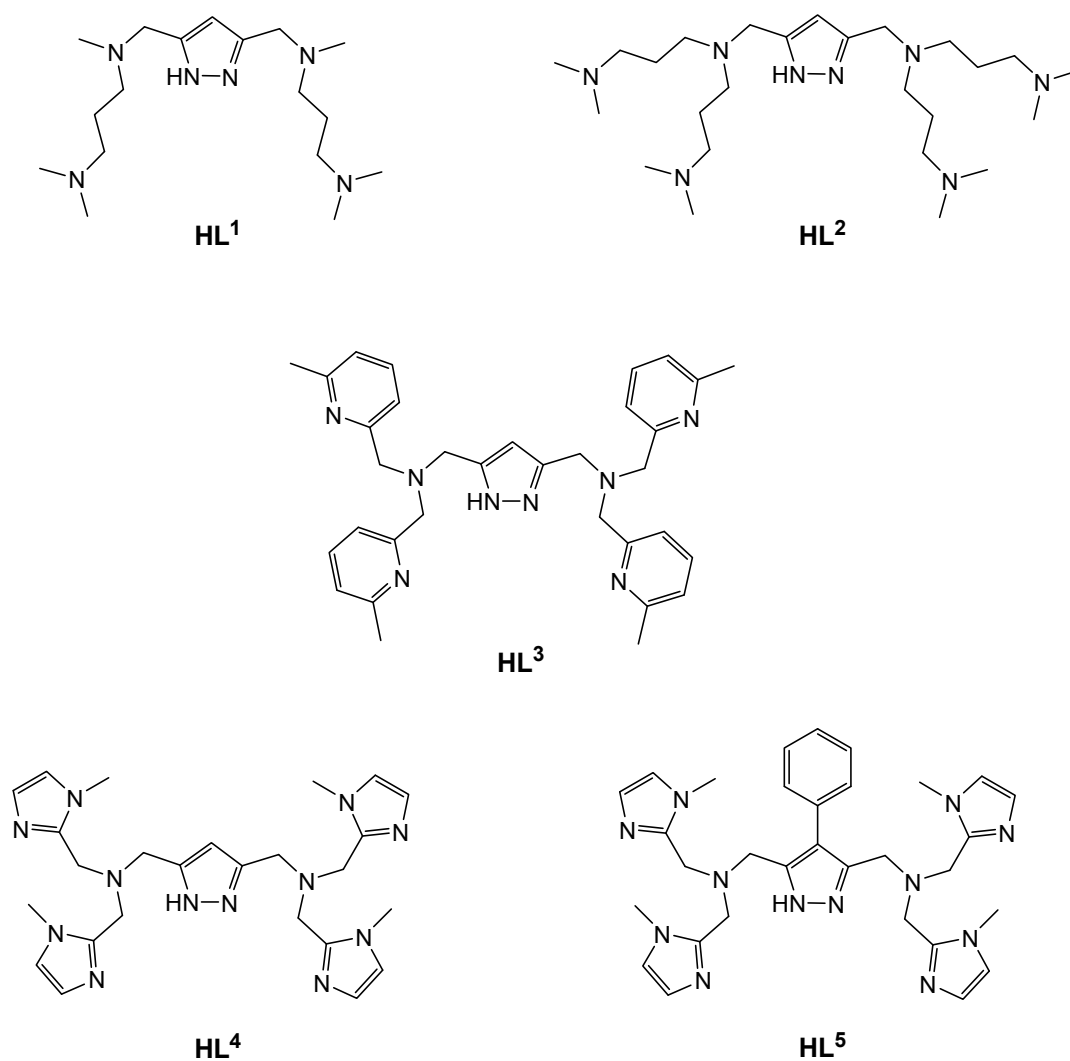


**Scheme 16.** Schematic representation of the  $\{N_4\}$  subunit **XVIII** and pyrazole-bridging ligand **XIX**.

The set of pyrazole-based ligands synthesized and used in this work is depicted in Figure 15. **HL**<sup>1</sup> and **HL**<sup>2</sup> have been reported previously<sup>71</sup> and represent pyrazole-based ligands with aliphatic side arms. This pair of ligands differs only by the number of additional  $N$ -donor-functionalities, which allows for the manipulation of the geometry of the copper ions in the complexes as well as the redox properties of the dicopper core. Presence of the pyridine- $N$ -donor compartments in ligand **HL**<sup>3</sup> provides for additional metal-to-ligand backbonding, which leads to a change in the redox properties of the copper ions. Such kind of electronic fine-tuning is not possible for ligands with aliphatic compartments.

The last two ligands **HL**<sup>4</sup> and **HL**<sup>5</sup> have binding compartments composed of imidazolyl groups. These new pyrazole-based ligands have been designed and prepared with the aim of further advancing the emulation of biological donor environments of copper ions in relevant

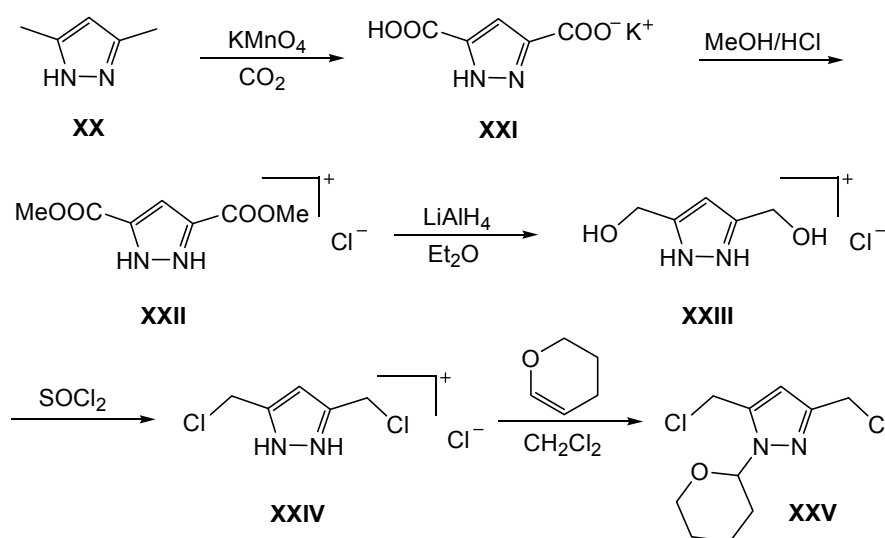
model complexes. The pendant imidazole donors in **HL**<sup>4</sup> and **HL**<sup>5</sup> significantly increase the biomimetic character of these ligands, and it is foreseen that these systems can be very interesting as building blocks for the synthesis of copper complexes that may exhibit promising catalytic properties. All ligands used were prepared via multi-step procedures.



**Figure 15.** Pyrazole-based ligands **HL**<sup>1</sup>-**HL**<sup>5</sup>.

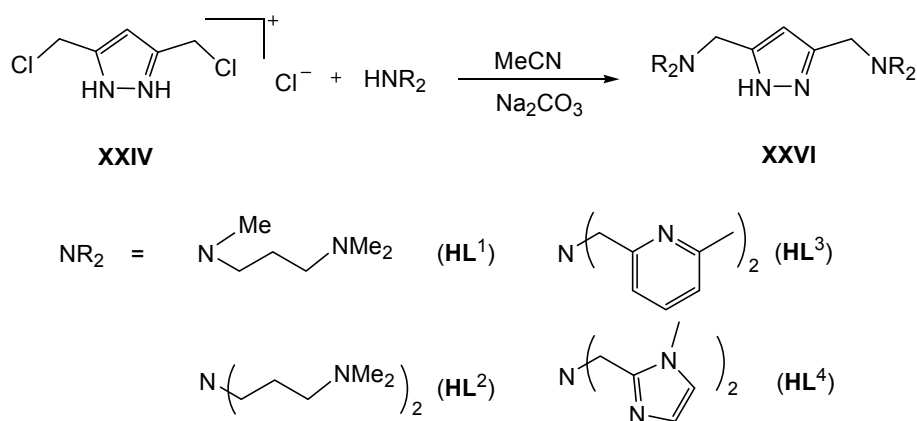
## 4.2 Synthesis of ligands

The herein described bis(aminomethyl)-substituted pyrazole-based ligands can be synthesized using the following procedure depicted in Schemes 10 and 11. At first, 3,5-bis(chloromethyl)-1-(tetrahydropyran-2-yl)pyrazole **XXV** has to be prepared according to the literature (Scheme 17).<sup>100,101,102</sup> By oxidation of 3,5-dimethylpyrazole **XX**, the mono potassium salt of 3,5-pyrazole dicarboxylic acid **XXI** can be obtained. Further esterification of **XXI** is performed under acidic conditions in methanol. Alcohol **XXIII** is obtained upon reduction of ester **XXII** in the presence of  $\text{LiAlH}_4$  in diethylether, and this former compound can thereafter be chlorinated using thionyl chloride, which at the same time serves as the solvent for this reaction, to yield 3,5-bis(chloromethyl)pyrazole **XXIV**. The last step in the preparation of 3,5-bis(chloromethyl)-1-(tetrahydropyran-2-yl)pyrazole **XXV** is protection of the NH-group of the pyrazole by 3,4-dihydro-2H-pyran in dichloromethane (DHP).



**Scheme 17.** Preparation of the 3,5-bis(chloromethyl)-1-(tetrahydropyran-2-yl)pyrazole **XXV**.

It has to be mentioned that protection of the pyrazole NH-functionality with DHP is not always a necessary step for the preparation of amine-based functional derivatives of pyrazoles. Depending on the amine used for the coupling with the bis(chloromethyl) derivative, the above-mentioned protection step can be excluded, and 3,5-bis(chloromethyl)pyrazole **XXIV** can directly undergo reaction with amines to yield the desired ligand with general structure **XXVI** (Scheme 18). This direct route works especially well for aliphatic and some aromatic amines.

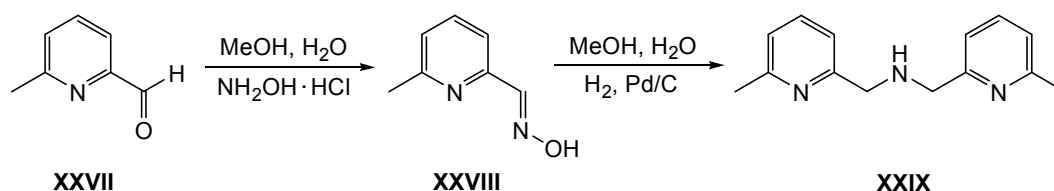


**Scheme 18.** Synthesis of ligands with aliphatic and aromatic side arms.

This advantage (excluding the NH-protection reaction) was applied in the synthesis of all ligands used, which increased their yields, as especially the deprotection of the pyrazole NH-unit is known to lead, in general, to significant product loss.

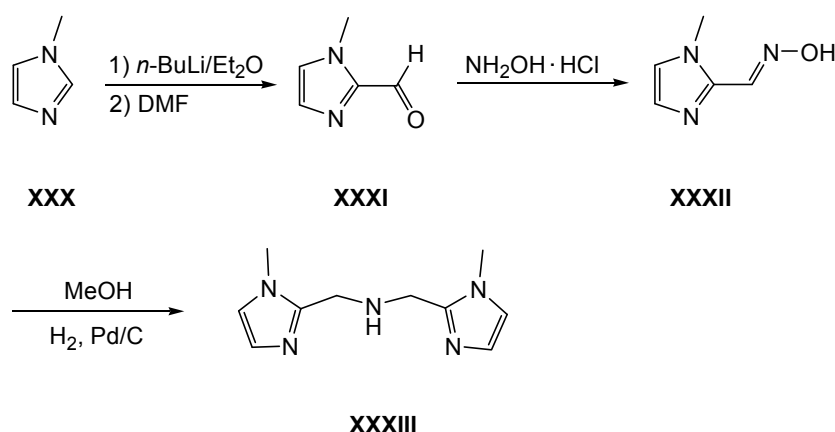
The amines used for the synthesis of ligands **HL**<sup>3</sup>, **HL**<sup>4</sup> and **HL**<sup>5</sup> were prepared in multistep syntheses following (modified) literature procedures.<sup>103</sup>

To obtain bis[(6-methyl-2-pyridyl)methyl]amine **XXIX**,<sup>103a</sup> 6-methylpyridine-2-carboxaldehyde **XXVII** was reacted with hydroxylamine hydrochloride, yielding 6-methylpyridine-2-oxime **XXVIII**. The last step in the preparation of this desired amine is hydrogenation of the oxime in a mixture of methanol/water (Scheme 19).



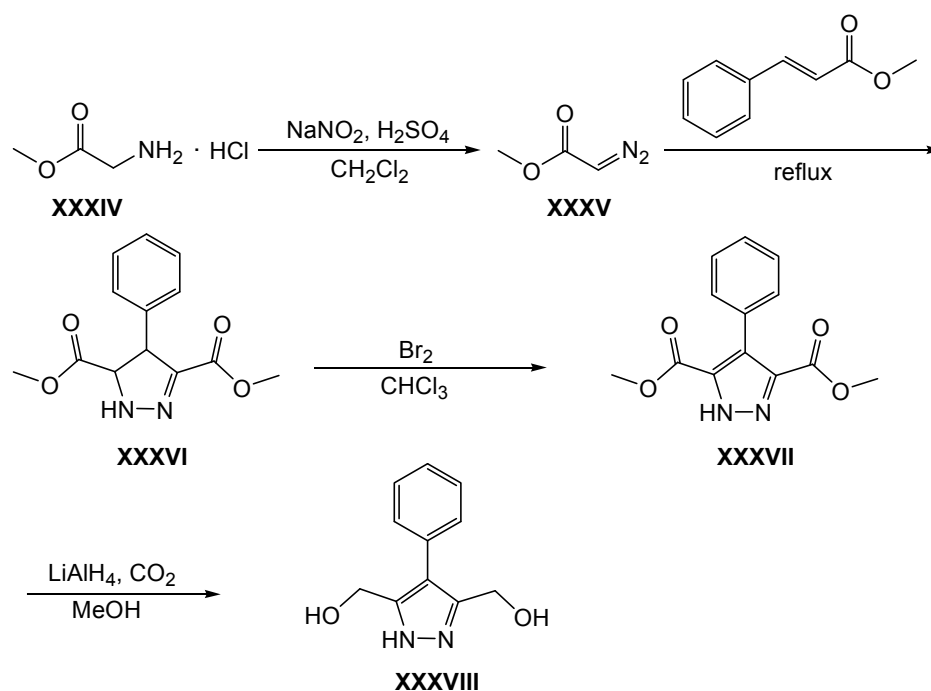
**Scheme 19.** Preparation of bis[(6-methyl-2-pyridyl)methyl]amine.

Bis[(1-methylimidazol-2-yl)-methyl]amine **XXXIII** was prepared via a four step synthetic route,<sup>103b,c</sup> starting from *N*-methylimidazole **XXX**, which was deprotonated by *n*-BuLi and then reacted with DMF, yielding *N*-methylimidazolyl-2-aldehyde **XXXI**. Preparation of *N*-methylimidazolyl-2-oxime **XXXII** was carried out in an analogous way as for **XXIX**, in the presence of hydroxylamine hydrochloride. Hydrogenation of the corresponding oxime was performed on Pd/C catalyst, yielding product **XXXIII** (Scheme 20).



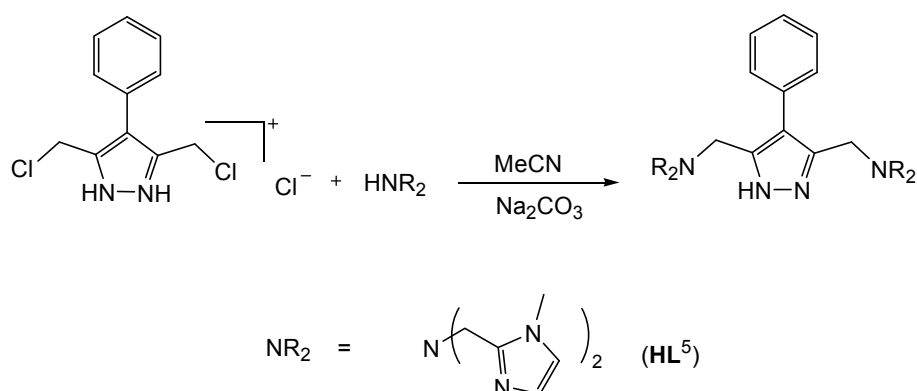
**Scheme 20.** Synthesis of bis[(1-methylimidazole-2-yl)-methyl]amine.

Inclusion of a phenyl group into the backbone of the central pyrazole unit, effectively yielding 3,5-bis(hydroxymethyl)-4-phenyl-pyrazole **XXXVIII**, requires drastic changes in the synthetic procedure to obtain this starting material. In this case, commercially available glycine methylester hydrochloride **XXXIV** was reacted with sodium nitrite in the presence of sulfuric acid, yielding diazoacetic acid methylester **XXXV** as orange oil.<sup>104</sup> Subsequently, **XXXV** was reacted with methylcinnamate to obtain the methylester of 4-phenylpyrazoline dicarboxylic acid **XXXVI**<sup>105</sup> which could be oxidized by bromine to the corresponding pyrazole analogue **XXXVII**. The end-product **XXXVIII** was cleanly obtained upon reduction of **XXXVII** with  $\text{LiAlH}_4$  in  $\text{Et}_2\text{O}$  (Scheme 21).



**Scheme 21.** Synthetic route for the preparation of 3,5-bis(hydroxymethyl)-4-phenyl-pyrazole.

**XXXVIII** could be further chlorinated using  $\text{SOCl}_2$  (as depicted in Scheme 10) and this derivative was then finally used for the coupling with amine **XXXIII** using the same conditions as described above (Scheme 22).



**Scheme 22.** Preparation of the ligand **HL<sup>5</sup>**.

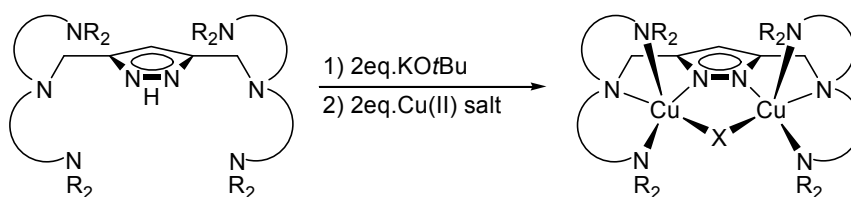
Thus, a new ligand **HL<sup>5</sup>**, with a 4-phenyl substituted pyrazole as the core of the ligand, was prepared as the first representative of a new family of pyrazole-based compartmental ligands featuring an aryl-substituted pyrazole ring.



## 5 Synthesis and characterization of complexes

### 5.1 Complex synthesis: general procedure

Pyrazole-bridging ligands **HL**<sup>1</sup>-**HL**<sup>5</sup>, each consisting of two tripodal tetradentate {N<sub>4</sub>} subunits bridged by a pyrazole motif, serve to form specific, targeted bimetallic copper complexes. The general route for preparing such complexes is depicted in Scheme 23. The nature of the side arms (aliphatic or aromatic) of the pyrazole-based ligands does not play any significant role when choosing the synthetic strategy. To obtain such dicopper species, the pyrazole ligand has to be dissolved in MeOH or MeCN, or in a mixture of these solvents, followed by addition of two equivalents of base. The first equivalent serves to deprotonate the pyrazole NH-functionality, which generates a dinucleating pyrazolate fragment, while the second equivalent of base is used to deprotonate either a solvent molecule or to abstract a proton from an H<sub>2</sub>O molecule, originating from the hydrated copper(II) salts employed.



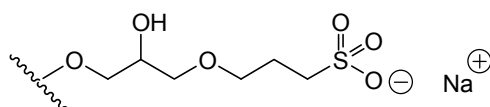
**Scheme 23.** Synthesis of the dicopper(II) complexes. The X ligand represents either a MeO⋯HOMe, an HO⋯HOH or an OH bridging pattern.

Subsequent addition of two equivalents of copper(II) salt leads to the formation of the desired dinuclear Cu-species, with each copper ion coordinated within one of the two tripodal {N<sub>4</sub>} binding pockets, with either a MeO⋯HOMe, an HO⋯HOH or  $\mu$ -OH motif, obtained after the second deprotonation step. From the wide range of available copper(II) salts, those containing large, weakly coordinated anions, such as ClO<sub>4</sub><sup>-</sup>, NO<sub>3</sub><sup>-</sup> or BF<sub>4</sub><sup>-</sup> were selected to be studied primarily. In these complex-formation reactions, KOtBu is normally used as a base in order to enable easy removal of the byproduct formed during the reaction, e.g. KClO<sub>4</sub>, by precipitation. The isolated copper complex can be redissolved in the appropriate solvent, whereafter slow diffusion of Et<sub>2</sub>O into this solution generally yields single crystals suitable for X-ray analysis.

### 5.1.1. Purification of complexes

Traces of the incompletely reacted amine **XXXIII** still present after the synthesis of ligands **HL**<sup>4</sup> and **HL**<sup>5</sup> proved to have a detrimental influence on the isolation of pure dicopper species, because of formation and co-crystallization of mononuclear copper complexes. Therefore, purification of each crude mixture of Cu-complexes was performed under gravity flow using Na<sup>+</sup> – loaded SP Sephadex C25 (40-125 μ) cation-exchange resin.

SP-Sephadex C25 consists of macroscopic beads that are synthetically derived from the polysaccharide dextran, with strongly acidic propylsulfate (sulfopropyl or SP) groups fixed on the surface (Scheme 24).



**Scheme 24.** Schematic representation of the “sulfopropyl” (SP) groups of the cationic exchange resin SP-Sephadex C25.

A solution of the particular copper complex subjected to this purification/separation procedure was prepared applying the same synthetic route described above with minor changes (only one equivalent of base was used). After addition of the copper salt, a further dilution of the reaction mixture with water to reach a ratio between organic solvent:water of 1:10 is required. The principle of ion-exchange column chromatography is based on interaction of the cationic part of the (in this case) Cu-complex present in the solution with the Sephadex column material; retention is dependent on the overall charge of the complex, with highly charged species (in the present study; multinuclear species) eluting slower than mononuclear analogues. Separation of the different complexes formed was carried out by washing the column with various concentrations of an aqueous solution of NaNO<sub>3</sub>.

The fraction of the singly charged mononuclear copper species derived from the incompletely reacted amine was collected after elution with 0.2 M NaNO<sub>3</sub> solution. Subsequent elution with 0.4 M NaNO<sub>3</sub> solution resulted in isolation of the main product of the complexation reaction, i.e. a multinuclear copper complex. Additional treatment of this main fraction

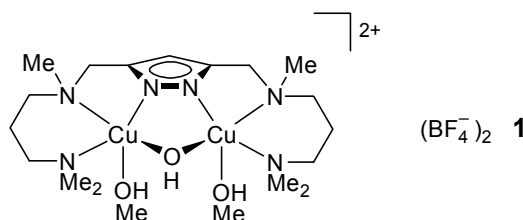
(changing of pH or solvents with regard to complex solubility) led to the formation and isolation of the desired dicopper species.

## 5.2 Copper(II) complexes of ligands **HL**<sup>1</sup> and **HL**<sup>2</sup>

In order to obtain a detailed understanding about the type of complexes formed both in solution and the solid state, the coordination behaviour of the two ligands **HL**<sup>1</sup> and **HL**<sup>2</sup>, containing functionalized aliphatic side arms, towards copper is studied. The influence of the reaction conditions on the formation of different types of dicopper complexes is discussed.

### 5.2.1 Structural characterization of copper complex with **HL**<sup>1</sup>

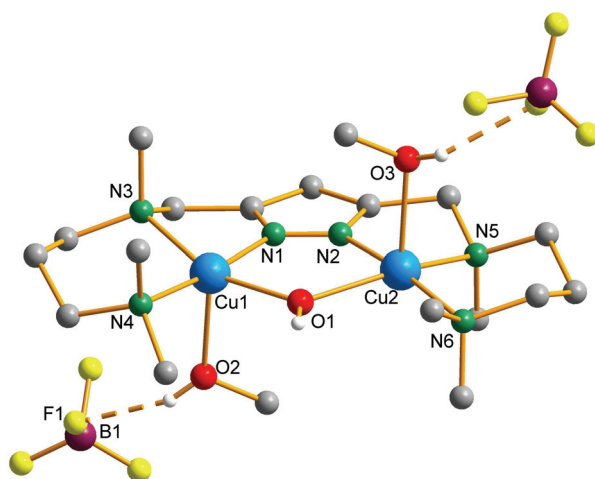
Reaction of **HL**<sup>1</sup> with two equivalents of KO<sup>t</sup>Bu in MeOH/MeCN, followed by addition of two equivalents of Cu(BF<sub>4</sub>)<sub>2</sub>·4H<sub>2</sub>O to the reaction mixture led to the formation of dinuclear copper complex **1** (Figure 16).



**Figure 16.** Structure of complex **1**.

Single crystals of complex **1**, obtained by diffusion of the Et<sub>2</sub>O into a methanol solution, were used for an X-ray crystallographic analysis. The molecular structure of the cation of **1** is shown in Figure 17.

As was previously described, pyrazole ligands such as **HL**<sup>1</sup>, with (relatively) long and flexible side arms, favor a short intramolecular copper-copper distance. Furthermore, depending on the number of N-donors, coordination of additional co-ligands (either solvent molecules or counter anions) can be observed.<sup>71</sup>



**Figure 17.** The molecular structure of complex **1**.

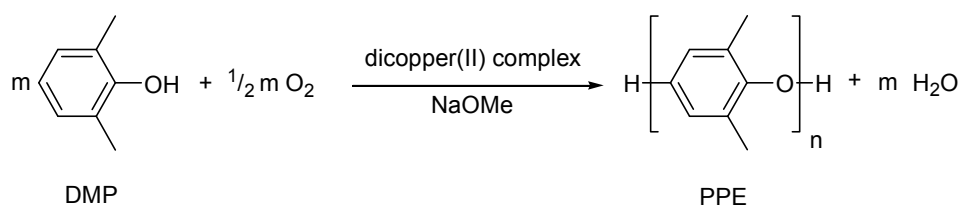
Two copper(II) ions are nested within their respective coordination pockets and are spanned by the bridging pyrazolate moiety. Each copper atom is in a roughly square planar coordination environment ( $\tau_{\text{Cu1}} = 0.23$ ,  $\tau_{\text{Cu2}} = 0.24$ ),<sup>106</sup> consisting of three N-donors from the pyrazolate ligand and an O atom from the  $\mu$ -OH-unit located within the bimetallic pocket. An additional axial position is occupied by a solvent molecule (MeOH) at a greater distance (2.25 – 2.28 Å), typical for Jahn-Teller distortion (Table 1). The distance between the copper atom and the oxygen atom from the co-ligand in complex **1** is short in comparison to known complexes based on the same ligand with aliphatic compartments, where the Cu-O separation is typically in the range from 2.32 to 2.36 Å. Fluorine atoms from two  $\text{BF}_4$  counter-anions and the additional axially coordinated MeOH ligands participate in hydrogen-bonding. The rather short  $\text{Cu}\cdots\text{Cu}$  distance of 3.60 Å is due to the long chelating side arms appended to the pyrazole, which provide formation of the small hydroxo-bridge, without any additionally included solvent molecule within the bimetallic pocket. The UV/vis spectroscopic measurements completely agreed with the persistence of the square planar coordination environment of the copper ions upon dissolution in MeCN, with only one observed  $d-d$  transition band at  $\lambda_{\text{max}} = 628$  nm.

**Table 1.** Selected intramolecular distances (Å) and angles (°) for complex **1**.

Distances			
Cu(1)-N(1)	1.849(6)	Cu(2)-N(6)	2.030(7)
Cu(1)-N(4)	1.996(5)	Cu(2)-N(5)	2.102(6)
Cu(1)-N(3)	2.113(7)	Cu(2)-O(1)	2.189(5)
Cu(1)-O(1)	2.115(7)	Cu(2)-O(3)	2.289(6)
Cu(1)-O(2)	2.250(6)	Cu(1)···Cu(2)	3.596(1)
Cu(2)-N(2)	1.871(8)		
Angles			
N(1)-Cu(1)-N(4)	173.5(3)	N(2)-Cu(2)-N(6)	172.5(3)
N(1)-Cu(1)-N(3)	79.0(3)	N(2)-Cu(2)-N(5)	81.6(3)
N(4)-Cu(1)-N(3)	98.8(3)	N(6)-Cu(2)-N(5)	98.3(3)
N(1)-Cu(1)-O(1)	86.0(3)	N(2)-Cu(2)-O(1)	82.8(3)
N(4)-Cu(1)-O(1)	94.6(3)	N(6)-Cu(2)-O(1)	95.2(3)
N(3)-Cu(1)-O(1)	159.6(2)	N(5)-Cu(2)-O(1)	158.1(2)
O(1)-Cu(1)-O(2)	95.2(2)	O(1)-Cu(2)-O(3)	97.1(2)
N(1)-Cu(1)-O(2)	92.8(3)	N(2)-Cu(2)-O(3)	90.0(3)
N(3)-Cu(1)-O(2)	99.2(2)	N(5)-Cu(2)-O(3)	98.1(2)
N(4)-Cu(1)-O(2)	93.6(2)	N(6)-Cu(2)-O(3)	97.4(3)

### 5.2.2 Previously studied catalytic activity of dicopper complexes

Dicopper(II) complexes based on a set of ligands with aliphatic side arms were previously tested as catalysts for the oxidative polymerization and coupling of 2,6-dimethylphenol (DMP) (Table 2). Poly(2,6-dimethylphenylene ether) (PPE, an important ingredient of high-performance engineering plastics) was the main product obtained under all chosen reaction conditions (Scheme 25).<sup>107</sup>



**Scheme 25.** Oxidative polymerization of DMP catalyzed by pyrazolate-based dicopper(II) complexes.

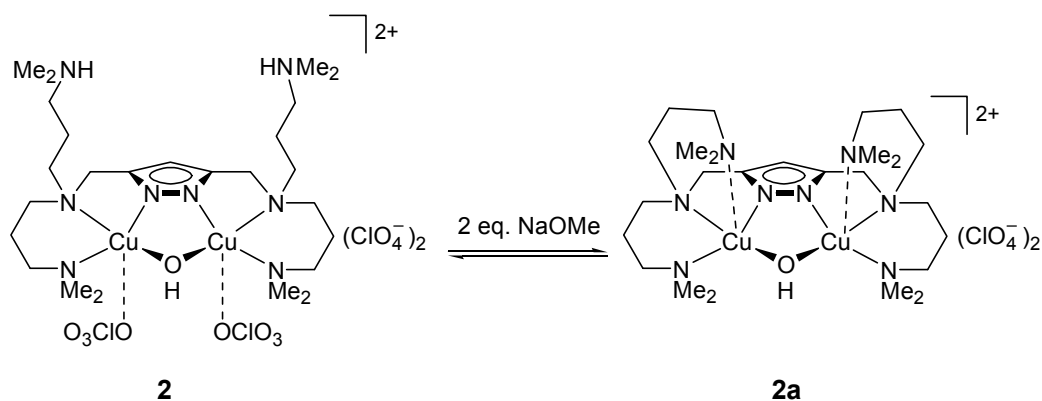
**Table 2.** Chelating side arms appended to the pyrazole unit and Cu...Cu separation (Å) found in the dicopper(II) complexes used for polymerization of DMP.

Aliphatic side arms	$d(\text{Cu}\cdots\text{Cu})$
	3.45
	4.09
	4.53
	3.54

\* side-arms of **HL**<sup>1</sup> in the present work

\*\* side-arms of **HL**<sup>2</sup> in the present work

Complex **2** (based on **HL**<sup>2</sup>)<sup>107,108</sup> was found to be the most active catalyst for the oxidative polymerization (C-O coupling), but activity only occurred when two additional equivalents of base (NaOMe) were added to the reaction mixture in MeCN. It was assumed that supplementary base was necessary for deprotonation of two dangling, protonated amine side arms, followed by the formation of complex **2a**. This latter complex, derived from **2** by deprotonation and coordination of two additional amine groups, was suggested to be the active species in the polymerization of DMP (Scheme 26).

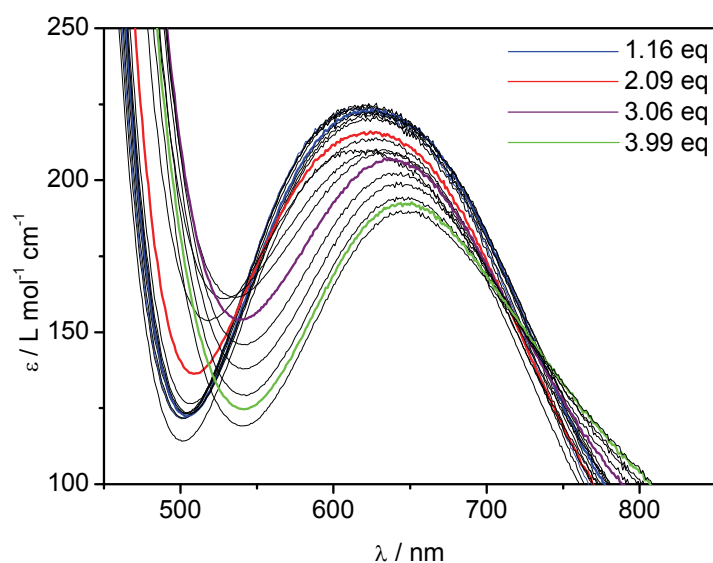


**Scheme 26.** Schematic representation of the assumed interconversion between **2** and **2a**.

Dicopper complex **2** resembles the structure found for complex **1**, with both copper atoms in identical square pyramidal coordination environments. Two *N*-dimethyl-aminopropyl groups of **HL**<sup>2</sup> are protonated and therefore remain uncoordinated; as such they can be considered analogous to the methyl groups in **HL**<sup>1</sup>. In this sense, the fifth, axial position of the copper atoms in **1** is occupied by coordinating solvent molecules, while in **2** coordination of the counter anions as co-ligands was observed in the same fashion.<sup>71</sup>

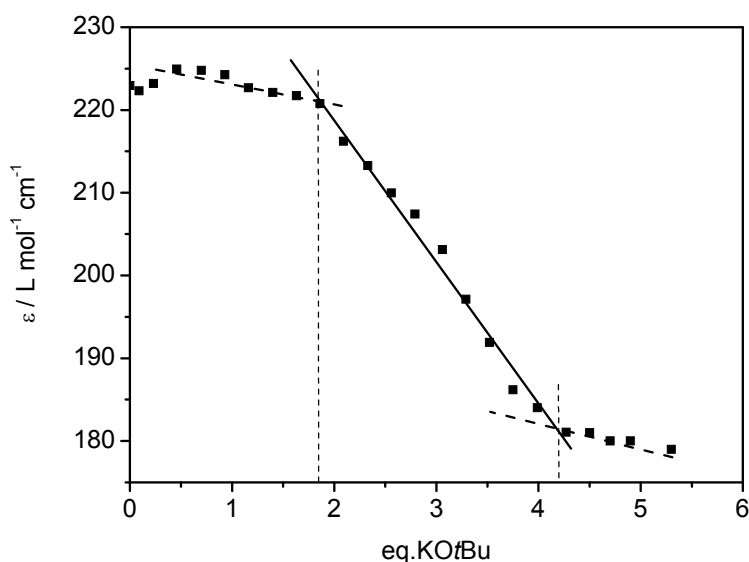
### 5.2.3 Equilibria in solution and structural characterization of complexes with **HL**<sup>2</sup>: unusual copper-dioxygen mediated amine to *N*-oxide transformation of **HL**<sup>2</sup>

In order to gain insight in the role of the supplementary base used during the activation of complex **2** and prior to any polymerization of DMP, the possible existence of an equilibrium between **2** and **2a** was studied. Dicopper complex **2** was dissolved in a mixture of MeOH/MeCN (0.0049 mol L<sup>-1</sup>) and addition of the KO<sup>t</sup>Bu solution (0.0098 mol L<sup>-1</sup>) was performed in a stepwise manner (Figure 18).



**Figure 18.** UV/vis titration of a solution of **2** in MeOH/MeCN with KOtBu.

The initial dicopper species **2** showed a characteristic absorption (*d-d* band) at  $\lambda_{\text{max}}$  of 618 nm and during titration with base, this maximum shifted gradually to lower energy, with the final value of 649 nm reached after four equivalents. However, no spectroscopic changes were observed when up to two equivalents of base were added and only the addition of a further two equivalents of KOtBu induced a shift towards weak ligand field (Figure 19).

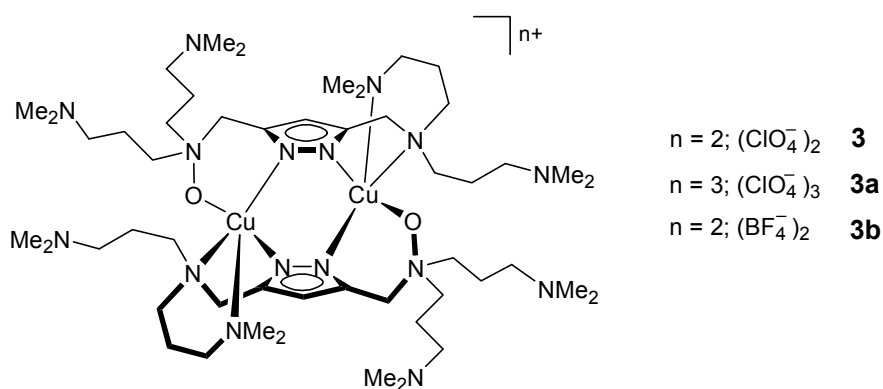


**Figure 19.** Changes in extinction coefficient depending on the amount of base added.



The necessity to add four equivalents of base to drive the (equilibrium) reaction to completion showed that the assumed single-step equilibrium between **2** and **2a** (see above) is most likely a more complicated multistep-process. One can propose that the protonated amine side arms in **2** are each losing one proton upon addition of the first two equivalents of base and thereafter loosely coordinate to the dicopper core. Coordination of the long, initially protonated side arms in the axial positions would not cause significant changes to the square pyramidal geometry of the copper ions, which is in a good agreement with the observed small shift of the band at 618 nm in the UV/vis spectrum. Further addition of the second two equivalents of base could then lead to deprotonation of two solvent molecules (MeOH), which would subsequently become coordinated to the copper ions via exchange with the initial co-ligand ( $\text{ClO}_4^-$ ). This exchange induces structural/electronic changes in the complex, as observed in the UV/vis spectrum, where finally formed species showed an absorption maximum at a  $\lambda_{\text{max}}$  of 649 nm.

Crystallization of the deprotonated species, anticipated to have the initially proposed structure as in **2a** was performed from the reaction mixture of **HL**<sup>2</sup> with two equivalents of KO<sup>t</sup>Bu and two equivalents of  $\text{Cu}(\text{ClO}_4)_2 \cdot 6\text{H}_2\text{O}$  in MeOH or EtOH. However, in sharp contrast with the expected results, the X-ray crystallographic analysis on two different kinds of crystals yielded the molecular structures **3** and **3a** (Figure 20). A similar structure **3b** was obtained when using  $\text{Cu}(\text{BF}_4)_2 \cdot 4\text{H}_2\text{O}$  as the copper salt (see below).



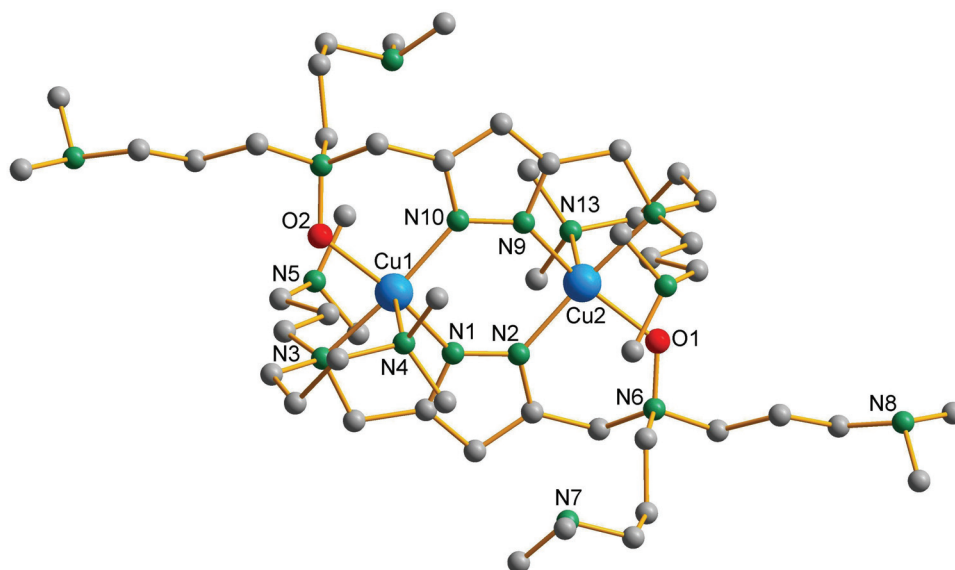
**Figure 20.** General structure of the *N*-oxide type of complexes **3**, **3a** and **3b**. **3a** contains a proton not localized in the X-ray structure.

The common feature shared between the different molecular structures found for **3-3b** is a drastic modification of the ligand, consisting of oxidation of one tertiary, bridgehead amine of

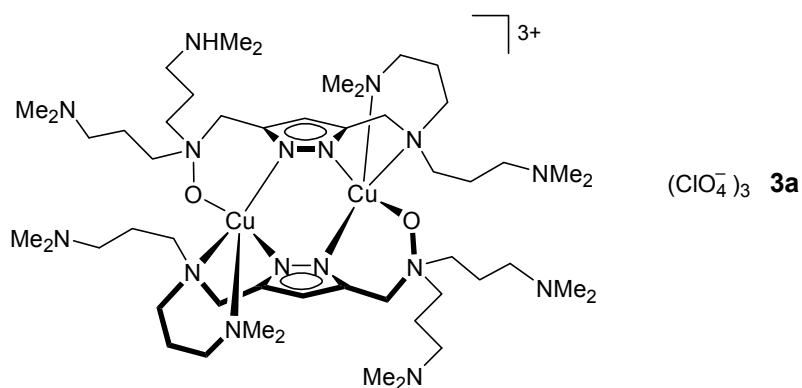
the side arms, yielding the *N*-oxide functionality. This oxidation results in the formation of an unexpected and unusual bonding motif, wherein the two copper atoms are coordinated to the oxygen atom of the oxidized amine (*N*-oxide) fragment.

The only difference observed in the molecular structures between **3** and **3a** (the molecular structure of the latter is depicted in Figure 21) is the protonated state of one of the uncoordinated *N*-dimethyl-aminopropyl groups in **3a**, which increases the amount of perchlorate counter anions and induces the asymmetric structure (i.e. the copper atoms are non-equivalent). The protonation also results in a distortion of the coordination geometry of the copper ions. Thus, whereas the crystallographically equivalent copper ions in **3** have almost perfect tetragonal geometry ( $\tau = 0.03$ ), in complex **3a** the  $\tau$ -value increases to around 0.20 for the second copper atom (Table 4).

In both complexes the copper atoms are ligated by three nitrogens from one of the (partly non-oxidized) coordinated ligands and the two remaining coordination positions are taken up by a nitrogen from the pyrazole unit and the oxygen atom of the *N*-O fragment stemming from the second coordinated ligand.



**Figure 21.** Molecular structure of the cation of **3a**.



**Figure 22.** Structure of the *N*-oxide type of complex **3a** which contains a proton not localized in the X-ray structure.

**Table 3.** Selected atom distances (Å) and angles (°) for complex **3a**.

Distances			
Cu(1)-O(2)	1.937(7)	Cu(2)-O(1)	1.967(6)
Cu(1)-N(1)	1.962(9)	Cu(2)-N(11)	2.125(11)
Cu(1)-N(10)	1.978(11)	Cu(2)-N(13)	2.359(8)
Cu(1)-N(3)	2.074(12)	Cu(1)···Cu(2)	3.931(2)
Cu(1)-N(4)	2.359(9)	N(6)-O(1)	1.386(12)
Cu(2)-N(9)	1.946(9)	N(14)-O(2)	1.434(12)
Cu(2)-N(2)	1.954(11)		
Angles			
O(2)-Cu(1)-N(1)	162.6(3)	N(9)-Cu(2)-N(2)	97.8(4)
O(2)-Cu(1)-N(10)	91.9(3)	N(9)-Cu(2)-O(1)	161.0(3)
N(1)-Cu(1)-N(10)	97.9(4)	N(2)-Cu(2)-O(1)	92.4(3)
O(2)-Cu(1)-N(3)	85.0(3)	N(9)-Cu(2)-N(11)	82.1(4)
N(1)-Cu(1)-N(3)	82.6(4)	N(2)-Cu(2)-N(11)	171.2(4)
N(10)-Cu(1)-N(3)	168.9(4)	O(1)-Cu(2)-N(11)	85.4(3)
O(2)-Cu(1)-N(4)	96.8(3)	N(9)-Cu(2)-N(13)	94.9(3)
N(1)-Cu(1)-N(4)	96.1(3)	N(2)-Cu(2)-N(13)	97.3(4)
N(10)-Cu(1)-N(4)	97.5(3)	O(1)-Cu(2)-N(13)	99.7(3)
N(3)-Cu(1)-N(4)	93.4(4)	N(11)-Cu(2)-N(13)	91.4(4)

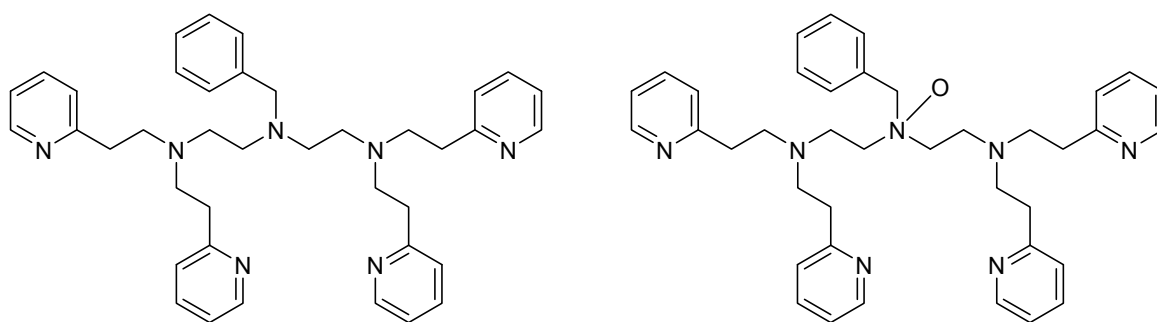
**Table 4.**  $\tau$ -value and the Cu...Cu distance (Å) for complexes **3**, **3a** and **3b**.

Complex	$\tau(\text{Cu1/Cu2})$	$d(\text{Cu}\cdots\text{Cu})$
<b>3</b>	0.03	3.92
<b>3a</b>	0.10/0.17	3.93
<b>3b</b>	0.06	3.92

The N-O bond distances in the *N*-oxide copper(II) complexes are in the range from 1.41 to 1.43 Å what is close to identical to those reported in the literature by Comba and co-workers.<sup>109</sup>

It has to be mentioned that the *N*-oxide complex is *only* formed during the long crystallization process (of up to one month). No *N*-oxide containing species were observed by means of ESI mass spectrometry in the reaction mixture before crystallization, while after crystallization the *N*-oxide species was clearly detected. Thus, for complex **3a**, where one of the side arms is protonated, signals at 1189, 1289 and 1389 *m/z* were observed, which confirm the presence of the species  $[\text{Cu}_2\text{L}^2_2\text{O}_2(\text{ClO}_4)]^+$ ,  $[\text{Cu}_2\text{L}^2_2\text{O}_2(\text{ClO}_4)_2]^+$  and  $[\text{Cu}_2\text{L}^2_2\text{O}_2(\text{ClO}_4)_3]^+$ , respectively, in MeOH solution.

Although very rarely observed, it was shown by Karlin and co-workers that such copper-dioxygen mediated amine to *N*-oxide transformation can be performed by a dicopper(I) complex based on a ligand with a built-in *N*-benzyl moiety (Figure 23).<sup>110</sup>



**Figure 23.** Ligand with a built-in *N*-benzylic active moiety used by Karlin and isolated *N*-oxide fragment, after decomposition of  $\text{Cu}_2^{\text{II}}\text{-O}_2$  species.

After reaction of the dinuclear copper(I) species with  $\text{O}_2$  at 0 °C to yield a dicopper(II)-peroxo species, oxidation of the benzylic nitrogen and formation of the corresponding *N*-oxide

fragment had occurred, as a result of the decomposition of the peroxo species. Moreover, a labeling experiment using  $^{18}\text{O}_2$  showed that the oxygen atom was derived from molecular dioxygen, which proved that the oxygen atom-transfer reaction was initiated by formation of the  $\text{Cu}_2^{\text{II}}\text{-O}_2$  active species.

The proposed oxidation pathway by Karlin, however, can not be applied to the present amine to *N*-oxide transformation reaction since the copper ions in the initially prepared dicopper complex are already in the oxidation state +2.

In order to determine the origin of the oxygen responsible for the oxidation of the tertiary amine, a copper salt with a non-oxygen containing counter-anion, such as  $\text{Cu}(\text{BF}_4)_2 \cdot 4\text{H}_2\text{O}$ , was used for the complex synthesis instead of the previously applied perchlorate salt. However, after approximately the same crystallization time, single crystals were again obtained and when the molecular structure was elucidated by X-ray crystallography, formation of dinuclear copper *N*-oxide complex **3b** was unequivocally proven. **3b** represents a close analogue of complex **3**, where two copper atoms are crystallographically equivalent, with almost perfect tetragonal geometry, and a  $d(\text{Cu}\cdots\text{Cu})$  equal to 3.92 Å.

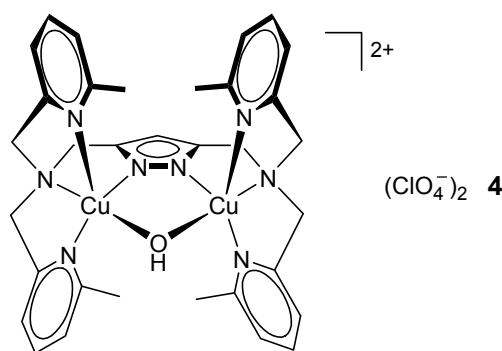
Unfortunately, complete exclusion of all potential sources of oxygen was not possible with the experimental methods described here, since in the first place crystallization was only induced when performed in the presence of ether, whereas within the second synthetic route, the applied copper tetrafluoroborate salt was hydrated.

The possible influence of aerial dioxygen was firstly elucidated by bubbling pure oxygen gas through a solution of **HL**<sup>2</sup> with two equivalents of KO<sup>*t*</sup>Bu and two equivalents of  $\text{Cu}(\text{ClO}_4)_2 \cdot 6\text{H}_2\text{O}$ , and monitoring the UV/vis spectrum of the solution. No spectroscopic changes in the *d-d* band region (618 nm) were observed during this procedure, indicating that formation of the *N*-oxide species is very slow, and only occurs during the crystallization period. To avoid the presence of any aerial dioxygen, reaction of **HL**<sup>2</sup> with two equivalents of KO<sup>*t*</sup>Bu and two equivalents  $\text{Cu}(\text{ClO}_4)_2 \cdot 6\text{H}_2\text{O}$  was performed under anaerobic conditions in a glove box. The crystalline compound formed under these conditions was analyzed by means of ESI-MS spectrometry. The only signal found in the ESI spectrum at 591 *m/z* corresponds to a  $[\text{Cu}_2\text{L}^2]^+$  species, which is typically present in the reaction mixture before crystallization. Unfortunately, no single crystals were obtained to structurally prove the role of aerial dioxygen. On the basis of these observations, it can be concluded that no formation of *N*-

oxide species takes place under anaerobic conditions, which implies that dioxygen is most likely responsible for the slow copper-dioxygen mediated amine to *N*-oxide transformation.

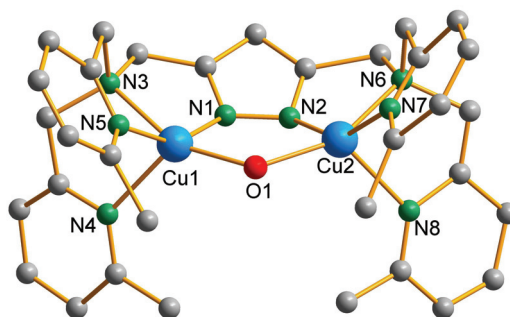
### 5.3 Characterization of a dicopper complex with the new ligand **HL**<sup>3</sup>

The coordination chemistry of a new pyrazole-based ligand with bis[(6-methyl-2-pyridyl)methyl]amine side arms towards copper(II) was studied. Reaction of **HL**<sup>3</sup> with two equivalents of KO<sup>*t*</sup>Bu in MeOH/MeCN, followed by addition of two equivalents of Cu(ClO<sub>4</sub>)<sub>2</sub>·6H<sub>2</sub>O to the reaction mixture led to the formation of dinuclear copper(II) complex [Cu<sub>2</sub>L<sup>3</sup>(OH)](ClO<sub>4</sub>)<sub>2</sub> **4** (Figure 24).



**Figure 24.** Schematic representation of complex **4**.

The single crystals isolated after diffusion of Et<sub>2</sub>O into CH<sub>2</sub>Cl<sub>2</sub>/MeCN proved of insufficient quality for a high-resolution X-ray crystallographic analysis and therefore a complete dataset could not be obtained. However, the measurements did allow for a rough estimation of intramolecular distances between atoms with high electron density (like Cu, N and O), so that key information can still be discussed for this structure. The corresponding approximation of the molecular structure of **4** is shown in Figure 25.



**Figure 25.** Molecular structure of the cation of **4**.

Two copper(II) ions are nested within their respective coordination pockets and are spanned by the bridging pyrazolate moiety. Both metal ions are five-coordinate with a slightly distorted trigonal bipyramidal geometry ( $\tau = 0.86$ ), in accordance with the solution UV/vis data, where a  $d-d$  transition band appeared at  $\lambda_{\text{max}} = 816$  nm. The coordination sphere of both copper atoms consists of four N-donors from the pyrazolate ligand (one of the central pyrazole core and three from the side arm fragments) and a fifth bridgehead O atom, presumably originating from a  $\mu\text{-OH}$  ligand, located within the bimetallic pocket. The approximate distance between the two copper atoms is *ca* 3.50 Å. This motif does not closely resemble the structural situation observed for some related  $\text{Ni}^{2+}$  and  $\text{Zn}^{2+}$  complexes of a pyrazole-derived ligand with bis(pyridyl methyl)amine side arms – without the methyl group in the 6-position – where the intramolecular metal-metal separation is larger than found for the two Cu ions in **4**. Thus, in these dinuclear nickel(II) and dizinc(II) complexes, because of the short methylene-spacers in the side arms of the ligand, the metal ions are bridged by an acetate ligand, resulting in metal-metal separations of *ca* 4.20 Å and 3.97 Å, respectively.<sup>111,112</sup> At the same time, a dicopper(II) complex derived from the ligand with short bis(pyridyl methyl)amine side arms showed a long intramolecular metal-metal separation of 4.30 Å where within the resulting bimetallic pocket, the F atom and a methanol molecule form a strong hydrogen bond.<sup>113</sup> The only reasonable signal, in terms of matching pattern, found in the ESI spectrum (MeCN solution), observed at 829  $m/z$ , presumably corresponds to  $[\text{Cu}_2\text{L}^3(\text{OH})(\text{MeCN})\text{ClO}_4]^+$ .

## 5.4 Copper complexes of the new bioinspired ligand **HL**<sup>4</sup>

With the aim of further advancing the emulation of biological donor environments in pyrazole-based ligands, the new ligand **HL**<sup>4</sup> that has binding compartments composed of imidazolyl groups has been prepared. To gain knowledge about the type of complexes with **HL**<sup>4</sup>, its coordination behaviour towards copper is studied. The complexation equilibria and the stability of copper(II) complexes of **HL**<sup>4</sup> in solution as well as crystallographic and magnetic studies of the different complexes in the solid state are discussed.

### 5.4.1. Elucidation of species distribution at different pH values

The first studies were focussed on the elucidation of species distribution. Potentiometric titrations were carried out in order to determine the  $pK_a$  values of the new ligand and to probe its copper(II) coordination chemistry. These studies were performed by Eva Anna Enyedy and Dr. Etelka Farkas at the University of Debrecen, Hungary.

*Ligand protonation constants:* Titrations were performed starting at acidic pH using a potassium hydroxide titrant. From the titration curves the deprotonation steps can be derived (see experimental part Figure 94 and Table 5). The processes occurring in the measurable pH-range between ca. pH 4 and 9 belong to the dissociation of one proton per protonated imidazole moiety. The difference between the sequential dissociation constants is higher (ca. 0.8 log units) than expected for statistical reason, which suggests some interaction (most probably through space) between the individual protonation sites. According to the experimental results, protonation of the pyrazole occurs only below pH 2 and the stability constant was not determined for this process.

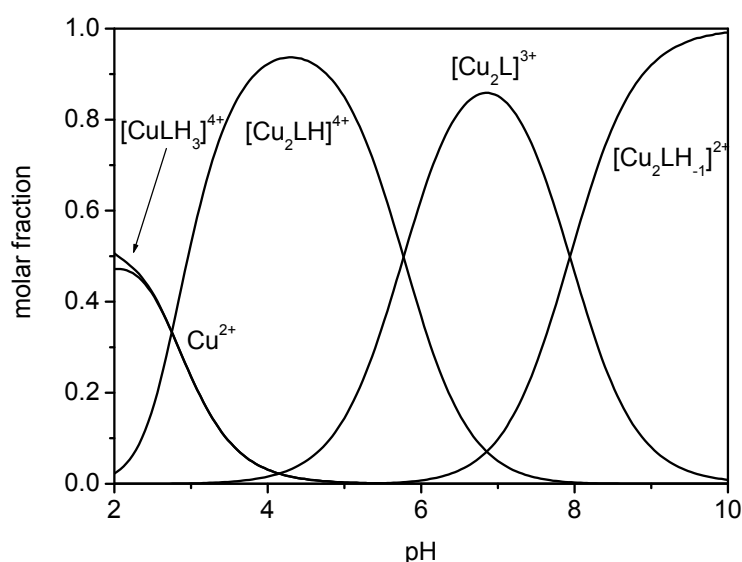


**Table 5.** Overall protonation constants ( $\log \beta$ ) and sequential dissociation constants ( $pK_a$ ) of the ligand **HL**<sup>4</sup> at 25°C;  $I = 0.2$  M (KCl)<sup>a</sup>, for the sake of simplification all species in solution will be further described using **HL** instead of **HL**<sup>4</sup>.

	$[\text{LH}_5]^{4+}$	$[\text{LH}_4]^{3+}$	$[\text{LH}_3]^{2+}$	$[\text{LH}_2]^+$
$\log \beta$	26.06(1)	20.78(1)	14.71(2)	7.77(1)
$pK_a$	5.28	6.07	6.94	7.77

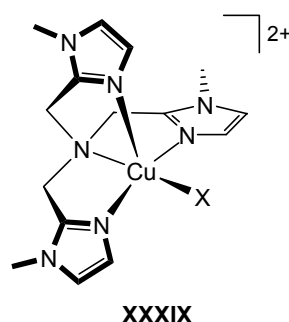
<sup>a</sup> Standard deviations are given in parenthesis

*Species distribution of copper complexes:* Titrations of **HL**<sup>4</sup> in the presence of various equivalents of Cu<sup>II</sup> were analyzed in batch calculations in which all titration curves are fitted at the same time with one model (see experimental part Figure 95 and Table 6). Evaluation of the titration curves shows that the Cu<sup>II</sup>-binding capabilities of **HL**<sup>4</sup> are high. Although free Cu<sup>II</sup> ions and the mononuclear species  $[\text{CuLH}_3]^{4+}$  are observable up to  $\sim$  pH 4, the dinuclear species  $[\text{Cu}_2\text{LH}]^{4+}$  is already formed at around pH 2 and becomes almost the sole species around pH 4 (Figure 26). This dinuclear complex, which is present at rather acidic conditions, presumably has a protonated (i.e. non-bridging) pyrazole unit.  $[\text{Cu}_2\text{L}]^{3+}$  starts to form above pH 4 and exists in solution up to pH 10.



**Figure 26.** Concentration distribution of the species formed between **HL**<sup>4</sup> and Cu<sup>II</sup> at 1:2 ligand to metal ratio.  $C_{\text{HL}}^4 = 1.5 \cdot 10^{-3}$  M.

It is the dominant species at pH 7 and most likely is a pyrazolato-bridged complex, where the heterocycle is deprotonated. A further deprotonation step leads to dinuclear  $[\text{Cu}_2\text{LH}_1]^{2+}$  which is the major species under more basic conditions. The calculated  $\text{p}K_a$  of 7.94 for  $[\text{Cu}_2\text{L}]^{3+}$  represents the acidity of a metal-bound water to give  $[\text{Cu}_2\text{LH}_1]^{2+}$ , i.e. the latter species is better described as  $[\text{Cu}_2\text{L}(\text{OH})]^{2+}$ . The  $\text{Zn}^{2+}$  complex of tris(2-(1-imidazolyl)methyl)amine shows a  $\text{p}K_a$  of 8.72 for a metal-bound water,<sup>114</sup> and the value for the corresponding mononuclear  $\text{Cu}^{\text{II}}$  system (Figure 27, with  $\text{X} = \text{H}_2\text{O}$ ) should be even higher.<sup>115</sup>



**Figure 27.** Schematic representation of the mononuclear copper complex with tris(2-(1-imidazolyl)methyl)amine and  $\text{X} = \text{H}_2\text{O}$ .

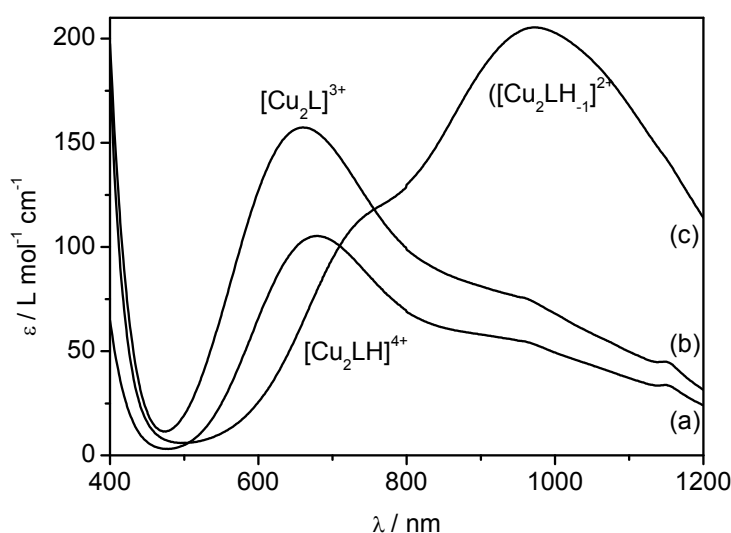
Hence, there is a clear increase in water acidity due to the bimetallic arrangement in  $[\text{Cu}_2\text{L}]^{3+}$ , and its relatively low  $\text{p}K_a$  value suggests a bridging position of the water or incorporation of the resulting hydroxide in a strongly hydrogen-bonded  $\text{O}_2\text{H}_3$  moiety within the bimetallic pocket. However, acidification of the Cu-bound water is less pronounced than in related pyrazolate-bridged systems with aliphatic N-donor side arms attached to the heterocycle.<sup>16</sup>

**Table 6.** Overall stability constants ( $\log \beta$ ) and some dissociation constants ( $\text{p}K_a$ ) for the complexes formed with  $\text{Cu}^{\text{II}}$  at  $25^\circ\text{C}$ ;  $I = 0.2 \text{ M}$  ( $\text{KCl}$ ).<sup>a</sup>

	$[\text{CuLH}_3]^{4+}$	$[\text{Cu}_2\text{LH}]^{4+}$	$[\text{Cu}_2\text{L}]^{3+}$	$[\text{Cu}_2\text{LH}_1]^{2+}$
$\log \beta$	26.36(4)	23.56(3)	17.79(8)	9.85(9)
$\text{p}K_a$		5.77	7.94	

<sup>a</sup> Standard deviations are given in parenthesis

UV/vis spectra were recorded for aqueous solutions containing **HL**<sup>4</sup> and two equivalents of Cu(NO<sub>3</sub>)<sub>2</sub> at pH 4.66, 6.55, and 9.40 in order to further characterize the species [Cu<sub>2</sub>LH]<sup>4+</sup>, [Cu<sub>2</sub>L]<sup>3+</sup>, and [Cu<sub>2</sub>LH<sub>1</sub>]<sup>2+</sup> present under those conditions (Figure 28). The spectral features of the [Cu<sub>2</sub>LH<sub>1</sub>]<sup>2+</sup> species at pH 9.40 indicate a trigonal bipyramidal coordination geometry for both copper ions ( $\lambda_{\text{max}} = 972$  nm), while the species [Cu<sub>2</sub>LH]<sup>4+</sup> and [Cu<sub>2</sub>L]<sup>3+</sup>, which are present at pH 4.66 and 6.55, respectively, have absorption maxima typical for copper in a square pyramidal environment ( $\lambda_{\text{max}} \approx 670$  nm; Table 7).<sup>116</sup>



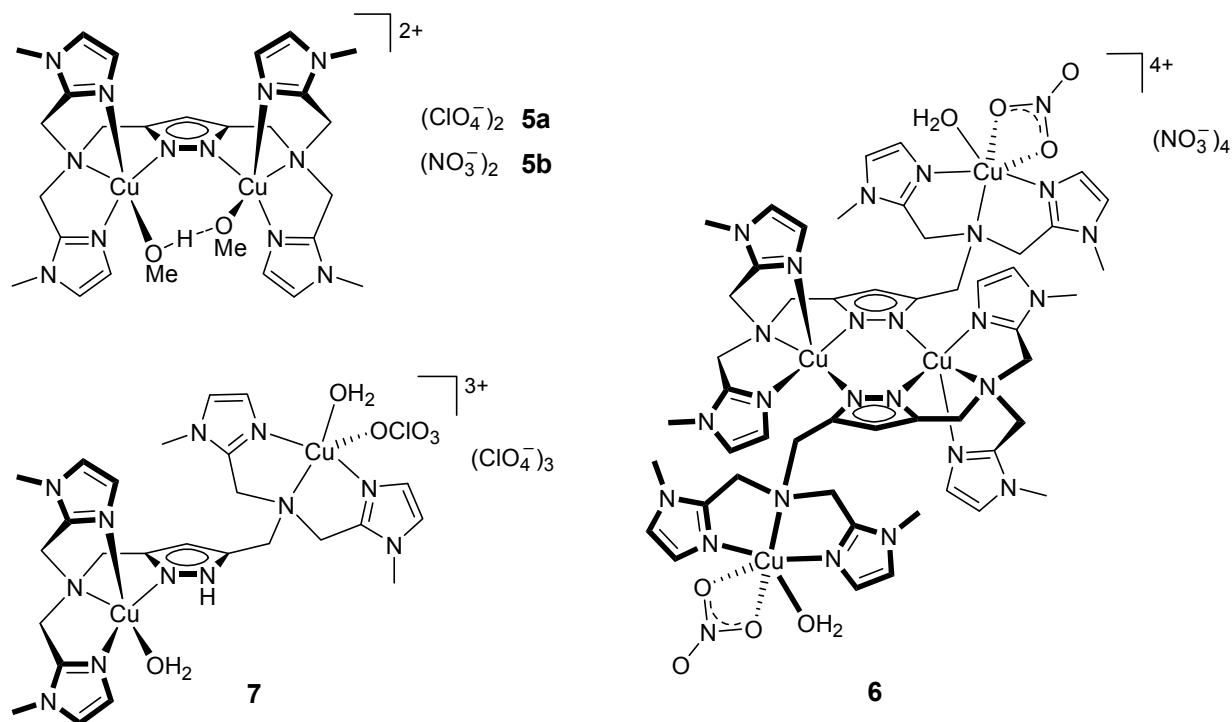
**Figure 28.** UV/vis spectra of **HL**<sup>4</sup> with 2 equivalents of Cu(NO<sub>3</sub>)<sub>2</sub> in H<sub>2</sub>O at pH 4.66 (a), 6.55 (b) and 9.40 (c).

**Table 7.** UV/vis data of **HL**<sup>4</sup> with 2 equivalents of Cu(NO<sub>3</sub>)<sub>2</sub> in aqueous solution at different pH and of individual complexes **5a**, **6**, and **7** in MeOH/MeCN (5:2) and in the solid state (diffuse reflectance);  $\lambda$  [nm] ( $\epsilon$  [L mol<sup>-1</sup>cm<sup>-1</sup>]).

species	H <sub>2</sub> O	complex	MeOH/MeCN (5:2)	Diffuse reflectance
[Cu <sub>2</sub> LH <sub>1</sub> ] <sup>2+</sup>	741 (110), 972 (204)	<b>5a</b>	730sh (135) 962 (269)	952
[Cu <sub>2</sub> L] <sup>3+</sup>	663 (157)	<b>6</b>	689 (281), 923 (272)	705, 918
[Cu <sub>2</sub> LH] <sup>4+</sup>	676 (105)	<b>7</b>	677 (96)	689

### 5.4.2 Structural characterization of complexes

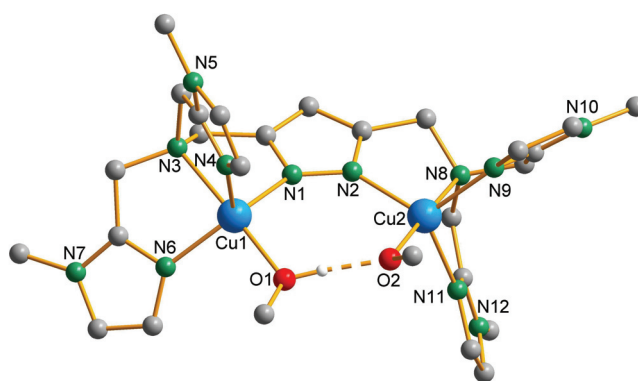
Three distinctly different copper(II) complexes **5a** - **7** of the pyrazole-based ligand **HL**<sup>4</sup> could be isolated after work-up at appropriate pH, reflecting the protonation state of the three different species  $[\text{Cu}_2\text{LH}]^{4+}$ ,  $[\text{Cu}_2\text{L}]^{3+}$ , and  $[\text{Cu}_2\text{LH}_1]^{2+}$  (Figure 29). Single crystals of **5a**, **5b**, **6**, and **7** were obtained and their molecular structures elucidated by X-ray crystallography.



**Figure 29.** Schematic representation of copper complexes of ligand **HL**<sup>4</sup> isolated under different pH conditions.

Addition of two equivalents of  $\text{Cu}(\text{NO}_3)_2$  to a  $\text{MeOH}/\text{H}_2\text{O}$  solution containing **HL**<sup>4</sup> and one equivalent of base ( $\text{KO}t\text{Bu}$ ) produced a green-blue reaction mixture that was subjected to ion-exchange chromatography using a SP-Sephadex C25 column. The first light-blue fraction was obtained after washing the column with a 0.2 M solution of  $\text{NaNO}_3$ . Interpretation of mass spectrometric signals ( $330\ m/z$   $[\text{C}_{10}\text{H}_{15}\text{N}_5\text{CuNO}_3]^+$ ,  $268\ m/z$   $[\text{C}_{10}\text{H}_{15}\text{N}_5\text{Cu}]^+$ ) led to the conclusion that the compound obtained is a mononuclear copper complex, derived from the incompletely reacted *N,N*-bis[2-(1-methylimidazolyl)methyl]amine side-arm during ligand synthesis, with an isolated yield of 4.5%.

Washing of the column with a 0.4 M solution of  $\text{NaNO}_3$  yielded the main blue aqueous fraction, which showed a characteristic maximum in the UV/vis spectrum at 656 nm (shifted in comparison to 663 nm due to the presence of  $\text{NaNO}_3$  in solution). By adjusting the pH of this solution to 9 and addition of  $\text{NaClO}_4$  a green powder precipitated that was crystallized from MeCN/MeOH/Et<sub>2</sub>O to yield complex **5a**. The corresponding nitrate salt **5b** could be prepared directly via the addition of two equivalents of base ( $\text{KO}^t\text{Bu}$ ) and two equivalents of  $\text{Cu}(\text{NO}_3)_2$  to a solution of **HL**<sup>4</sup>, followed by crystallization from MeCN/MeOH/Et<sub>2</sub>O. Molecular structures of the cations of **5a** and **5b** are very similar, and the molecular structure of the former is shown in Figure 30.



**Figure 30.** Molecular structure of the cation of **5a**.

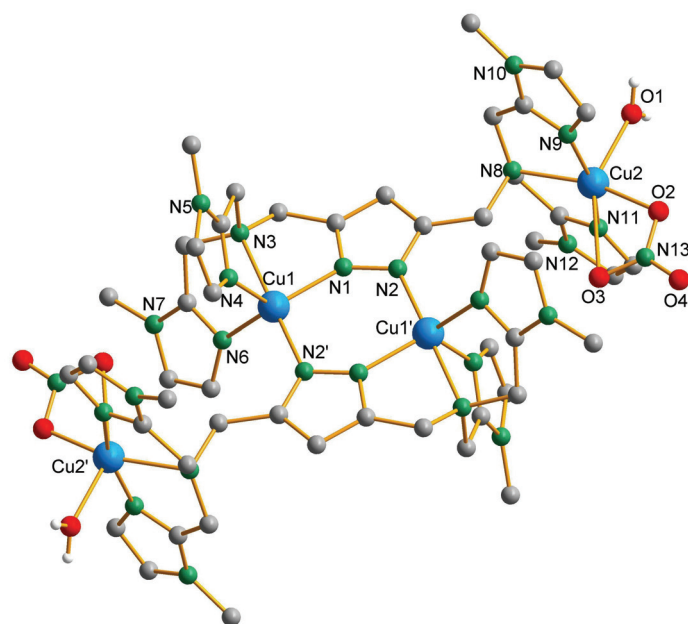
**Table 8.** Selected atom distances (Å) and angles (°) for complex **5a**.

Distances			
Cu1–O1	1.915(2)	Cu2–N2	2.007(3)
Cu1–N1	2.030(3)	Cu2–N8	2.111(3)
Cu1–N3	2.129(3)	Cu2–N9	2.085(3)
Cu1–N4	2.080(3)	Cu2–N11	2.087(3)
Cu1–N6	2.013(3)	Cu1···Cu2	4.3405(6)
Cu2–O2	1.929(3)	O1–O2	2.407(4)
Angles			
O1–Cu1–N1	96.4(1)	O2–Cu2–N8	174.8(1)
O1–Cu1–N3	177.3(1)	O2–Cu2–N9	104.2(1)
O1–Cu1–N4	101.5(1)	O2–Cu2–N11	96.9(1)
O1–Cu1–N6	96.4(1)	N2–Cu2–N8	80.3(1)

N1–Cu1–N3	80.8(1)	N2–Cu2–N9	118.5(1)
N1–Cu1–N4	109.1(1)	N2–Cu2–N11	121.4(1)
N1–Cu1–N6	124.2(1)	N8–Cu2–N9	80.1(1)
N3–Cu1–N4	81.0(1)	N8–Cu2–N11	78.8(1)
N3–Cu1–N6	81.4(1)	N9–Cu2–N11	110.7(1)
N4–Cu1–N6	119.47(1)	O1–H1–O2	173(5)
O2–Cu2–N2	99.8(1)		

The two copper ions in **5a** reside within the adjacent {N<sub>4</sub>} ligand compartments of **L**<sup>4</sup> and are bridged by the pyrazolate ring, as anticipated. Both metal ions are five-coordinate with a slightly distorted trigonal bipyramidal geometry ( $\tau = 0.88$ ), in accordance with the solution UV/vis data for [Cu<sub>2</sub>LH<sub>1</sub>]<sup>2+</sup>. The pyrazolate-N and the two imidazole-N atoms constitute the equatorial planes, while axial positions are occupied by the tertiary N atoms of the ligand backbone and by the O atoms of a MeO⋯HOMe moiety located within the bimetallic pocket. This motif closely resembles the situation observed for some Ni<sup>2+</sup>, Cu<sup>2+</sup> and Zn<sup>2+</sup> complexes of related pyrazole-derived ligands with pyridyl or aliphatic N-donor chelate substituents, where it was shown that the accessible range of metal-metal separations is determined by the length of the side arms appended to the pyrazole.<sup>15,16,81b,117</sup> The rather short side arms of **HL**<sup>4</sup> give five-membered chelate rings and thus enforce rather large Cu⋯Cu distances that prevent a small hydroxide or methoxide ligand from spanning the two metal ions. Incorporation of an additional MeOH solvent molecule then furnishes the MeO⋯HOMe bridging unit observed for **5a** ( $d(\text{Cu}\cdots\text{Cu}) = 4.34 \text{ \AA}$ ). Such units have previously been shown to undergo rapid ligand exchange with e.g. water.<sup>117d</sup> Therefore the species [Cu<sub>2</sub>LH<sub>1</sub>]<sup>2+</sup> that is present in aqueous solution at high pH most certainly contains an analogous HO⋯HOH bridge and should thus best be formulated as [Cu<sub>2</sub>L(O<sub>2</sub>H<sub>3</sub>)]<sup>2+</sup>.

A tetranuclear copper complex **6** could be isolated directly from the blue aqueous solution obtained after ion-exchange chromatography (see above). The protonation state of **6** relates it to the species [Cu<sub>2</sub>L]<sup>3+</sup> that predominates in solution around neutral pH, i.e. the pyrazole is deprotonated but no additional hydroxide is present. The absorption maximum in the UV/vis spectrum at 656 nm (shifted in comparison to 663 nm due to the presence of NaNO<sub>3</sub> in solution) confirms the close relation between **6** and [Cu<sub>2</sub>L]<sup>3+</sup>. The molecular structure of the cation of **6** is shown in Figure 31.



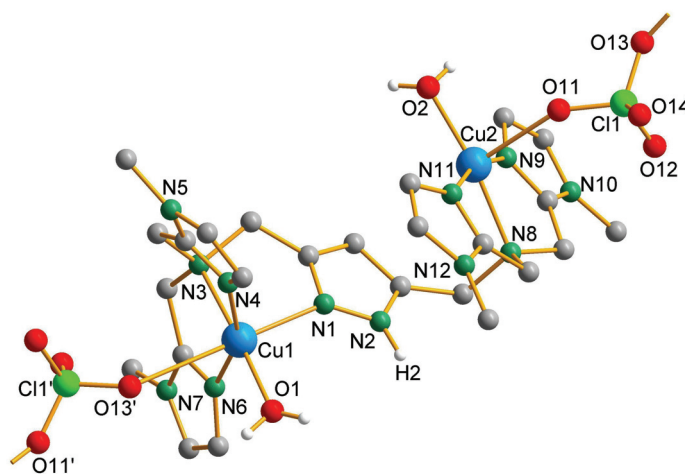
**Figure 31.** Molecular structure of the cation of **6**.

**Table 9.** Selected atom distances (Å) and angles (°) for complex **6**.

Distances			
Cu1–N1	2.020(2)	Cu2–O2	1.996(2)
Cu1–N2'	1.949(2)	Cu2–O3	2.651(2)
Cu1–N3	2.117(2)	Cu2–N8	2.111(2)
Cu1–N4	2.106(2)	Cu2–N9	1.941(2)
Cu1–N6	2.074(2)	Cu2–N11	1.952(2)
Cu2–O1	2.222(2)	Cu1...Cu1'	3.8674(6)
Angles			
N1–Cu1–N2'	100.72(8)	O1–Cu2–O2	100.31(8)
N1–Cu1–N3	79.93(8)	O1–Cu2–N8	96.23(8)
N1–Cu1–N4	119.64(8)	O1–Cu2–N9	92.41(9)
N1–Cu1–N6	119.71(8)	O1–Cu2–N11	88.62(8)
N2'–Cu1–N3	174.15(8)	O2–Cu2–N8	163.40(7)
N2'–Cu1–N4	95.70(8)	O2–Cu2–N9	95.77(8)
N2'–Cu1–N6	103.90(8)	O2–Cu2–N11	99.77(8)
N3–Cu1–N4	79.04(8)	N8–Cu2–N9	82.03(8)
N3–Cu1–N6	80.59(8)	N8–Cu2–N11	81.97(8)
N4–Cu1–N6	111.51(8)	N9–Cu2–N11	163.98(9)

Unexpectedly, X-ray crystallographic analysis of **6** revealed a dimeric arrangement of two  $\{\text{Cu}_2\text{L}\}$  subunits that features a central bis(pyrazolato) bridged dicopper(II) core. These two copper(II) ions have an almost perfect trigonal bipyramidal  $\{\text{N}_5\}$  coordination environment ( $\tau = 0.91$ ), where one of the apical Cu-N bonds is slightly elongated at  $d(\text{Cu1-N3}) = 2.12 \text{ \AA}$ . The remaining ligand side arms are dangling and host the other two copper ions, whose coordination spheres consist of three side arm N atoms and one water molecule. An overall square pyramidal geometry of those outer metal ions is completed by an O-bound nitrate, but taking into account the additional weak interaction of the metal with a second O atom of the nitrate ( $\text{Cu2-O3} = 2.65 \text{ \AA}$ ) increases the coordination number to six and extends the coordination sphere to a strongly Jahn-Teller-distorted octahedron.

Acidification of the blue solution of **6** obtained after ion-exchange chromatography (see above) to  $\sim \text{pH } 4$  by the addition of aqueous  $\text{HClO}_4$  yielded crystalline material of complex **7** that relates to the solution species  $[\text{Cu}_2\text{LH}]^{4+}$ . As was already concluded from the titration data, **7** has a non-deprotonated pyrazole. The molecular structure of its cation is shown in Figure 32.



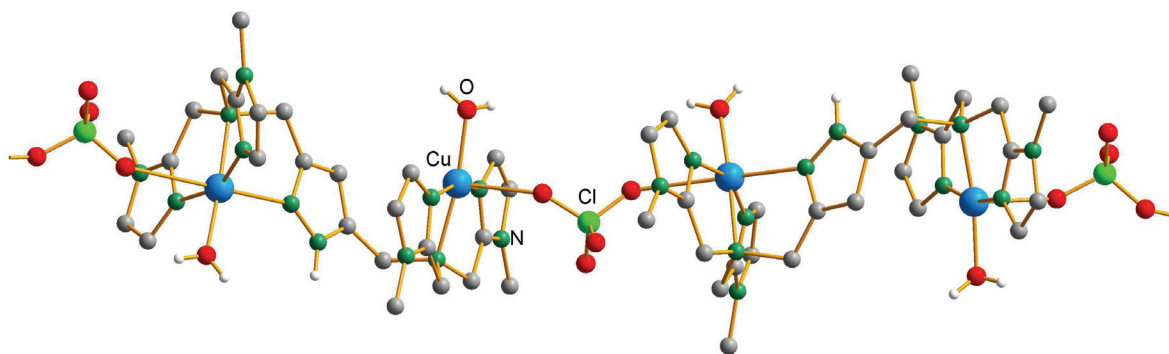
**Figure 32.** Molecular structure of the cation of **7**.



**Table 10.** Selected atom distances (Å) and angles (°) for complex **7**.

Distances			
Cu1–O1	1.990(3)	Cu2–O2	1.955(3)
Cu1–O13	2.761(4)	Cu2–O11	2.398(4)
Cu1–N1	2.244(4)	Cu2–N8	2.076(3)
Cu1–N3	2.146(3)	Cu2–N9	1.945(4)
Cu1–N4	1.946(4)	Cu2–N11	1.957(4)
Cu1–N6	1.945(4)	Cu1···Cu2	6.7645(8)
Angles			
O1–Cu1–N1	102.1(1)	O2–Cu2–O11	86.6(2)
O1–Cu1–N3	177.1(2)	O2–Cu2–N8	172.0(2)
O1–Cu1–N4	98.7(2)	O2–Cu2–N9	99.6(2)
O1–Cu1–N6	96.0(2)	O2–Cu2–N11	96.0(2)
N1–Cu1–N3	80.7(1)	O11–Cu2–N8	101.1(2)
N1–Cu1–N4	103.2(2)	O11–Cu2–N9	93.4(2)
N1–Cu1–N6	92.4(2)	O11–Cu2–N11	88.8(2)
N3–Cu1–N4	80.9(1)	N8–Cu2–N9	81.9(2)
N3–Cu1–N6	83.4(1)	N8–Cu2–N11	82.5(2)
N4–Cu1–N6	155.8(2)	N9–Cu2–N11	164.4(2)

Complex **7** can be described as one-half of **6**, since protonation of the pyrazolate splits the central bis(pyrazolato) dicopper core and leaves only one of the copper ions coordinated to the non-bridging pyrazole fragment. Cu1 is found in an octahedral coordination environment, ligated equatorially by three N-donors from the side arm of **HL**<sup>4</sup> and an O atom from a water molecule. Axial positions are occupied by the distant N-donor from pyrazole (2.24 Å) and a perchlorate counter-anion at an even greater distance (2.76 Å), typical for a Jahn-Teller elongated situation. The second metal is again nested in the dangling chelate arm compartment and is five-coordinate ( $\tau = 0.13$ ) with an additional water in the equatorial and a perchlorate-O in the axial position. A three-dimensional network is built up by H-bonds between coordinated water molecules, perchlorate anions and the NH-unit of the pyrazole. A one-dimensional chain is represented in Figure 33, where the dicopper pyrazole bridged compartments are connected by a  $\mu$ -bidentate perchlorate bridge via two copper ions from the different units (Cu1–O13' (2.76 Å), Cu2–O11 (2.39 Å)).



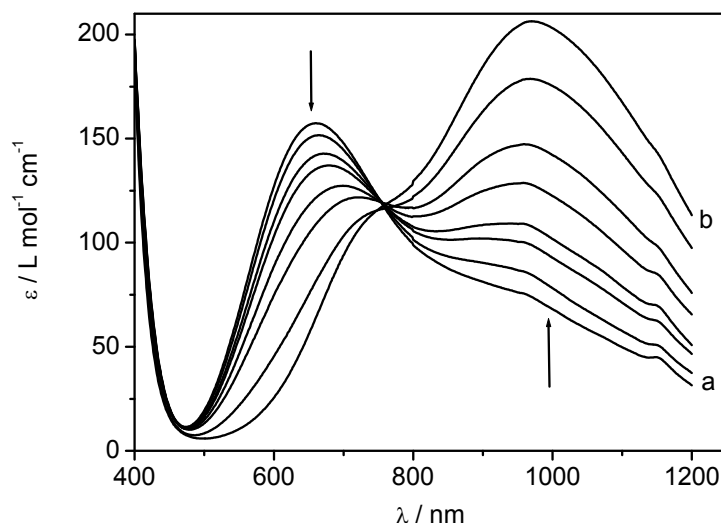
**Figure 33.** Schematic representation of the one-dimensional chain of **7**.

### 5.4.3 Spectroscopic properties of the complexes and equilibria in solution

UV/vis spectra of the three complexes **5a**, **6**, and **7** have been recorded in MeOH/MeCN (5:2) solution as well as in the solid state (diffuse reflectance). Table 7 (see page 52) compares findings for the ligand-field bands for the species in aqueous solution at different pH as well as for the isolated compounds. Absorption maxima in the diffuse reflectance spectra are in accordance with the coordination geometries observed crystallographically, i.e. trigonal bipyramidal for **5a** (broad *d-d* absorption at  $\sim 950$  nm), tetragonal for **7** (weak ligand field band at  $\sim 690$  nm) and the presence of both signatures in the case of **6** ( $\lambda_{\text{max}}$  is also affected by the type of donor atoms). Similar spectra were observed for each complex in MeOH/MeCN solution, implying that no major structural changes occur upon redissolving the crystalline solids. The same is true for species in aqueous solution at the respective pH except for **6**. In the latter system the broad *d-d* absorption at  $\sim 920$  nm seen in the diffuse reflectance spectra and in MeOH/MeCN solution is strongly diminished in aqueous solution around neutral pH. Since a trigonal bipyramidal situation (characterized by the *d-d* band at  $\sim 920$  nm) is observed for the central bis(pyrazolato) bridged dicopper(II) core in **6**, it is reasonable to assume that in aqueous solution the dimeric aggregate largely breaks apart to give bimetallic species  $[\text{Cu}_2\text{L}(\text{H}_2\text{O})_x]^{3+}$ . It should be noted that pH-potentiometry cannot differentiate between bimetallic  $[\text{Cu}_2\text{L}]^{3+}$  and its dimeric aggregate  $[(\text{Cu}_2\text{L})_2]^{6+}$ .

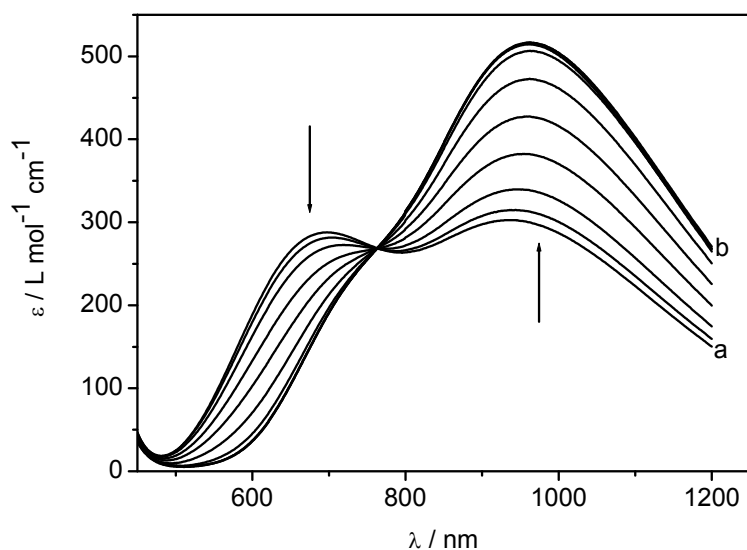
Equilibria in solution between the three different complexes was monitored by UV/vis spectroscopy upon titration with a base, starting at pH 4.66. Dicopper complex **7** was dissolved in 0.1 M  $\text{NaNO}_3$  (in order to prevent precipitation of the perchlorate salt **5a** at higher pH), with only  $[\text{Cu}_2\text{LH}]^{4+}$  present in solution at pH 4.66. After stepwise addition of base ( $\text{NaOtBu}$ ), the initial dicopper complex was fully converted into  $[\text{Cu}_2\text{L}]^{3+}$  at pH 6.55.

Further addition of base led to subsequent formation of  $[\text{Cu}_2\text{LH}_1]^{2+}$  (which is suggested to represent the dinuclear species **5b'** with a  $\text{HO}\cdots\text{HOH}$  bridge). This becomes the only species at pH 9.40 (Figure 34).



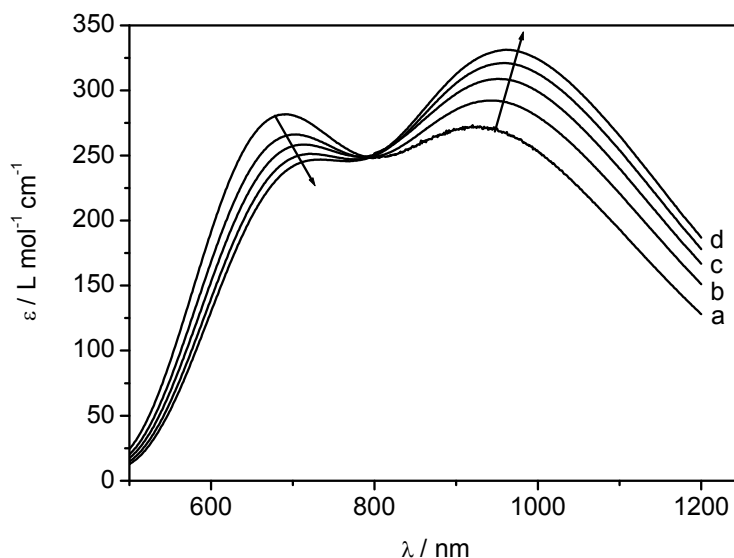
**Figure 34.** UV/vis titration of a solution of **7** in 0.1 M  $\text{NaNO}_3$  with  $\text{NaOtBu}$  between pH 6.55 (a) and pH 9.40 (b).

The appropriate amount of base necessary to convert tetranuclear **6** into dicopper(II) complex **5b** was established by titration of complex **6** with base ( $\text{KOtBu}$ ) in  $\text{MeOH}/\text{MeCN}$  (5:2) solution. The concentration of complex **6** was varied in the range from 0.0059 to 0.0027  $\text{mol L}^{-1}$ . Titrations were performed by varying the ratio complex:base from 0.1:1.0 to 2.01:1.0. Complete conversion of tetranuclear **6** into dinuclear **5b** was observed after addition of two equivalents of  $\text{KOtBu}$ , consistent with the structural data: two equivalents of base should be required to split the dimeric species into its bimetallic  $\{\text{Cu}_2\text{L}\}$  constituents, concomitant with formation of the  $\text{MeO}\cdots\text{HOMe}$  bridge (Figure 35).



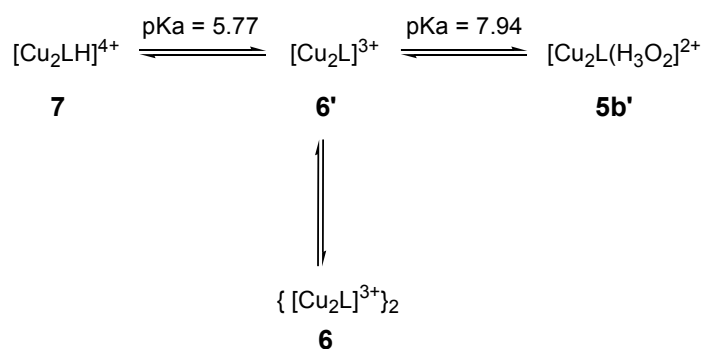
**Figure 35.** UV/vis titration of a solution of **6** in MeOH/MeCN (5:2) with KO $t$ Bu: solution of **6** without KO $t$ Bu (a) and with 2 eq. KO $t$ Bu (b).

During the course of these studies, an additional concentration dependence was observed for **6** (Figure 36), suggesting an equilibrium between the tetranuclear complex and a putative dinuclear species **6'** around neutral pH. A concentrated solution of complex **6** (0.01 M in MeOH/MeCN (5:2)) showed two bands at 689 nm and 923 nm, in accordance with the two types of copper ions found in the solid state (square pyramidal and trigonal bipyramidal). Dilution of this solution causes a shift of the absorption envelope from 923 to 962 nm and from 689 to 710 nm, with concomitant increase in intensity for the former and decrease in intensity for the latter band. Spectral features for **6'** are reminiscent of those seen for **5a**. The equilibrium thus induces a structural reorganization of the copper centers from square pyramidal to trigonal bipyramidal upon dilution, which is likely associated with dissociation of the tetranuclear complex into bimetallic species [Cu<sub>2</sub>L]<sup>3+</sup> (**6'**).



**Figure 36.** UV/vis spectra of **6** at different concentrations: 0.01 M (a); 0.005 M (b); 0.003 M (c); 0.002 M (d) in MeOH/MeCN (5:2).

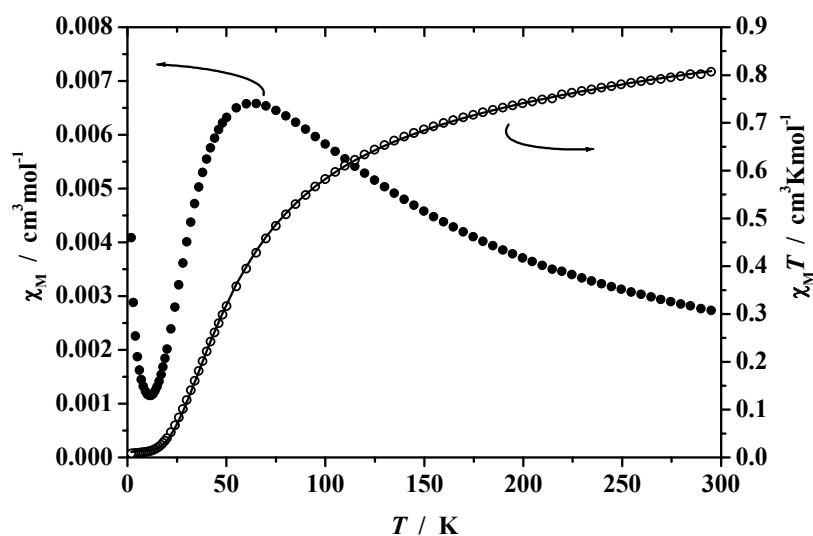
Above described overall equilibria between the three different complexes in 0.1 M aqueous solution of NaNO<sub>3</sub> is depicted in Scheme 27.

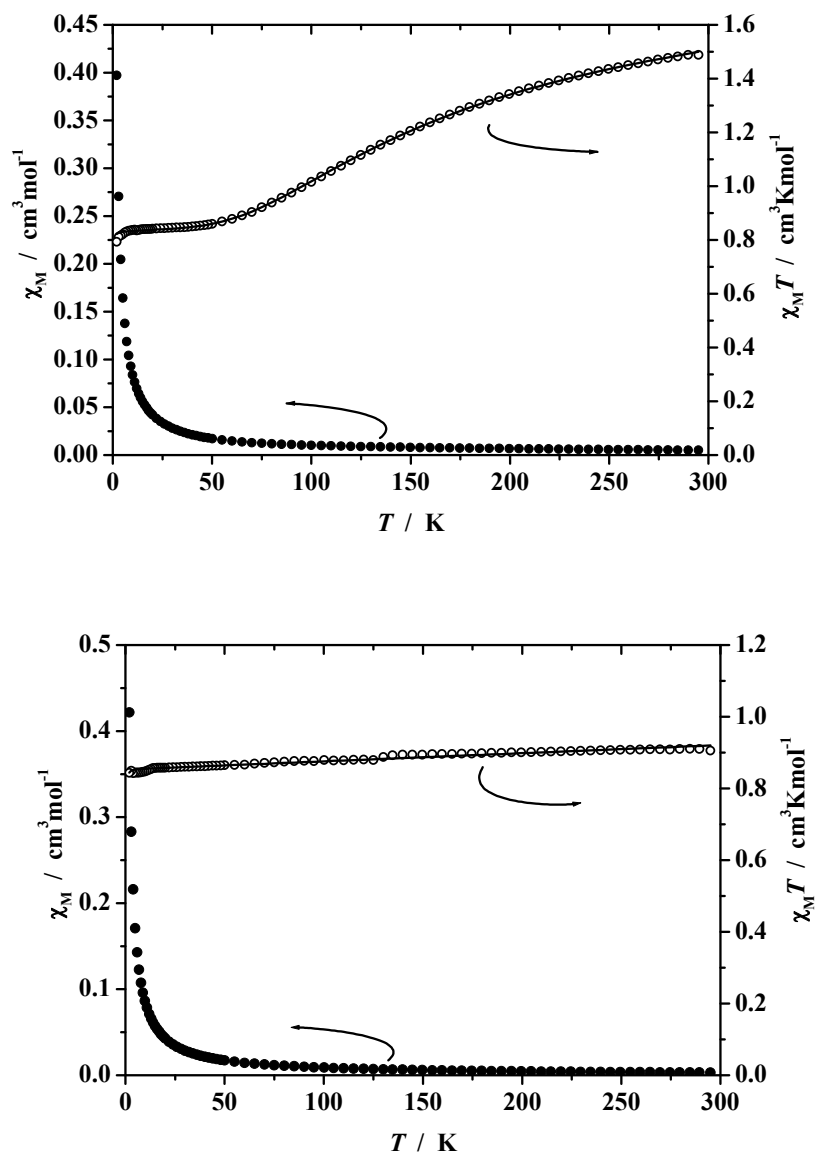


**Scheme 27.** Schematic representation of the overall equilibria between three complexes in 0.1 M NaNO<sub>3</sub> solution: dinuclear species **7** at pH = 4.66; tetranuclear species **6** at pH = 6.55; dinuclear species **6'** formed upon dissociation of **6** at neutral pH; dinuclear species **5b'** at pH = 9.40 with a HO···HOH bridge.

#### 5.4.4. Magnetic properties

Magnetic susceptibilities for powdered samples of **5a**, **6**, and **7** were measured at two different magnetic fields (2000 G and 5000 G) in a temperature range from 2.0 K to 295 K. No significant field dependence was observed for any of the complexes. The temperature dependence of the magnetic susceptibility  $\chi_M$  and of the product  $\chi_M T$  for the three distinct systems is depicted in Figure 37.





**Figure 37.** Plots of  $\chi_M$  (solid circles) and  $\chi_M T$  (open circles) versus temperature for **5a** (top), **6** (middle) and **7** (bottom) at 5000 G; the solid black lines represent the calculated curve fits (see text).

The observed  $\chi_M T$  value at 295 K for dicopper complex **7** is  $0.91 \text{ cm}^3 \cdot \text{K} \cdot \text{mol}^{-1}$  ( $2.63 \mu_B$ ), which indicates the presence of two uncoupled copper(II) ions ( $2.62 \mu_B$  for  $g = 2.14$ ). In contrast to **5a** and **6**,  $\chi_M T$  remains almost constant over a wide temperature range and shows only a slight linear decrease when the temperature is lowered to 2 K, which is a signature for complexes without magnetic interaction.

Experimental data for both dinuclear complexes **5a** and **7** were modelled by using a fitting procedure to the appropriate Heisenberg-Dirac-van-Vleck (HDvV) spin Hamiltonian for

isotropic exchange coupling and Zeeman splitting, equation (1).<sup>118</sup> A Curie-Weiss behaved paramagnetic impurity ( $\rho$ ) with spin  $S = 1/2$  and temperature-independent paramagnetism ( $TIP$ ) were included according to  $\chi = (1 - \rho) \cdot \chi + \rho \cdot \chi_{\text{mono}} + TIP$ .<sup>119</sup> Susceptibility data for the tetranuclear complex **6** were treated in a model that assumes an exchange-coupled bis( $\mu$ -pyrazolato) bridged dicopper(II) core according to equation (1), but with an additional single-ion Curie term for two well-separated non-interacting copper(II) ions (with  $g_2$ ). Calculated curve fits are shown as solid lines in Figure 37, and best fit parameters for all complexes are summarized in Table 11.

$$H = -2J\vec{S}_1\vec{S}_2 + g\mu_B(\vec{S}_1 + \vec{S}_2)\vec{B} \quad (1)$$

**Table 11.** Best fit parameters of magnetic data analyses for complexes **5a**, **6** and **7**.

complex	<b>5a</b>	<b>6</b>	<b>7</b>
$g_1$	2.07	2.06	2.14
$g_2$	-	2.11	-
$J, \text{cm}^{-1}$	-35.3	-100.6	0
$\rho, \%$	2.9	1.9	0.3
$TIP, \text{cm}^3 \cdot \text{mol}^{-1}$	3.09E-4	4.13E-4	2.27E-4

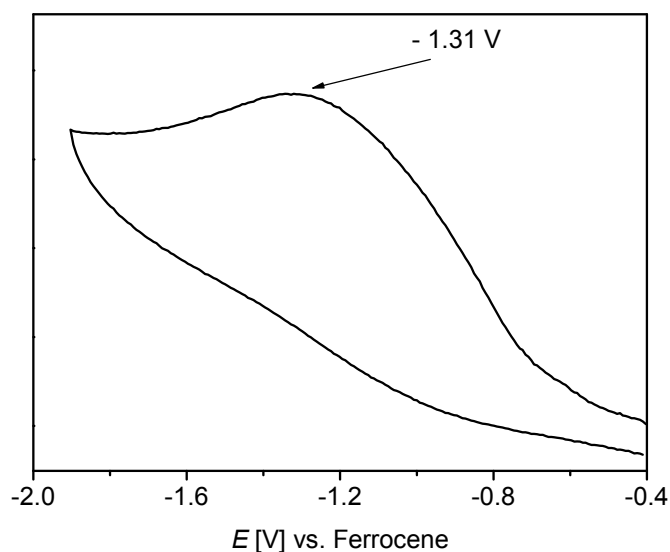
The differences in the magnetic properties for **5a**, **6** and **7** can be rationalized on the basis of the crystallographic findings. Tetranuclear **6** has two different types of copper ions: two metal ions constitute the bis( $\mu$ -pyrazolato) bridged core ( $d(\text{Cu1} \cdots \text{Cu1}') = 3.86 \text{ \AA}$ ) and two further ones are coordinated to the remaining ligand side arms and are well separated from the central core ( $d(\text{Cu1} \cdots \text{Cu2}') = 8.31 \text{ \AA}$ ). Antiferromagnetic coupling is observed only within the pyrazolate-bridged core, while the constant value of  $\chi_M T$  ( $0.84 \text{ cm}^3 \text{Kmol}^{-1}$ ) below 50 K confirms the presence of two additional uncoupled copper(II) ions. Two different  $g$  values (2.06 and 2.11) were observed for complex **6**, in agreement with the proposed model. The magnitude of the antiferromagnetic interaction in **5a** containing a single pyrazolate bridge is  $-35.3 \text{ cm}^{-1}$ , which is much lower than for the central part of complex **6** ( $-100.6 \text{ cm}^{-1}$ ) with its doubly pyrazolato-bridged dicopper(II) core. It can be safely concluded that the primary pathway for the magnetic interaction is through the pyrazolate bridges, whereas coupling through the H-bonded  $\text{MeO} \cdots \text{HOME}$  moiety in **5a** should be negligible. The value for the antiferromagnetic interaction in **6**, however, is still relatively small compared to data for



various other bis( $\mu$ -pyrazolato) bridged dicopper(II) compounds.<sup>120,121,122</sup> This can be ascribed to the trigonal bipyramidal coordination geometry imposed by the tripodal tetradentate  $\{N_4\}$  ligand compartments of **HL**<sup>4</sup> and the resulting orientation of the magnetic  $d_{z^2}$  orbital of each metal ion, which represents a quite rare situation in copper pyrazolate chemistry.<sup>123</sup> The bridging pyrazolate groups in **6** are positioned in such a way that one N atom occupies an axial site on one copper while the other N atom occupies an equatorial site on the second copper, and consequently the overlap of the magnetic  $d_{z^2}$  orbitals with ligand orbitals of the metal xy plane is relatively weak. In contrast, many other known dicopper(II) complexes that are spanned by two pyrazolato bridges feature square planar or tetragonal metal ions where the magnetic  $d_{x^2-y^2}$  orbitals are located within the plane of the bridging heterocycles.<sup>120,123</sup> This latter situation establishes a much more efficient coupling pathway and  $J$  values in the order of  $-200\text{ cm}^{-1}$ . It should be noted that additional parameters such as the deviation from co-planarity of the pyrazolate planes,<sup>124</sup> the Cu-N-N angle,<sup>125</sup> the bending angles  $\delta_{\text{pz-bend}}$  (representing the dihedral angle of the pyrazolate plane relative to the Cu-N-N-Cu plane),<sup>123</sup> and possibly the terminal donor atoms have been found to also contribute to the strength of the antiferromagnetic coupling in bis(pyrazolato) bridged dicopper(II) scaffolds. The magnetic behaviour of dicopper complex **7**, which does not feature a pyrazolate-bridging motif but a large Cu $\cdots$ Cu distance of 6.76 Å, is in accordance with the absence of any efficient exchange pathway and the lack of any significant coupling between the two metal ions. The slight linear decrease of  $\chi_M T$  upon lowering the temperature to 2 K in this case is merely due to the  $TIP$  ( $2.27\text{E-}4\text{ cm}^3\text{mol}^{-1}$ ).

#### 5.4.5 Cyclovoltammetry

Cyclovoltammetric measurements on dicopper(II) complex **5a** revealed only one irreversible reduction process at  $E_p^{\text{Red}} = -1.3\text{ V}$  versus the  $\text{Cp}_2\text{Fe}/\text{Cp}_2\text{Fe}^+$  couple. The cyclic voltammogram of **5a** is depicted in Figure 38.



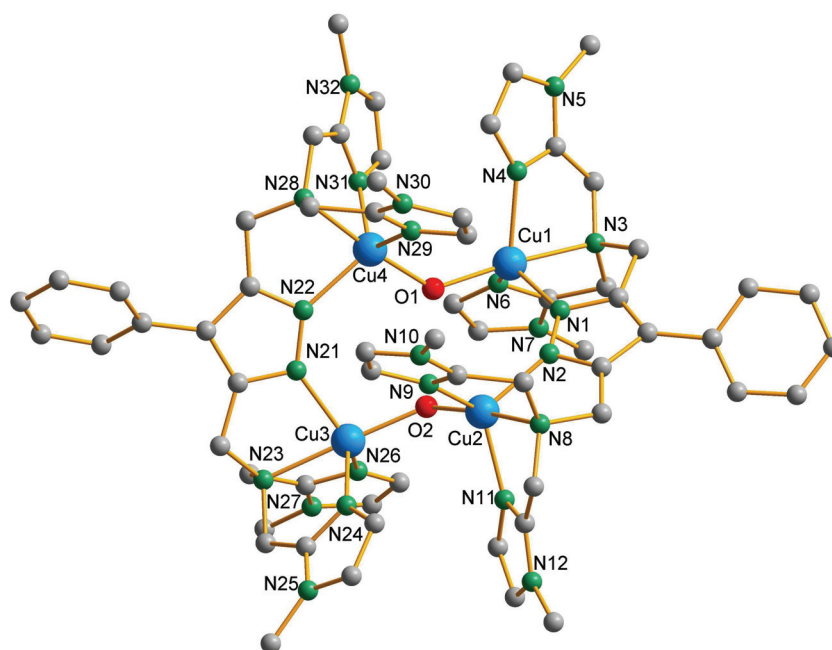
**Figure 38.** Cyclic voltammogram of **5a** in MeCN (0.1 M  $N^nBu_4PF_6$ , 100  $mV \cdot s^{-1}$ ); peak potentials in Volts versus  $Cp_2Fe/Cp_2Fe^+$  couple.

The reduction occurred only at low potential, which illustrates the significant stability of the dicopper(II) species.<sup>74,108</sup> Moreover, the irreversible nature of the reduction most likely is caused by the drastic differences between copper(II) and copper(I) regarding their structural and electronic requirements. Electrochemical production of the copper(I) species is presumably supported by a structural reorganisation relative to the initial dicopper(II) species, i.e. dissociation of the bridging  $MeO \cdots HOME$  unit, which possesses a very low affinity to copper(I) ions. The preferences in coordination geometry for the copper(I) ion formed upon reduction could also modify the overall structural motif found in **5a** by disruption of the strongly chelating, dinucleating character of the ligand as observed in the dicopper(II) species, resulting in an expulsion of one of the side arms to generate a preferable coordination pocket for the copper(I) ion, as for example observed in complex **9** (see section 7.6.4). However, the irreversible nature of the electrochemically induced redox-process clearly does not affect the activity of dicopper(II) complex **5a** as an oxidation catalyst, in particular for the oxidative C-C coupling of TMP (see section 6.3). The single observable reduction peak can be assigned to a  $2e^-$  reduction of the  $Cu^{II}Cu^{II}$  species to yield the corresponding  $Cu^I Cu^I$  analogue or to only  $1e^-$  reduction of the initial dicopper(II) species resulting in the formation of a mixed-valence  $Cu^I Cu^{II}$  species. The oxidation process is taking place at high potentials (not shown in the Figure 38,  $\sim 1.7$  V) and occurs most probably in concert with oxidation of the solvent used for these measurements.

### 5.5 Characterization of a copper complex with the new ligand HL<sup>5</sup>

The new ligand **HL**<sup>5</sup>, based on 4-phenyl pyrazole as the core framework, was prepared as the first representative of a new family of substituted pyrazole-based compartmental ligands featuring an arylated pyrazole ring. This substitution of a phenyl group instead of a proton is expected to significantly change the solubility of the copper complexes derived from ligands featuring this building block and at the same time influence the properties of the molecule (packing) in the solid state and hopefully enhance the isolation of crystalline samples.

The standard synthetic route was applied for the synthesis of copper complexes. Addition of two equivalents of Cu(NO<sub>3</sub>)<sub>2</sub> to a MeOH/MeCN solution containing **HL**<sup>5</sup> and two equivalents of base (KO<sup>*t*</sup>Bu) produced a green reaction mixture, from which single crystals were obtained by diffusion of Et<sub>2</sub>O that were suitable for an X-ray crystallographic analysis. The resultant molecular structure of the cation of **8** is depicted in Figure 39.



**Figure 39.** Molecular structure of the cation of **8**.

Surprisingly, formation of the kindred tetranuclear species took place instead of the expected dinuclear. This tetranuclear complex **8** possesses two independent dinuclear units that are bridged by two  $\mu$ -OH ligands. All four copper atoms are ligated by four N atoms, i.e. one from the pyrazolate-unit, two from the imidazoles in the side arm and the tertiary N atom of the ligand backbone, and by the O atom from the bridging OH unit. This ligation results in an

almost perfect trigonal bipyramidal geometry for Cu3 ( $\tau = 0.95$ ) and Cu4 ( $\tau = 0.92$ ) as well as for the other two copper atoms ( $\tau = 0.95$ ) (Table 12).

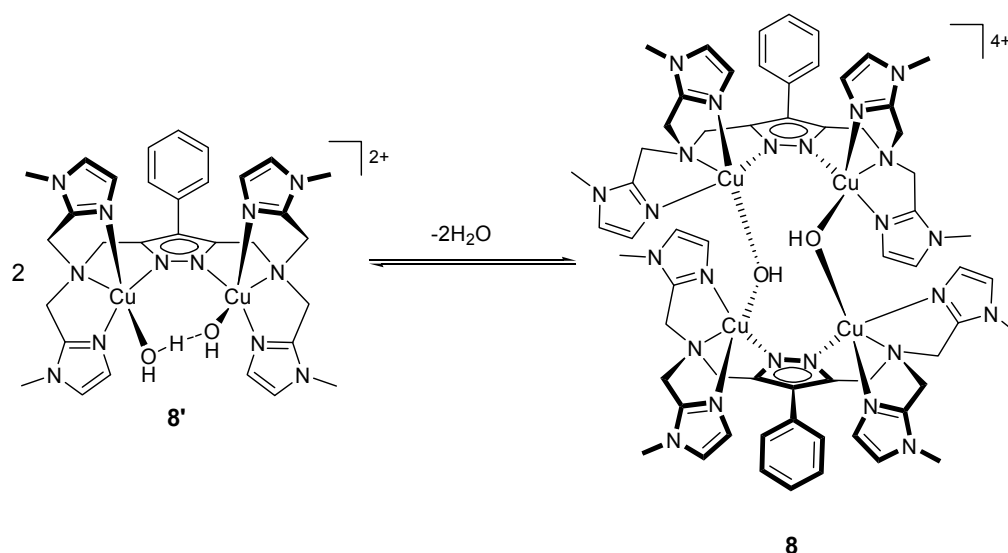
**Table 12.** Selected intramolecular distances (Å) and angles (°) for complex **8**.

Distances			
Cu(1)-O(1)	1.911(3)	Cu(3)-N(24)	2.123(3)
Cu(1)-N(1)	1.975(4)	Cu(3)-N(23)	2.130(3)
Cu(1)-N(6)	2.011(4)	Cu(4)-O(1)	1.895(3)
Cu(1)-N(3)	2.136(3)	Cu(4)-N(22)	2.041(3)
Cu(1)-N(4)	2.136(4)	Cu(4)-N(29)	2.043(4)
Cu(2)-O(2)	1.935(3)	Cu(4)-N(31)	2.090(4)
Cu(2)-N(9)	2.032(4)	Cu(4)-N(28)	2.111(4)
Cu(2)-N(2)	2.056(3)	Cu(1)···Cu(2)	4.2895(7)
Cu(2)-N(11)	2.063(4)	Cu(1)···Cu(3)	5.4999(6)
Cu(2)-N(8)	2.116(4)	Cu(1)···Cu(4)	3.4877(7)
Cu(3)-O(2)	1.943(3)	Cu(2)···Cu(3)	3.5249(7)
Cu(3)-N(21)	2.017(3)	Cu(2)···Cu(4)	4.6024(8)
Cu(3)-N(26)	2.062(3)	Cu(3)···Cu(4)	4.3774(7)
Angles			
O(1)-Cu(1)-N(1)	99.91(14)	O(2)-Cu(3)-N(21)	101.19(13)
O(1)-Cu(1)-N(6)	96.26(14)	O(2)-Cu(3)-N(26)	97.95(13)
N(1)-Cu(1)-N(6)	123.54(17)	N(21)-Cu(3)-N(26)	120.35(14)
O(1)-Cu(1)-N(3)	173.79(14)	O(2)-Cu(3)-N(24)	102.16(13)
N(1)-Cu(1)-N(3)	79.75(14)	N(21)-Cu(3)-N(24)	112.90(14)
N(6)-Cu(1)-N(3)	78.96(15)	N(26)-Cu(3)-N(24)	117.21(14)
O(1)-Cu(1)-N(4)	107.80(14)	O(2)-Cu(3)-N(23)	177.73(13)
N(1)-Cu(1)-N(4)	111.20(15)	N(21)-Cu(3)-N(23)	80.38(12)
N(6)-Cu(1)-N(4)	114.36(17)	N(26)-Cu(3)-N(23)	79.82(13)
N(3)-Cu(1)-N(4)	77.95(14)	N(24)-Cu(3)-N(23)	78.61(13)
O(2)-Cu(2)-N(9)	98.91(14)	O(1)-Cu(4)-N(22)	104.47(13)
O(2)-Cu(2)-N(2)	105.83(13)	O(1)-Cu(4)-N(29)	98.84(14)
N(9)-Cu(2)-N(2)	114.22(16)	N(22)-Cu(4)-N(29)	117.54(14)
O(2)-Cu(2)-N(11)	97.18(15)	O(1)-Cu(4)-N(31)	97.56(15)

N(9)-Cu(2)-N(11)	121.91(15)	N(22)-Cu(4)-N(31)	114.46(14)
N(2)-Cu(2)-N(11)	114.07(15)	N(29)-Cu(4)-N(31)	118.68(16)
O(2)-Cu(2)-N(8)	175.17(14)	O(1)-Cu(4)-N(28)	174.82(13)
N(9)-Cu(2)-N(8)	80.17(18)	N(22)-Cu(4)-N(28)	80.58(13)
N(2)-Cu(2)-N(8)	78.79(15)	N(29)-Cu(4)-N(28)	79.55(14)
N(11)-Cu(2)-N(8)	79.44(19)	N(31)-Cu(4)-N(28)	79.07(16)

The bridging OH<sup>-</sup> ligands between two dicopper units induce an enlargement of the copper-copper distance within the independent bimetallic core to 4.60 Å for  $d(\text{Cu}2\cdots\text{Cu}4)$ , compared to the usual distance observed in dinuclear copper(II) complexes with related imidazole side arms (see section 5.4.2). However, the distance between two copper atoms belonging to different bimetallic subunits that are connected by a  $\mu\text{-OH}$  ligand is rather small ( $d(\text{Cu}1\cdots\text{Cu}4) = 3.49$  Å).

The structural features were reflected perfectly in the corresponding UV/vis spectrum, where one  $d-d$  transition band for copper ions in a trigonal bipyramidal environment at  $\lambda_{\text{max}}$  of 995 nm was observed with the typical additional shoulder at  $\lambda_{\text{max}}$  of 726 nm. Unfortunately, it was not possible by means of UV/vis spectroscopy to distinguish between the isolated tetranuclear species and the related dinuclear complex, which presumably forms in solution through dissociation of the former, since the dinuclear species, should have similar spectroscopic features.



**Scheme 28.** Equilibrium in aqueous solution between tetranuclear species **8** and dinuclear species **8'**.

The ESI spectrum of the MeCN solution of **8** confirmed the presumed dissociation process resulting in formation of dinuclear subunit **8'** with MeO...HOMe or HO...HOH bridging motif (depending on the solvent used) within the bimetallic pocket (Scheme 28), as for example observed in **5a**. The observed signals in the ESI spectrum at 703, 766 and 827  $m/z$  are typical for dinuclear copper(II) species, as they correspond to  $[\text{Cu}_2\text{L}^5]^+$ ,  $[\text{Cu}_2\text{L}^5(\text{NO}_3)]^+$  and  $[\text{Cu}_2\text{L}^5(\text{NO}_3)_2]^+$ , respectively.

The dissociation of the tetranuclear species is very important for the subsequent catalytic reactions studied with this system, in particular for the oxidative C-C coupling of 4-ethylphenol, where dicopper(II) species are shown to act as the catalyst (see section 9).

## 5.6 Comparison of the spectroscopic and structural features of the copper complexes

In order to analyze and compare the geometries, both in solid state and solution, of the copper ions in the complexes described in this chapter, values for the important parameters  $\tau$  and  $\lambda_{\text{max}}$  are summarized in Table 13.

**Table 13.**  $\tau$  values and  $\lambda_{\text{max}}$  for selected copper complexes.

Complex	$d(\text{Cu}\cdots\text{Cu})$ [ $\text{\AA}$ ]	$\tau$	$\lambda_{\text{max}}$ [nm] ( $\epsilon$ [ $\text{L mol}^{-1} \text{cm}^{-1}$ ])*
<b>1</b>	3.59	0.23/0.24	628 (282)
<b>4</b>	$\sim 3.5$	0.86	816 (291)
<b>5a</b>	4.34	0.88	730sh (135) 962 (269)
<b>6</b>	3.87	0.91	689 (281), 923 (272)
<b>7</b>	6.76	0.13	677 (96)
<b>8</b>	3.48/4.60	0.83/0.95	995 (280), 726sh (135)

\*UV/vis spectra in solution (see experimental part)

In the crystal structure of **5a**, two copper ions were found to be in almost perfect trigonal bipyramidal  $\{\text{N}_4\text{O}\}$  coordination environment, and this is reflected nicely in the UV/vis spectrum, with an absorption maximum at 962 nm. In case of a slightly distorted square pyramidal geometry of the copper ions, as in complex **1**,  $\lambda_{\text{max}}$  is typically found at lower value, and the observations prove the accordance between the solid state and solution

structure for this species. The presence of two geometrically different copper ions in complex **6** should give rise to two bands in the UV/vis spectrum for both square pyramidal and trigonal bipyramidal copper, and this was indeed confirmed. Moreover, equilibrium between dinuclear and tetranuclear species was occurred in some cases.

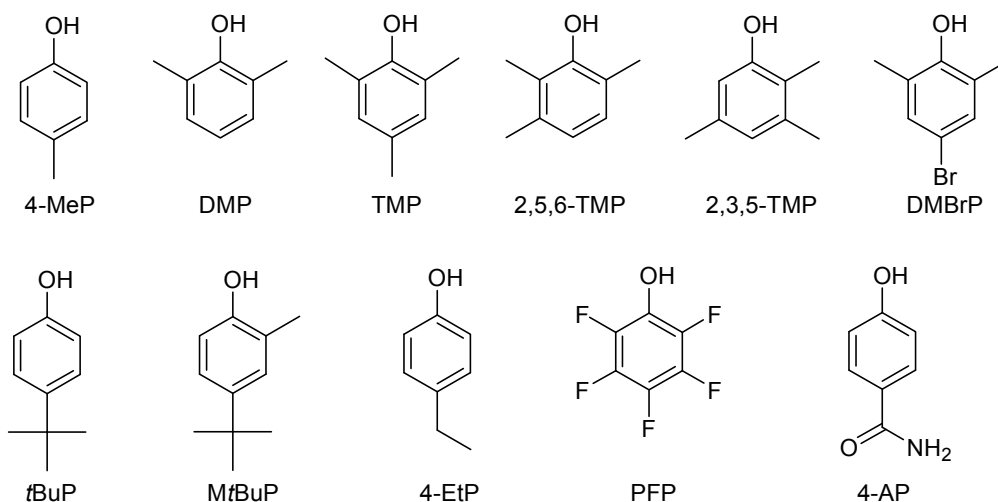
From the observed correlations between significant structural parameters of both the solid state and solution structure, it can be safely implied that the structures, as determined by X-ray crystallography for isolated crystalline forms of these complexes, are clearly retained when in solution. This not only leads to the full characterization of these species, but more importantly shows the high structural stability of these pyrazolate-based ligand systems and their Cu-complexes. This in turn might allow the use of solution spectroscopic techniques as elegant and credible tools for the elucidation of e.g. the characterization of specific intermediates when these Cu-species are employed as catalysts.

## 6 Bioinspired oxidation reactions of phenols

Unprecedented and highly interesting catalytic activity of the pyrazolate-based dicopper(II) complex with binding compartments composed of imidazolyl groups (complex **5a**) in phenol oxidation will be discussed in detail. Substrate binding to the dicopper site was investigated by spectroscopic techniques and solid-state X-ray crystallography, using phenols that are inert to oxidation. A subtle interplay of reaction conditions and substrate specific properties enabled the determination of different kinds of organic products after catalysis. Mechanistic insight in the studied oxidation reactions is provided from a combination of spectroscopic studies.

### 6.1 Screening of the phenol substrates

In order to test the reactivity of the pyrazolate-based dicopper(II) complex **5a** as a catalyst in bioinspired phenol oxidation, a screening of a range of phenol substrates was performed. It was envisioned that these very different phenols might show dissimilar tendencies to undergo chemical transformations during catalysis (Figure 40).



**Figure 40.** The set of the phenols screened for activity with dicopper complex **5a**.

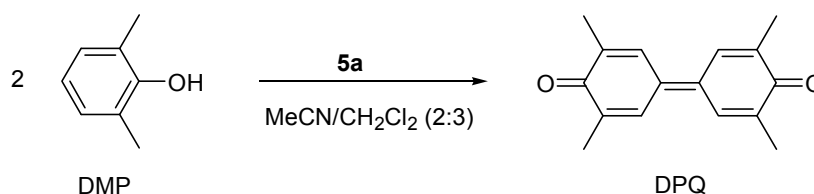
The nature of the substituents on the phenol ring has a large influence on the reactivity observed with the chosen dinuclear Cu-complex **5a**, leading to a wide variety of products and



unexpected modes of activation of the phenolic substrates. Thus, electron rich DMP and TMP are shown to easily undergo C-C coupling in the respective *para*-positions, catalyzed by dicopper(II) complex **5a** (see section 6.2 and 6.3). 4-Ethylphenol, a phenol with unsubstituted *ortho*-positions, is found to be a particularly reactive substrate for C-C oxidative coupling in the *ortho*-position (see section 9). Presence of the extremely reactive bromo substituent in the *para*-position of 4-bromo-2,6-dimethylphenol (DMBrP) directs the catalysis towards oxidative C-O coupling, with formation of a polymeric material, analogous to PPE (see section 11). Phenols with strong electron-withdrawing properties, such as pentafluorophenol (PFP) and 4-hydroxybenzamide (4-AP), are inert to any kind of Cu-catalyzed oxidation reaction and are therefore applied as model substrates to elucidate phenol binding to the dicopper active core (see section 8.2). Possible correlations between the observed activities of the screened phenols and their electronic and steric properties will be discussed in detail within the following chapters of the present work.

## 6.2 Oxidative C-C coupling of 2,6-dimethylphenol

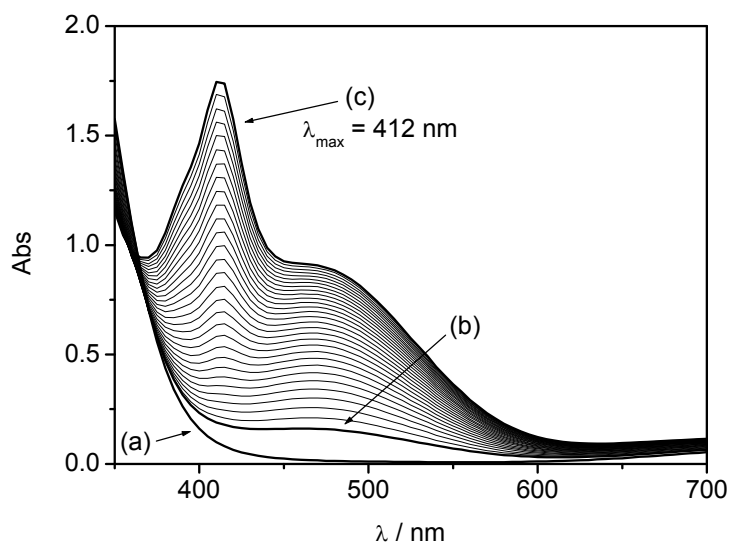
2,6-dimethylphenol (DMP) is known to be oxidized in the presence of a copper-catalyst to yield the C-O coupled polymeric product poly(2,6-dimethylphenylene ether) (PPE). Therefore, to test the catalytic activity of the newly prepared dicopper complex **5a**, featuring pendant imidazolyl side arms, DMP was chosen as the initial substrate. In marked contrast to previous results obtained with pyrazolate-based dicopper(II) complexes having aliphatic side arms (see section 5.2.2), whereby DMP was selectively converted to yield PPE, complex **5a** was found to catalyze the oxidation of DMP in a very different manner. Thus, in the presence of **5a**, DMP underwent C-C oxidative coupling, yielding 3,3',5,5'-tetramethyl-4,4'-diphenoquinone (DPQ) as the main product (Scheme 29), with no traces of C-O coupled polymer found. Notably, DPQ is normally observed as by-product in the synthesis of PPE, but few selective processes have so far been devised to form DPQ as the main product from copper-catalyzed oxidative coupling of DMP.<sup>126</sup>



**Scheme 29.** Oxidative coupling of DMP catalyzed by dicopper complex **5a**.

Using catalyst **5a** instead of the previously employed mononuclear copper systems<sup>88,89</sup> allowed the C-C coupling to be performed under mild conditions, avoiding high temperatures and long reaction times.<sup>126</sup> The standard conditions used for the C-C coupling as well as the C-O coupling reactions of phenols require the use of additional base (e.g. triethylamine) to activate the phenolic substrate and enable interaction with the Cu-catalyst, whereas **5a** already contains a highly basic methanolate that can act as an internal base. The catalytic reaction of DMP with aerial dioxygen as oxidant and in the presence of **5a** takes place without addition of base and at room temperature.

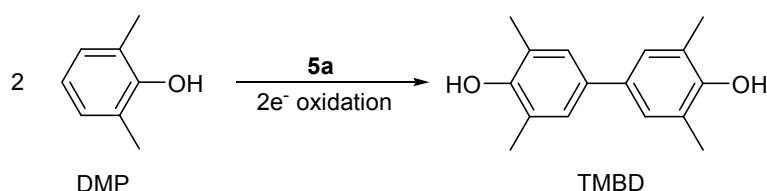
The C-C coupling reaction of DMP to DPQ was monitored using time-resolved stopped-flow UV/vis spectroscopy (Figure 41).



**Figure 41.** UV/vis spectra at different stages of the oxidative coupling of DMP (initial concentration of **5a** =  $4 \cdot 10^{-4}$  mol·L<sup>-1</sup>; initial concentration of DMP =  $2 \cdot 10^{-3}$  mol·L<sup>-1</sup>; L = 1.0 cm; solvent: MeCN; (a) starting solution of **5a**; (b) a few seconds after addition of TMP (red solution); (c) 6 minutes after addition of DMP (absorption spectrum of the formed DPQ as indicated by the intense absorption band at 412 nm).

Measurements were performed in the range from 350 to 900 nm, as no *d-d* bands from the dicopper complex **5a** are to be expected in this region. Drastic changes were already observed a few seconds after addition of DMP, with the appearance of an intense band at  $\lambda_{\text{max}}$  472 nm ( $\epsilon \sim 1500 \text{ L}\cdot\text{mol}^{-1}\cdot\text{cm}^{-1}$ ). DPQ started to form after 3 minutes of reaction, as indicated by the intense absorption band at 412 nm (Figure 41 (c)).

This  $4e^-$  oxidation of DMP to DPQ in the presence of aerial dioxygen can not be performed in one step, as only  $2e^-$  can be taken up by the initial complex **5a** (assuming a  $\text{Cu}^{\text{II}}\text{Cu}^{\text{II}}$  to  $\text{Cu}^{\text{I}}\text{Cu}^{\text{I}}$  redox-process). The overall reaction therefore likely proceeds via formation of an intermediate organic product. In accord with this hypothesis, it was observed that under anaerobic conditions the oxidative coupling reaction was halted after formation of the 3,3',5,5'-tetramethylbiphenyl-4,4'-diol (TMBD) (Scheme 30).



**Scheme 30.**  $2e^-$  oxidative C-C coupling of DMP under anaerobic conditions.

This  $2e^-$  oxidative C-C coupling of DMP ( $1e^-$  per DMP molecule) under anaerobic conditions can only take place in parallel with reduction of the initial dicopper complex **5a**. In order to elucidate the above-mentioned aspects of this C-C coupling reaction, it was deemed logical to switch to the related compound 2,4,6-trimethylphenol (TMP) and investigate if substitution of the reactive *para*-position would alter or possibly even totally block the reactivity of **5a**. This would then allow a study of the coordination of ‘unreactive’ phenols to the dicopper core of **5a** and provide insights to elucidate some factors guiding the activity of **5a**.

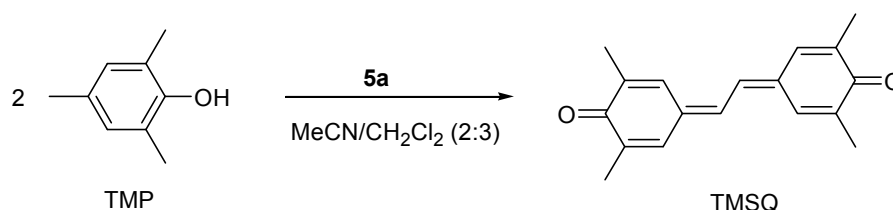
### 6.3 Oxidative C-C coupling of 2,4,6-trimethylphenol

The copper-mediated oxidation of 2,4,6-trimethylphenol (TMP) with oxygen as an oxidant has been dominated by the formation of known oxygenated products such as 4-hydroxy-3,5-dimethylbenzaldehyde, 2,6-dimethyl-*p*-benzoquinone and 4-alkoxy-2,6-dimethylphenols.<sup>96b,c</sup> As a consequence, the oxidative coupling of TMP at the benzylic carbon in the *para*-position

is rarely observed and has so far required the use of excess strong oxidants to proceed.<sup>127</sup> The only reported incident of selective oxidative C-C coupling of TMP to yield stilbenequinone was achieved in the presence of dioxygen and a mononuclear copper complex, as published by Tsushida and co-workers.<sup>128</sup>

As mentioned in the previous paragraph, despite the remarkable selectivity towards C-C coupling that was evidenced for DMP, it was hypothesized that with TMP as substrate, such reactivity would not be observed, as the *para*-position is blocked for direct aryl-aryl C-C coupling.

The same reaction conditions as used for the copper-catalyzed oxidative coupling of DMP were applied, where TMP was added to a solution of **5a** in a mixture of MeCN/CH<sub>2</sub>Cl<sub>2</sub>. Red crystals, which separated from the reaction mixture after standing overnight, could be isolated and fully characterized by a combination of X-ray crystallography and spectroscopic methods. It was thereby revealed that the product obtained corresponded to 3,3',5,5'-tetramethylstilbene-4,4'-quinone (TMSQ) (Scheme 31).

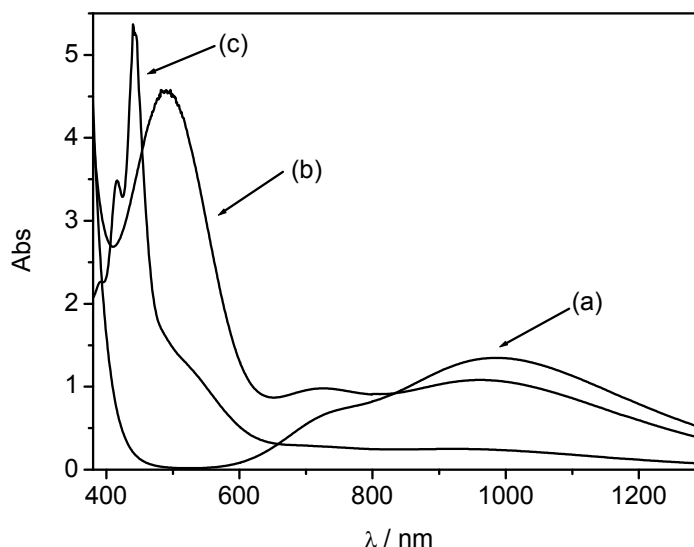


**Scheme 31.** Oxidative C-C coupling of TMP catalyzed by **5a**.

The high-yield formation of TMSQ under the applied reaction conditions established that dicopper complex **5a**, incorporating functional imidazolyl side arms, shows remarkable and significant selectivity towards the oxidative C-C coupling with both DMP and TMP as substrates.

The reaction was followed in time by means of UV/vis spectroscopy. The electronic spectrum of **5a** in MeCN/CH<sub>2</sub>Cl<sub>2</sub> showed a band at  $\lambda_{\text{max}}$  989 nm ( $\epsilon = 269 \text{ L}\cdot\text{mol}^{-1}\cdot\text{cm}^{-1}$ ) with a shoulder at 724 nm, corresponding to *d-d* transitions of copper(II) ions in a trigonal bipyramidal environment (Figure 42 (a)). Significant changes were observed directly after addition of TMP (Figure 42 (b)), namely the appearance of an intense band at  $\lambda_{\text{max}}$  495 nm ( $\epsilon \sim 1500$

$\text{L}\cdot\text{mol}^{-1}\cdot\text{cm}^{-1}$ ) and a shift of the  $\text{Cu}^{\text{II}}$ -based  $d-d$  transition band to 960 nm. Formation of the product (TMSQ) began after a relatively long incubation period (2 h) and the intense absorption band of the product is detected at 440 nm ( $\epsilon \sim 96000 \text{ L}\cdot\text{mol}^{-1}\cdot\text{cm}^{-1}$  in  $\text{CH}_2\text{Cl}_2$ ) (Figure 42 (c)).



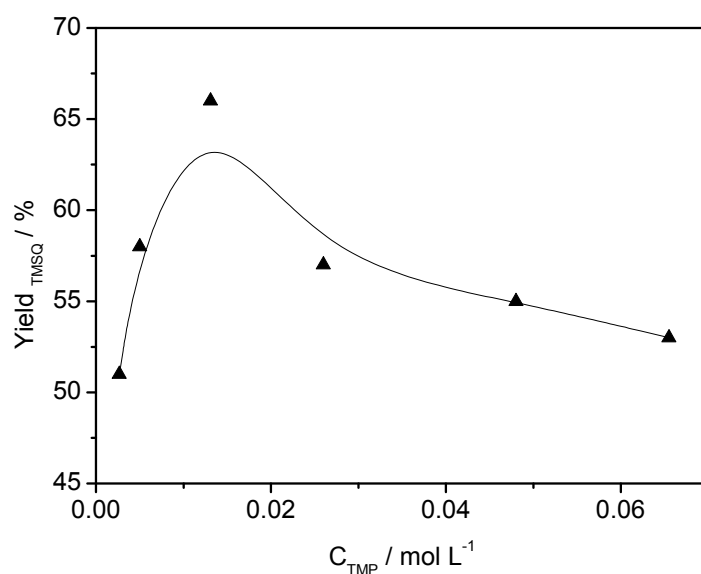
**Figure 42.** UV/vis spectra at different stages of the oxidative coupling of TMP (initial concentration of **5a** =  $0.005 \text{ mol}\cdot\text{L}^{-1}$ ; initial concentration of TMP =  $0.025 \text{ mol}\cdot\text{L}^{-1}$ ;  $L = 1.0 \text{ cm}$ ; solvent:  $\text{MeCN}/\text{CH}_2\text{Cl}_2$  4:6 v/v): (a) starting solution of **5a**; (b) a few minutes after addition of TMP (red solution); (c) 8 h after addition of TMP (absorption spectrum of the formed TMSQ scaled by a factor 90).

One notable difference with the related reactivity observed for DMP with complex **5a** is that the oxidative C-C coupling of TMP to yield TMSQ is an overall 6e-process ( $3e^-$  per TMP molecule), which implies a rather complicated reaction pathway and hence intriguing mechanistic considerations. Further studies on the mechanism of C-C coupling of TMP will be discussed in details (see section 7).

## 7 Investigations of the mechanism of C-C coupling of TMP

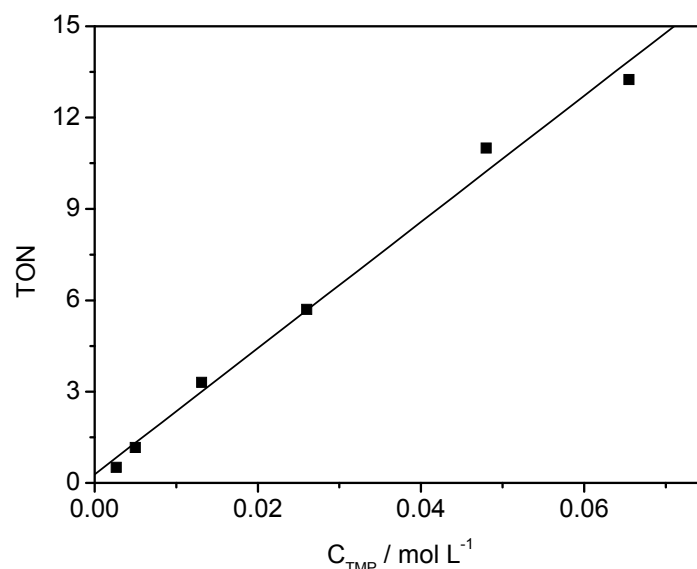
### 7.1 Determination of the optimal reaction conditions for C-C-coupling of TMP

Optimization of the reaction conditions was first of all focussed on improving the yield of TMSQ, which was targeted by studying the solvent influence on the catalytic performance. The yield of TMSQ was determined by means of UV/vis spectroscopy, with the aid of the intense absorption band of this product at 440 nm ( $\epsilon \sim 96000 \text{ L}\cdot\text{mol}^{-1}\cdot\text{cm}^{-1}$ ). It was found that reactions performed in a 2:3 mixture of MeCN/CH<sub>2</sub>Cl<sub>2</sub> provided the highest yield of TMSQ, approximately 65%. Further studies were concentrated on the influence of the substrate (TMP) to catalyst **5a** (S/C) ratio on the yield of TMSQ. Six identical samples of the dicopper(II) complex **5a** in MeCN/CH<sub>2</sub>Cl<sub>2</sub> (2:3) with identical concentration (0.0024 M) were prepared and TMP was added as a solid to each solution, but with varying initial concentration (0.0026 M, 0.0050 M, 0.0131 M, 0.0260 M, 0.0480 M, 0.0655 M). The red coloured mixtures were stirred for 24h at room temperature and after appropriate dilution of the reaction samples with CH<sub>2</sub>Cl<sub>2</sub>, UV/vis spectra were recorded. The experimental data showed that the yield in TMSQ was only slightly dependent on the ratio TMP:**5a**, with the most optimal S/C ratio at 5:1 (TMP (0.0131 M):**5a** (0.0024 M)), giving 66% of TMSQ (Figure 43).



**Figure 43.** Dependence of the yield of TMSQ on the S/C ratio, as followed by UV/vis spectroscopy, with a constant concentration in catalyst **5a** (0.0024 M).

The TON number (expressed as mole substrate converted per mole catalyst used) increased linearly with the concentration of TMP employed in the reaction, which is a clear indication for high catalyst stability and good overall performance of the catalytic active dicopper complex (Figure 44).



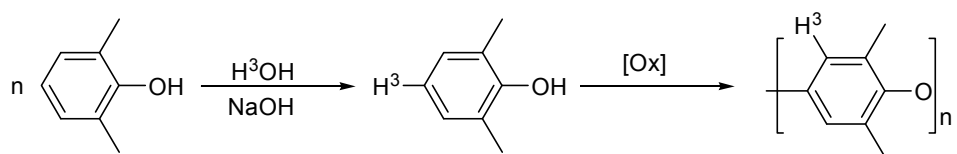
**Figure 44.** Turnover numbers for formation of TMSQ (after 24 h for each sample).

Thus, as the catalytic activity of **5a** was determined to not be strongly dependent on the substrate to catalyst ratio, S/C 5:1 ratio was chosen as standard condition for further studies. The temperature profile of the yield in TMSQ was not investigated, because it was reasoned that the oxidative C-C coupling of TMP with copper catalyst **5a** could attract the greatest interest when selectively conducted under very mild conditions, i.e. at room temperature and in the absence of excess base or other additives.

## 7.2 Investigations with deuterated TMP substrate

It is known that 2,6-dimethylphenol (DMP) can be oxidized in the presence of a copper-catalyst, to yield the C-O coupled polymeric product poly(2,6-dimethylphenylene ether) (PPE) as well as the C-C coupled product 3,3',5,5'-tetramethyl-4,4'-diphenquinone (DPQ). Many studies were done in order to investigate the mechanism of the oxidative polymerization of DMP (see section 3.2) and it was shown that the reaction can proceed through free radical intermediates and, moreover, that migration of the H-atom from the *para*-

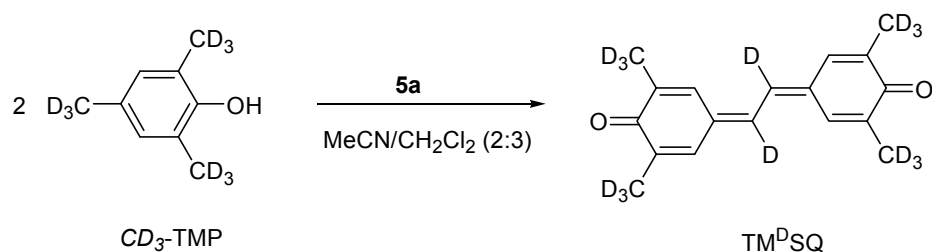
position to the *meta*-position of the phenol is taking place during the polymerization process (Scheme 32).<sup>129</sup>



**Scheme 32.** H-atom migration during the C-O coupling of DMP.

With the aim to further elucidate the mechanism of the oxidative C-C coupling of TMP, such an H-atom migration pathway had to be considered as a possible step in the mechanism. Therefore, NMR spectroscopy was used to clarify whether this was indeed a viable option to take into account for the overall mechanistic picture for this reaction.

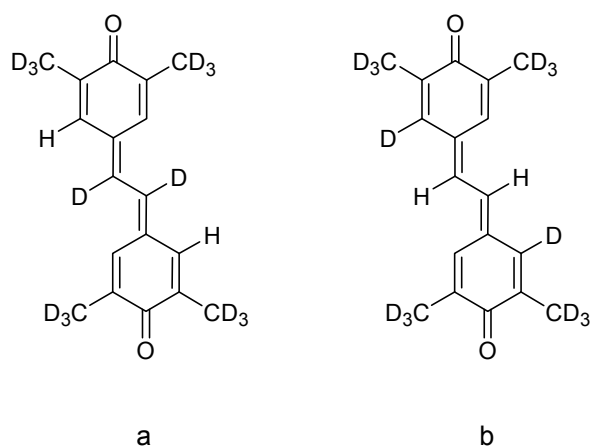
First of all, the substrate with fully deuterated  $\text{CH}_3$ -groups ( $\text{CD}_3$ -TMP) was prepared (via standard Raney-Ni catalyzed H/D exchange for TMP, using  $\text{D}_2\text{O}$  as the deuterium source)<sup>130</sup> and tested in the C-C coupling. Under the same reaction conditions as for the C-C coupling of TMP,  $\text{CD}_3$ -TMP smoothly underwent reaction to yield  $\text{TM}^{\text{D}}\text{SQ}$  – the analogue of TMSQ with deuterated  $\text{CH}_3$ -groups (Scheme 33).



**Scheme 33.** Oxidative C-C coupling of  $\text{CD}_3$ -TMP catalyzed by **5a**.

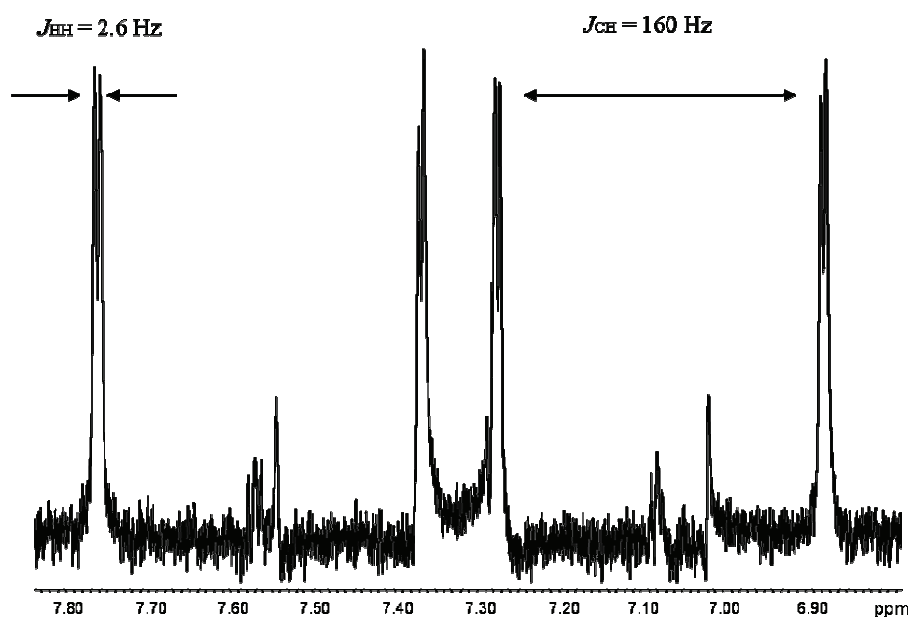
The formed product  $\text{TM}^{\text{D}}\text{SQ}$  was straightforwardly characterized by standard  $^1\text{H}$  and  $^{13}\text{C}$  NMR spectroscopy, but the obtained results did not allow any unambiguous distinction between products formed with or without possible H-atom migration (Figure 45).





**Figure 45.** Two possible  $\text{TM}^{\text{D}}\text{SQ}$  products formed: (a) without H-atom migration; (b) with H-atom migration.

Further determination of the  $\text{TM}^{\text{D}}\text{SQ}$  structure was carried out using Heteronuclear Multiple Quantum Correlation (HMQC) and Heteronuclear Multiple Bond Correlation (HMBC) NMR techniques. Both of them are two-dimensional inverse C,H-correlation techniques that provide information about the carbon (or other heteroatoms) to hydrogen connectivity. HMQC is selective for direct C-H coupling interactions, while HMBC will give longer range couplings (two- to four-bond coupling) between heteroatom nuclei. The 1D HMQC spectrum of  $\text{TM}^{\text{D}}\text{SQ}$  was recorded in  $\text{CDCl}_3$  (Figure 46).



**Figure 46.** 1D HMQC spectrum of  $\text{TM}^{\text{D}}\text{SQ}$  in  $\text{CDCl}_3$ .

Two signals for two protons from TM<sup>D</sup>SQ, which appear at  $\delta$  7.02 and 7.50 ppm in the <sup>1</sup>H NMR spectrum, show a mutual coupling with a coupling constant  $J_{HH}$  of 2.6 Hz, as well as short range C-H coupling with  $J_{CH} = 160$  Hz. The observed value for the  $J_{HH}$  coupling is typical for aromatic protons in *meta*-position to each other, as found in the proposed structure for TM<sup>D</sup>SQ formed without H-atom migration, i.e. structure (a). It has to be mentioned that in case H-atom migration would have occurred (structure (b)), the corresponding 1D HMQC spectrum should include signals corresponding to a H,H *trans* coupling with a value for the coupling constant  $J_{HH}$  of ~7-10 ppm.

The HMBC method, which is selective for longer range couplings (two- to four-bond coupling), was applied to obtain additional evidence about the actual structure of TM<sup>D</sup>SQ and to support the preliminary conclusion, that no H-atom migration takes place during its formation. In the recorded HMBC spectrum both protons from TM<sup>D</sup>SQ resonating at  $\delta$  7.02 and 7.50 ppm in the <sup>1</sup>H NMR spectrum, showed four bond coupling to the carbonyl C-atom (C=O) at 185 ppm, which is possible only in the case of proposed structure (a).

On the basis of these results, it can be safely concluded that the oxidative C-C coupling of TMP in the presence of **5a** and dioxygen is taking place without H-atom migration from the *para* CH<sub>3</sub>-group to the *meta*-position of the aromatic ring.

### 7.3 Discussion of the nature of the UV/vis Charge Transfer band of dicopper phenolate complexes

Addition of DMP and TMP substrates to a green solution of dicopper(II) complex **5a** in MeCN led to a colour change of the solution from green to red with concomitant appearance of an intense band at  $\lambda_{max} = 472$  and 495, respectively. These spectral changes are most likely occurred do to the coordination of a phenolate to one of the copper(II) ions of complex **5a** owing to a methanolate-phenolate exchange. Appearance of such an intense band in UV/vis spectrum upon addition of phenols to various copper complexes was observed in similar systems.<sup>131,132,133</sup> and, moreover, this band was characterized as a ligand-to metal charge-transfer band (LMCT).

In order to determine the nature of the observed charge-transfer band, addition of the various phenol substrates to a green solution of **5a** was performed. Identical colour change, as for

DMP and TMP was observed, with concomitant appearance of an intense band with  $\lambda_{\max}$  in the range from 390 to 500 nm (Table 14).

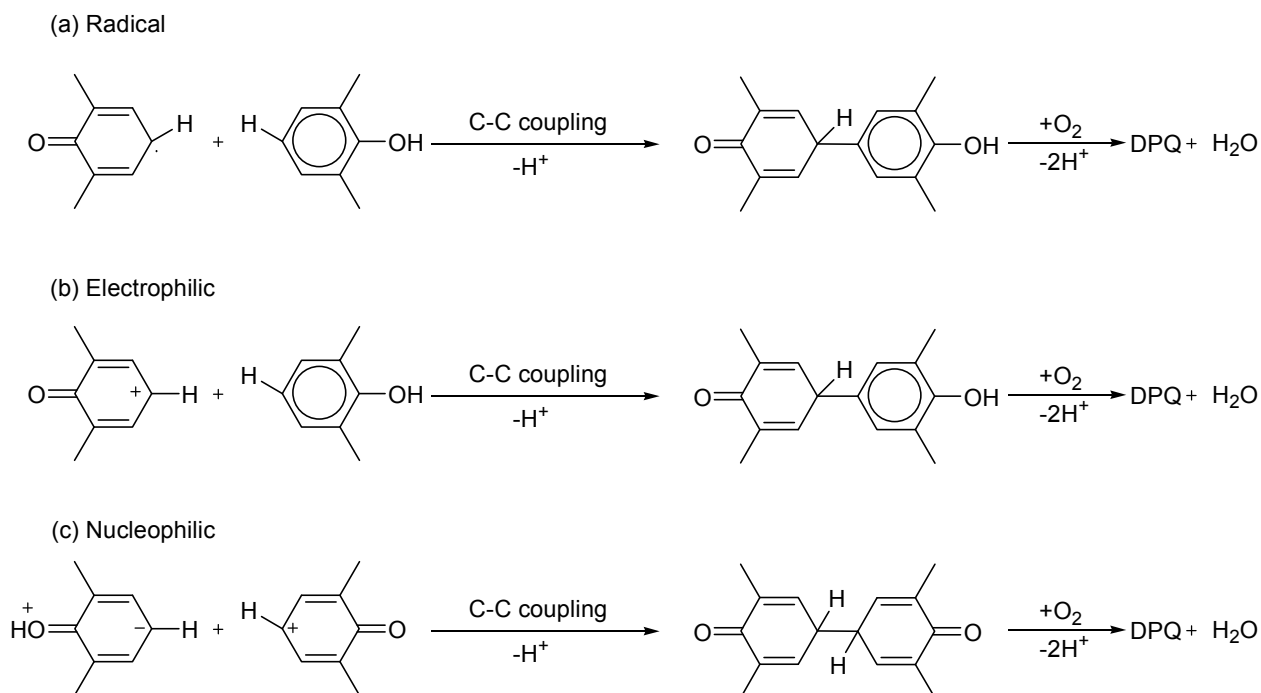
**Table 14.** Various phenols used for complexation studies with dicopper complex **5a** and  $\lambda_{\max}$  of the CT band of the corresponding phenolate adducts.

phenol	$\lambda_{\max}$ (nm)
4-MeP	457
DMP	472
TMP	495
<i>t</i> BuP	455
4-AP	440
PFP	397

A clear trend was observed in  $\lambda_{\max}$  for the different phenols used, in particular for the three methyl-substituted phenols 4-MeP, DMP and TMP. The energy of the charge-transfer transition of these copper-phenolate complexes will decrease with an increase in the ability of the coordinated phenol to donate electron density (originating from the CH<sub>3</sub>-groups on the phenol) to one of the copper ions, resulting in a shift of the charge-transfer (CT) band in the UV/vis spectrum to higher wavelength, i.e. lower energy. Therefore, the charge-transfer band in these particular cases was identified as a ligand-to-metal (LMCT) band, from the phenolate to the copper(II) ion. The presence of strong electron-withdrawing groups (e.g. F or CONH<sub>2</sub>) on the phenol induces a rather big shift of the CT band to lower wavelength, as clearly seen in the UV/vis spectrum of the copper pentafluorophenol adduct ( $\lambda_{\max}$  397 nm). Previous studies on the determination of the nature of charge-transfer band for mononuclear copper-phenolate complexes with simple amine ligands (e.g. pyridine) using substituted chlorophenols have shown that the presence of strong electron-withdrawing groups typifies the CT band as a metal-to-ligand charge transfer.<sup>131</sup> Therefore the CT band of the copper pentafluorophenolate adduct may possibly be better qualified as a metal-to-ligand charge transfer (MLCT) band.

## 7.4 Determination of the nature of the adduct formed upon the addition of TMP

Oxidative C-C coupling of phenols, in particular DMP, as catalyzed by copper complexes, including dicopper species **5a**, can be envisioned to occur via three different mechanistic pathways depicted in Scheme 34.



**Scheme 34.** Mechanistic pathways proposed for the oxidative C-C coupling of DMP.<sup>134</sup>

Previous studies have shown that treatment of DMP with a radical initiator like benzoyl peroxide produced the 2,6-dimethyl-2,5-cyclohexadienone radical<sup>135,136</sup>, which will mainly undergo C-C coupling yielding DPQ as the product. On these grounds, the formation of DPQ is believed to be a radical process, where DMP coordinates to a copper(II) ion with further formation of a copper(I)-phenoxyl radical adduct.

In this sense, the unusual C-C coupling of TMP catalyzed by dicopper(II) complex **5a** can in principle also occur via the three mentioned mechanistic pathways. In order to elucidate and determine the most plausible mechanistic route, Raman and EPR spectroscopy were applied as useful instruments to investigate the phenol binding within the dicopper pocket, with a further possibility to identify the reactive species formed upon substrate coordination,

particularly distinguishing between copper(II)-phenolate and copper(I)-phenoxyl radical character.

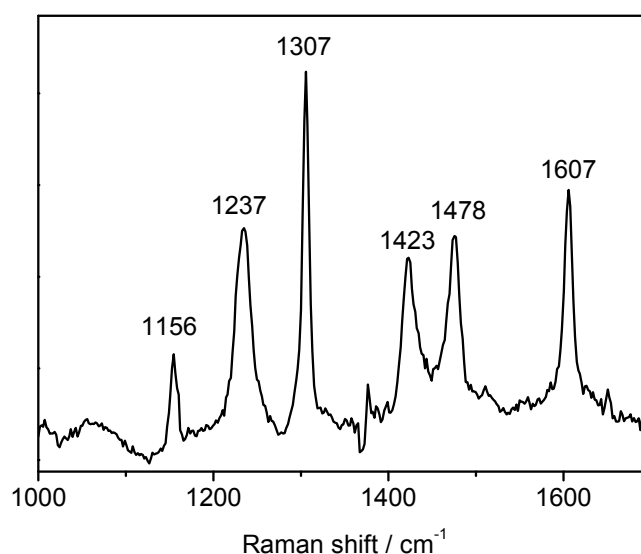
#### 7.4.1. Raman spectroscopy

Coordination of the TMP substrate to the dicopper core of **5a** during the oxidative C-C coupling reaction was proven by means of UV/vis spectroscopy, particularly through the observation of an intense band with  $\lambda_{\text{max}}$  of 495 nm ( $\epsilon \sim 1500 \text{ L mol}^{-1} \text{ cm}^{-1}$ ). This band was assigned to a phenolate-to-copper LMCT transition, based on the relative shift in the UV/vis spectrum depending on the substituents in the phenol ring (see section 7.3). These studies are in good agreement with reported literature data for various TACN-supported mono- and bis(phenolate) copper(II) complexes, with  $\lambda_{\text{max}}$  in the range of  $\sim 430\text{--}540 \text{ nm}$  ( $\epsilon \sim 1000\text{--}2000 \text{ L mol}^{-1} \text{ cm}^{-1}$ ).<sup>137,138,139</sup> In marked contrast to the spectroscopic features observed for such copper-phenolate complexes, the UV/vis absorption spectra of the  $\text{Cu}^{\text{II}}$ -phenoxyl radical complexes show an intense CT band at  $\lambda_{\text{max}} \sim 390\text{--}430 \text{ nm}$  ( $\epsilon \sim 3000\text{--}8000 \text{ L mol}^{-1} \text{ cm}^{-1}$ ) that is generally assigned to the phenoxyl  $\pi\text{--}\pi^*$  transition on the basis of enhancements of radical ring Raman modes upon laser excitation (vide infra).<sup>138,139,140</sup> This initial spectroscopic observation already strongly suggests that coordination of a molecule of TMP within the bimetallic pocket of **5a** leads to the formation of the copper(II)-phenolate and not to a copper(I)-phenoxyl radical complex. It should be noted, however, that spectral characteristics of a copper(I)-phenoxyl radical might be somewhat different from those of a copper(II)-phenoxyl radicals.

Resonance Raman spectroscopy is particularly useful for gaining insight into the structural and electronic properties of both metal-phenoxyl radical as well as metal-phenolate species, and moreover, to distinguish between them.<sup>138,139,140,141,142,143,144</sup> Laser excitation into the  $\pi\text{--}\pi^*$  UV/vis band ( $\lambda_{\text{max}} \sim 400 \text{ nm}$ ) of TACN-supported mono- and bis(phenoxyl radical) copper(II) and zinc(II) complexes – prepared by chemical or electrochemical oxidation of those copper-phenolate compounds – resulted in resonance Raman spectra very similar to those of free phenoxyl radicals,<sup>145,146</sup> with two dominant features at  $\sim 1500 \text{ cm}^{-1}$  ( $\nu_{7a}$ , predominantly C-O stretching) and  $\sim 1600 \text{ cm}^{-1}$  ( $\nu_{8a}$ ,  $C_{\text{ortho}}\text{--}C_{\text{meta}}$  ring stretching). The  $\nu_{7a}$  band in these complexes occurs at  $\sim 250 \text{ cm}^{-1}$  higher energy than in the metal-phenolate precursors, indicative of increased C-O double bond character in the coordinated phenoxyl radicals.

The Raman spectra of the copper(II)-phenolate complexes generally show a set of multiple features between 1100 and 1600  $\text{cm}^{-1}$  that are typical for metal-tyrosinase sites in proteins at 1174, 1270, 1500, and 1598  $\text{cm}^{-1}$  (see also section 8.1).

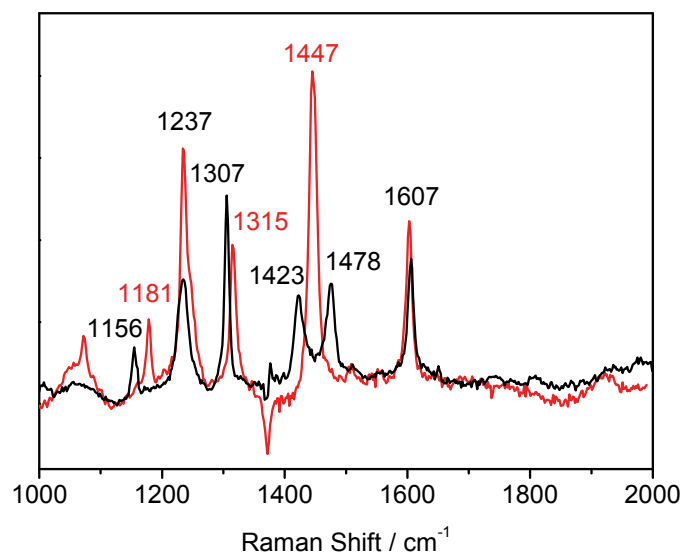
Therefore, Resonance Raman spectroscopy was used in order to provide additional evidence for the formation of either the copper(II)-phenolate or the copper(I)-phenoxyl radical active species upon the coordination of TMP. Because of the spectroscopic features observed in the UV/vis spectrum, laser excitation was performed at 488 nm, into the LMCT band of the adduct with a band at 495 nm. TMP was added to the green solution of dicopper(II) complex **5a** and the Raman spectrum of the resulting red solution was recorded (Figure 47).



**Figure 47.** Resonance Raman spectrum of the mixture of **5a** and TMP in MeCN;  $\lambda_{\text{ex}} = 488$  nm, solvent signals are subtracted.

Typical features for a phenolate coordinated to copper(II) were observed in the Raman spectrum with bands at 1156 ( $\nu_{9a}$  C-H bending), 1237 ( $\nu_{7a}$  C-O stretching), and 1607  $\text{cm}^{-1}$  ( $\nu_{8a}$   $C_{\text{ortho}}-C_{\text{meta}}$  ring stretching). The remaining three signals could not be identified, but they most probably represent the C-H bending and C-C stretching bands of the TMP substrate molecule. For thorough assignment of the characteristic vibrations corresponding to the coordinated phenolate-ring, in particular for the copper-phenolate adduct derived from **5a** and TMP, a model  $CD_3$ -TMP substrate with fully deuterated methyl groups was used. The modified TMP substrate is also active in the oxidative C-C coupling in the *para*-position and behaves in the same fashion towards the dicopper catalyst (i.e. formation of the copper-phenolate adduct, ultimately yielding the C-C coupled product  $\text{TM}^{\text{D}}\text{SQ}$ ; see section 7.2). The Raman spectrum

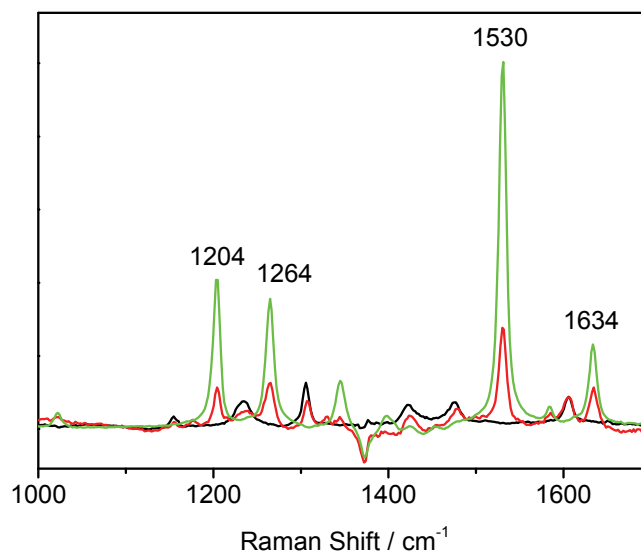
of the reaction mixture of **5a** with  $CD_3$ -TMP was recorded under the same conditions as with TMP and is depicted in Figure 48.



**Figure 48.** Resonance Raman spectra:  $\lambda_{ex} = 488$  nm; black line - mixture of **5a** and TMP in MeCN; red line - mixture of **5a** and  $CD_3$ -TMP in MeCN, solvent signals are subtracted.

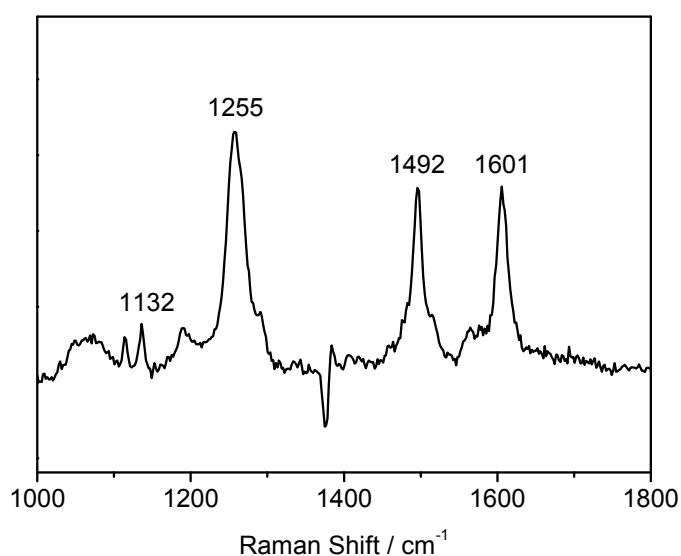
Two peaks at 1237 and 1607  $cm^{-1}$  in the original Raman spectrum with TMP remained unaffected by the introduction of the  $CD_3$ -groups in the phenol ring. This result is in good agreement with the definition of the stretching character of the two mentioned signals:  $\nu_{7a}$  (C-O stretching) and  $\nu_{8a}$  ( $C_{ortho}$ - $C_{meta}$  ring stretching) which should not have any C-H contribution. A strong influence of the  $CD_3$ -groups on the other stretching values of the phenol ring is indicated by the observed shifts of the signals at 1156 and 1307  $cm^{-1}$  to higher wavenumbers ( $\Delta\nu$  of +25  $cm^{-1}$  and +8  $cm^{-1}$ ). Therefore, any contribution of the  $CH_3$ -groups on the two mentioned bands can be excluded and, moreover, introduction of the  $CD_3$ -groups influenced only the C-H bending of the phenol ring itself. This is in good agreement with the fact that the signal at 1156  $cm^{-1}$  is assigned as C-H bending of the phenolate-ring for *para*-substituted phenols.<sup>147</sup>

Moreover, the oxidative C-C coupling of TMP catalyzed by **5a** to yield TMSQ was followed by Raman spectroscopy over a period of  $\sim 8$  h. Formation of the quinone product had already started after 2 h of reaction time (Figure 49) as indicated by the appearance of signals at 1204, 1264, 1530 and 1634  $cm^{-1}$  assigned to TMSQ, which most likely correspond to C-H bending (first signal), C-O and the ring C-C stretching vibrations (two last signals), respectively.



**Figure 49.** Resonance Raman spectra:  $\lambda_{\text{ex}} = 488$  nm; black line - mixture of **5a** and TMP in MeCN; red line - mixture of **5a** and TMP after 140 min; green line - TMSQ in MeCN, solvent signals are subtracted.

In order to learn more about the spectroscopic features of the dinuclear copper(II)-phenolate adducts with **5a**, dicopper complex **5a** was reacted with various phenols that are inert in any kind of oxidation reaction, focussing in particular on 2-methyl-4-*tert*-butylphenol (MtBuP). Laser excitation into the LMCT band of the copper-phenolate adduct with MtBuP ( $\lambda_{\text{max}} \sim 475$  nm) led to the resonance effect in the Raman spectrum depicted in Figure 50.



**Figure 50.** Resonance Raman spectrum of the mixture of **5a** and MtBuP in MeCN;  $\lambda_{\text{ex}} = 488$  nm, solvent signals are subtracted.



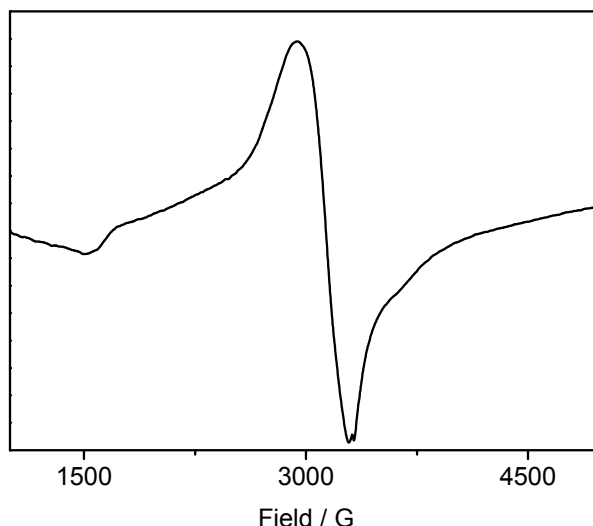
The Raman spectrum of the copper(II)-phenolate complex formed upon addition of *MtBuP* showed typical features for phenolate-ring deformation at 1132, 1255, 1492 and 1601  $\text{cm}^{-1}$ . Hence, the detected signals appeared in the same range as for the copper-phenolate species with the active TMP substrate and the only difference observed is the absence of the signals at 1307, 1423 and 1478  $\text{cm}^{-1}$ ; these presumably correspond to some modified copper(II)-phenolate active species formed further on in the catalytic reaction with TMP or to a TMP molecule coordinated within the bimetallic pocket itself.

The Raman measurements clearly allow the species formed upon coordination of the TMP within the bimetallic pocket of **5a** to be described as a copper(II)-phenolate adduct.

#### 7.4.2 EPR studies

The use of EPR spectroscopy is very limited in case a phenoxyl radical is coordinated to copper(II), due to the antiferromagnetic coupling between the unpaired electron of the copper(II) ion and the electron of the radical species. Therefore, in order to gain insight into the spectroscopic properties of the coordinated phenoxyl radical without interference from features due to the  $d^9$   $\text{Cu}^{\text{II}}$  ion, many studies were performed on the  $\text{Zn}^{\text{II}}$ -phenoxyl radical analogs.<sup>139,143,148</sup> The EPR spectra of these complexes exhibit an  $S = \frac{1}{2}$  signal centered at  $g \sim 2.0$ , similar to those for free phenoxyl radicals.<sup>149</sup>

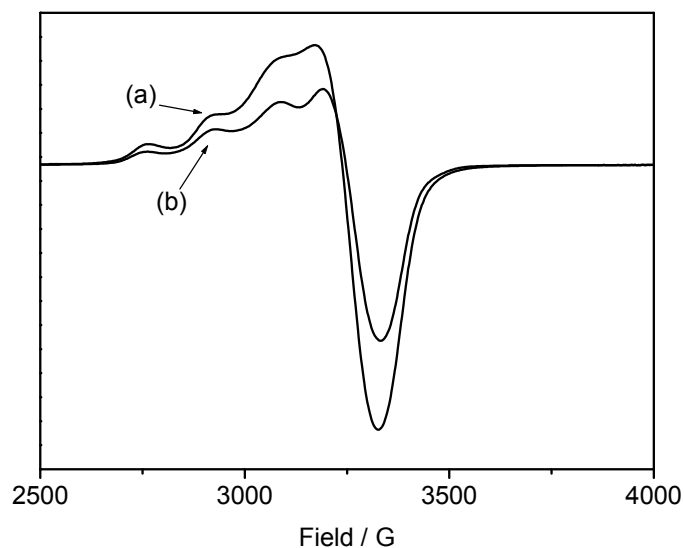
It was shown, by means of both UV/vis and Raman spectroscopy, that coordination of the TMP substrate to the dicopper(II) core of **5a** led to formation of a dicopper(II)-phenolate species. EPR studies of the red solution containing this dicopper(II)-phenolate species at room temperature were not informative: the broad signal, observed for dicopper(II) complex **5a** (which is typical for dinuclear copper(II) complexes with pyrazole-based ligands at room temperature) remained completely unchanged upon addition of TMP. Studies at lower temperature (120 K) revealed the same result. This broad signal with a weak half-field signal, characteristic for an exchange-coupled antiferromagnetic dicopper(II) system in the case of **5a** appears as the result of significant interaction between the two copper(II) ions and only at very low temperature (15 K) this complex is EPR-silent, due to antiferromagnetic coupling (see section 5.4.4) and an  $S = 0$  ground state (Figure S1).



**Figure 51.** EPR spectrum of **5a** in MeCN glass at 50 K.

On the one hand it can be argued that this particular interaction between two copper(II) ions is also observed in the dicopper(II)-phenolate species, leading to the same EPR behaviour as for **5a**. On the other hand, the broad signal in the EPR spectrum of the red solution can be interpreted as stemming from a copper(II)copper(I)-phenoxyl radical species, which would also yield a spectrum for an exchange-coupled system, and might not be very different from that of **5a**.

With the idea to exclude any interaction between the  $d^9$  copper(II) ions upon coordination of the TMP molecule, a model dinuclear copper-zinc complex was synthesized to perform analogous EPR studies on a system where the second metal ion is EPR silent. To a solution of the deprotonated ligand **HL**<sup>4</sup> in MeCN/MeOH (1:1, v/v) one equivalent of both  $\text{Cu}(\text{ClO}_4)_2 \cdot 6\text{H}_2\text{O}$  and  $\text{Zn}(\text{ClO}_4)_2 \cdot 6\text{H}_2\text{O}$  were added. The obtained blue-green solution was additionally treated with one equivalent of KO<sup>*t*</sup>Bu to establish a hydrogen-bonded  $\text{MeO} \cdots \text{HOME}$  bridge between the two metal ions. The EPR spectrum of the frozen solution of this copper-zinc complex was measured at 15 K (Figure 52).



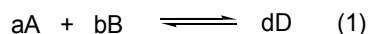
**Figure 52.** EPR spectra at 15 K: (a) frozen solution of the  $\text{Cu}^{\text{II}}\text{Zn}^{\text{II}}$  model complex; (b) frozen solution of the  $\text{Cu}^{\text{II}}\text{Zn}^{\text{II}}$  complex after addition of TMP.

A characteristic four-line pattern, expected for an isolated  $d^9$   $\text{Cu}^{\text{II}}$  ion, was observed in the EPR spectrum of the  $\text{Cu}^{\text{II}}\text{Zn}^{\text{II}}$  complex, which confirmed the presence of the mixed metal species (the other possibly formed species, i.e.  $\text{Cu}^{\text{II}}\text{Cu}^{\text{II}}$  and/or  $\text{Zn}^{\text{II}}\text{Zn}^{\text{II}}$ , are EPR silent at 15 K). No significant changes were observed upon the addition of TMP substrate to the solution of the  $\text{Cu}^{\text{II}}\text{Zn}^{\text{II}}$  complex, which strongly suggests formation of the copper(II)-phenolate adduct also with this dinuclear complex. Surprisingly, the colour of the solution changed from blue-green to green without formation of the typical red colour of copper(II)-phenolate complexes. In this light, it can be assumed that the presence of the second copper(II) ion is necessary for the characteristic CT transition band to occur. Unfortunately, all attempts to crystallize the  $\text{Cu}^{\text{II}}\text{Zn}^{\text{II}}$  species led to formation of the dicopper(II) or dizinc(II) complexes as crystalline compounds.

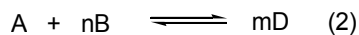
## 7.5 Determination of the amount of coordinated phenol

### 7.5.1 General

Job's Method,<sup>150</sup> also called the Method of Continuous Variation, is a simple and effective approach to determine the stoichiometry for any chemical reaction with a general description as in Eq (1).



This equation can be rewritten into the form of (2) by dividing all coefficients by "a".



where  $n = b/a$  and  $m = d/a$ .

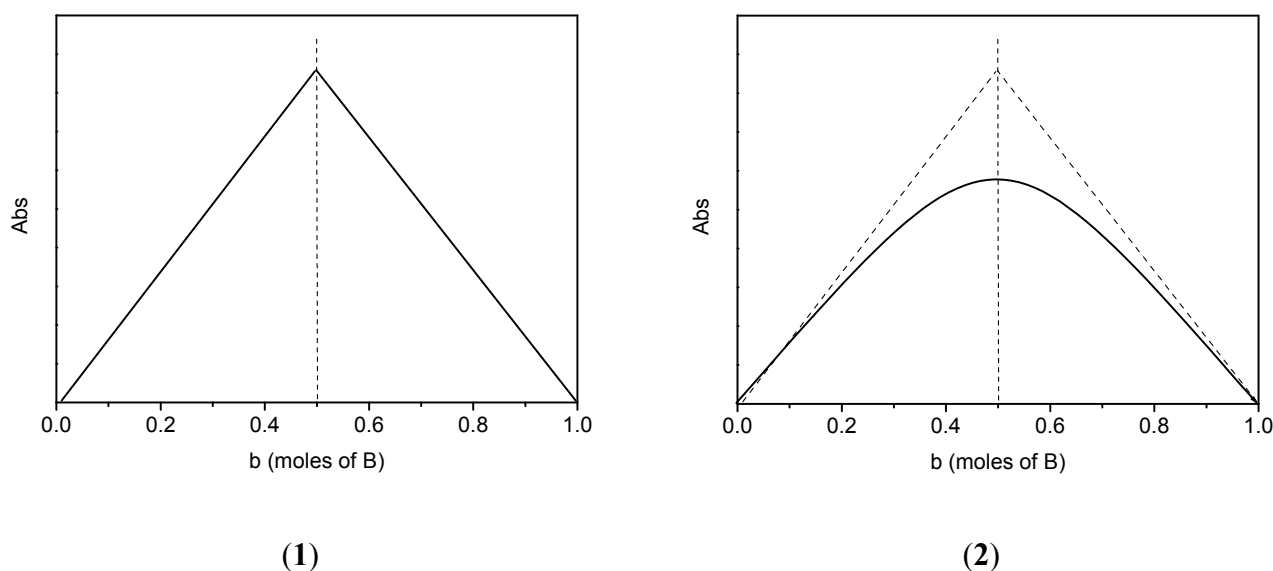
Job's method is based on the following fact: *if a series of solutions is prepared, each containing the same total number of moles of A and B, but a different ratio R of moles B to moles A, the maximum amount of product D is obtained in the solution in which  $R = n$  (the stoichiometric ratio)*. This method is therefore useful and practical when information is sought about the formation of particular ligand-adducts of metal complexes or to deduce the maximum number of substrates B capable of coordinating to a given metal species A. To implement Job's Method experimentally, one prepares a series of solutions containing a fixed total number of moles of A and B, but in which their ratio R is systematically varied from large to small, and then measures the amount of product obtained in each solution (e.g. via UV/vis spectroscopy). Then the amount of product (in case of UV/vis measurements represented by the absorption value) is plotted *versus* the molar fraction in B (b), and a maximum in the plot is obtained at the initially unknown value of n (amount of the coordinated compound), that can be calculated with the simple equation  $n = b/a$  (Table 15).

**Table 15.** Relation between b value obtained experimentally from Job's plot and n (amount of the coordinated compound).

b	n
0.33	0.5
0.50	1
0.66	2
0.75	3
0.80	4

Thus, for the present systems, a series of solutions was prepared by mixing different volumes of equimolar solutions of the two components (i.e. the appropriate dicopper complex A and phenol substrate B), followed by dilution to a constant volume to give solutions with identical total molar concentrations but different molar fractions. The UV/vis spectrum for each sample

was then recorded. If a single, stable complex is formed, i.e. one that shows no appreciable dissociation, a plot of the absorbance versus the mole fraction of reactant B (phenol) gives a characteristic triangular correlation (Figure. 53 (1)). The mole fraction of the maximum of this plot, the apex of the triangle, indicates the molar composition of the formed complex. However, if a weak complex is formed, a very curved plot results (Figure. 53 (2)).

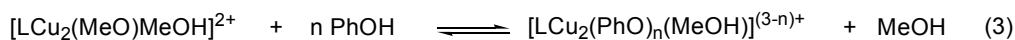


**Figure 53.** Schematic representation of Job's plots of stable (not dissociated) (1) and weak (2) complexes.

For a moderately stable complex, the molar composition of the complex can be obtained from the point of intersection of the tangents to the curve. However, for complexes where the dissociation constant  $K_d$  (see Eq. (4)) is too large, the value for  $n$  can not be determined very reliably using the continuous variations method as described by Job.

### 7.5.2 Job plot of TMP with dicopper complex **5a**

Coordination of a phenol substrate like TMP to the dicopper complex **5a** can be described with the equilibrium reaction given in Eq. (3). Methanolate, which serves as internal base, undergoes exchange with phenol substrate, resulting in release of a methanol molecule and formation of a dicopper(II)-phenolate species. However, depending on the reaction conditions, coordination of more than one phenol molecule is conceivable.

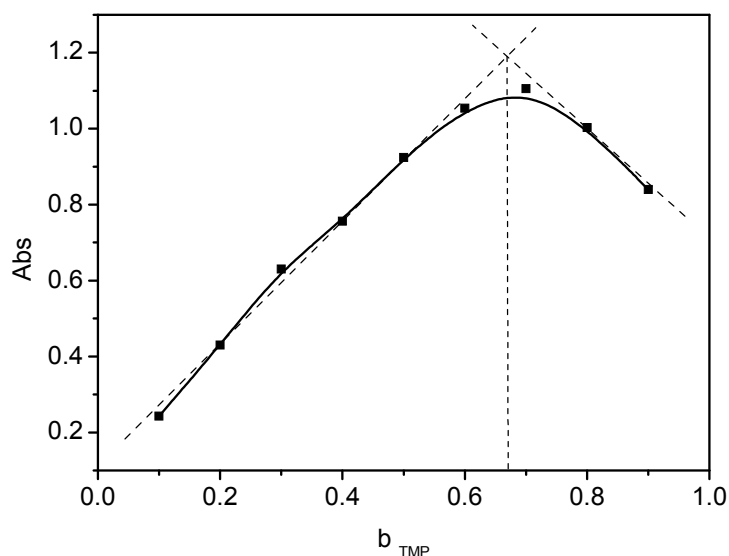


Solutions of the dicopper complex and phenol used to perform a Job experiment were equimolar with concentrations equal to  $C_0$ . Taking this into account, the maximum number of coordinated phenol molecules  $n$  can be calculated accurately from the equation  $n = b/a$  only when  $K_d$  (dissociation constant of phenolate adduct, Eq. (4)) is significantly smaller than  $C_0$  and can therefore be ignored in Eq. (5).

$$K_d = \frac{[\text{LCu}_2(\text{MeO})\text{MeOH}]^{2+} [\text{PhOH}]^n}{[\text{LCu}_2(\text{PhO})_n]^{(3-n)+}} = \frac{[\text{A}] [\text{B}]}{[\text{D}]} \quad (4)$$

$$\frac{b}{a} = \frac{K_d + nC_0}{K_d + C_0} \sim n \quad (5)$$

Because of the further reactivity of the dicopper(II)-phenolate species formed after addition of TMP to **5a**, determination of the stoichiometry for the C-C coupling reaction of TMP to yield TMSQ was performed using time-resolved stopped-flow UV/vis spectroscopy. In the presence of dioxygen, solutions of substrate and complex in MeCN (total concentration of 47 mM) were mixed in different ratios, and the reaction was followed until the phenolate-to-copper LMCT band at  $\lambda_{\text{max}}$  495 nm had reached its maximum. The corresponding absorption value for each mixture was plotted *versus* the molar fraction in phenol (b) (Figure 54). The maximum amount of TMP coordinated to the dicopper core of complex **5a** was found to be 2 (Table 15).



**Figure 54.** Job plot of TMP with dicopper complex **5a**,  $\lambda_{\text{max}} = 495$  nm.

The curved plot shows that the dicopper(II)-phenolate complex formed upon coordination of TMP within the bimetallic pocket exhibits fairly low overall stability owing to moderate binding of the phenolate (strong enough to accomplish appropriate activation of the total substrate fragment and therefore reactivity to occur, but weak enough to ensure that the product leaves after reaction and is thus isolable) and substantial dissociation occurs, which is indeed necessary to enable the further reaction steps with final formation of TMSQ.

The maximum number of coordinated TMP molecules indicated by the Job plot measurements requires careful consideration, since the copper-phenolate species is not very stable, and therefore the approximation  $K_d \ll C_0$  and the corresponding simplification in Eq. (5) are invalid. Nevertheless, it can be assumed that coordination of two TMP molecules to the dicopper core in **5a** requires some structural changes in the bimetallic core, which shows that catalytic oxidative C-C coupling of TMP to TMSQ is a complicated process.

In order to perform further studies on the formation of copper-phenolate species in solution and to gain knowledge about the driving force needed to accomplish activation of TMP as the key step for the reaction to occur, various phenols that are inert to any kind of oxidation reactions catalyzed by **5a** were applied as model substrates. The binding of these phenols was proven by detection of the phenolate-to-copper LMCT band using UV/vis spectroscopy. Job's technique described above was applied in order to determine the stoichiometry upon binding of the model phenol substrates to the dicopper complex **5a**.

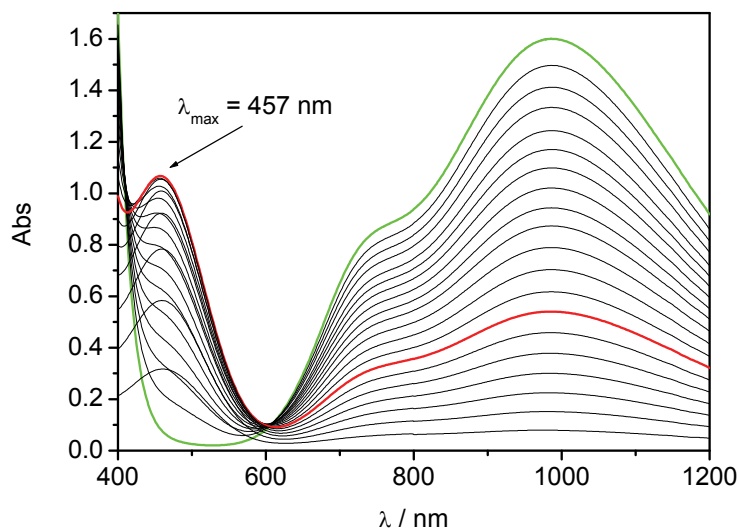
### 7.5.3 Job plot of 4-methylphenol and 4-*tert*-butylphenol with dicopper complex **5a**

Initial model studies on the binding of phenol substrates to the dicopper core in **5a** were performed using *p*-cresol (4-MeP), an analogue of TMP. Addition of *p*-cresol to a green solution of **5a** in MeCN led to a visible colour change of the solution from green to red with appearance of an LMCT band at  $\lambda_{\text{max}}$  457 nm in the UV/vis spectrum. No spectroscopic changes were observed after storing the red solution in air for one week, which confirmed the “inert nature” of 4-MeP in any kind of transformation in the presence of **5a**.

*This unreactivity of p-cresol compared to DMP and TMP, particularly in the copper-catalyzed oxidative para C-C coupling, could be explained by the varying number of electron-donating CH<sub>3</sub>-groups on the aromatic ring of each phenol, which are most likely responsible for activation of the substrate while coordinated to the dicopper core in 5a. Additional CH<sub>3</sub>-groups not only ensure a stronger binding of the phenolate to the copper ion (as reflected in the  $\lambda_{\text{max}}$ , section 7.3) but also enhance the formation of a reactive species. Thus, for any further reactivity to occur (formation of C-C coupled product) the presence of at least two CH<sub>3</sub>-groups on the phenol substrate is required.*

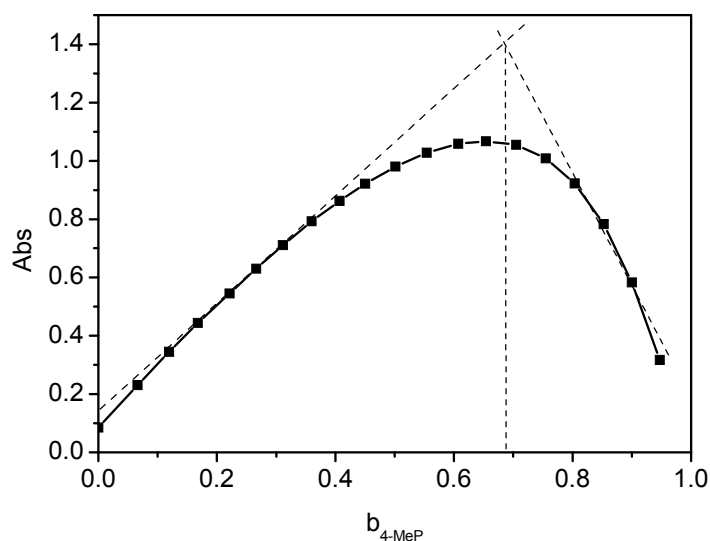
The Job plot of 4-MeP (as well as other model phenol substrates) with **5a** was performed in a slightly different manner compared to the previous experiments described in this chapter. The initial solution of dicopper complex **5a** in MeCN was diluted further in a stepwise manner (each dilution representing a certain complex to phenol ratio R) by addition of a solution of phenol with a constant concentration. Thus, for the Job plot of 4-MeP with **5a**, solutions with a concentration of 48 mM were used and the UV/vis spectrum of the mixture was recorded after each dilution step (Figure 55). It has to be mentioned that a dilution effect for the band of interest ( $\lambda_{\text{max}} = 457$  nm) could be observed during the experiment as reflected in UV/vis spectrum, but only after the maximum absorbance (and therefore the maximum number of coordinated phenol) of the dicopper(II)-phenolate species was reached.





**Figure 55.** UV/vis spectrum of the mixture after each dilution step: green line (initial dicopper complex **5a**); red line (solution of **5a** and 4-MeP with a maximum absorbance).

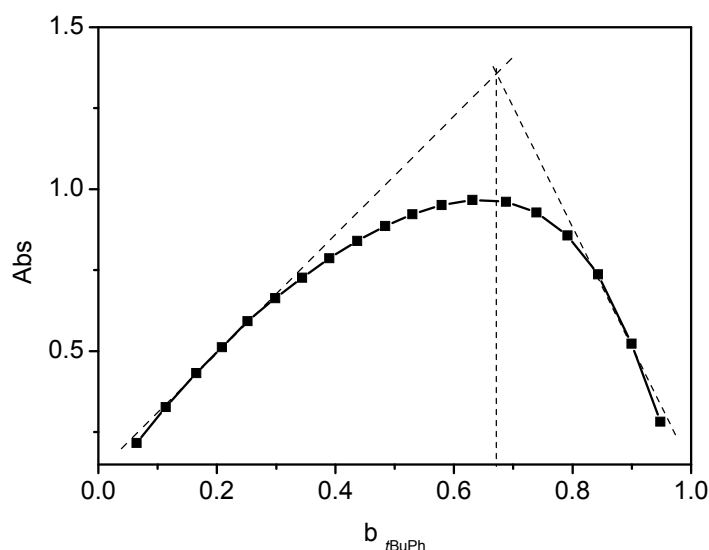
From the Job plot depicted in Figure 56 it can be deduced that a maximum of two molecules of 4-MeP can be coordinated to the dicopper core of complex **5a**, similar to the situation with TMP.



**Figure 56.** Job plot of *p*-cresol with dicopper complex **5a**,  $\lambda_{\text{max}} = 457$  nm.

A Job plot of 4-*tert*-butylphenol *t*BuP with **5a** was performed using 49 mM solutions of both components. The corresponding absorption value of the LMCT band ( $\lambda_{\text{max}} = 455$  nm) for each mixture after dilution was plotted *versus* the molar fraction in *t*BuP (*b*) (Figure 57). The

maximum number of *t*BuP molecules coordinated to the dicopper core of complex **5a** was also found to be two.



**Figure 57.** Job plot of *t*BuP with dicopper complex **5a**,  $\lambda_{\text{max}} = 455$  nm.

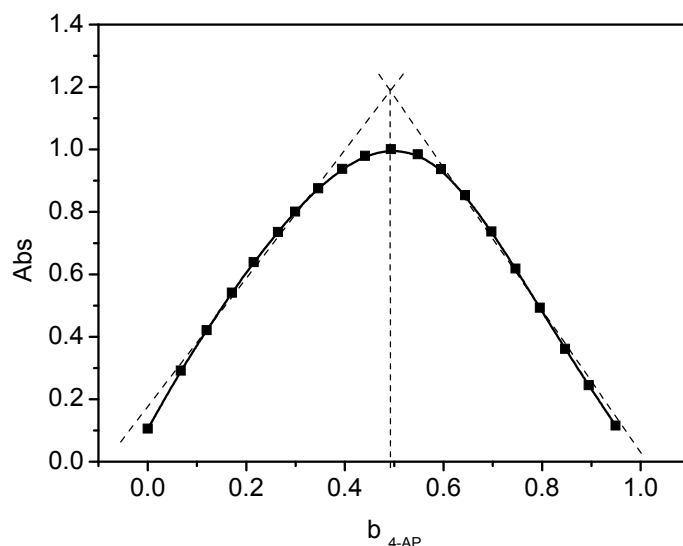
The curved shape for this Job plot - as in the case of 4-MeP - shows that the dicopper-phenolate complex formed upon coordination of *t*BuP to the dicopper complex exhibits rather low stability, but in contrast to TMP this low stability does not induce any further reactivity and results only in dissociation of the phenolate species. This became evident when all attempts to crystallize any of the observed alkyl-substituted dicopper-phenolate species only led to regeneration and isolation of the initial dicopper(II) complex **5a**, indicative of significant dissociation of the phenolate species under these conditions.

Based on these results, it can be assumed that a key factor required for further reaction to occur is not the number of coordinated phenol substrates, as the Job plot experiments have indicated the same values for TMP, 4-MeP and *t*BuP, but the electronic and steric properties of the substituents on the phenol ring.

#### 7.5.4 Job plot of 4-hydroxybenzamide and pentafluorophenol with dicopper complex **5a**

Further studies on the binding of phenol molecules within the dicopper pocket of **5a** were done using phenols with electron-withdrawing groups, like pentafluorophenol (PFP) and 4-

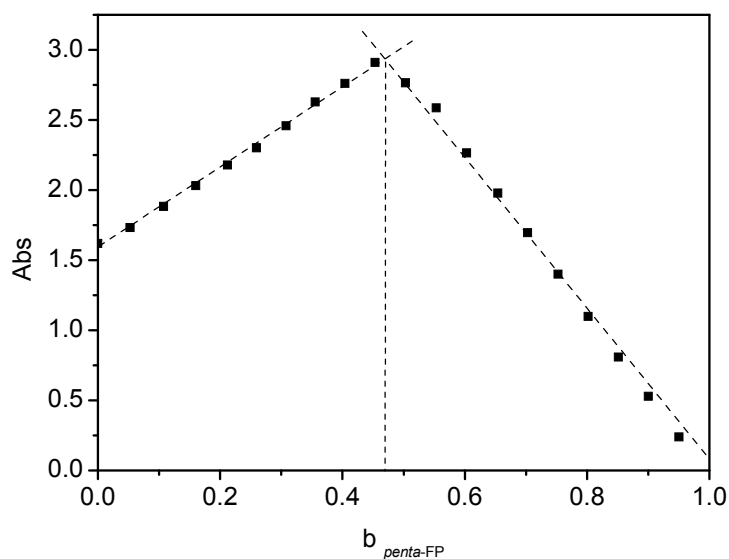
hydroxybenzamide (4-AP). Addition of 4-AP to a solution of **5a** in MeCN led to the formation of a yellow-green solution with an LMCT band at  $\lambda_{\text{max}}$  446 nm, which is in sharp contrast to the previously described observations after phenol addition, where red solutions were obtained. The highest absorption value reached in the Job plot experiment corresponded to a complex with a 1 to 1 ratio of 4-AP and **5a** (Figure 58).



**Figure 58.** Job plot of 4-AP with dicopper complex **5a**,  $\lambda_{\text{max}} = 446$  nm.

In this case only one phenol molecule is able to coordinate to the dicopper core. The slightly curved plot (the deviation from a perfect triangular shape is significantly smaller than for any of the phenols discussed in section 7.5.3) shows that the dicopper phenolate complex exhibits moderate stability and dissociation of the phenolate species is still likely to occur to some degree in solution. Nonetheless, crystallization of a solution of **5a** with excess of 4-AP in MeCN by slow diffusion with Et<sub>2</sub>O led to the formation of a crystalline compound. Single crystals were used for an X-ray crystallographic analysis and the formation of a complex with only one coordinated 4-AP molecule was unambiguously proven (see section 8.2).

The UV/vis spectrum of the yellow-green solution formed after addition of PFP to dicopper complex **5a** in MeCN showed an intense CT band at  $\lambda_{\text{max}}$  397 nm. Formation of a very stable copper-pentafluorophenolate complex was evidenced by a Job's experiment, as the corresponding plot of absorbance versus the mole fraction  $b$  of PFP featured the characteristic triangular correlation (Figure 59). The optimal value of  $b \sim 0.5$  implies that this stable complex contains only one coordinated pentafluorophenolate molecule.



**Figure 59.** Job plot of PFP with dicopper complex **5a**,  $\lambda_{\text{max}} = 397$  nm.

Single crystals of this phenolate adduct were obtained and coordination of only one PFP molecule was unequivocally proven by X-ray crystallography (see section 8.2).

A set of Job experiments carried out with different phenols as substrate molecules clearly showed that the deciding factor for C-C oxidative coupling to occur - after coordination of the phenol substrate has taken place - is not the number of coordinated phenols, but the electronic properties of the substituents on the phenol ring. Moreover, stable (mono)phenolate adducts could be isolated and even crystallized in case of strong electron-withdrawing substituents on the phenol ring.

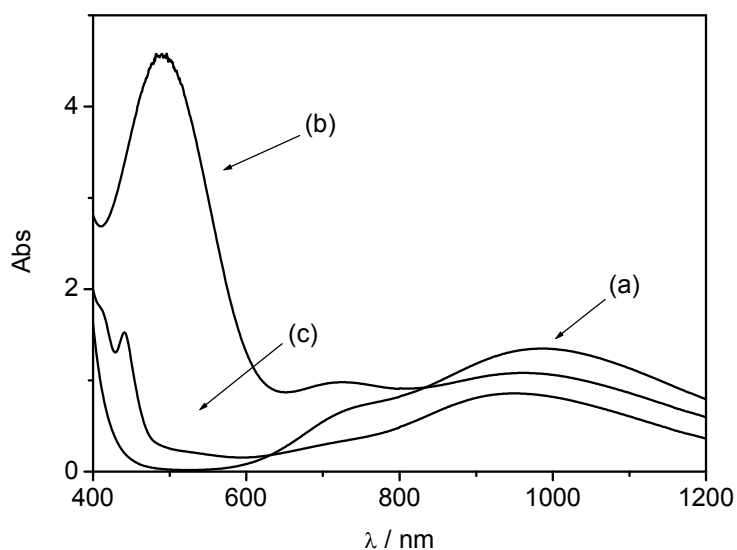
## 7.6 Mechanistic studies of C-C coupling of TMP under anaerobic conditions

The catalytic oxidative C-C coupling of TMP to yield TMSQ, catalyzed by dicopper complex **5a** and with dioxygen as the oxidant, is an overall 6-electron process ( $3e^-$  per TMP molecule) which implies a rather complicated overall reaction pathway. The formation of TMSQ as the final product is expected to proceed through a series of intermediate species, each of which presumably requires the formation of an at least partially reduced dicopper species. The proposed reaction pathway is described in more detail in section 12. Therefore, initial mechanistic studies were performed under anaerobic conditions with the aim to determine the

role of dioxygen in the oxidative C-C coupling of TMP and to trap possible intermediates (both organic compounds and copper species).

### 7.6.1 UV/vis studies under N<sub>2</sub>-atmosphere

Addition of TMP to a green solution of **5a** (Figure 60 (a)) under an N<sub>2</sub>-atmosphere led to the same spectroscopic changes as for the analogous reaction in the presence of dioxygen, i.e. instantaneous formation of a red solution with concomitant appearance of an intense LMCT band at  $\lambda_{\text{max}}$  495 nm ( $\epsilon \sim 1500 \text{ L}\cdot\text{mol}^{-1}\cdot\text{cm}^{-1}$ ) and a shift of the Cu<sup>II</sup>-based *d-d* transition band from 989 nm to 960 nm (Figure 60 (b)). This shift indicates slight geometric changes of the copper ion/ions from trigonal bipyramidal to square planar geometry upon substitution of methanolate for phenolate within the bimetallic pocket.



**Figure 60.** UV/vis spectra at different stages of the oxidative coupling of TMP under anaerobic conditions (initial concentration of **5a** =  $0.005 \text{ mol}\cdot\text{L}^{-1}$ ; initial concentration of TMP =  $0.025 \text{ mol}\cdot\text{L}^{-1}$ ; solvent: MeCNCN/CH<sub>2</sub>Cl<sub>2</sub> 4:6 v/v): (a) starting solution of **5a**; (b) a few minutes after addition of TMP (red solution); (c) 48 h after addition of TMP (only traces of TMSQ are observed).

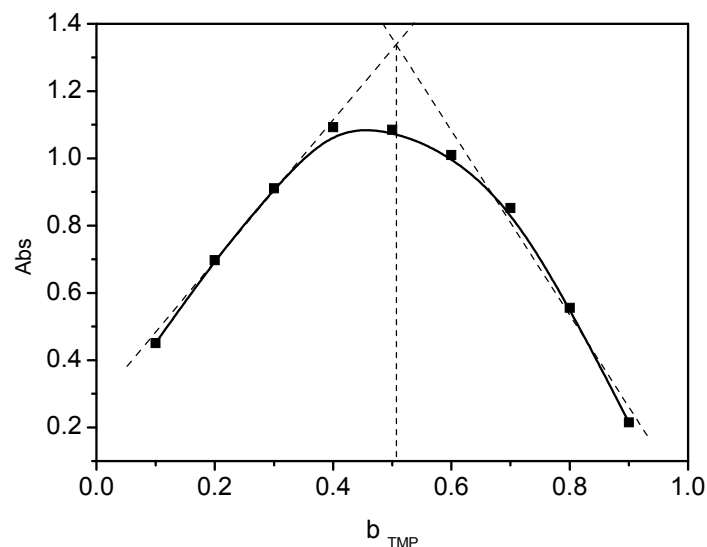
Complete disappearance of the charge-transfer band was observed within 48 h, concomitant with formation of a yellow-green solution with a Cu<sup>II</sup>-based *d-d* transition band at  $\lambda_{\text{max}}$  947 nm. Only traces of the TMSQ product were detected; this product has a very large extinction

coefficient  $\varepsilon$  of *ca.* 96000 L·mol<sup>-1</sup>·cm<sup>-1</sup> and therefore even traces already show up quite pronounced in the UV/vis spectrum (Figure 60 (c)). The yellow-green solution formed after this first reaction step can be stored under an N<sub>2</sub>-atmosphere indefinitely, without any observable spectroscopic and visual changes. For any further oxidation reaction to occur the presence of dioxygen is required. Addition of O<sub>2</sub> induced an instantaneous colour change from yellow-green to the initially observed red colour and the product TMSQ started to form 10 minutes after introducing dioxygen to the catalytic system.

It was deemed interesting to study the coordination of TMP within the bimetallic pocket of **5a** in the absence of oxygen, since in this case the reaction can be halted at the first intermediate stage and only stoichiometric processes can take place.

### 7.6.2 Job plot of TMP with **5a** under anaerobic conditions

Determination of the stoichiometry for the reaction of TMP with dicopper complex **5a** in the absence of dioxygen was performed using time-resolved stopped-flow UV/vis spectroscopy. Solutions of the TMP substrate and the complex in MeCN (50 mM) were prepared in an N<sub>2</sub>-filled glove box and then mixed in different ratios; and the reaction was followed until the LMCT band at 495 nm had reached its maximum (after 9 min for each sample). Absorption maxima for each mixture were plotted *versus* the molar fraction in TMP (Figure 61). In contrast to the results obtained from the Job plot experiments in the presence of O<sub>2</sub>, where two TMP molecules were found to be interacting with dicopper complex **5a**, the maximum number of TMP molecules coordinating to **5a** under an N<sub>2</sub>-atmosphere was found to be only one.

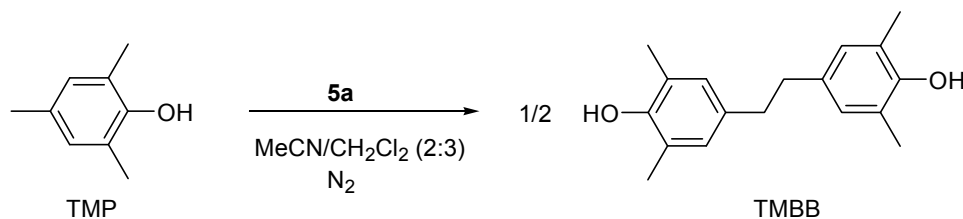


**Figure 61.** Job plot of TMP with **5a** under anaerobic conditions,  $\lambda_{\text{max}} = 495$  nm.

From these studies it can be concluded that coordination of TMP within the bimetallic pocket of **5a** occurs under anaerobic conditions as well, while further formation of TMSQ can take place only in the presence of dioxygen. Disappearance of the charge-transfer band and formation of the yellow-green solution indicate the complete absence of the initially formed copper-phenolate species after 48 h of reaction under anaerobic conditions, which is clear evidence for its participation in the oxidative coupling reaction.

### 7.6.3 Trapping of the intermediates under anaerobic conditions

The observation that under anaerobic conditions the reaction can be halted at what appears to be an intermediate stage of the overall oxidative coupling reaction, encouraged to attempt the synthesis of this organic intermediate on a sufficiently large scale to allow its isolation and characterization. Thus, 250 mmol of TMP and 50 mmol of dicopper complex **5a** were reacted under an inert atmosphere to generate, after flash chromatography, a white powder. The product could be identified as 4,4'-dihydroxy-3,3',5,5'-tetramethylbibenzyl (TMBB) (Scheme 35).

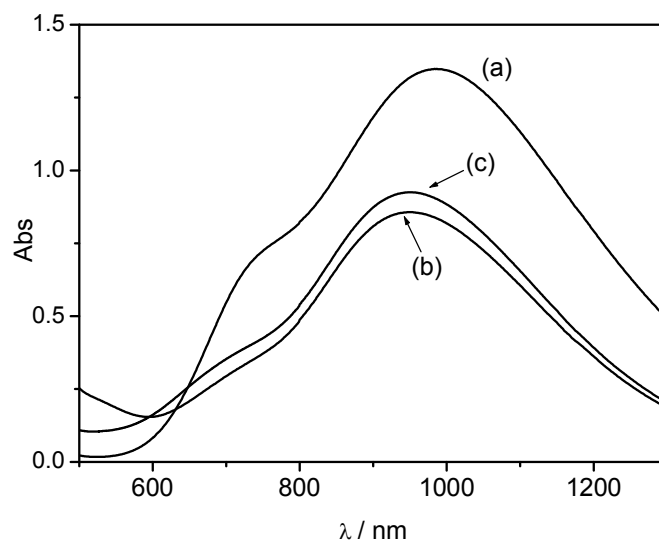


**Scheme 35.** C-C coupling of TMP catalyzed by **5a** under an N<sub>2</sub>-atmosphere.

This overall  $2e^-$  process (based on the product) proceeds stoichiometrically via abstraction of an electron from TMP by the dicopper system. In this case only one out of the five equivalents of TMP used in the reaction can undergo a chemical transformation to yield TMBB, which was indeed confirmed by  $^1\text{H}$  NMR studies. Around 80 % (4 equivalents) of TMP was found to be unreacted after the first reaction step in the glove box and the other 20% (1 equivalent) underwent C-C coupling to form TMBB in 100% yield based on redox equivalents corresponding to formation of the dicopper complex in its  $\text{Cu}^{\text{I}}\text{Cu}^{\text{II}}$  state. This intermediate organic species (when isolated) is stable in air and can be further oxidized to TMSQ by oxygen *only* in the presence of the original dicopper complex **5a**: upon exposure of TMBB to O<sub>2</sub> in the presence of **5a** the initially observed charge-transfer band ( $\lambda_{\text{max}} = 495 \text{ nm}$ ) reappeared in the UV/vis spectrum and instantaneous formation of TMSQ was observed.

In order to spectroscopically prove the formation of a dinuclear mixed-valence  $\text{Cu}^{\text{I}}\text{Cu}^{\text{II}}$  species after formation of TMBB under an N<sub>2</sub>-atmosphere, an independently synthesized model  $\text{Cu}^{\text{I}}\text{Cu}^{\text{II}}$  complex was used for comparison. A solution of **HL**<sup>4</sup> in a mixture of MeCN/CH<sub>2</sub>Cl<sub>2</sub> was treated with 1 equivalent of KO<sup>*t*</sup>Bu to deprotonate the pyrazole NH-unit, and 1 equivalent of both  $\text{Cu}(\text{ClO}_4)_2 \cdot 6\text{H}_2\text{O}$  and  $[\text{Cu}(\text{MeCN})_4](\text{ClO}_4)$  were subsequently added, yielding a light-green solution. The UV/vis spectrum of the resulting solution, with an equal concentration as for the experiment performed with **5a**, was recorded in an inert atmosphere (Figure 62 (c)).





**Figure 62.** UV/vis spectra under anaerobic conditions: (initial concentration of **5a** = 0.005 mol·L<sup>-1</sup>; initial concentration of TMP = 0.025 mol·L<sup>-1</sup>; solvent: MeCN/CH<sub>2</sub>Cl<sub>2</sub> 4:6 v/v): (a) starting solution of **5a**; (b) 48 h after addition of TMP; (c) 0.005 mol·L<sup>-1</sup> solution of the model Cu<sup>I</sup>Cu<sup>II</sup> complex).

The overall spectral features of the solution of the model Cu<sup>I</sup>Cu<sup>II</sup> complex, and most notably the absorption maximum at  $\lambda_{\text{max}}$  947 nm (as well as the approximate value for the extinction coefficient), are very similar to those observed in the UV/vis spectrum of the yellow-green solution formed after reaction and storage for 48 h in the nitrogen filled glove box.

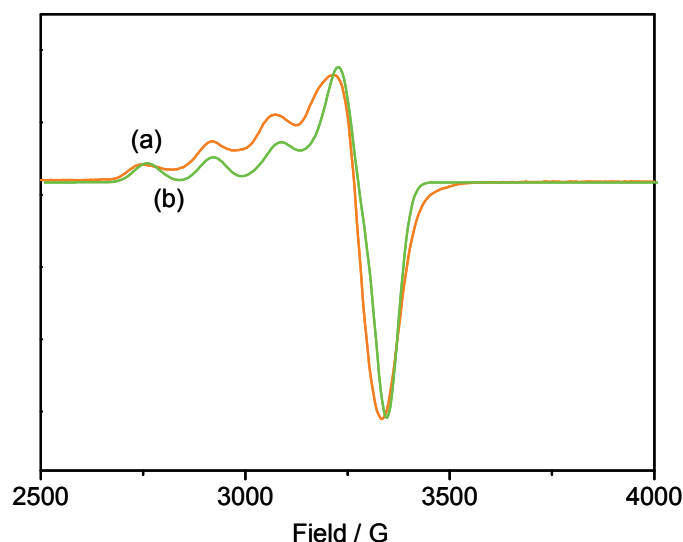
*Therefore, on the basis of these results, the yellow-green solution was characterized as a mixture of stoichiometrically formed TMBB and mixed-valence Cu<sup>I</sup>Cu<sup>II</sup> complex, generated by partial reduction of the original dicopper(II) complex **5a**.*

#### 7.6.4 Evidence for the formation of a mixed-valence Cu<sup>I</sup>Cu<sup>II</sup> species

Formation of the mixed-valence Cu<sup>I</sup>Cu<sup>II</sup> species after 48 h of storage in an N<sub>2</sub>-atmosphere was also proven by means of EPR spectroscopy. Copper(II) is especially amenable to EPR investigation, because it has only one unpaired electron and in addition, the <sup>63</sup>Cu and <sup>65</sup>Cu (nuclear spin 3/2) nuclei give rise to a characteristic four-line pattern because of electron-nuclei-spin interaction, denoted by the hyperfine parameter A.

The initial dicopper(II) complex **5a** is EPR-silent (under the low temperature conditions used for the measurements: 15 K) due to the strong antiferromagnetic interaction (see section 5.4.4 and 7.4.2) between the two copper ions, brought about by the bridging pyrazolate unit. On this basis, it can be reasoned that a dinuclear mixed-valence  $\text{Cu}^{\text{I}}\text{Cu}^{\text{II}}$  species should be detectable at low temperature.

First of all, the X-band EPR spectroscopic measurement of a frozen solution of the independently synthesized  $\text{Cu}^{\text{I}}\text{Cu}^{\text{II}}$  model complex in MeCN glass was recorded at 15 K (Figure 63 (a)).

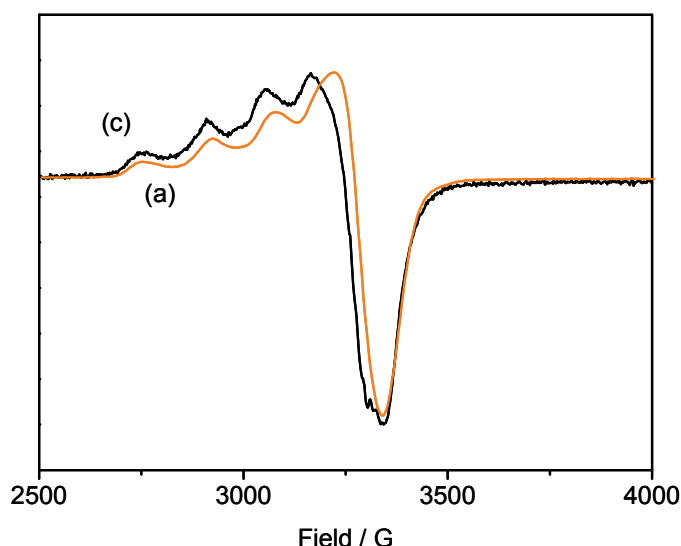


**Figure 63.** EPR spectra at 15 K: (a)-red line, frozen solution of the  $\text{Cu}^{\text{I}}\text{Cu}^{\text{II}}$  model complex; (b)-green line, simulated spectrum.

The red line (a) represents the recorded EPR spectrum and the green line (b) is the corresponding simulated spectrum. A typical four-line pattern is observed, which is characteristic for a non-perturbed  $\text{Cu}^{\text{II}}$  ion. Since under the conditions applied for these measurements any other copper species that is possibly present, i.e. traces of  $\text{Cu}^{\text{II}}\text{Cu}^{\text{II}}$  and/or  $\text{Cu}^{\text{I}}\text{Cu}^{\text{I}}$  – both species can in principle have formed during the direct synthesis of the mixed-valence  $\text{Cu}^{\text{I}}\text{Cu}^{\text{II}}$  complex - would be EPR-silent, this signal was attributed to the mixed-valence copper species. The data for the simulated spectrum revealed  $g_{\parallel}(2.25) > g_{\perp}(2.06)$  and  $|A_{\parallel}| = 157 \text{ G}$  are typical of a five-coordinate square pyramidal structure around  $\text{Cu}^{\text{II}}$  ion.<sup>151</sup> At the same time, the overall UV/vis features of the solution of the model  $\text{Cu}^{\text{I}}\text{Cu}^{\text{II}}$  complex are characteristic for a copper ion in trigonal bipyramidal geometry. The relation between observed EPR and UV/vis spectroscopic features can not be explained at the present moment.

The EPR spectrum of the reaction mixture after storage in glove box was recorded under the same conditions and it is depicted in Figure 64 (c) together with the EPR spectrum of the model  $\text{Cu}^{\text{I}}\text{Cu}^{\text{II}}$  complex Figure 64 (a). The same four-line pattern as for the model complex was observed. It has to be mentioned that the shape of the spectrum of the reaction mixture (c) indicates the presence of at least two different mixed-valence species in solution with most likely similar features, possibly due to the presence of TMBB or excess TMP, and therefore simulation was not performed.

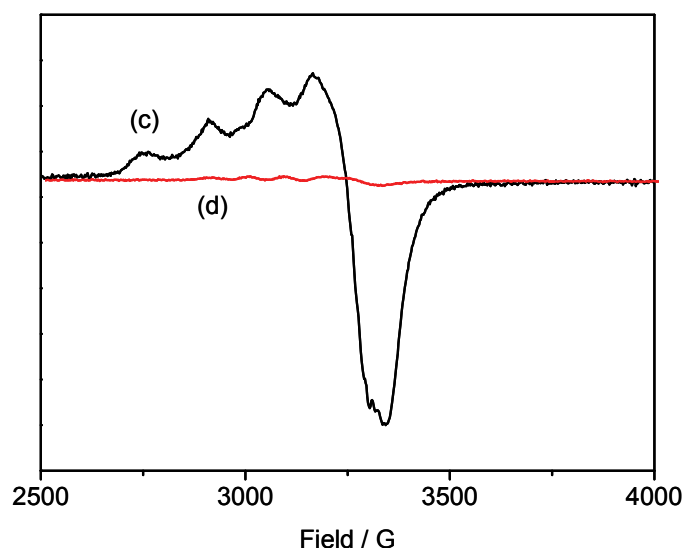
The single most important conclusion that can be drawn from these measurements is that the unprecedented formation of a mixed-valence  $\text{Cu}^{\text{I}}\text{Cu}^{\text{II}}$  species, brought about by the reduction of one of the copper ions in complex **5a**, is clearly observable after the first reaction step, i.e. the oxidative C-C coupling of two molecules of TMP to yield TMBB. This first step does proceed under anaerobic conditions.



**Figure 64.** EPR spectra at 15 K: (a)-red line, frozen solution of the model  $\text{Cu}^{\text{I}}\text{Cu}^{\text{II}}$  complex; (c)-black line, yellow-green solution after 48 h of storage in glove box.

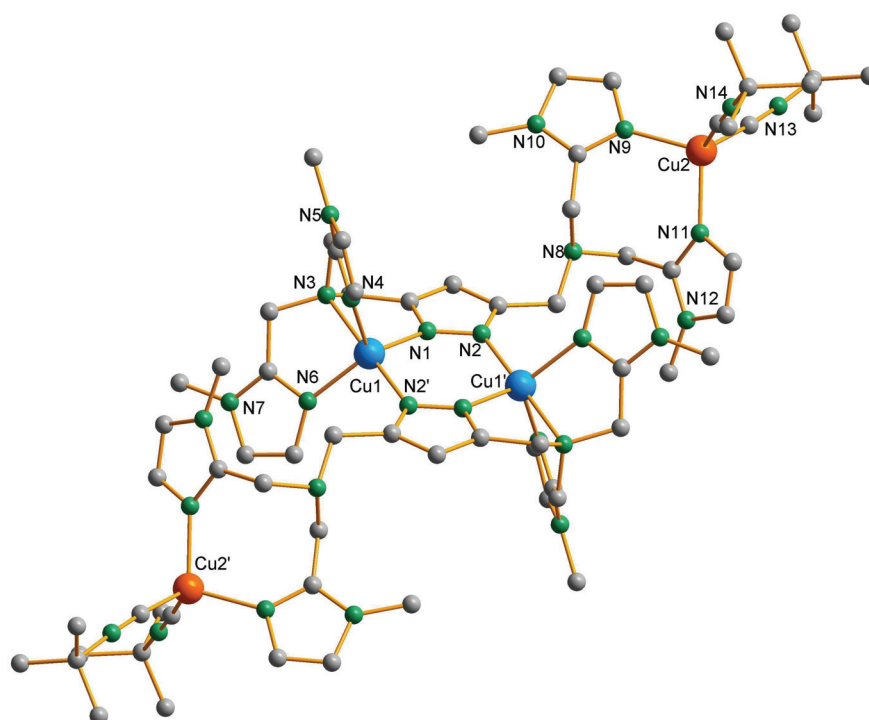
To further investigate the nature of the copper species generated under anaerobic conditions, and after formation of the organic product TMBB was complete, it was first attempted to obtain suitable crystals from the reaction medium. Unfortunately, under these conditions (direct crystallization from the reaction mixture after first reaction step under anaerobic conditions), only green powder was formed. To enhance the stability of the relevant copper complex formed after the oxidative coupling and to trap proposedly a mixed-valence  $\text{Cu}^{\text{I}}\text{Cu}^{\text{II}}$  species, two equivalents of *tert*-butyl isocyanide (per dicopper complex) were added to the

obtained yellow-green solution (see above). Addition of the strong  $\sigma$ -donor isocyanide co-ligand led to the disappearance of the typical four-line pattern for copper(II) (Figure 65 (d)).



**Figure 65.** EPR spectra at 15 K: (a)-black line, yellow-green frozen solution after 48 h of storage in glove box; (c)-red line, yellow-green solution after addition of  $(\text{CH}_3)_3\text{CNC}$ .

Coordination of the strong  $\sigma$ -donor isocyanide ligand was implied by the colour change to intense green. Isolation of the complex was achieved by slow diffusion of the acetonitrile solution with  $\text{Et}_2\text{O}$ . Characterization by IR spectroscopy revealed the presence of two bands at  $\nu_{\text{CN}}$  2173 and 2151  $\text{cm}^{-1}$ , indicative of two isocyanide ligands on a  $\text{Cu}^{\text{I}}$  center. Molecular structure of the complex formed was determined by X-ray crystallography. Figure 66 shows the molecular structure of complex **9**, while Table 16 contains selected data for intramolecular atom distances and angles. The anticipated mixed-valence  $\text{Cu}^{\text{I}}\text{Cu}^{\text{II}}$  motif is clearly preserved in this structure, but instead of the expected dinuclear species, this complex exists in the related dimeric form in the solid state. Such a dimerisation has most probably taken place due to the coordination of the strong  $\sigma$ -donor isocyanide co-ligands which induces a rearrangement of the mixed-valence dinuclear  $\text{Cu}^{\text{I}}\text{Cu}^{\text{II}}$  core and coordination of the  $\text{Cu}^{\text{I}}$  ions to the dangling chelate side arms, concomitant with formation of the central bis( $\mu$ -pyrazolato) dicopper(II) core. These two copper(II) ions reside in the complex in the same coordination mode as in **6**, which is reflected by an almost perfect trigonal bipyramidal  $\{\text{N}_5\}$  coordination environment ( $\tau = 0.98$ ), where one of the apical Cu-N-bonds is slightly elongated, with a  $d(\text{Cu1-N3})$  of 2.12 Å.



**Figure 66.** Molecular structure of the cation of **9**.

**Table 16.** Selected intramolecular distances (Å) and angles (°) for complex **9**.

Distances			
Cu(1)-N(2)'	1.946(3)	Cu(2)-C(31)	1.939(5)
Cu(1)-N(1)	2.025(3)	Cu(2)-N(11)	2.060(3)
Cu(1)-N(4)	2.071(4)	Cu(2)-N(9)	2.077(4)
Cu(1)-N(6)	2.075(4)	Cu(1)···Cu(1)'	3.847(1)
Cu(1)-N(3)	2.121(3)		
Cu(2)-C(26)	1.924(4)		
Angles			
N(2)'-Cu(1)-N(1)	101.59(13)	N(4)-Cu(1)-N(3)	79.30(14)
N(2)'-Cu(1)-N(4)	97.81(14)	N(6)-Cu(1)-N(3)	80.02(14)
N(1)-Cu(1)-N(4)	115.76(14)	C(26)-Cu(2)-C(31)	114.73(19)
N(2)'-Cu(1)-N(6)	101.34(14)	C(26)-Cu(2)-N(11)	113.59(16)
N(1)-Cu(1)-N(6)	116.11(14)	C(31)-Cu(2)-N(11)	104.95(16)
N(4)-Cu(1)-N(6)	118.86(14)	C(26)-Cu(2)-N(9)	106.35(17)
N(2)'-Cu(1)-N(3)	177.10(14)	C(31)-Cu(2)-N(9)	111.99(17)
N(1)-Cu(1)-N(3)	79.97(13)	N(11)-Cu(2)-N(9)	104.91(14)

The coordination sphere of each of the two Cu<sup>I</sup> ions consists of two side arm N atoms and two isocyanide co-ligands, resulting in a perfect tetrahedral geometry typical for Cu<sup>I</sup> ions. The observed distance between copper and the carbon from the isocyanide co-ligand (~ 1.93 Å) is slightly longer than for previously described copper(I) systems stabilized by various isocyanide ligands.<sup>152,153,154,155</sup>

This is in good agreement with the features of the EPR spectrum obtained after addition of the isocyanide co-ligand: two copper(II) ions are strongly antiferromagnetically coupled via the pyrazole unit resulting in the formation of a bis( $\mu$ -pyrazolato) dicopper(II) core. The two copper(I) ions in this complex are EPR-silent.

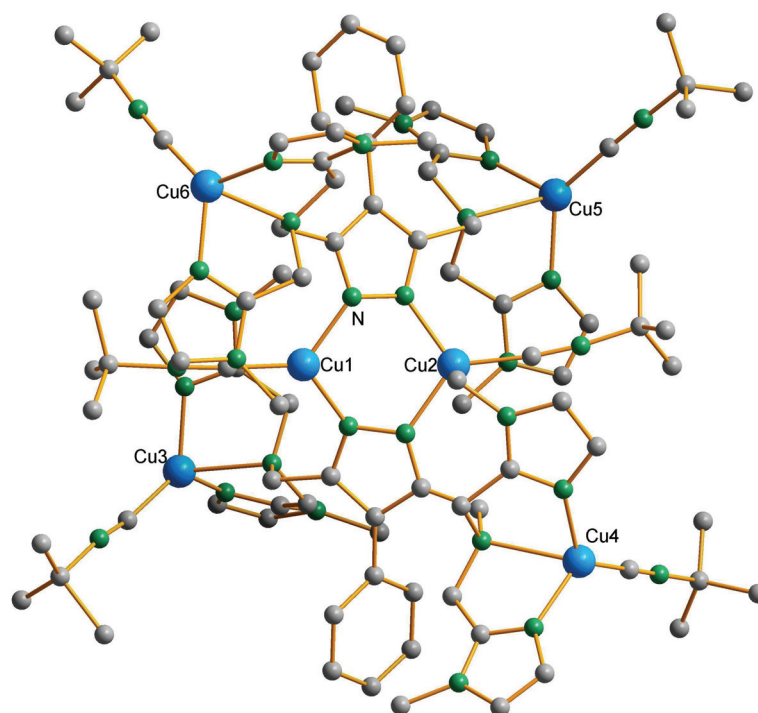
Taking this in account, it can be concluded that the yellow-green solution largely contains an EPR active, dinuclear mixed-valence Cu<sup>I</sup>Cu<sup>II</sup> complex and also that addition of *tert*-butyl isocyanide induces a dimerisation of this species due to the coordination of the strong  $\sigma$ -donor isocyanide, resulting in a rearrangement of the mixed-valence Cu<sup>I</sup>Cu<sup>II</sup> core and formation of a stable bis( $\mu$ -pyrazolato) dicopper(II) motif.

## 7.7 Coordination behaviour of the new ligand **HL**<sup>5</sup> towards copper(I)

The pyrazolate ligand **HL**<sup>5</sup>, substituted in the 4-position by a phenyl group, was applied to study the coordination behaviour of the present new generation of ligands with pendant bis[(1-methylimidazole-2-yl)-methyl]amine side arms towards copper(I). Moreover, the information gained from the solid state structures and spectroscopic properties of these copper(I) complexes was considered very useful to determine the nature of various intermediate species formed upon reduction of the initial copper(II) species during oxidation and oxygenation reactions catalyzed by copper complexes with pyrazole-based ligands.

Reaction of **HL**<sup>5</sup> with one equivalent of KO<sup>*t*</sup>Bu (for deprotonation of the pyrazole NH-unit) in MeCN, followed by addition of two equivalents of [Cu(MeCN)<sub>4</sub>](PF<sub>6</sub>) to the reaction mixture, was performed under strict anaerobic conditions. After stirring of the light-yellow reaction mixture for 2 h, one equivalent of *tert*-butyl isocyanide (per copper atom) was added. Characterization of the resultant crystalline material by IR spectroscopy revealed the presence of a band at  $\nu_{\text{CN}}$  2164 cm<sup>-1</sup>, indicative of the presence of one isocyanide ligand per Cu<sup>I</sup> center. The single crystals of complex **10** that could be isolated after diffusion of Et<sub>2</sub>O into a MeCN

solution proved to be of insufficient quality for a high-resolution X-ray crystallographic analysis and therefore a complete dataset could not be obtained. However, a rough estimation of intramolecular distances between key atoms (like Cu and N) was possible on the basis of these measurements. The corresponding approximation of the molecular structure of **10** is shown in Figure 67.



**Figure 67.** Molecular structure of the cation of **10**.

Instead of the expected dinuclear species, this complex exists as a hexanuclear species. Six copper atoms are coordinated to two ligands overall, with one additional isocyanide co-ligand per copper atom. The four outer copper(I) atoms that are nested in the dangling chelate side arms have distorted tetrahedral geometry. The two remaining copper(I) ions are bridged by the two pyrazolate cores of the respective ligands, which results in the formation of the central bis( $\mu$ -pyrazolato) dicopper(I) core. Coordination of one additional isocyanide fragment per Cu leads to completion of the trigonal planar coordination environment for both central copper(I) atoms.

It is assumed that formation of this structural motif is promoted by coordination of the strong  $\sigma$ -donor isocyanide co-ligands, which induce a rearrangement of the putative dicopper(I) core that may have formed initially. It was clearly shown by means of  $^1\text{H}$  NMR spectroscopy that

the ratio between pyrazole ligand and *tert*-butyl isocyanide in the resulting copper(I) complex in solution is 1 to 3 (based on the integration ratio).

On these grounds it was proven that complex **10** exists in both, solid state and solution as hexanuclear species. These experiments show that pyrazole-based ligands substituted with bis[(1-methylimidazole-2-yl)-methyl]amine pockets can serve as a host for copper(I) and that such complexes can be stabilized in the presence of strong  $\sigma$ -donor co-ligands.

### 7.8 Time-dependent concentration profiles of TMP, TMBB and TMSQ during catalysis with **5a**

In order to learn about the formation of the C-C coupled intermediate TMBB as well as of the oxidized product TMSQ over time under catalytic conditions, the concentration profiles of TMBB and TMP were measured by  $^1\text{H}$  NMR spectroscopy, while the formation of TMSQ was followed by UV/vis spectroscopy.

#### *NMR monitoring:*

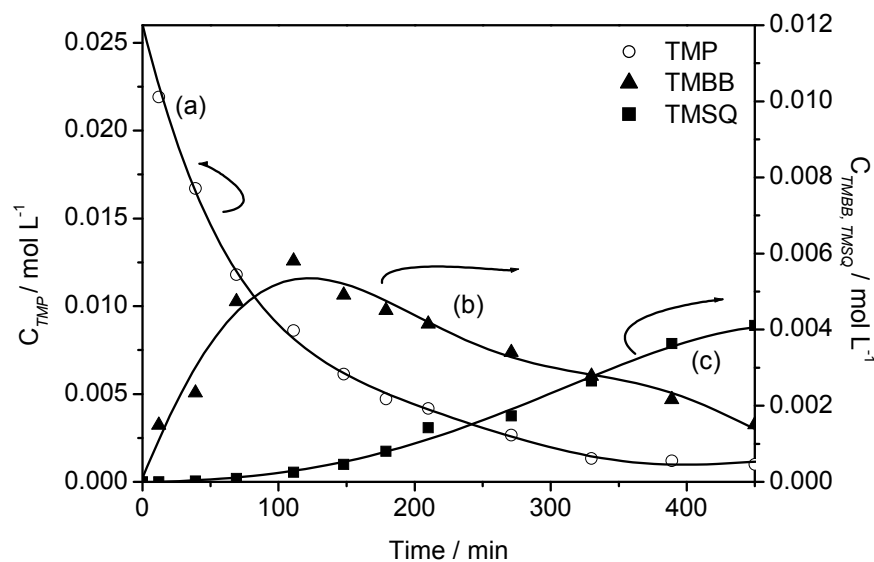
NMR monitoring was performed under aerobic conditions using the standard reaction conditions applied. To a 0.005 M solution of dicopper(II) complex **5a**, a 0.025 M solution of TMP was added, resulting in a final volume of 64 mL of MeCN/ $\text{CH}_2\text{Cl}_2$  (4:6). 1,2,4,5-Tetrabromobenzene was used as an internal standard to allow calculation of the yield of the formed TMBB and the conversion of TMP during 8 h reaction time. Aliquots of the reaction mixture (4 mL) were passed through a silica column using  $\text{CH}_2\text{Cl}_2$  as eluent (final washing was performed using a mixture of  $\text{CH}_2\text{Cl}_2/\text{MeOH}$  9:1) to quench the reaction by removal of the copper complex. After silica chromatography, solvents were removed *in vacuo* and  $^1\text{H}$  NMR spectra of the resulting residues were measured in  $\text{CDCl}_3$ . The concentrations of the formed TMBB as well as of the remaining TMP substrate were calculated from  $^1\text{H}$  NMR data using the relative integrals of the signal at 6.76 ppm for TMP and at 6.80 ppm for TMBB (Figure 68 (a), (b)) and the signal for tetrabromobenzene at 7.80 ppm as internal standard.

#### *UV/vis monitoring:*

UV/vis monitoring of the formation of the final product TMSQ was carried out using the same amounts of complex **5a** and TMP as applied in the previous experiment. Aliquots of the



reaction mixture (1 mL) were diluted with  $\text{CH}_2\text{Cl}_2$ , skipping the chromatographic procedure for removal of the copper complex, and UV/vis spectra were measured over a reaction time of 8 h. The observed yield in TMSQ (absorption values at 440 nm ( $\epsilon = 96000 \text{ L}\cdot\text{mol}^{-1}\cdot\text{cm}^{-1}$  in  $\text{CH}_2\text{Cl}_2$ ) were used for calculations) after 8 h was found to be 38 % (Figure 68 (c)). In case of a longer reaction time (24 h and longer) the yield of the C-C coupled product increased to 66 %.

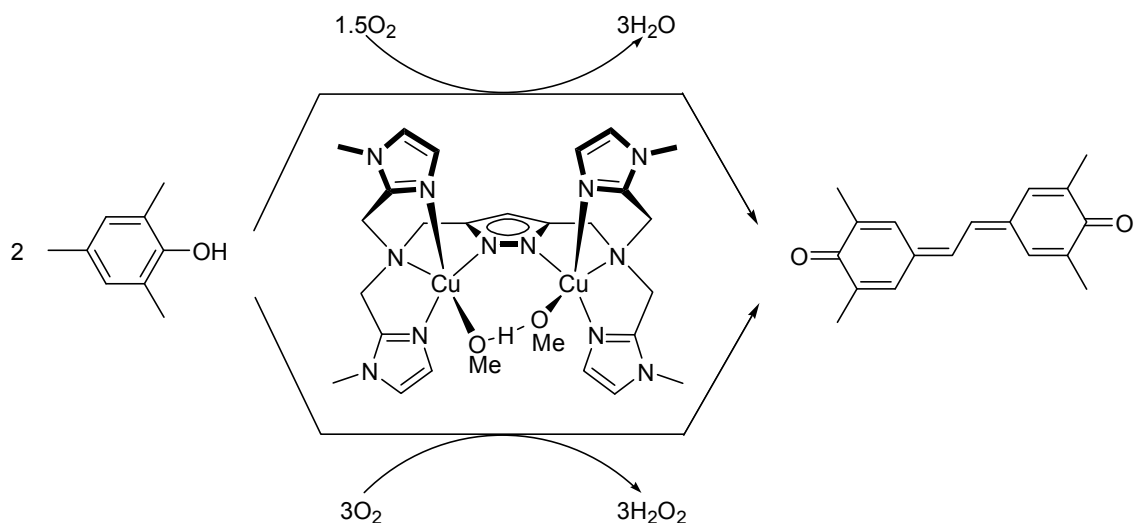


**Figure 68.** Time-dependent concentration profiles of TMP (a), TMBB (b) and TMSQ (c) (starting concentration of **5a** =  $0.005 \text{ mol}\cdot\text{L}^{-1}$ , concentration of TMP =  $0.025 \text{ mol}\cdot\text{L}^{-1}$ , solvent: MeCN/ $\text{CH}_2\text{Cl}_2$  4:6 v/v).

An exponential decay was observed for the concentration profile of TMP, whereas the concentration of TMBB reached a maximum within 2 h, concurrent with the rapid formation of TMSQ.

## 7.9 Determination of the $\text{O}_2$ derived by-product in the C-C coupling reaction

Oxidative C-C coupling of TMP to TMSQ catalyzed by **5a** in the presence of dioxygen can result in either  $\text{H}_2\text{O}_2$  or  $\text{H}_2\text{O}$  as the reduction product (Scheme 36). These scenarios differ by the stoichiometry of substrate to oxidant ( $\text{O}_2$ ). Determination of the reduction product is important for a full understanding of the mechanism behind this unusual Cu-catalyzed reaction with TMP.



**Scheme 36.** Oxidative C-C coupling of TMP:  $\text{H}_2\text{O}_2$  and  $\text{H}_2\text{O}$  are possible reduction products.

The possible formation of  $\text{H}_2\text{O}_2$  can be probed by some chemical tests that selectively detect the presence of this species, in the way described below.<sup>108</sup>

First the TMP substrate was oxidized to the product TMSQ in the presence of dicopper(II) catalyst **5a** under aerobic conditions until the absorption at  $\lambda_{\text{max}}$  440 nm had reached the arbitrary value of one in the UV/vis spectrum. The reaction was then quenched with an equimolar amount of a 0.005 M  $\text{H}_2\text{SO}_4$  solution and the product TMSQ as well as residual TMP were removed by extraction with  $\text{CH}_2\text{Cl}_2$ . To 5 ml of the remaining solution was added 2 ml of  $\text{H}_2\text{O}$  in the reference cell. In the sample cell 2 ml of a 0.3 M KI solution and catalytic amounts of lactoperoxidase - for specific acceleration of the oxidation of  $\text{I}^-$  to  $\text{I}_3^-$  - were added. The development of the absorption band at  $\lambda_{\text{max}}$  353 ( $\epsilon = 26\,000 \text{ L mol}^{-1} \text{ cm}^{-1}$ ) for the resulting  $\text{I}_3^-$  species, which can *only* be formed in the presence of  $\text{H}_2\text{O}_2$ , was followed by UV/vis spectroscopy. The blank experiment, without substrate present, was performed using the same procedure. Additionally, the possible formation of  $\text{H}_2\text{O}_2$  as the reduction product during the C-C coupling was checked by using test strips from Merck.

Both tests applied were clearly negative, which convincingly shows that during the oxidative C-C coupling of TMP to TMSQ  $\text{H}_2\text{O}_2$  is not formed. This means that water is formed as the reduction product, implying that 1.5 molar equivalents of  $\text{O}_2$  is needed per molecule of TMSQ formed.

## 8 Adducts with model substrate molecules

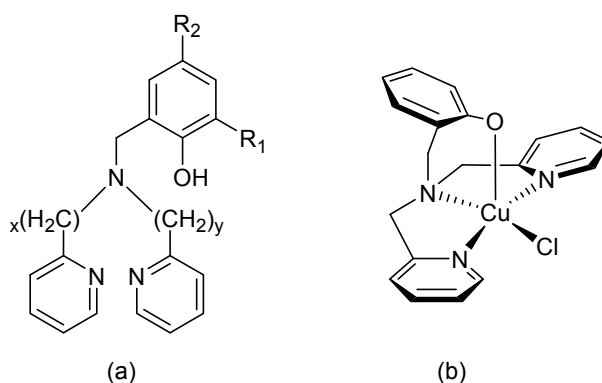
Coordination of the TMP substrate within the bimetallic pocket of the dicopper core of **5a** prior to oxidative C-C coupling occurs under both aerobic and anaerobic conditions, as was shown by means of UV/vis spectroscopy (i.e. the Job experiment), in particular by the observation of a phenolate-to-copper CT band at a  $\lambda_{\text{max}}$  of 495 nm. Resonance Raman spectroscopy also provided evidence for the formation of the dicopper(II)-phenolate species upon coordination of TMP.

In order to gain structural insight in the possible coordination behaviour of TMP towards copper catalyst **5a**, a selected range of phenolic and diphenolic substrates (as models for TMBB), all of have redox potentials that prevent any Cu-mediated reactivity, was studied. The interaction between these model substrates and **5a** in solution is investigated spectroscopically and molecular structures of dicopper-phenolate complexes with PFP and 4-AP as model substrates are discussed.

### 8.1 Copper(II)-phenolate complexes

Recently, considerable emphasis has been placed on the detailed study of the properties of Cu<sup>II</sup>-phenolate complexes, because of their postulated involvement in a range of biological and catalytic processes. Thus, Cu<sup>II</sup>-phenolate units have been proposed as intermediates in the catalytic cycles of metalloenzymes (e.g. galactose oxidase,<sup>156</sup> tyrosinase<sup>157</sup>) as well as in synthetic catalysis (e.g. alcohol oxidation,<sup>158</sup> phenol polymerization<sup>159</sup>).<sup>160</sup> The known Cu<sup>II</sup>-phenolate complexes exhibit coordination numbers ranging from 4 to 6, as is typical for the coordination chemistry of Cu<sup>II</sup>. In addition, the phenolates in most of these compounds usually are incorporated as part of multidentate ligand systems; complexes with simple, exogenous phenolate ligands are less common.<sup>161</sup>

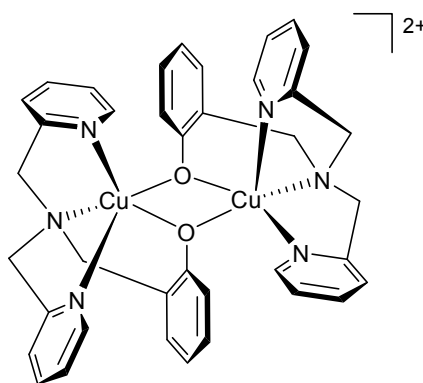
Several research groups have used ligands that have bis(pyridyl)alkylamines linked to a single phenol as a common design feature (Figure 69 (a)). These ligands represent a class of compounds where the phenol unit is incorporated into multidentate ligand systems.



**Figure 69.** (a) General representation of the bis(pyridyl)alkylamine ligand framework  $HL^{Ph}$  ( $x, y = 1$  or  $2$ ,  $R_1, R_2 =$  alkyl substituents); (b) schematic representation of the structure of the  $Cu^{II}$ -phenolate complex with  $x = y = 1$ ,  $R_1 = R_2 = H$ .

This basic tripodal ligand design has been varied by adjusting the length of the alkyl chain linking the pyridine and tertiary amine donors ( $x$  and  $y$ ), as well as by changing the phenol ring substituents ( $R_1$  and  $R_2$ ). Numerous mononuclear complexes of the general formula  $[L^{Ph}CuX]$  ( $X$  is a monoanionic donor ligand, such as  $Cl^-$  or  $CH_3CO_2^-$ ;  $L^{Ph}$  is a phenolate-containing bis(pyridyl)alkylamine ligand) have been prepared and some of them have been structurally characterized (molecular formula is depicted in Figure 69 (b)). Typical features of these compounds include a phenolate-to-copper(II) CT transition in their UV/vis spectrum ( $\lambda_{max} \sim 380\text{--}450\text{ nm}$ ) as well as axial signals in their EPR spectrum.<sup>162</sup>

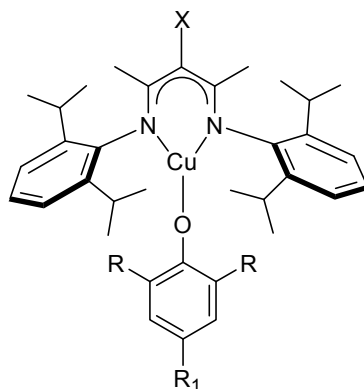
When the complex syntheses using bis(pyridyl)alkylamine/phenol ligands were performed in the absence of a strong monoanionic donor (e.g. with  $Cu(ClO_4)_2$ ,  $Cu(BF_4)_2$ , or  $CuSO_4$ ), dimeric complexes of the formulation  $[LCu]_2^{2+}$  were isolated.<sup>162d,e,163</sup> A representative structure of one such dimeric complex is shown in Figure 70.



**Figure 70.** Schematic representation of a dimeric copper(II) complex with a phenolate-derived multidentate ligand.

All structurally characterized complexes are similar to the depicted one and show two  $\text{Cu}^{\text{II}}$  ions in square pyramidal geometry, with slight trigonal bipyramidal distortion. The metal ions are bridged by two phenolates, one from each ligand. Like the monomeric complexes discussed above, the UV/vis spectra of the dimeric complexes exhibit a phenolate-to-copper(II) CT band (around 440 nm) as well as  $d-d$  transitions at a lower energy (around 630 nm).

A recent example of a complex with a simple, exogenous phenolate ligand incorporated into a Cu-complex was reported by Tolman and co-workers (Figure 71).<sup>132</sup> Dark green, three-coordinate  $\beta$ -diketiminato-containing copper(II)-phenolate complexes were spectroscopically characterized and - in case of  $\text{R} = \text{H}$  and  $\text{R}_1 = \text{OMe}$  in the *para*-position of the phenol ring - the molecular structure was solved by X-ray crystallography.



**Figure 71.** Schematic representation of the general structure of three-coordinate copper(II)-phenolate complexes with  $\beta$ -diketiminato ligands.

The UV/vis spectrum of the complex with coordinated 4-*tert*-butylphenol showed intense ( $\epsilon \sim 1000\text{--}3000 \text{ L mol}^{-1} \text{ cm}^{-1}$ ) absorption bands at  $\lambda_{\text{max}} \sim 450, 625$  and  $700 \text{ nm}$  and on the basis of the resonance Raman experiments it was suggested that the absorption at  $\lambda_{\text{max}} \sim 625 \text{ nm}$  possessed at least partial phenolate-to-copper(II) LMCT character. The Raman spectrum of a  $\text{CH}_2\text{Cl}_2$  solution of the mononuclear copper(II) complex with 4-*tert*-butylphenolate ligand was measured using  $633 \text{ nm}$  laser excitation. The set of multiple features found between  $1100$  and  $1600 \text{ cm}^{-1}$  are typical of metal-phenolate complexes and metal-tyrosinase sites in proteins,<sup>164</sup> with those at  $1174, 1270, 1500$ , and  $1598 \text{ cm}^{-1}$  being diagnostic for coordinated phenolates that have a substituent at the *para*-position.<sup>147,165</sup> The bands at  $1174$  and  $1270 \text{ cm}^{-1}$  were assigned as C-H bending and C-O stretching modes, respectively, and those at  $1500$  and

1598 cm<sup>-1</sup> were attributed to ring C-C stretching vibrations for the coordinated phenolate ligand.

In this light, elucidation of the phenol binding within the dicopper core of **5a** is of great interest not only in the frame of the present work but also with a general sense to investigate the behaviour of phenolic substrates towards dinuclear copper species.

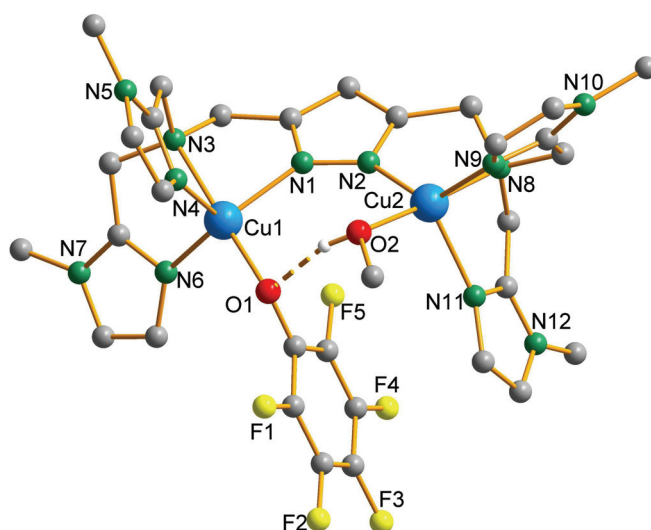
## 8.2 Characterization of the adducts with 4-hydroxybenzamide and pentafluorophenol

With the aim to learn about the formation and structure of possible intermediates in the catalytic oxidative C-C coupling reactions studied, the coordination chemistry of dicopper complex **5a** towards phenolic substrates that can not display any Cu-mediated reactivity was investigated. Pentafluorophenol (PFP) and 4-hydroxybenzamide (4-AP) were applied as model substrates to study the binding of the phenol within the bimetallic pocket of **5a**. Reedijk and co-workers have shown that PFP can be used as an effective instrument to study the behaviour of phenolic substrates towards a copper catalyst. Thus, their copper catalyst based on the neocuproine ligand was shown to form a mononuclear copper complex, and formation of the presumably active dinuclear copper species during the catalysis was proven by using PFP as model substrate.<sup>99</sup> Trapping of the active species was performed in the presence of base, which served as the second co-ligand to form a self-assembled l-phenoxo-l-methoxo-bridged dinuclear copper species with a mononucleating non-bridging ligand, namely neocuproine (see Figure 14 in section 3.3). The two copper(II) ions in the resulting complex are in square pyramidal environments and both the PFP and the methoxide are coordinated in a bridging mode to both copper ions. This type of coordination is governed by the possibility of two mononuclear copper species to assemble through the interaction of bridging co-ligands, whereby the Cu...Cu distance is determined solely by the phenolate and methoxide ligands. Therefore, the two copper ions are only 3.14 Å apart.

Taking in account the completely different nature of the present dicopper(II) catalytic system, where two copper ions are already bridged by a pyrazole unit that features short *N,N*-bis[2-(1-methylimidazolyl)methyl]amine side arms, the PFP substrate, which is inactive in any Cu-mediated oxidation reactions, can possibly show a new coordination mode within the bimetallic pocket of **5a**.

It was clearly shown (see section 7.5.4) that the presence of strong electron-withdrawing groups (e.g. F or CONH<sub>2</sub>) on the phenol shifts the redox potentials and renders the phenolic substrates inert towards any kind of oxidation reactions. The perfect triangular shape of the corresponding Job plots, particularly with PFP as a substrate, shows that the formed dicopper-pentafluorophenolate complex exhibits significant stability and dissociation of the phenolate species does not occur to any significant extent in solution. Moreover, stable copper-phenolate complexes with these phenols can be formed as a result of the coordination of only one substrate molecule.

The crystallization attempts were performed in the presence of dioxygen using a tenfold excess of pentafluorophenol relative to dicopper complex **5a**. Yellow-green single crystals of copper-phenolate adduct **11**, suitable for X-ray crystallographic analysis, were formed after layering the reaction mixture with Et<sub>2</sub>O overnight (Figure 72).



**Figure 72.** Molecular structure of the cation of **11**.

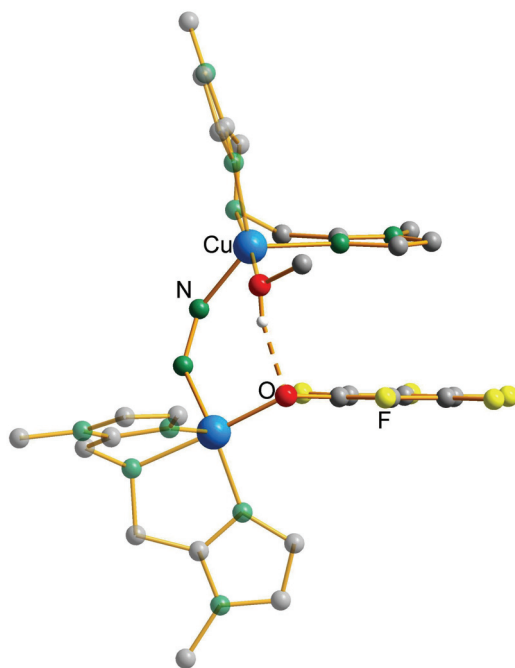
**Table 17.** Selected intramolecular distances (Å) and angles (°) for complex **11**.

Distances			
Cu(1)-O(1)	1.938(5)	Cu(2)-N(2)	1.970(5)
Cu(1)-N(6)	2.004(5)	Cu(2)-N(9)	2.025(5)
Cu(1)-N(1)	2.015(5)	Cu(2)-N(8)	2.088(5)
Cu(1)-N(4)	2.100(6)	Cu(2)-N(11)	2.147(5)
Cu(1)-N(3)	2.104(5)	Cu(1)⋯Cu(2)	4.309(1)

Cu(2)-O(2)	1.960(5)		
Angles			
O(1)-Cu(1)-N(6)	101.7(2)	O(2)-Cu(2)-N(2)	95.3(2)
O(1)-Cu(1)-N(1)	99.4(2)	O(2)-Cu(2)-N(9)	99.5(2)
N(6)-Cu(1)-N(1)	127.8(2)	N(2)-Cu(2)-N(9)	132.5(2)
O(1)-Cu(1)-N(4)	95.6(2)	O(2)-Cu(2)-N(8)	176.0(2)
N(6)-Cu(1)-N(4)	116.7(2)	N(2)-Cu(2)-N(8)	80.8(2)
N(1)-Cu(1)-N(4)	107.8(2)	N(9)-Cu(2)-N(8)	82.6(2)
O(1)-Cu(1)-N(3)	175.3(2)	O(2)-Cu(2)-N(11)	101.6(2)
N(6)-Cu(1)-N(3)	82.0(2)	N(2)-Cu(2)-N(11)	116.9(2)
N(1)-Cu(1)-N(3)	80.3(2)	N(9)-Cu(2)-N(11)	103.9(2)
N(4)-Cu(1)-N(3)	80.1(2)	N(8)-Cu(2)-N(11)	81.1(2)

A methanol-phenolate bridge between the two copper(II) centers was found in the molecular structure of the complex. Formation of such bridge proves that a methanolate-to-phenolate exchange has taken place at one Cu ion, effectively forming an ArO...HOMe bridge between the copper(II) centers. This closely matches the situation that is assumed to occur upon coordination of the active TMP substrate to **5a**. The methanolate-for-phenolate exchange causes only slight changes in the coordination spheres of both copper ions (both metal ions are five-coordinated,  $\tau_{\text{Cu1}} = 0.80$ ;  $\tau_{\text{Cu2}} = 0.73$ ), which is reflected well in the UV/vis spectrum. For the resulting complex **11** the copper-based *d-d* transition band was also observed at  $\lambda_{\text{max}}$  989 nm, and a charge-transfer band appeared at  $\lambda_{\text{max}}$  of 397 nm with an extinction coefficient that is typical for copper(II)-phenolate compounds (*ca.* 1240 L mol<sup>-1</sup> cm<sup>-1</sup>). Moreover, the molecular structure indicates an additional stabilization due to  $\pi$ - $\pi$  stacking interaction between the C<sub>6</sub>F<sub>5</sub>-ring and one imidazole unit of the ligand (interplane distance 3.88 Å, angle 4.5°, Figure 73).





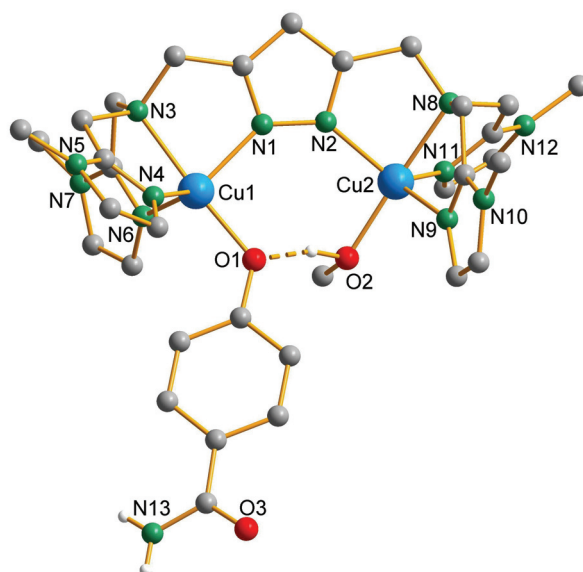
**Figure 73.** Side view of the molecular structure of the cation of **11**; for clarity the carbon atoms of the pyrazole core are omitted.

As was supposed and intended when designing ligand **HL**<sup>4</sup>, the large separation between the copper(II) ions in complex **5a** ( $d(\text{Cu}\cdots\text{Cu}) = 4.34 \text{ \AA}$ ) is conditional for coordination of the PFP within the bimetallic core to only one of the copper ions, resulting in an almost unchanged copper-copper distance ( $4.31 \text{ \AA}$ ). The molecular structure of **11** also confirmed preliminary results from the Job plot experiment, where it was shown that coordination of only one PFP is optimal, thereby forming a very stable copper(II)-phenolate species.

In order to exclude any specific influence of substituents on the phenol ring on the interaction between the dicopper complex and the phenol substrate, 4-hydroxybenzamide was applied as a second model substrate to elucidate the phenol binding to the dicopper core of **5a**.

The slightly curved Job plot of 4-AP with dicopper complex **5a** (see section 7.5.4) showed that the dicopper phenolate adduct exhibits moderate stability and dissociation of the phenolate species is still likely to occur to some degree in solution. From the performed Job plot experiment it was concluded that only one phenol molecule is able to coordinate to the dicopper core. Such an interaction in solution between 4-AP and dicopper complex **5a** was unambiguously proven after analysis of single crystals that were obtained by slow diffusion of

Et<sub>2</sub>O into a MeCN solution of **5a** in the presence of excess of 4-AP. The molecular structure of the cation of **12** is depicted in Figure 74.



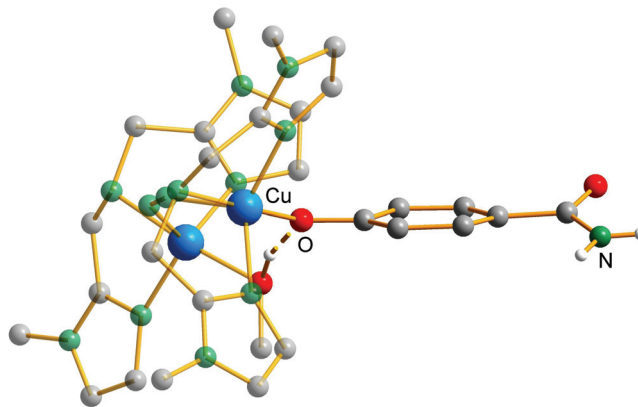
**Figure 74.** Molecular structure of the cation of **12**.

**Table 18.** Selected intramolecular distances (Å) and angles (°) for complex **12**.

Distances			
Cu(1)-O(1)	1.919(7)	Cu(2)-N(2)	2.015(8)
Cu(1)-N(1)	2.024(8)	Cu(2)-N(9)	2.053(8)
Cu(1)-N(4)	2.040(8)	Cu(2)-N(11)	2.064(8)
Cu(1)-N(6)	2.087(8)	Cu(2)-N(8)	2.086(8)
Cu(1)-N(3)	2.114(8)	Cu(1)···Cu(2)	4.387(2)
Cu(2)-O(2)	1.953(7)		
Angles			
O(1)-Cu(1)-N(1)	95.7(3)	O(2)-Cu(2)-N(2)	99.8(3)
O(1)-Cu(1)-N(4)	99.8(3)	O(2)-Cu(2)-N(9)	94.3(3)
N(1)-Cu(1)-N(4)	120.0(3)	N(2)-Cu(2)-N(9)	117.3(3)
O(1)-Cu(1)-N(6)	102.4(3)	O(2)-Cu(2)-N(11)	102.7(3)
N(1)-Cu(1)-N(6)	115.0(3)	N(2)-Cu(2)-N(11)	120.7(3)
N(4)-Cu(1)-N(6)	117.3(3)	N(9)-Cu(2)-N(11)	114.8(3)
O(1)-Cu(1)-N(3)	176.0(3)	O(2)-Cu(2)-N(8)	174.3(3)
N(1)-Cu(1)-N(3)	80.6(3)	N(2)-Cu(2)-N(8)	81.0(3)

N(4)-Cu(1)-N(3)	80.9(3)	N(9)-Cu(2)-N(8)	80.5(3)
N(6)-Cu(1)-N(3)	80.6(3)	N(11)-Cu(2)-N(8)	81.5(3)

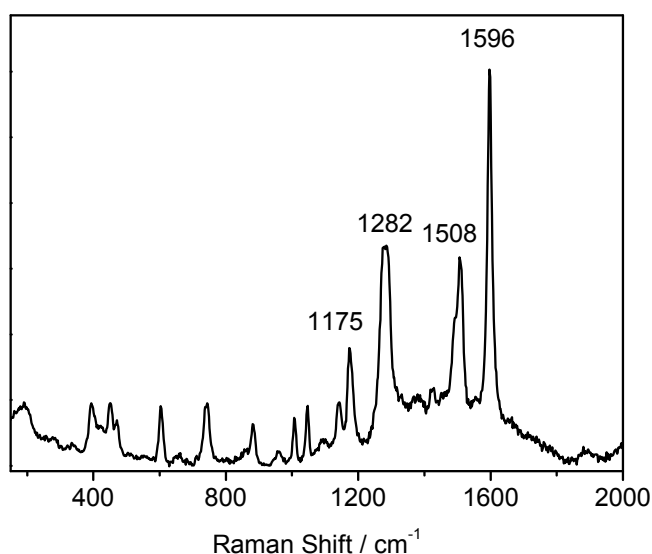
The two copper ions in **12** reside within the adjacent {N<sub>4</sub>} ligand compartments and are bridged by the pyrazolate core. Both metal ions are five-coordinate with almost perfect trigonal bipyramidal geometries ( $\tau_{\text{Cu1}} = 0.93$ ;  $\tau_{\text{Cu2}} = 0.90$ ). The pyrazolate-N and the two imidazole-N atoms constitute the equatorial plains, while axial positions are occupied by the tertiary N atoms of the ligand backbone and by the O atoms of the ArO...HOMe moiety located within the bimetallic pocket ( $d(\text{Cu}\cdots\text{Cu}) = 4.39 \text{ \AA}$ ). The slightly larger Cu...Cu distance found in **12** in comparison to both **5a** and **11** could be explained by the absence of the  $\pi$ - $\pi$  stacking interaction between the C<sub>6</sub>F<sub>5</sub>-ring and one imidazole unit of the ligand. Thus, in the molecular structure of the dicopper-phenolate complex **12**,  $\pi$ - $\pi$  stacking interactions are absent. The coordinated 4-hydroxybenzamidate ligand is directed out from the bimetallic pocket and away from the imidazole rings. This presumably contributes to the lower binding affinity compared to the PFP adduct **11** and leads to a lengthening of the Cu...Cu distance (Figure 75).



**Figure 75.** Side view of the molecular structure of the cation of **12**; for clarity the carbon atoms of the pyrazole core are omitted.

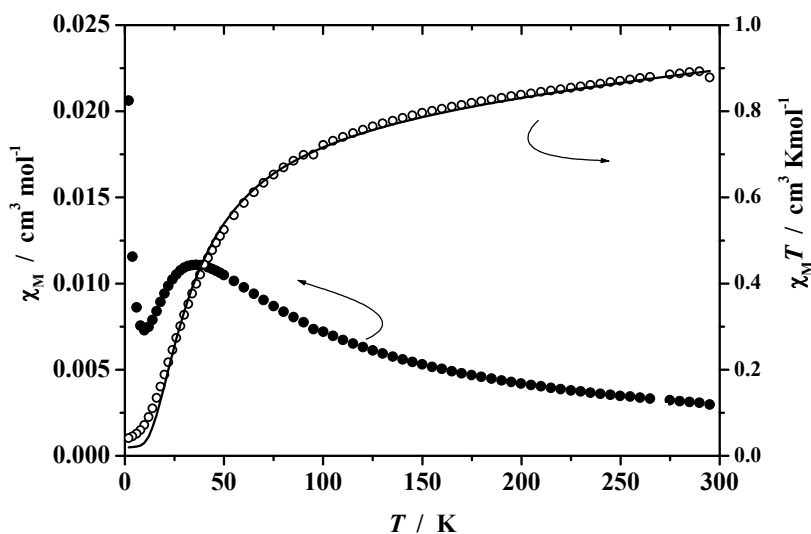
As was observed for **11**, formation of the dicopper-phenolate complex **12** did not result in any major changes in the Cu  $d$ - $d$  region in the UV/vis spectrum, confirming that the coordination spheres of both copper ions are largely unchanged. The phenolate-to-copper CT transition band appeared at 446 nm.

Resonance Raman spectroscopy has been particularly useful for gaining insight into the structural and electronic properties of the dicopper(II)–phenolate complexes, in particular for complex **12**. Laser excitation (488 nm) into the UV/vis CT transition band of **12** results in a resonance Raman spectrum that is very similar to those of other coordinated phenolates,<sup>132,165</sup> with three dominant features at 1175 cm<sup>-1</sup> ( $\nu_{9a}$ , predominantly a C-H phenol stretching), 1282 cm<sup>-1</sup> ( $\nu_{7a}$ , C-O stretching) and 1596 cm<sup>-1</sup> ( $\nu_{8a}$ ,  $C_{ortho}$ - $C_{meta}$  ring stretching). The Raman spectrum of **12** is depicted in Figure 76.



**Figure 76.** Solid state Raman spectrum of the dicopper(II)-phenolate complex **12**.

Magnetic susceptibility data for a powdered sample of **12** were measured at two different magnetic fields (2000 G and 5000 G) in a temperature range from 2.0 K to 295 K. No significant field dependence was observed. The temperature dependence of the magnetic susceptibility  $\chi_M$  and of the product  $\chi_M T$  for **12** is depicted in Figure 77.



**Figure 77.** Plots of  $\chi_M$  (solid circles) and  $\chi_M T$  (open circles) versus temperature for **12** at 5000 G; the solid black line represents the calculated curve fits (see text).

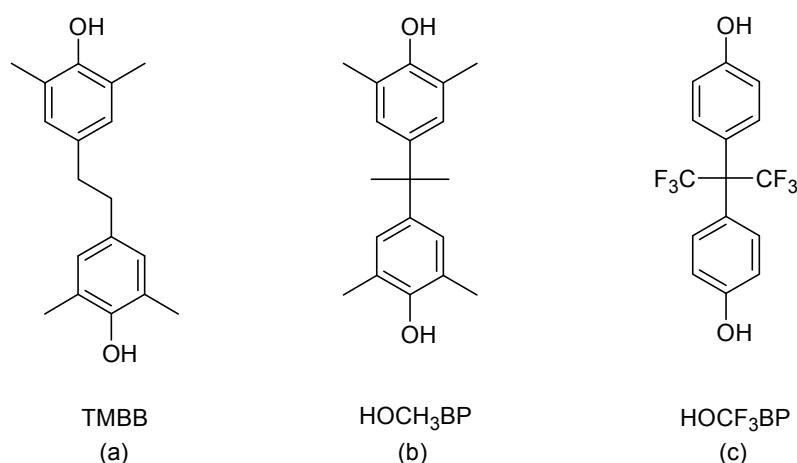
The observed  $\chi_M T$  value for **12** at 295 K is  $0.89 \text{ cm}^3 \cdot \text{K} \cdot \text{mol}^{-1}$  ( $2.65 \mu_B$ ), which matches the value expected for two uncoupled copper(II) ions ( $2.57 \mu_B$ ).  $\chi_M T$  decreases upon lowering the temperature and reaches zero below 15 K, indicating an  $S = 0$  ground state, which is also evident from the broad maximum of the  $\chi_M$  versus  $T$  curve that occurs around 40 K. This is a typical signature for dinuclear copper complexes with relatively strong intramolecular antiferromagnetic coupling. The increase of  $\chi_M$  at very low temperatures is presumably due to small amounts of paramagnetic impurities. Parameters according to the model described on page 65 are  $J = -20.90 \text{ cm}^{-1}$ ,  $g = 2.10$ ,  $\rho \sim 5.0 \%$ ,  $TIP = 4.34 \cdot 10^{-4}$ .

### 8.3 4,4'-isopropylidene-bis(2,6-dimethylphenol) and 4,4'-(hexafluoroisopropylidene)diphenol as model substrates for TMBB

Studies of the oxidative C-C coupling of TMP under anaerobic conditions showed that 4,4'-dihydroxy-3,3',5,5'-tetramethylbibenzyl (TMBB) was the first intermediate formed (see section 7.6.3). For any further reaction (i.e. oxidation to TMSQ) to occur the presence of both dioxygen and copper complex **5a** are required. Upon exposure of the yellow-green mixture, formed after storing the reaction mixture in the glove box for 48 h, to molecular dioxygen or air, an intense charge-transfer band ( $\lambda_{\text{max}} = 495 \text{ nm}$ ) again appeared in the UV/vis spectrum. In this case, no incubation period was observed, in contrast to the first oxidation step that

leads to formation of TMBB, and instantaneous formation of TMSQ occurred. It was shown that when 5 equivalents of TMP were used relative to **5a**, only one substrate molecule underwent coupling to yield TMBB in a stoichiometric reaction, while the remaining four equivalents did not react. Taking this in account, instantaneous formation of TMSQ after exposure of the yellow-green mixture to O<sub>2</sub> can presumably take place only upon coordination of the formed TMBB intermediate within the dicopper core of **5a** (Figure 78 (a)). This observation also justifies the conclusion that the 2e<sup>-</sup> oxidation of TMP to TMBB is the rate limiting step, while the further 4e<sup>-</sup> oxidation of TMBB to TMSQ occurs very rapidly.

Assuming that coordination of TMBB within the bimetallic pocket of the catalyst **5a**, which was regenerated after reoxidation of the Cu<sup>I</sup>Cu<sup>II</sup> species by dioxygen, actually takes place and is necessary for the subsequent reaction, 4,4'-isopropylidene-bis(2,6-dimethylphenol) (HOCH<sub>3</sub>BP) and 4,4'-(hexafluoroisopropylidene) diphenol (HOCF<sub>3</sub>BP) were applied as model substrates to study the binding of TMBB to **5a** (Figure 78 (b,c)).



**Figure 78.** Intermediate species TMBB (a) and model substrates HOCH<sub>3</sub>BP (b) and HOCF<sub>3</sub>BP (c).

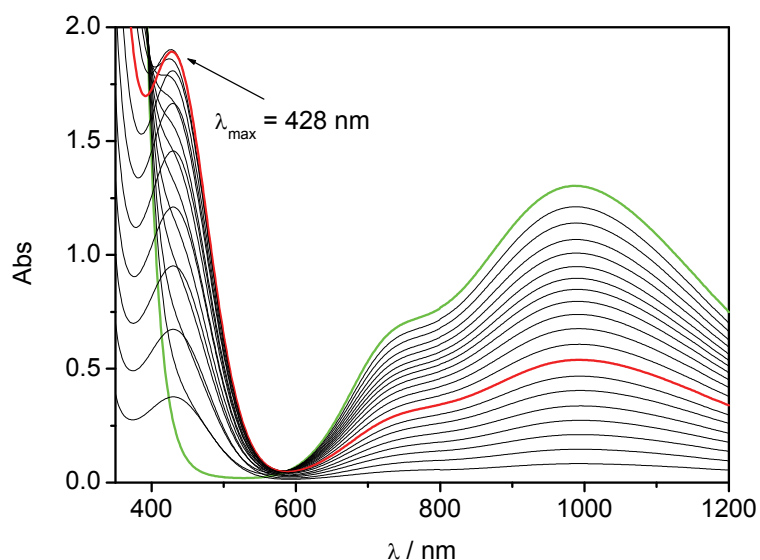
The model diphenols as well as TMBB contain two OH-groups as potential active units for binding to dicopper complex **5a**. This might be the reason for the rapid formation of TMSQ upon exposure of the yellow-green solution to O<sub>2</sub>, i.e. either coordination of TMBB as a monodentate ligand to **5a** or as a bridging ligand between two **5a** species.

The absence of any possibility to build up a conjugated C-C system - as present in TMSQ - gives rise to the inert behaviour of these two model substrates towards any kind of oxidation reactions. On the one hand, 4,4'-isopropylidenebis(2,6-dimethylphenol) (HOCH<sub>3</sub>BP) possesses very similar structural features as the active TMBB intermediate, with phenol rings

that are substituted only by aliphatic CH<sub>3</sub>-groups in both *ortho*-positions. On the other hand, use of the second model substrate HO CF<sub>3</sub>BP, which contains strong electron-withdrawing CF<sub>3</sub>-groups, will also allow studies on the binding to **5a**, while at the same time chances for the isolation of single crystals may be better, as observed with PFP.

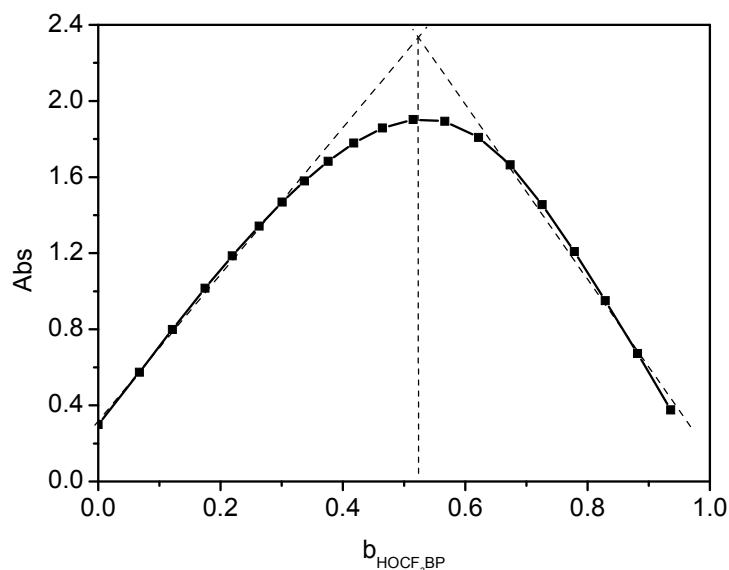
In order to distinguish between the two proposed coordination modes of TMBB with **5a** (see above) Job's method was applied as a useful instrument to determine the stoichiometry for the reaction occurring. Thus, in case of monodentate coordination of diphenols, the optimal value of *b* (molar fraction in diphenol) should be equal to ~ 0.5, meaning the formation of a 1:1 complex of diphenol and **5a**. The bridging coordination mode of the applied diphenols implies formation of a 1:2 complex of diphenol and **5a**, which would lead to an expected value of 0.33 for *b*.

The Job plot of HO CF<sub>3</sub>BP with **5a** was performed using the dilution technique (see section 7.5.3). The initial solution of dicopper complex **5a** in MeCN was diluted further in a stepwise manner by addition of a solution of diphenol with a constant concentration. The UV/vis spectrum of the mixture was recorded after each dilution step (Figure 79).



**Figure 79.** UV/vis spectra for the titration of **5a** with HO CF<sub>3</sub>BP after each dilution step: green line (initial dicopper complex **5a**); red line (solution of **5a** and HO CF<sub>3</sub>BP with a maximum absorbance).

The corresponding absorption value of the LMCT band at λ<sub>max</sub> 428 nm for each mixture was plotted *versus* the molar fraction in diphenol (*b*) (Figure 80).

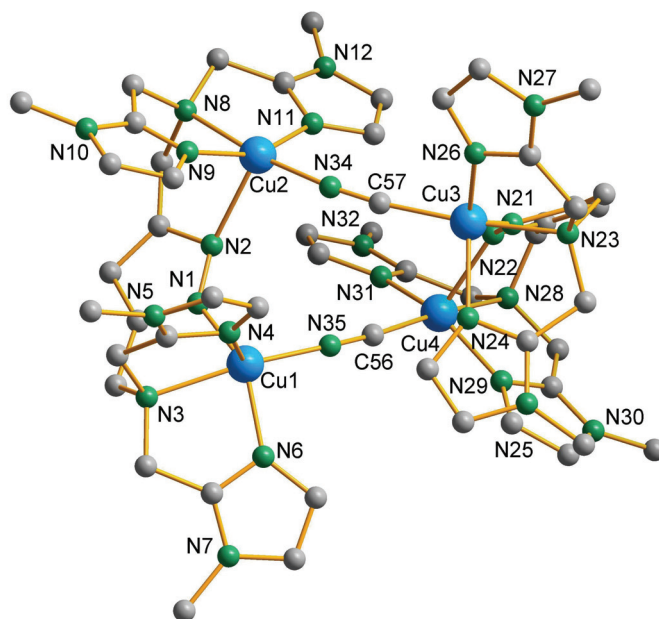


**Figure 80.** Job plot of HOCF<sub>3</sub>BP with dicopper complex **5a**,  $\lambda_{\text{max}} = 428$  nm.

From the obtained Job plot it can be concluded that formation of a dicopper-diphenolate species took place and moreover, that the formed species contained only one HOCF<sub>3</sub>BP ( $b \sim 0.5$ ) molecule per dicopper unit. The slightly curved plot shows that the dissociation of the diphenolate species is still likely to occur to some degree in solution.

It was not possible to perform the identical Job plot experiment with HOCH<sub>3</sub>BP as described above for HOCF<sub>3</sub>BP: addition of the substrate HOCH<sub>3</sub>BP to a green solution of **5a** in MeCN initially led to the usual formation of a red coloured copper-phenolate species, but this proved to be only a short-lived complex, as a further unexpected colour change to deep green occurred within ten minutes. The same colour change was also observed, but at a significantly slower rate, for the red mixture of HOCF<sub>3</sub>BP with **5a** obtained after the Job experiment, while this was subjected to a crystallization attempt. Slow diffusion of Et<sub>2</sub>O into the red mixture of HOCF<sub>3</sub>BP and **5a** induced the formation of dark green crystals. Surprisingly, an unexpected tetranuclear copper complex was isolated (Figure 81).





**Figure 81.** Molecular structure of the cation of tetranuclear complex **13**.

**Table 19.** Selected intramolecular distances (Å) and angles (°) for complex **13**.

Distances			
Cu(1)-N(1)	1.952(2)	Cu(3)-N(24)	2.112(3)
Cu(1)-N(35)	1.969(3)	Cu(3)-N(23)	2.143(2)
Cu(1)-N(6)	1.987(3)	Cu(4)-C(56)	1.958(3)
Cu(1)-N(3)	2.178(2)	Cu(4)-N(31)	1.965(3)
Cu(1)-N(4)	2.189(2)	Cu(4)-N(29)	1.979(3)
Cu(2)-N(11)	1.958(2)	Cu(4)-N(28)	2.159(3)
Cu(2)-N(9)	1.970(2)	Cu(4)-N(22)	2.186(3)
Cu(2)-N(34)	1.982(3)	Cu(1)···Cu(2)	4.4169(5)
Cu(2)-N(8)	2.164(2)	Cu(1)···Cu(3)	5.6224(5)
Cu(2)-N(2)	2.257(2)	Cu(1)···Cu(4)	5.0210(5)
Cu(3)-C(57)	1.957(3)	Cu(2)···Cu(3)	5.0241(5)
Cu(3)-N(21)	2.015(2)	Cu(2)···Cu(4)	5.3618(5)
Cu(3)-N(26)	2.021(3)	Cu(3)···Cu(4)	4.4632(5)
Angles			
N(1)-Cu(1)-N(35)	95.04(11)	C(57)-Cu(3)-N(21)	100.73(10)
N(1)-Cu(1)-N(6)	144.89(10)	C(57)-Cu(3)-N(26)	96.70(11)
N(35)-Cu(1)-N(6)	95.28(11)	N(21)-Cu(3)-N(26)	128.28(13)

N(1)-Cu(1)-N(3)	79.18(10)	C(57)-Cu(3)-N(24)	105.46(11)
N(35)-Cu(1)-N(3)	163.18(10)	N(21)-Cu(3)-N(24)	105.63(10)
N(6)-Cu(1)-N(3)	81.34(10)	N(26)-Cu(3)-N(24)	115.86(12)
N(1)-Cu(1)-N(4)	106.12(10)	C(57)-Cu(3)-N(23)	174.86(11)
N(35)-Cu(1)-N(4)	117.41(10)	N(21)-Cu(3)-N(23)	78.27(10)
N(6)-Cu(1)-N(4)	98.59(10)	N(26)-Cu(3)-N(23)	80.21(10)
N(3)-Cu(1)-N(4)	79.41(9)	N(24)-Cu(3)-N(23)	79.62(10)
N(11)-Cu(2)-N(9)	156.45(10)	C(56)-Cu(4)-N(31)	96.84(11)
N(11)-Cu(2)-N(34)	94.93(10)	C(56)-Cu(4)-N(29)	97.01(12)
N(9)-Cu(2)-N(34)	101.65(10)	N(31)-Cu(4)-N(29)	148.13(11)
N(11)-Cu(2)-N(8)	79.95(10)	C(56)-Cu(4)-N(28)	172.94(11)
N(9)-Cu(2)-N(8)	82.05(10)	N(31)-Cu(4)-N(28)	80.67(10)
N(34)-Cu(2)-N(8)	173.26(11)	N(29)-Cu(4)-N(28)	82.10(11)
N(11)-Cu(2)-N(2)	104.18(9)	C(56)-Cu(4)-N(22)	104.74(11)
N(9)-Cu(2)-N(2)	87.85(9)	N(31)-Cu(4)-N(22)	108.57(10)
N(34)-Cu(2)-N(2)	104.42(10)	N(29)-Cu(4)-N(22)	95.39(11)
N(8)-Cu(2)-N(2)	81.23(9)	N(28)-Cu(4)-N(22)	82.33(10)

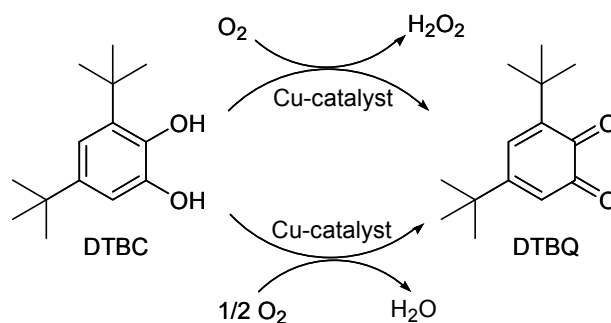
The same structural motif as for tetranuclear complex **8** is observed for **13** with the only difference being the bridging ligand. Thus, in complex **13** two dicopper units are bridged by  $\mu$ -CN ligands, while in tetranuclear complex **8** two  $\mu$ -OH groups are spanning two dicopper units (see section 5.5). The Cu-C<sub>CN</sub> (~1.96 Å) and Cu-N<sub>CN</sub> (~1.97 Å) atom distances are in agreement with a related *end-on* cyano-bridged dicopper complex reported in the literature.<sup>166</sup> All four copper atoms are ligated by four N atoms, i.e. one from the pyrazolate-unit, two from the imidazoles in the side arm and by the tertiary N atom of the ligand backbone. The coordination environment of Cu3 and Cu4 is completed by C atoms from the bridging CN-groups, while the remaining Cu1 and Cu2 ions are coordinated to the N atom from the same CN-groups. In marked contrast to copper complex **8**, this ligation results in a distorted trigonal bipyramidal geometry only for Cu3 ( $\tau = 0.76$ ) while the other copper atoms are in a distorted square pyramidal coordination environment (Cu1:  $\tau = 0.31$ ; Cu2:  $\tau = 0.28$  and Cu4:  $\tau = 0.40$ ). These structural features were perfectly reproduced in the corresponding UV/vis spectrum in solution, as *d-d* transition bands were observed for a trigonal bipyramidal copper ion at  $\lambda_{\text{max}}$  of 879 nm as well as for copper ions in a square pyramidal environment at  $\lambda_{\text{max}}$  of 671 nm.

The ESI spectrum of a MeCN solution of **13** did not reveal the presence of this particular tetranuclear species in solution. However, FAB mass spectrometry allowed the detection of complex **13** with signals at 627, 728, 754 and 1508  $m/z$ , which correspond to  $[\text{Cu}_2\text{L}^4]^+$ ,  $[\text{Cu}_2\text{L}^4(\text{ClO}_4)]^+$ ,  $[\text{Cu}_2\text{L}^4(\text{CN})(\text{ClO}_4)]^+$  and  $[\text{Cu}_4\text{L}^4_2(\text{CN})_2(\text{ClO}_4)_2]^+$ , respectively.

In the IR spectrum of **13** a characteristic  $\nu_{\text{CN}}$  stretch for *end-on* bridging cyano-fragments was observed at  $2173\text{ cm}^{-1}$ , which is very close to the value found for the related tetranuclear system reported by Karlin and co-workers.<sup>166</sup> This reported tetranuclear copper complex was formed from a dicopper(II)-hydroperoxo species through nucleophilic attack on the nitrile solvent used for reaction. In this light, the source of the CN-group incorporated into the structure of complex **13** is most likely acetonitrile used for reaction. Unfortunately, the mechanistic aspects and the prerequisites for the observed MeCN oxidation are not clear till now, especially since in the present case the copper ions in the initial complex **5a** are already in the oxidation state +2, whereas the complex used by Karlin starts out as a copper(I) species that activates dioxygen.

#### 8.4 A tetrachlorocatechol-adduct of dicopper(II) complex **5a**

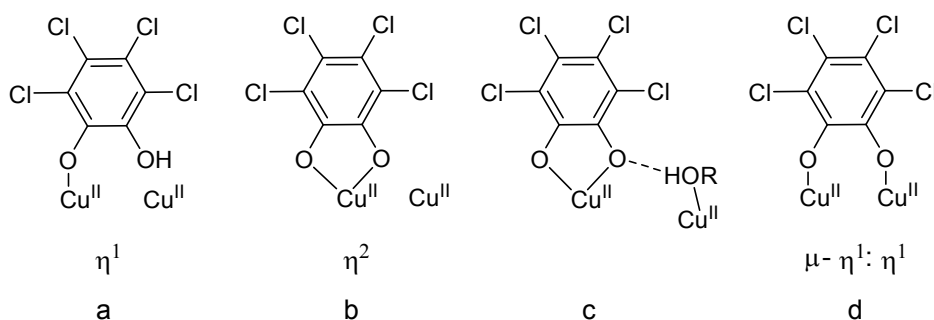
Oxidation of catechols to the corresponding quinones is catalyzed by the *type 3* copper center in the enzyme catechol oxidase. Nowadays, many studies are focussed on investigating the mechanism behind this catalytic reaction. A plethora of mono- and dinuclear copper complexes have been synthesized and investigated as biomimetic catalysts for the catechol oxidation,<sup>65,11</sup> in most cases using 3,5-di-*tert*-butylcatechol (DTBC) as the model substrate.<sup>72,75,78a,108,167,168,169,170</sup> The bulky *tert*-butyl groups of DTBC prevent unwanted side reactions such as ring opening or polymerization of the resulting quinone. Depending on the particular Cu catalyst used, either  $\text{H}_2\text{O}_2$  or  $\text{H}_2\text{O}$  may result as the reduction product (Scheme 37).



**Scheme 37.** Possible pathways for catechol oxidation catalyzed by a copper-based catalyst.

To study the possible modes of substrate binding within the dicopper core and to gain structural insight on the dicopper(II)-catecholate intermediate species formed during the catalytic reaction, tetrachlorocatechol (TCC) is usually employed as a structural mimic of the DTBC substrate, since TCC shows no tendency to undergo oxidation. Various mononuclear copper-catecholate complexes were structurally characterized,<sup>171</sup> while only few examples of dicopper systems with coordinated TCC have been reported.<sup>170,71</sup>

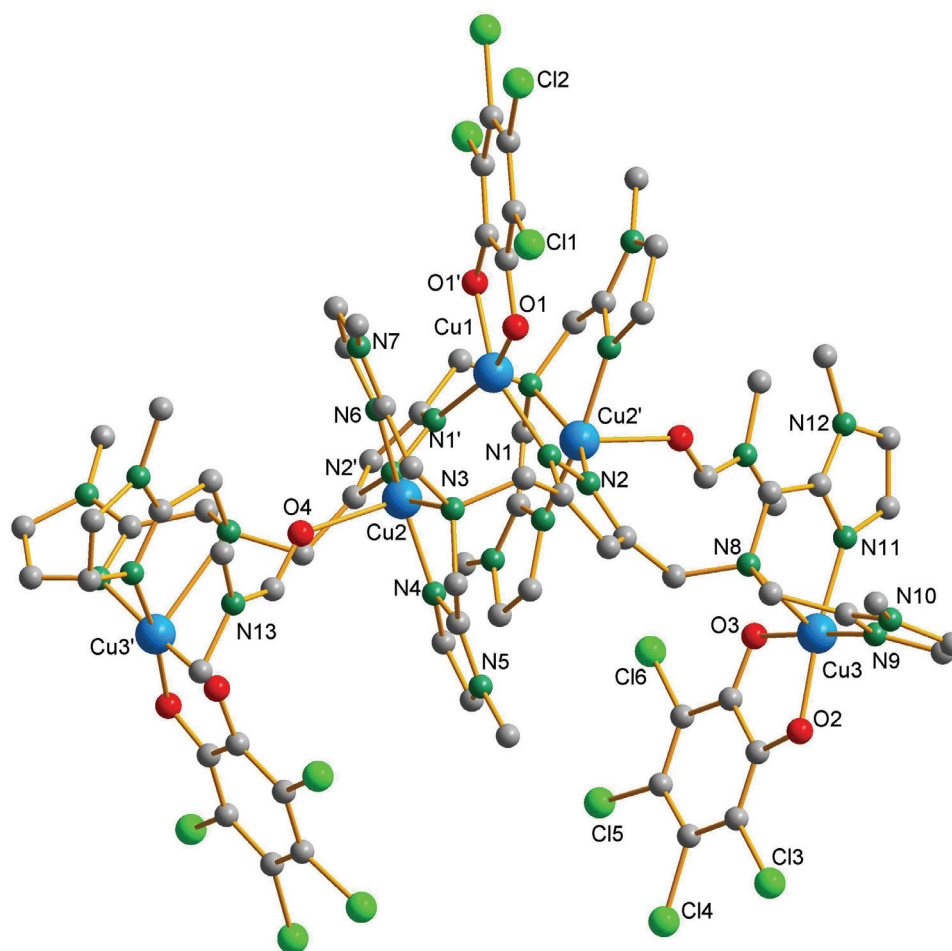
Several different binding modes for TCC within the bimetallic pocket are possible (Scheme 38): the  $\eta^1$ -mode represents monodentate coordination to only one of the copper ions (a), the  $\eta^2$ -mode, in which TCC acts as a bidentate ligand (b) which may be complemented by H-bonding to a solvent molecule of the second copper ion (c), and  $\mu$ - $\eta^1$ : $\eta^1$ -mode, which represents a bridging coordination to both copper ions of a dinuclear complex (d).



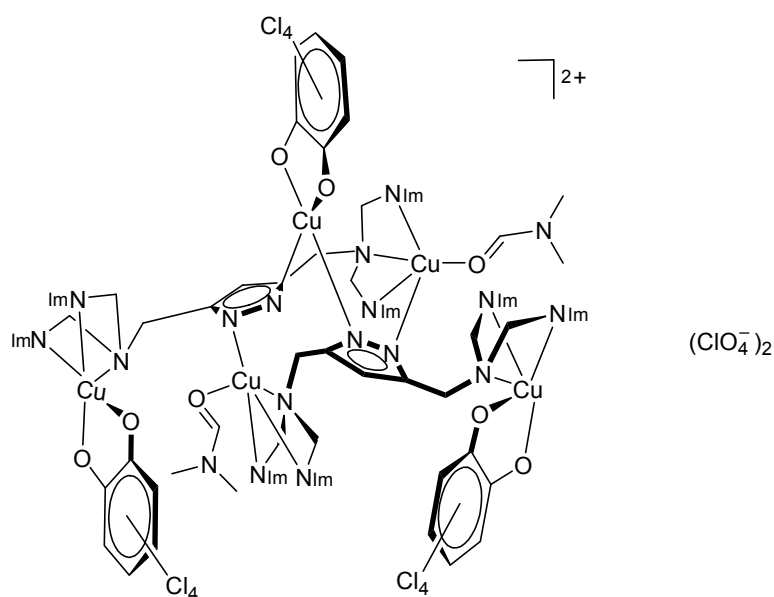
**Scheme 38.** Possible binding motifs of TCC within a dicopper core.

In order to investigate the coordination behaviour of the dicopper complex **5a** towards not only phenols but also *o*-diphenols, and to extend the library of the possible modes of substrate binding for dicopper complexes with pyrazolate-based ligands, TCC was reacted with the newly synthesized bioinspired dicopper(II) complex **5a**. To a solution of **HL**<sup>4</sup> in methanol

were added two equivalents of KO $t$ Bu and subsequently, after 10 min of stirring, two equivalents of Cu(ClO $_4$ ) $_2$ ·6H $_2$ O. The reaction was completed by addition of 1 equivalent of tetrachlorocatechol, which was pretreated with 1 equivalent of KO $t$ Bu to deprotonate one of the OH-groups. The colour of the reaction mixture changed from green to dark-brown. After the solvent was evaporated, the crude residue was dissolved in a MeCN/DMF mixture from which single crystals of complex **14** were obtained upon slow diffusion of Et $_2$ O. The molecular structure of the cationic part of **14** is shown in Figure 82.



**Figure 82.** Molecular structure of the cation of **14**.



**Figure 83.** Schematic representation of complex **14**: for clarity the *N*-methylimidazole is depicted as N<sub>Im</sub>.

**Table 20.** Selected intramolecular distances (Å) and angles (°) for complex **14**.

Distances			
Cu(1)-O(1)'	1.912(4)	Cu(3)-O(3)	1.931(4)
Cu(1)-O(1)	1.912(4)	Cu(3)-N(11)	1.979(5)
Cu(1)-N(1)	1.987(4)	Cu(3)-N(9)	1.982(5)
Cu(1)-N(1)'	1.987(4)	Cu(3)-N(8)	2.470(4)
Cu(2)-N(4)	1.942(4)	Cu(1)···Cu(2)	3.1801(8)
Cu(2)-N(6)	1.951(4)	Cu(1)···Cu(3)	8.3560(9)
Cu(2)-N(2)'	1.965(4)	Cu(2)···Cu(3)	9.0634(9)
Cu(2)-N(3)	2.106(4)	Cu(2)···Cu(2)'	4.955(1)
Cu(2)-O(4)	2.312(3)	Cu(3)···Cu(3)'	12.817(1)
Cu(3)-O(2)	1.920(4)	Cu(2)···Cu(3)'	5.9133(9)
Angles			
O(1)'-Cu(1)-O(1)	86.8(2)	N(6)-Cu(2)-O(4)	82.71(14)
O(1)'-Cu(1)-N(1)	156.90(15)	N(2)'-Cu(2)-O(4)	115.21(15)
O(1)-Cu(1)-N(1)	93.62(17)	N(3)-Cu(2)-O(4)	88.44(14)
O(1)'-Cu(1)-N(1)'	93.62(17)	O(2)-Cu(3)-O(3)	85.50(17)
O(1)-Cu(1)-N(1)'	156.90(15)	O(2)-Cu(3)-N(11)	169.61(18)

N(1)-Cu(1)-N(1)'	94.8(2)	O(3)-Cu(3)-N(11)	91.34(18)
N(4)-Cu(2)-N(6)	163.30(19)	O(2)-Cu(3)-N(9)	91.76(19)
N(4)-Cu(2)-N(2)'	98.94(17)	O(3)-Cu(3)-N(9)	175.04(17)
N(6)-Cu(2)-N(2)'	97.51(17)	N(11)-Cu(3)-N(9)	92.1(2)
N(4)-Cu(2)-N(3)	82.45(17)	O(2)-Cu(3)-N(8)	112.82(16)
N(6)-Cu(2)-N(3)	81.35(17)	O(3)-Cu(3)-N(8)	100.43(15)
N(2)'-Cu(2)-N(3)	156.09(15)	N(11)-Cu(3)-N(8)	77.48(16)
N(4)-Cu(2)-O(4)	92.83(14)	N(9)-Cu(3)-N(8)	76.82(17)

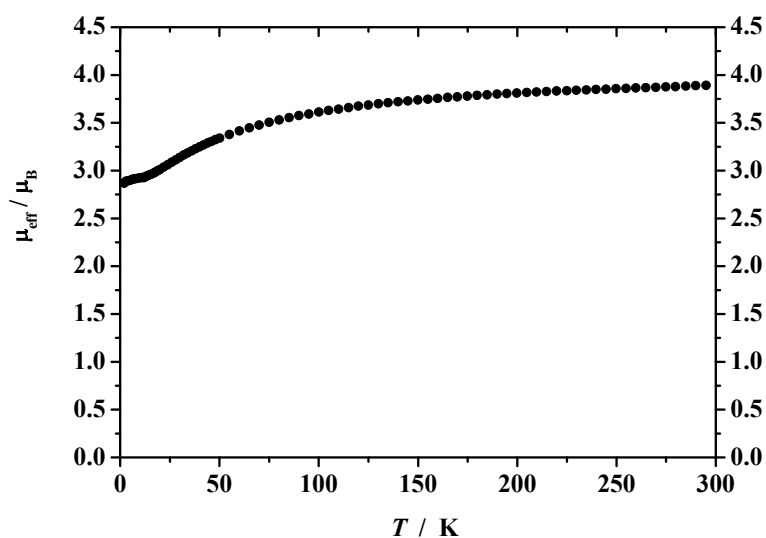
Surprisingly, an unusual pentanuclear copper complex was isolated instead of the expected dinuclear species. This can be explained by the significant flexibility of the pyrazolate ligand system, especially in the case of a polydentate imidazolyl side arms. These chelate arms incorporated into ligand **HL**<sup>4</sup> possess a very high affinity towards copper, which in some cases results in coordination of copper ions solely in the side arm unit without involving the pyrazole core, as observed in **6**, for example. Such a coordination motif induces a dimerization of the dinuclear species formed or even leads to more complicated structural features as observed in **14**.

Two ligands and five copper atoms are incorporated in the molecular structure of complex **14** and moreover, three TCC molecules are bound to three of the copper atoms. The structure possesses overall  $C_2$ -symmetry. One of the copper atoms (Cu1) has a distorted tetragonal geometry, whilst being coordinated to N-atoms of two different pyrazolate units. The coordination sphere is completed by a TCC molecule which is  $\eta^2$ -coordinated in the bidentate binding mode. A copper atom of the second type (Cu2) is ligated by four N-atoms (three from the side arm of one ligand subunit and an additional pyrazole N-atom of the second ligand involved) and one additional oxygen atom from a DMF molecule used for crystallization, resulting in almost perfect square pyramidal geometry ( $\tau = 0.11$ ). The remaining side arms of the two ligands have rotated away from the pyrazole core and host the remaining copper atom (Cu3), whose coordination sphere consists of three side arm N atoms. An overall square pyramidal geometry ( $\tau = 0.11$ ) of this outer metal ion is completed by the  $\eta^2$  – bound TCC molecule.

Signals at 1183, 937, 872 and 627  $m/z$  were observed in the ESI MS spectrum of a MeCN solution of **14**, which confirm the presence of the species  $[\text{Cu}_3\text{L}^4(\text{TCC})_2]^+$ ,  $[\text{Cu}_2\text{L}^4(\text{TCC})(\text{MeOH})_2]^+$ ,  $[\text{Cu}_2\text{L}^4(\text{TCC})]^+$  and  $[\text{Cu}_2\text{L}^4]^+$ , respectively. The structural features were perfectly reflected in the UV/vis spectrum in MeCN solution, where two  $d-d$  transition

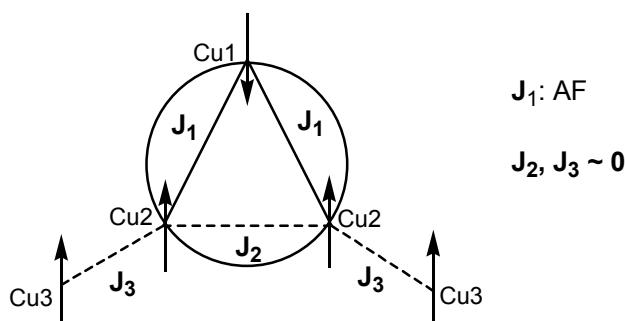
bands were observed: a typical *d-d* band for a tetragonally coordinated copper center (Cu1) with  $\lambda_{\text{max}} = 917$  nm, and a high energy *d-d* transition for square pyramidal copper ions (Cu2 and Cu3) with a band at  $\lambda_{\text{max}} = 702$  nm.

The magnetic susceptibility of a powdered sample of **14** was measured at two different magnetic fields (2000 G and 5000 G) in a temperature range from 2.0 K to 295 K. No significant field dependence was observed. The temperature dependence of the effective magnetic moment  $\mu_{\text{eff}}$  is depicted in Figure 84.



**Figure 84.** Plot of  $\mu_{\text{eff}}$  versus temperature at 2000 G for **14**.

The magnetic moment of  $3.86 \mu_{\text{B}}$  at 295 K closely matches the value expected for five uncoupled copper(II) ions (Scheme 39) while upon decreasing the temperature to 2 K, only three uncoupled copper(II) ions remained ( $3.00 \mu_{\text{B}}$ ).



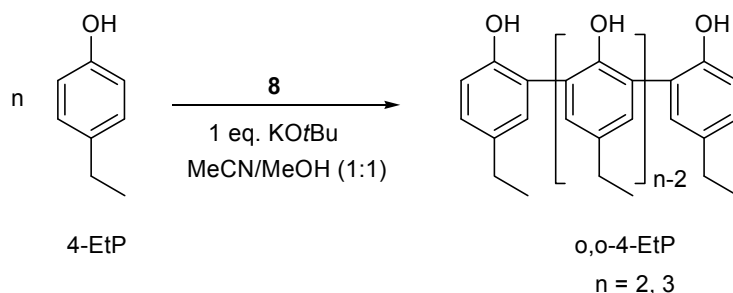
**Scheme 39.** A qualitative picture showing the alignment of the spin moment of the electrons in the pentanuclear copper complex **14**.



The observed antiferromagnetic interaction can take place only between three copper atoms bridged by a pyrazole unit ( $d(\text{Cu1}\cdots\text{Cu2}) = 3.18 \text{ \AA}$ ) resulting in a spin value of  $\frac{1}{2}$ . Two outer copper atoms (Cu3) remained uncoupled and the overall spin value for the whole system at low temperature is  $\frac{3}{2}$ .

## 9 Oxidative *ortho*-C-C coupling of 4-ethylphenol catalyzed by **8**

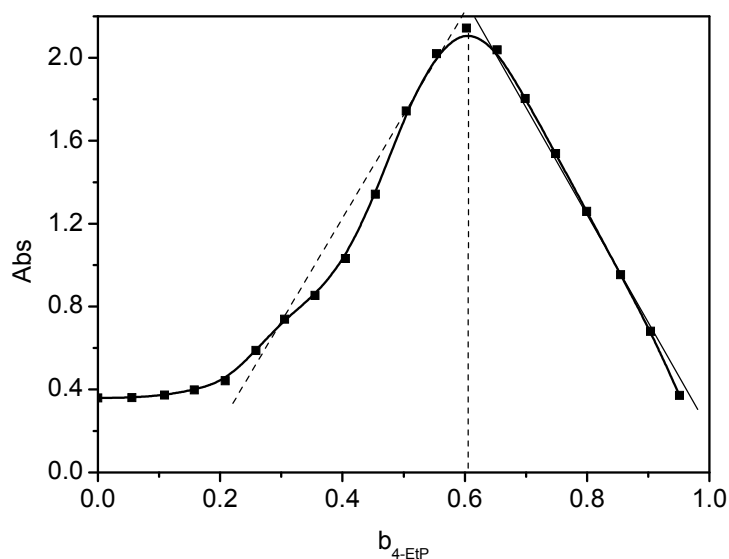
In marked contrast to the observed selective oxidative C-C coupling of TMP in the *para*-position to yield TMSQ, the substrate 4-ethylphenol (from here on abbreviated as 4-EtP) was found to undergo C-C coupling in the *ortho*-position yielding an unique oligomeric compound o,o-4-EtP (Scheme 40). Apparently, steric congestion at the *para* substituent in 4-EtP favors C-C coupling in the *ortho*-position to occur. Therefore, the only accessible positions for any C-C coupling are the carbons that are in the *ortho*-positions to the phenol, as coupling in *meta*-position is electronically not preferable in terms of stability of a reactive intermediate (cf. resonance structures of aromatic substitution reactions).



**Scheme 40.** Oxidative C-C coupling of 4-EtP in the *ortho*-position catalyzed by **8**.

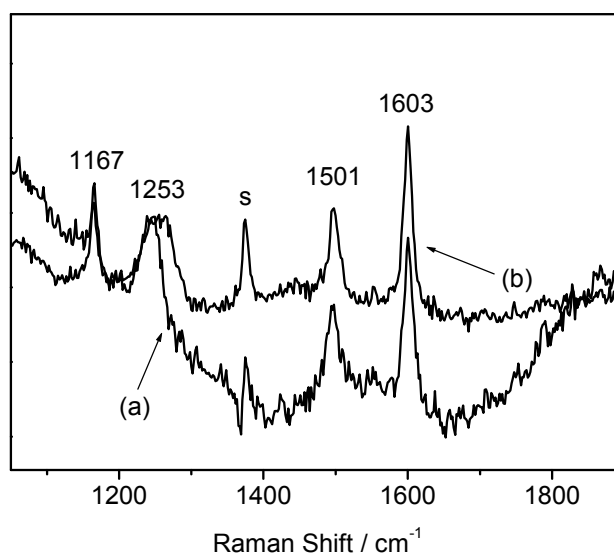
The catalyst used for performing the oxidative C-C coupling of 4-EtP was based on the ligand **HL**<sup>5</sup> with a phenyl substituent in the backbone of the pyrazole core. Unfortunately, crystallization of the dinuclear copper(II) complexes derived from this ligand did not result in formation of crystals suitable for X-ray analysis (opposite to what was expected and intended when this ligand backbone was designed), and only in one case the tetranuclear complex **8** was structurally characterized. As discussed in section 5.5, this particular tetranuclear species is most likely present only in the solid state, and on the basis of ESI spectrometry a dissociation process is assumed to be operative in solution, resulting in the formation of dinuclear subunit **8'** with a MeO...HOMe or HO...HOH bridging motif (depending on the solvent used) within the bimetallic pocket (see Scheme 28 in section 5.5), as observed in **5a**. This dinuclear species **8'** was considered as the active species during the oxidative C-C coupling of 4-EtP. Contrary to the C-C coupling of TMP, for the observed coupling of 4-EtP to occur, the presence of one additional equivalent of external base (KOtBu) is required.

Addition of the substrate to a MeCN solution of **8** without additional base resulted in appearance of the copper(II)-phenolate CT band at 453 nm. No significant shift of the copper *d-d* transition band was observed, which is a typical feature for simple coordination of the phenol molecule within the bimetallic pocket via replacement of bound H<sub>2</sub>O/MeOH, and without any further oxidation occurring. Observation of the reaction mixture over time showed that the intensity of this CT band remained unchanged, indicating that this copper(II)-phenolate species is unreactive. Unfortunately, studies on the stoichiometry between copper complex and 4-EtP by Job's method were unsuccessful due to significant dissociation of the phenolate species in solution under these conditions. <sup>1</sup>H NMR analysis of the reaction mixture after 24 h and after separation of all copper species passing the solution over a silica column revealed the presence of the starting 4-EtP as the only organic material. UV/vis studies were carried out with the reaction mixture including one additional equivalent of base. Addition of base led to a shift of the LMCT band to higher wavelength, with a maximum at 473 nm, concurrent with an increase in the intensity of this band. These observations indicate a shift of the reaction equilibrium towards the formation of the copper(II)-phenolate species and therefore Job's method was applied to study the stoichiometry between **8** and the phenolate derived from 4-EtP. Unfortunately, this particular technique does not allow investigations on the interaction between the dicopper complex and 4-EtP in the presence of only one equivalent of base (as used for the reaction). Therefore, a Job experiment was performed using a solution of completely deprotonated 4-EtP. From the Job plot depicted in Figure 85 it was deduced that a maximum of two phenolate molecules can be coordinated to the dicopper core.



**Figure 85.** Job plot of **8** with 4-EtP in MeCN,  $\lambda_{\text{max}} = 473$  nm.

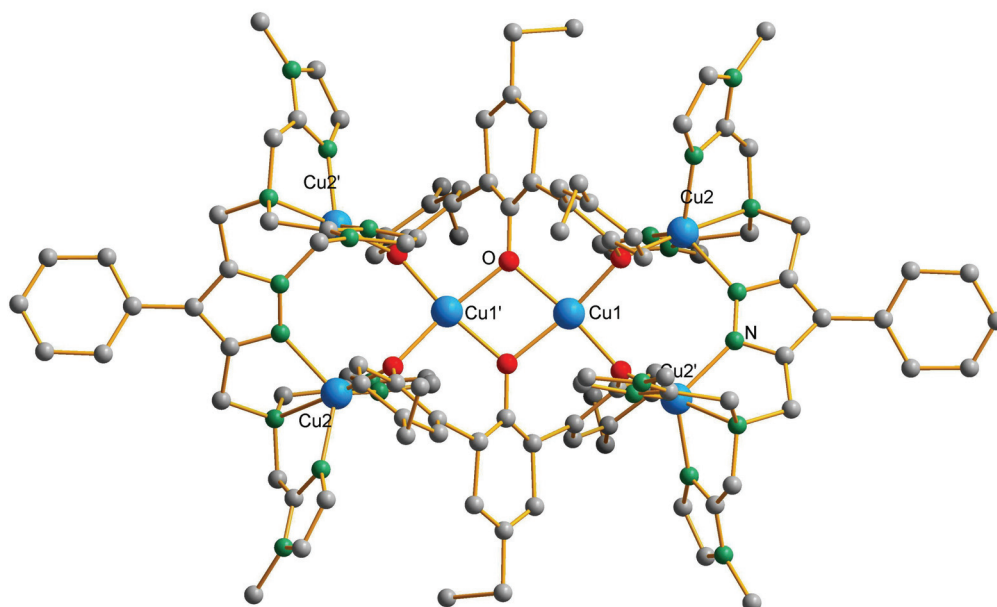
To further study the influence of base on the reaction between **8** and 4-EtP, Raman spectroscopy was applied. First of all, the Raman spectrum of the reaction mixture without supplementary base was recorded (Figure 86 (a)).



**Figure 86.** Resonance Raman spectra of the reaction mixture of **8** and 4-EtP in MeCN;  $\lambda_{\text{ex}} = 488$  nm; (a) mixture without KOtBu; (b) mixture with one equivalent of KOtBu; s denotes not fully subtracted solvent peak.

Laser excitation was performed at 488 nm, i.e. into the LMCT band of the copper(II)-phenolate adduct at 453 nm. Typical features were observed in the Raman spectrum for a phenolate coordinated to copper(II) (as for example observed in case of phenolate adduct with M<sub>t</sub>BuP, see section 7.4.1), with bands at 1167, 1253, 1501, and 1603 cm<sup>-1</sup>. Addition of base did not induce any changes in the Raman spectrum, proving that the identical dicopper(II)-phenolate species is formed under both conditions (Figure 86 (b)).

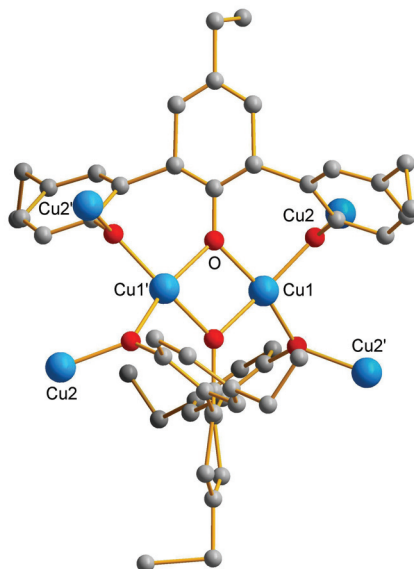
Slow diffusion of Et<sub>2</sub>O into a solution of **8** and 4-EtP with one equivalent of KO<sup>t</sup>Bu led to formation of the black crystals. The X-ray crystallographic measurements allowed only a rough estimation of the molecular structure, because of the presence of disordered solvent molecules for which no satisfactory model for the disorder could be found. The corresponding approximation of the molecular structure of **15** is shown in Figure 87.



**Figure 87.** Molecular structure of the cationic part of complex **15**. Average positions of the carbon atoms of the central phenolate unit were calculated from the disordered atomic positions, initially available from the X-ray data analysis.

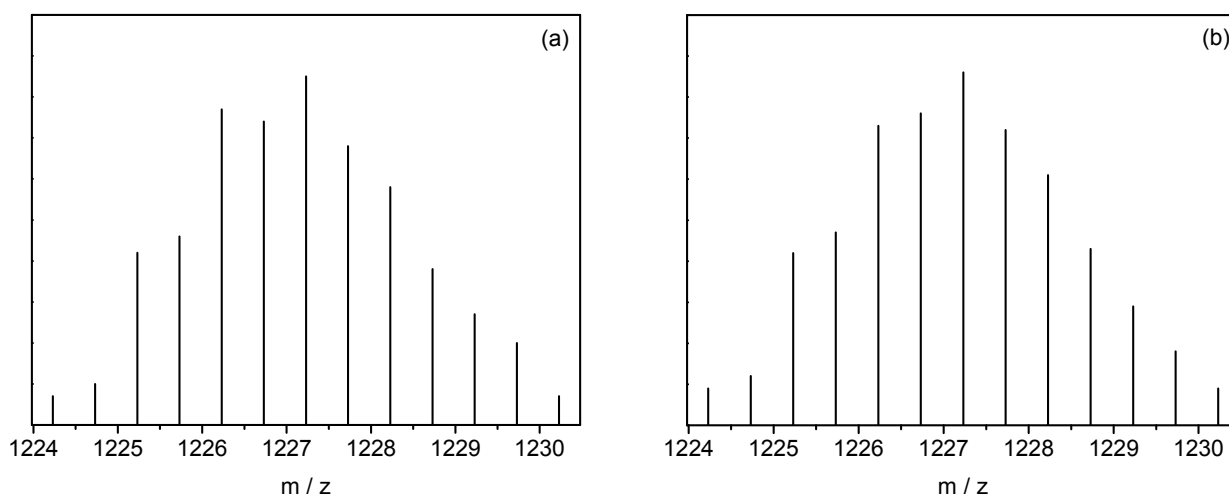
The formed oligonuclear complex **15** consists of two outer pyrazolate-based dicopper subunits with the copper atoms (Cu2 and Cu2') hosted within the chelate arm compartments and bridged by pyrazole, as anticipated. The coordination of Cu2/Cu2' is completed by a phenolate-O atom from the central Cu<sub>2</sub>O<sub>6</sub> part of the complex, which has apparently been formed via C-C coupling of 4-EtP. Coupling in both *ortho*-positions of the central 4-EtP

fragment yielded a unique 2,2',5',2''-triphenol species that acts as a bridging ligand for all six copper atoms present in the molecular structure. Each phenolate unit bridges two copper ions, resulting in a distorted square planar geometry for the two copper atoms located in the center of the molecule (Figure 88).



**Figure 88.** Selected part of the cation of the molecular structure of complex **15**: Nitrogen- and carbon-atoms of the pyrazole ligands are omitted for clarity.

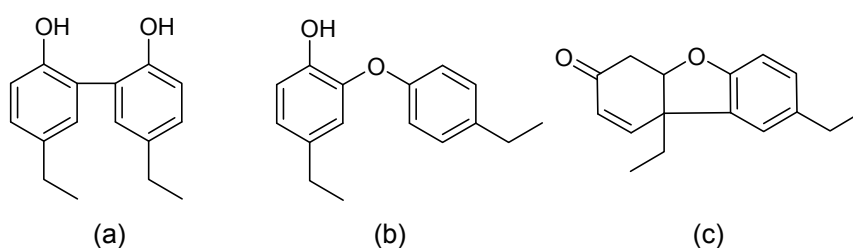
Stability of such a hexanuclear species in solution was proven by means of ESI high resolution mass spectrometry, whereby a doubly charged cation  $[M-2(\text{ClO}_4)]^{2+}$  (M is complex **15**) was detected at 1224.23  $m/z$  (calcd. 1224.22790  $m/z$  (Figure 89)).



**Figure 89.** High resolution ESI-spectrum of complex **15** in MeCN: (a) observed signal; (b) simulated isotope pattern for the fragment  $[M-2(\text{ClO}_4)]^{2+}$ .

The UV/vis spectrum in the solid state (diffuse reflectance) showed three signals at  $\lambda_{\text{max}}$  of 427, 633 and 1039 nm, which are in good agreement with the coordination environments of the copper ions found in the crystal structure. Thus, the signal at 1039 nm corresponds to the *d-d* transition band of the copper ions in a trigonal bipyramidal geometry (Cu2, Cu2'), while the absorption maximum at 633 nm is typically assigned to a *d-d* band for copper in a square planar coordination mode (Cu1, Cu1'). The coordinated triphenol unit implies the presence of a copper-to-phenolate CT transition band, found in the solid state UV/vis spectrum at 427 nm. These spectroscopic features were also found in some other copper complexes with incorporated phenolate subunits.<sup>172</sup> The UV/vis spectrum of an acetonitrile solution of **15** showed only two *d-d* bands at 972 and 732 nm for the copper ions in a trigonal bipyramidal and square planar coordination mode, respectively. The observed differences in UV/vis spectra in the solid state and solution imply some structural preorganization in the hexanuclear copper complex **15** upon dissolving.

Analysis of the reaction mixture after crystallization of this complex by means of GC-MS spectrometry revealed the presence of 4-EtP (122 *m/z*) and three isomers of the dimeric derivative of 4-EtP at 242 *m/z*. The small difference observed in the fragmentation of these isomers (for two of these isomers loss of a CH<sub>3</sub>-group was observed, while in the third a C<sub>2</sub>H<sub>5</sub>-group was split off) did not allow the determination of the exact structure of the three isomers. Based on the studies with *p*-cresol reported in literature<sup>173</sup> it can be assumed that during the oxidative *ortho*-C-C coupling of 4-EtP different coupling modes have taken place resulting in the formation of three isomers depicted in Figure 90.



**Figure 90.** Proposed structures of three isomers of the dimeric derivative of 4-EtP.

There are three most probable possibilities to form dimers during the C-C coupling, i.e. an *ortho-ortho* C-C coupling to form dimer (a), an *ortho* C-O-C coupling to yield dimer (b), and an *ortho-para* C-C coupling to form a structural analogue to the Pummerer's ketone.

The trimeric product derived from 4-ethylphenol (362 *m/z*), which was found in the crystal structure, was detected only in traces, while any other oligomeric compounds derived from 4-

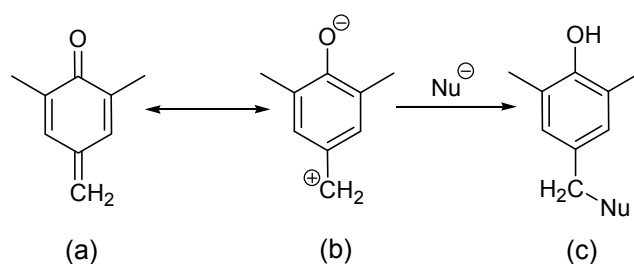
EtP were not observed in the GC-MS spectrum. These oligomeric compounds may did not form at all or their absence can either be caused by (unexpected) strong interaction of these oligomers with the column material used for the measurements or a low tendency of these species to become ionized, resulting in insufficiently low concentrations for detection in the GC-MS set-up.

On the basis of these results, it can be concluded that C-C coupling of the substrate 4-EtP preferably occurs in the *ortho*-position, as was found in the crystal structure of **15**. Most likely, this reaction mechanistically proceeds via an initially formed bisphenol species, as detected by GC mass spectrometry.



## 10 Nucleophilic 1,6-addition of MeOH to 2,4,6-trimethylphenol

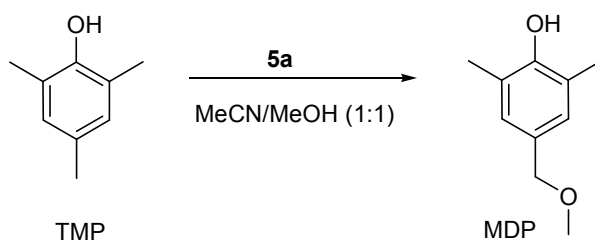
Derivatives of 2,4,6-trimethylphenol functionalized at the 4-position are very important organic compounds for industrial purposes<sup>174,175</sup> as well as for fundamental research.<sup>176,177</sup> It is known that the synthetic pathway to produce *para*-substituted 2,4,6-trimethylphenol derivatives may involve a benzoquinone methide intermediate (Scheme 41 (a)).<sup>99</sup>



**Scheme 41.** Benzoquinone methide (a), its zwitterionic resonance form (b), *para*-substituted product after nucleophilic addition (c).

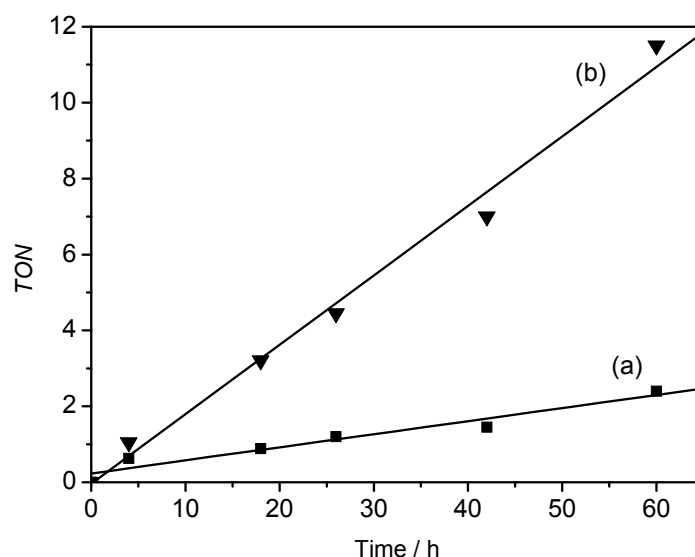
*para*-Benzoquinone methide exists only as a short-lived species in dilute solution, and has a limited stability.<sup>178</sup> Considering the existence of such a highly reactive *para*-benzoquinone methide species, formation of 4-methoxy-2,6-dimethylphenol could be explained as a result of nucleophilic attack by methoxide, formed from a deprotonated methanol molecule, to a quinone methide.<sup>99</sup> Work previously reported by Reedijk and co-workers on the nucleophilic addition to TMP made use of the copper system [CuCl<sub>2</sub>-(neocuproine)<sub>2</sub>-NaOMe] to mediate a four-electron process to convert TMP, via ketal formation and subsequent hydrolysis, to yield 4-hydroxy-3,5-dimethylbenzaldehyde **XVII** (see section 3.3, Scheme 15).

2,4,6-Trimethylphenol, which undergoes selective oxidative C-C coupling catalyzed by dicopper(II) complex **5a** in MeCN/CH<sub>2</sub>Cl<sub>2</sub> (see section 6.3), can yield distinctly different products upon changing the reaction conditions, most notably by varying the reaction medium. Thus, addition of MeOH to a reaction mixture of **5a** and TMP in MeCN after 10 minutes of reaction time led to 1,6-nucleophilic addition of MeOH to the methyl-group of TMP in the *para*-position, resulting in the formation of 4-methoxy-2,6-dimethylphenol (MDP) (Scheme 42).



**Scheme 42.** 1,6-nucleophilic addition of MeOH to TMP catalyzed by **5a**.

Standard reaction conditions as for the oxidative C-C coupling of TMP were initially used to perform the 1,6-nucleophilic addition of MeOH to TMP. 4 ml of MeOH was added after 10 minutes to a reaction mixture of **5a** and five equivalents of TMP in 4 ml of MeCN. The yield of 4-methoxy-2,6-dimethylphenol was determined by means of  $^1\text{H}$ -NMR spectroscopy, using 1,3,5-trimethoxybenzene as internal standard. Formation of MDP was established after detection of the characteristic signal in the  $^1\text{H}$  NMR spectrum at 3.34 ppm for the  $\text{CH}_3$ -group of the resulting ether fragment. The reaction was followed for 60 h after which time MDP was formed in 48% yield, corresponding to a TON of 2.5 (Figure 91 (a)). Together with the formation of 4-methoxy-2,6-dimethylphenol as the major product, traces of 4-hydroxy-3,5-dimethylbenzaldehyde were observed. Use of a bigger excess of TMP (50 eq.) led to formation of MDP with a total turnover number of 12, after 60 h (Figure 91 (b)).



**Figure 91.** Turnover numbers for formation of MDP: (a) 5 equivalents TMP; (b) 50 equivalents TMP.

As was previously described (see section 5.4.2), dicopper complex **5a** contains a MeO··HOMe bridge within the bimetallic pocket. It was furthermore established that upon coordination of the phenolic substrate to one of the copper(II) ions, the OH-group of the phenol becomes deprotonated due to the presence of the methoxide ligand that is acting as a internal base, and a methanol molecule is released. In order to prove that 1,6-addition of ‘exogenous’ methanol added to the reaction mixture was taking place, CD<sub>3</sub>OD was used as nucleophile. The reaction was performed under the same conditions, using 5 equivalents excess of TMP but instead CD<sub>3</sub>OD was added after 10 min of reaction time (Scheme 43).



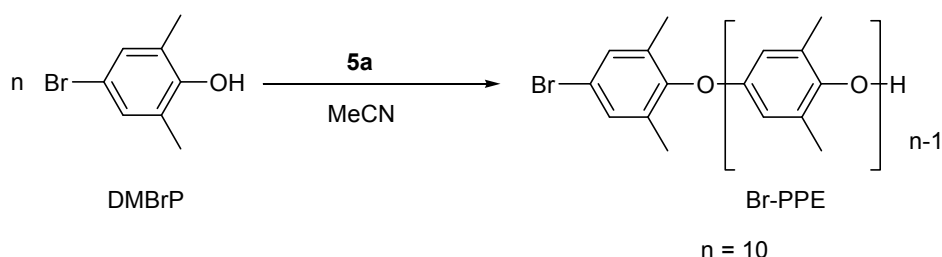
**Scheme 43.** 1,6-nucleophilic addition of CD<sub>3</sub>OD to TMP catalyzed by **5a**.

Analysis of the reaction mixture by <sup>1</sup>H NMR spectroscopy after 40 h confirmed the formation of <sup>D</sup>MDP, where nucleophilic addition on the *para*-methyl group has occurred with incorporation of the fully deuterated OCD<sub>3</sub>-group, resulting in the complete absence of the signal for the protons of the OCH<sub>3</sub>-group at 3.34 ppm, while again only traces of 4-hydroxy-3,5-dimethylbenzaldehyde were detected.

The observed 1,6-addition of MeOH and *d*<sup>4</sup>-MeOH catalyzed by dicopper complex **5a** shows the significant potential of this complex to act as a versatile catalyst in different kinds of phenol oxidations besides the C-C coupling reaction, which can be used in the future to generate new organic compounds, not only by means of C–C bond formation but in particular also by C–N and C–O bond making reactions.

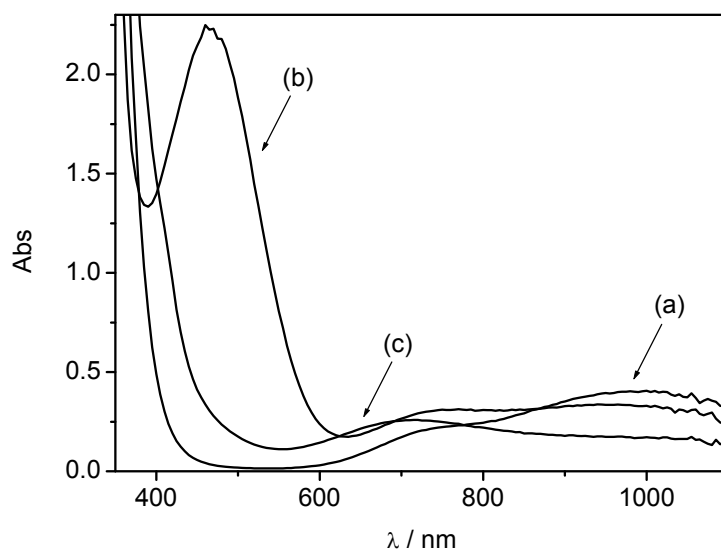
## 11 Oxidative C-O coupling of 4-bromo-2,6-dimethylphenol catalyzed by **5a**

4-bromo-2,6-dimethylphenol (from here on abbreviated as DMBrP), which was initially applied as a model substrate to study phenol binding to the dicopper complex **5a**, since it was thought to be “inert” and should not participate in any Cu-mediated catalytic reaction, was in fact shown to undergo oxidative C-O coupling to yield a oligomeric compound Br-PPE in the presence of **5a** and dioxygen (Scheme 44).

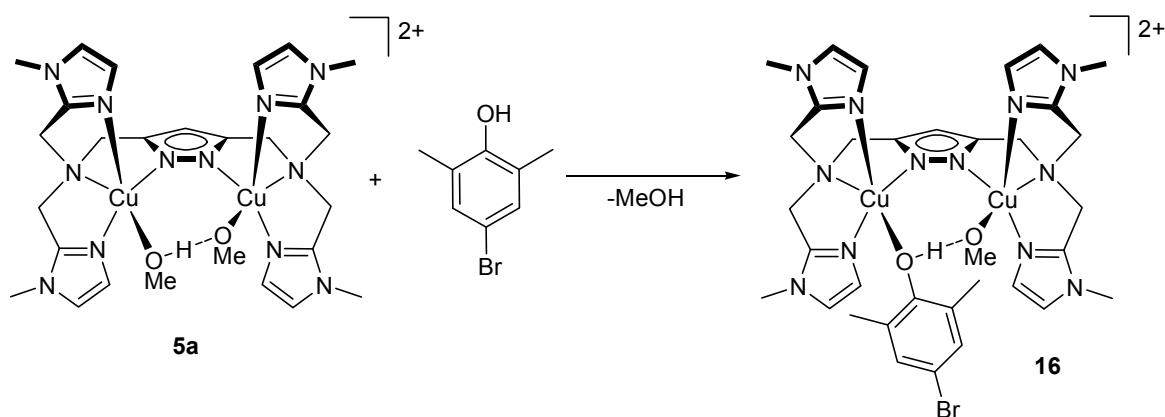


**Scheme 44.** Oxidative C-O coupling of DMBrP catalyzed by **5a**.

The reaction was followed in time by means of UV/vis spectroscopy. The electronic spectrum of the green solution of **5a** in MeCN showed a *d-d* band at  $\lambda_{\text{max}}$  989 nm with a shoulder at 724 nm, corresponding to transitions of copper(II) ions in a trigonal bipyramidal environment (Figure 92 (a)). Addition of the DMBrP led to an immediate colour change from green to red, reflected in the UV/vis spectrum through the appearance of an intense charge-transfer band at  $\lambda_{\text{max}}$  465 nm and a shift of the Cu<sup>II</sup>-based *d-d* transition band to 960 nm (Figure 92(b)). These observations indicate that also with this substrate a dicopper(II)-phenolate species **16** (Scheme 45) is formed through deprotonation and exchange with the methanolate fragment.



**Figure 92.** UV/vis spectra at different stages of the oxidative C-O coupling of DMBrP (initial concentration of **5a** = 0.001 mol·L<sup>-1</sup>; initial concentration of DMBrP = 0.021 mol·L<sup>-1</sup>; L = 1.0 cm; solvent: MeCN: (a) starting solution of **5a**; (b) a few seconds after addition of DMBrP (red solution); (c) 12 min after addition of DMBrP.

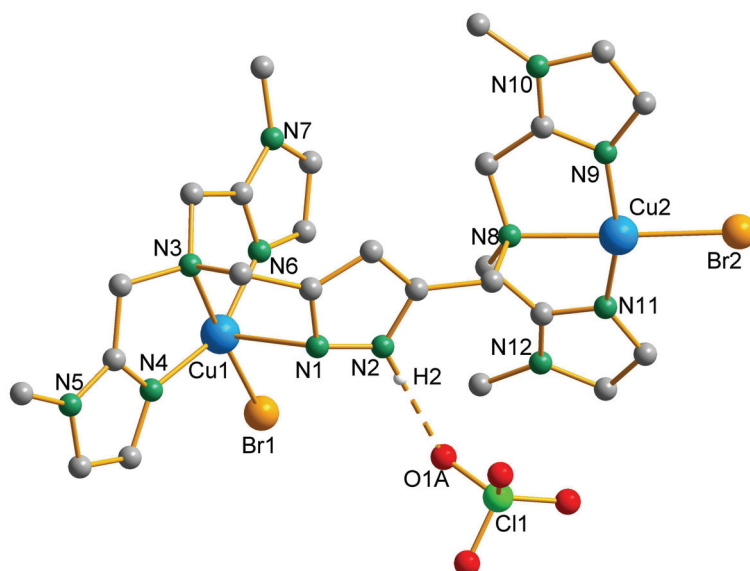


**Scheme 45.** Coordination of the DMBrP within the bimetallic pocket of **5a**.

Somewhat surprisingly and in contrast to the results obtained with TMP as the substrate (see section 6.3), rapid disappearance of the formed copper(II)-phenolate species occurred within 10 minutes, concomitant with a colour change of the reaction mixture to deep green (Figure 92 (c)). The UV/vis spectrum of the resultant solution showed the typical *d-d* transition band at  $\lambda_{\text{max}}$  695 nm for a copper(II) ion in square pyramidal coordination environment. Polymeric Br-PPE precipitated from the green solution as a white powder within the next 10 minutes.

Analysis of the white precipitate by means of EI mass spectrometry proved the polymeric nature of the material, as it was found that the polymer chain consisted of at least ten phenol ether moieties with a peak at 1282  $m/z$ , which corresponds to  $[\text{C}_{80}\text{H}_{80}\text{O}_{10}\text{Br}]^+$ . Further studies on the exact polymer composition were not performed.

Slow evaporation of the deep green solution at room temperature led to the accumulation of blue crystals, suitable for X-ray analysis.



**Figure 93.** Molecular structure of the cation of complex **17** including one  $\text{ClO}_4^-$  anion to indicate the H-bonding with the pyrazole NH-unit. The second one is omitted for clarity.

The molecular structure of complex **17** (Figure 93) revealed the constitution of a structural analogue of **7**, where the pyrazole N-atom is protonated. This protonation induces a splitting of the ( $\mu$ -pyrazolato) dicopper core found in **5a** and leaves only one of the copper ions coordinated to the now non-bridging pyrazole fragment. Thus, Cu1 is nested in a distorted square pyramidal coordination environment ( $\tau = 0.31$ ), ligated by four N-donors, including all three nitrogens from the side arm of the ligand, and a Br atom. The second metal is hosted by the dangling chelate arm compartment and is four-coordinated by three N-donors from the side arm and one additional Br atom resulting in a distorted square planar geometry. Additional H-bonding is observed between the NH-unit of the pyrazole and a perchlorate anion (H2-O1A (2.02 Å)).

**Table 21.** Selected atom distances (Å) and angles (°) for complex **17**.

Distances			
Cu(1)-N(4)	1.923(7)	Cu(2)-N(9)	1.895(8)
Cu(1)-N(6)	1.939(8)	Cu(2)-N(11)	1.899(8)
Cu(1)-N(3)	2.150(8)	Cu(2)-N(8)	2.130(6)
Cu(1)-Br(1)	2.3791(17)	Cu(2)-Br(2)	2.3594(13)
Cu(1)-N(1)	2.382(6)	Cu(1)···Cu(2)	8.014(1)
Angles			
N(4)-Cu(1)-N(6)	156.4(3)	N(3)-Cu(1)-N(1)	80.9(2)
N(4)-Cu(1)-N(3)	81.3(3)	Br(1)-Cu(1)-N(1)	94.25(18)
N(6)-Cu(1)-N(3))	82.4(4)	N(9)-Cu(2)-N(11)	160.7(4)
N(4)-Cu(1)-Br(1)	99.3(2)	N(9)-Cu(2)-N(8)	82.6(3)
N(6)-Cu(1)-Br(1)	98.4(3)	N(11)-Cu(2)-N(8)	81.7(3)
N(3)-Cu(1)-Br(1)	175.09(18)	N(9)-Cu(2)-Br(2)	97.1(2)
N(4)-Cu(1)-N(1)	104.1(2)	N(11)-Cu(2)-Br(2)	98.0(2)
N(6)-Cu(1)-N(1)	90.0(3)	N(8)-Cu(2)-Br(2)	177.66(19)

Such structural changes in the complex **5a** after performing the oxidative C-O coupling of DMBrP are most likely caused by the presence of HBr that is formed as a by-product. It can be assumed that after coordination of one DMBrP molecule to the dicopper(II) complex **5a**, the formation of phenoxyl radicals is taking place and further polymerization proceeds via a radical pathway. In the meantime a lot of studies have shown that C-O coupling, in particular of DMP, can also occur via coupling of phenoxonium cations with phenolate anions.<sup>179</sup> Both mechanistic pathways include release of the H-atom from the *para*-position in DMP, which in the present case is replaced by a Br-atom. Liberation of Br<sup>-</sup>, which then binds to the dicopper active site of **5a**, led to the structural reorganization, resulting in formation of the complex **17**. No further mechanistic studies were performed on the C-O polymerization of DMBrP.

## 12 Discussion of the proposed mechanism for C-C coupling of TMP

On the basis of the currently available results, as they are discussed in this thesis, the following mechanism for the oxidative C-C coupling of TMP ( $3e^-$  overall per TMP molecule) can be proposed (Scheme 46). The mechanism illustrated below has to be considered only as a preliminary working scheme, as some details are still not totally clear.

### *Coordination of TMP within the bimetallic pocket of 5a:*

Coordination of the TMP substrate to the dicopper(II) complex **5a** was proven by UV/vis spectroscopy, where an intense band appeared at  $\lambda_{\max}$  495 nm ( $\epsilon \sim 1500 \text{ L}\cdot\text{mol}^{-1}\cdot\text{cm}^{-1}$ ) upon the addition of TMP to the solution of **5a**. This band was identified as a ligand-to-metal charge-transfer (LMCT) absorption from the phenolate to the copper ion, based on the shift in the UV/vis spectrum to higher wavelength in the order 4-methylphenol (4-MeP), 2,6-dimethylphenol (DMP) and 2,4,6-trimethylphenol (TMP), and the characteristic Raman signatures. Such spectroscopic changes were attributed to coordination of a phenolate to one of the copper(II) ions of complex **5a** owing to a methanolate-phenolate exchange, concomitant with release of the methanol molecule.

Studies on the determination of the stoichiometry for the reaction of TMP with dicopper complex **5a** showed that under aerobic conditions a maximum of two molecules of TMP can coordinate to **5a**, resulting in formation of a copper(II)-phenolate species, for which the exact structure is so far unclear. Furthermore, based on identical studies with model substrates such as 4-methylphenol and 4-*tert*-butylphenol, it was revealed that a key factor required for further reaction to occur is not the number of coordinated phenol substrates, but the substitution pattern and the resulting electronic properties of the phenol ring. In addition, a distinct influence of the steric factors on the further reactivity of the copper(II)-phenolate species was proven. Thus, formation of an unreactive phenolate species was observed with 2,3,5-trimethylphenol (2,3,5-TMP) and 2,5,6-trimethylphenol (2,5,6-TMP) as substrate molecules. This clearly shows that the presence of substituents in the *meta*-position(s) of the phenol ring is blocking any further reactivity.





*Adducts with model substrate molecules:*

Copper(II)-phenolate complexes with phenolic substrates such as pentafluorophenol (PFP) and 4-hydroxybenzamide (4-AP), that do not display any Cu-mediated reactivity, were fully characterized. Structural features of these model complexes have proven that the assumed methanolate-phenolate exchange occurs upon coordination of phenols and revealed a likely mode of interaction between phenols and dicopper complex **5a**. It was shown that coordination of the phenolic molecule occurred only to one of the copper ions in **5a** and that the adduct formed is additionally stabilized by  $\pi$ - $\pi$  stacking interaction (in case of pentafluorophenol) between the imidazole and phenol rings, as well as by H-bonding between the phenolate-O and a methanol molecule that is coordinated to the adjacent copper ion within the bimetallic pocket.

*Active species:*

The nature of the active species formed upon coordination of the TMP substrate within the bimetallic pocket of **5a** is the key point in the mechanism. It is believed that C-C coupling of the related substrate DMP occurs via a radical pathway, which would imply the formation of a copper(II)copper(I)-phenoxyl radical species for the studied system with TMP as well. This assumption is not supported by the features observed with UV/vis spectroscopy. Addition of the TMP to **5a** induces the appearance of an LMCT band at 495 nm, which is more characteristic for a copper(II)-phenolate species. Resonance Raman spectroscopy was particularly useful and allowed to gain insight into the structural and electronic properties of the species formed. It was shown that interaction of TMP and **5a** results in formation of a copper(II)-phenolate species. Typical features for a phenolate coordinated to copper(II) were observed in the Raman spectrum at 1156 ( $\nu_{9a}$  C-H bending), 1237 ( $\nu_{7a}$  C-O stretching), and 1607  $\text{cm}^{-1}$  ( $\nu_{8a}$   $C_{ortho}$ - $C_{meta}$  ring stretching). Moreover, EPR studies on the reaction of a model  $\text{Cu}^{\text{II}}\text{Zn}^{\text{II}}$  complex with TMP did not reveal any evidence for the formation of phenoxyl radicals. In this light, it is proposed that the ground state of the adduct can be described as a dicopper(II)-phenolate. However, it can not be excluded that this is in equilibrium with a copper(II)copper(I) phenoxyl radical species (which might also be a thermally accessible excited state species) which is then responsible for further reactions to occur.

Based on studies reported in the literature on the nucleophilic 1,6-addition of small molecules to TMP catalyzed by a mononuclear copper system,<sup>99</sup> it is believed that one of the possible pathways is formation of a highly active benzoquinone methide intermediate after the first  $2e^-$  oxidation step of TMP. It was proposed that the *para*-benzylic proton of TMP is activated *via*

coordination of the phenolate to the copper center and this  $1e^-$  transfer induces the polarization of the benzylic C–H bond, resulting in a rearrangement of the aromatic ring to a highly reactive quinone methide. The same kind of 1,6-addition of both MeOH as well as  $d^4$ -MeOH to TMP was observed using complex **5a** as catalyst. However, there is no evidence for the formation of a putative highly active methide intermediate after initial  $2e^-$  oxidation of TMP for the present system, since it would require formation of the fully reduced  $Cu^I Cu^I$  species, which is not observed experimentally.

*Formation of the initial products:*

Formation of the first organic product TMBB in 100% yield through a stoichiometric reaction (from the 5 equivalents of TMP used only 1 equivalent underwent oxidation) was proven by means of  $^1H$  NMR spectroscopy. This process is taking place under both aerobic and anaerobic conditions. However, under an  $N_2$ -atmosphere, the reaction is halted after the formation of TMBB. The  $1e^-$  transfer that occurs upon activation of coordinated TMP implies reduction of only one copper in complex **5a**, which was fully confirmed by trapping of the resulting mixed-valence copper species with the strong  $\sigma$ -donor ligand *tert*-butyl isocyanide. These results are in good agreement with studies on the stoichiometry between **5a** and TMP using Job's method under anaerobic conditions: *it was clearly shown that only one TMP molecule is coordinated to the dicopper core and is able to induce a  $1e^-$  transfer to the  $Cu^{II}$  ion it is bound to, resulting in formation of TMBB in a stoichiometric fashion.* The formed mixed-valence  $Cu^I Cu^{II}$  species after release of the TMBB molecule can *not* be reoxidized under anaerobic conditions. Presence of the  $Cu^I Cu^{II}$  species after this first oxidation step was also proven by means of EPR spectroscopy showing a four-line pattern that is characteristic for a mononuclear copper(II) system.

In marked contrast with these observations, it was discovered that in the presence of dioxygen two molecules of TMP were found to interact with copper complex **5a**, which is most likely the result of several parallel processes: *under aerobic conditions the mixed-valence  $Cu^I Cu^{II}$  species formed after release of TMBB is reoxidized and able to bind either another TMP molecule or the TMBB intermediate, to finally form the product TMSQ. In this light, the Job plot of TMP with **5a** under aerobic conditions represents a mixture of different species formed during the overall reaction, resulting in the average amount of two coordinated TMP molecules.*

The stoichiometrically formed TMBB can be further oxidized in air *only* in the presence of the parent dicopper complex **5a**. Therefore aerial dioxygen is required for the reoxidation of the mixed-valence  $\text{Cu}^{\text{I}}\text{Cu}^{\text{II}}$  species formed after the first reaction step.

The  $4e^-$  oxidation reaction of TMBB to yield TMSQ most likely occurs via formation of a second organic intermediate, concurrent with generation of another mixed-valence  $\text{Cu}^{\text{I}}\text{Cu}^{\text{II}}$  species. Unfortunately, detection of the second organic intermediate was not possible under both aerobic (formation in non-isolated yield) and anaerobic conditions (rapid formation of TMSQ from TMBB).

*H<sub>2</sub>O<sub>2</sub> test:*

It was convincingly shown that  $\text{H}_2\text{O}_2$  is not formed during the oxidative C-C coupling of TMP to TMSQ. This means that water is formed as the reduction product, implying that 1.5 molar equivalents of  $\text{O}_2$  is needed per molecule of TMSQ formed.

## 13 Conclusions

In the present thesis the design-concept for pyrazole-based ligands, which makes use of the fact that the anionic pyrazolate unit has a high tendency to span two metal ions in a  $\mu$ - $\eta^1:\eta^1$  *exo*-bidentate fashion, was applied for a range of copper complexes and moreover, the coordination spheres of the individual copper ions as well as the intramolecular metal-metal separation were properly tuned. Ligand **HL**<sup>2</sup> with *N*-dimethyl-aminopropyl groups was shown to undergo an unusual copper mediated amine to *N*-oxide transformation. The formed copper complexes with bound *N*-oxide were structurally characterized. On the basis of selected performed studies, it was concluded that this kind of amine to *N*-oxide transformation is taking place only during the crystallization procedure and in the presence of aerial dioxygen. No formation of *N*-oxide species was observed under anaerobic conditions.

Furthermore, new pyrazole-based ligands with bio-inspired bis[(1-methylimidazole-2-yl)-methyl]amine chelating side arms in the 3- and 5-positions of the heterocyclic core were prepared and fully characterized. The coordination behaviour of these new ligands (**HL**<sup>4</sup> and **HL**<sup>5</sup>) towards copper was elucidated and it was shown that these ligands form very stable copper complexes. Determination of the different species formed in solution, depending on the pH (in particular for complexes based on a ligand with appended bis[2-(1-methylimidazolyl)methyl]aminomethyl chelate arms) was successfully performed by potentiometric and spectroscopic methods and all relevant copper complexes were structurally characterized.

Properly characterized copper complexes, in particular **5a**, with carefully tuned and desired properties, were applied as catalysts in different types of oxidation reactions of phenolic substrates. In particular, it was shown that dicopper complex **5a** catalyzes the unusual oxidative C-C coupling of 2,4,6-trimethylphenol (TMP) to yield TMSQ. Moreover, the formation and structure of intermediates in the catalytic reactions of TMP were elucidated by means of various spectroscopic methods (i.e. Raman, EPR, NMR and UV/vis spectroscopy). On the basis of these studies it was shown that C-C coupling of TMP is taking place only in the presence of dicopper complex **5a** and dioxygen as oxidant. The mixed-valence Cu<sup>I</sup>Cu<sup>II</sup> species which is formed after the first oxidation step of TMP was trapped using the strong  $\sigma$ -donor isocyanide ligand and structurally characterized. Furthermore, the first organic

intermediate formed during the catalytic C-C coupling reaction - TMBB - was isolated. It was clearly shown that further oxidation of this biphenol intermediate is possible only in the presence of initial dicopper complex **5a** and therefore, aerial dioxygen is required for the oxidation of the mixed-valence  $\text{Cu}^{\text{I}}\text{Cu}^{\text{II}}$  species formed after the first reaction step. Dicopper(II)-phenolate complexes with 4-hydroxybenzamide and pentafluorophenol substrates that were considered inert to any oxidation reaction were successfully prepared, which revealed a mode of interaction between phenols and dicopper complex **5a**. It was shown that coordination of the phenolic molecule occurred only to one of the copper ions in **5a** and that the adduct formed is additionally stabilized by  $\pi$ - $\pi$  stacking interaction (in case of pentafluorophenol) between the imidazole and phenol rings as well as by H-bonding between the phenolate-O and methanol molecule that is coordinated to the adjacent copper ion within the bimetallic pocket.

The ground state of the key species in the C-C coupling reaction of TMP was characterized as a dicopper(II)-phenolate, which was proven by means of Raman and EPR spectroscopy.

All these above-mentioned studies provided a better understanding of the principles/factors that govern the catalytic oxidation activity towards phenols of pyrazolate-based complexes reminiscent of *type 3* dicopper sites, and allowed to propose a preliminary mechanism for the oxidative C-C coupling of TMP.

In addition, it was shown that, depending on the reaction conditions applied, dicopper complex **5a** can catalyze the 1,6-nucleophilic addition of several small molecules such as MeOH to TMP. The observed 1,6-addition of MeOH and  $d^4$ -MeOH catalyzed by dicopper complex **5a** showed the significant potential of this complex to act as a versatile catalyst in different kinds of phenol oxidations besides the C-C coupling reaction. This can be used in the future to generate new organic compounds, not only by means of C-C bond formation but in particular also by C-N and C-O bond making reactions.

Furthermore, a C-O bond forming reaction with 4-bromo-2,6-dimethylphenol was shown to occur in the presence of **5a** as catalyst to yield a polymeric phenylene ether.

Finally, *ortho* C-C coupling of 4-ethylphenol to yield an oligomeric compound can be also performed using an analogue to copper complex **5a** based on a pyrazole ligand (**HL**<sup>5</sup>) with a modified backbone. An oligonuclear copper complex **15** that represent an intermediate in the described reaction was crystallized and structurally characterized.

All these studies have shown the vital potential of a new class of bioinspired copper complexes, based on biorelevant pyrazole ligands, to act as catalysts in various oxidation reactions of phenols. Moreover, this work presents mechanistic insight, in particular on the unusual oxidative C-C coupling of TMP to yield TMSQ. These results will undoubtedly provide the significant background necessary to advance future studies on bioinspired phenol oxidation reactions.

*Every time we set ourselves to learn, we have to labor as hard as anyone can. The limits of our learning will be determined by our nature.*

*The Wheel of Time*

*Carlos Castaneda*

## 14 Experimental section

### 14.1 General

*Equipment:* Preparations of air sensitive materials were carried out under nitrogen atmosphere using standard Schlenk techniques or in the N<sub>2</sub>-filled glove box. All glassware was dried by heating under vacuum.

*Solvent purification:* Solvents were purified and dried by established procedures, in particular: Aceton (calcium hydride), Acetonitrile (phosphorus pentoxide), Dichloromethane (calcium hydride), Diethylether (sodium/potassium), Tetrahydrofuran (sodium/potassium), Ethanol (sodium), Methanol (magnesium).

*Elemental analysis:* Microanalyses were performed by the Analytisches Labor des Anorganisch-Chemischen Instituts der Universität Göttingen using a CHN-O-Rapid from the company Elementar.

*Infrared spectroscopy:* IR spectra (as KBr pellets) were recorded with a Digilab Excalibur. The given intensity in the experimental section is abbreviated as follows:

vs	very strong
s	strong
m	medium
w	weak

*UV/vis spectroscopy:* UV/vis spectra of solutions and solids (diffuse reflectance) were recorded with a Varian Cary 5000 spectrometer at room temperature using quartz cuvettes (L = 1 cm).

*Mass spectrometry:* Mass spectra were measured with a Finnigan MAT 95 (FAB-MS), a Finnigan MAT LCQ (HR-ESI-MS) and with an Applied Biosystems API 2000 (ESI-MS). For the FAB-MS measurement 3-nitrobenzylalcohol (3-NBA) or glycerine were used as matrix. EI spectra were recorded with a Finnigan MAT 8200 (70 eV).



*NMR:* NMR spectra were recorded with a Bruker Avance 200 ( $^1\text{H}$ : 200.13 MHz,  $^{13}\text{C}$ : 50.3 MHz), 500 ( $^1\text{H}$ : 500.13 MHz,  $^{13}\text{C}$ : 125.7 MHz) and with a Bruker 900 MHz NMR-Spektrometer (52mm) at room temperature. The residual solvent signal was used as the chemical shift reference ( $\text{CDCl}_3$ :  $\delta_{\text{H}} = 7.24$ ,  $\delta_{\text{C}} = 77.0$ ), ( $(\text{CD}_3)_2\text{SO}$ :  $\delta_{\text{H}} = 2.54$ ,  $\delta_{\text{C}} = 40.45$ ) and ( $\text{CD}_3\text{CN}$ :  $\delta_{\text{H}} = 1.96$ ,  $\delta_{\text{C}} = 118.26$ ) relative to external trimethylsilane ( $\delta = 0$ ). Abbreviated as follows: s (singlet), d (doublet), t (triplet), m (multiplet).

*Magnetic measurements:* Magnetic data were measured with a Quantum-Design MPMS-5S SQUID magnetometer equipped with a 5 Tesla magnet in the range from 295 K to 2 K. The powdered samples were contained in a gel bucket and fixed in a non-magnetic sample holder.

*Stopped-Flow measurement:* Stopped-Flow measurements were performed using Bio-Logic stopped-flow module SFM-20 with gas tight glass syringers Hamilton 1010C at room temperature.

*Raman spectroscopy:* Resonance Raman spectra were obtained using LabRAM HR Vis (400-1100 nm) with open-electrode CCD detector. Excitation was provided by an  $\text{Ar}^+$  ion laser. The laser line, 488.7 nm, was chosen to coincide with the intense absorption transition of the copper(II)-phenolate species. Sample concentrations were approximately 5-6 mM in dicopper complexes **5a** or **8**. All measurements were carried out at room temperature in MeCN.

*GC-MS measurement:* GC-MS spectra were recorded using Finnigan INCOS 50 with connected gas chromatograph Varian 3400.

*Cyclovoltammetry:* Redox properties have been examined by cyclovoltammetry in MeCN/0.1 M  $[\text{NBu}_4]\text{PF}_6$  at room temperature. A glassy carbon electrode was used as a working electrode, platinum as a counter electrode and SCE (Ag-electrode) as reference electrode. All spectra were measured versus the  $\text{Cp}_2\text{Fe}/\text{Cp}_2\text{Fe}^+$  couple.

*EPR measurements:* X-band EPR were measured on a Bruker ELEXSYS E 500 spectrometer, equipped with a digital temperature control ER 4131 VT using helium as coolant.

*Chemicals:*

3,5-Bis(chloromethyl)-1-(tetrahydropyran-2-yl)pyrazole<sup>100,101,102</sup>

Bis[(6-methyl-2-pyridyl)methyl]amine **XXIX**,<sup>103a</sup>

Bis[(1-methylimidazol-2-yl)-methyl]amine<sup>103b,c</sup>

3,5-Bis(hydroxymethyl)-4-phenyl-pyrazole<sup>104</sup>

*CD*<sub>3</sub>-TMP<sup>130</sup>

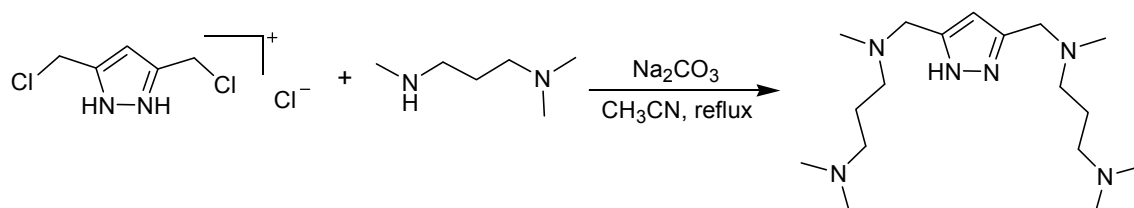
All other chemicals were purchased from commercial sources (Merck, Aldrich, Lancaster and Grüssing) and used as received.

**Caution!** Although no problems were encountered in this work, transition metal perchlorate complexes are potentially explosive and should be handled with proper precautions.

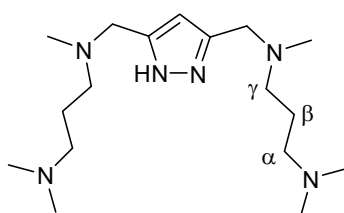
## 14.2 Synthesis of ligands **HL**<sup>1</sup>-**HL**<sup>5</sup>

Ligands **HL**<sup>1</sup> and **HL**<sup>2</sup> were prepared by modified literature procedure<sup>15a</sup>

*ligand **HL**<sup>1</sup>:*



3,5-Bis(chloromethyl)pyrazole hydrochloride (4.02 g, 20 mmol) and *N,N,N'*-trimethyl-1,3-propanediamine (5.0 g, 40 mmol) were dissolved in 600 mL of MeCN and Na<sub>2</sub>CO<sub>3</sub> (24.38 g, 0.23 mol, pre-dried at 100-120°C and 10<sup>-3</sup> mbar) was added to this solution. The reaction mixture was refluxed for 4 days while stirring. After filtration to remove insolubles, the solvent was evaporated and the residue was dried at 60°C and 10<sup>-3</sup> mbar for 12 h. **HL**<sup>1</sup> was obtained as light yellow oil.



Yield: 3.95 g, 61 %

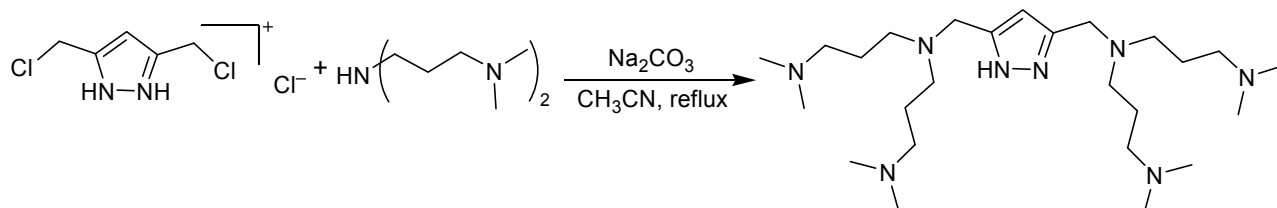
Empirical formula: C<sub>17</sub>H<sub>36</sub>N<sub>6</sub>

Molecular weight: 324.5 g/mol

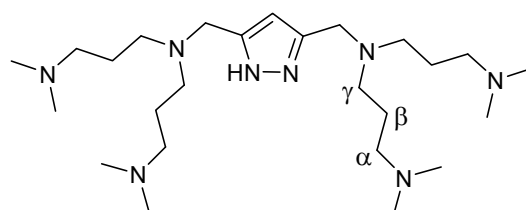
<sup>1</sup>H-NMR (CDCl<sub>3</sub>) δ (ppm): 1.32 (p, *J* = 7.2 Hz CH<sub>2</sub> (β), 4H), 1.87 (s, CH<sub>3</sub>, 12H), 1.88 (s, CH<sub>3</sub>, 6H), 1.96 (t, *J* = 7.2 Hz, CH<sub>2</sub> (α), 4H), 2.05 (t, *J* =

	7.2 Hz, CH <sub>2</sub> (γ), 4H), 3.21 (s, pz-CH <sub>2</sub> , 4H), 5.68 (s, pz-CH, 1H)
<sup>13</sup> C-NMR (CDCl <sub>3</sub> ) δ (ppm):	26.2 (CH <sub>2</sub> (β)), 43.4 (CH <sub>3</sub> ), 46.4 (CH <sub>3</sub> ), 52.3 (pz-CH <sub>2</sub> ), 55.2 (CH <sub>2</sub> (α)), 55.8 (CH <sub>2</sub> (γ)), 104.9 (pz-C <sup>4</sup> ), pz-C <sup>3/5</sup> not observed
MS (EI) <i>m/z</i> (%):	324 (35) [C <sub>17</sub> H <sub>36</sub> N <sub>6</sub> ] <sup>+</sup> 238 (15) [C <sub>17</sub> H <sub>36</sub> N <sub>6</sub> – (CH <sub>2</sub> ) <sub>3</sub> N(CH <sub>3</sub> ) <sub>2</sub> ] <sup>+</sup> 210 (50) [C <sub>17</sub> H <sub>36</sub> N <sub>6</sub> – N(CH <sub>3</sub> )(CH <sub>2</sub> ) <sub>3</sub> N(CH <sub>3</sub> ) <sub>2</sub> ] <sup>+</sup>
Elemental analysis (%):	for C <sub>17</sub> H <sub>36</sub> N <sub>6</sub> calcd.: C 62.92, H 11.18, N 25.90 found: C 61.12, H 11.28, N 25.77

**ligand HL<sup>2</sup>:**

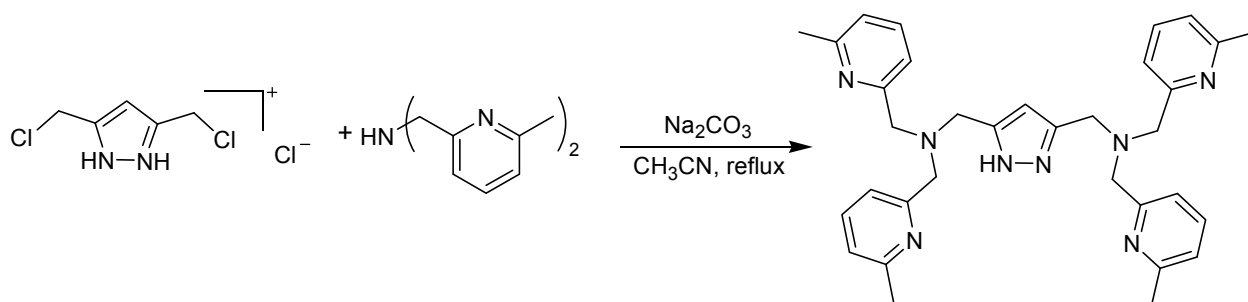


3,5-Bis(chloromethyl)pyrazole hydrochloride (4.02 g, 20 mmol) and N,N-bis-(3-dimethylaminopropyl)amine (7.48 g, 40 mmol) were dissolved in 700 mL of MeCN and Na<sub>2</sub>CO<sub>3</sub> (24.38 g, 0.23 mol, pre-dried at 100-120°C and 10<sup>-3</sup> mbar) was added to this solution. The reaction mixture was refluxed for 3 days while stirring. After filtration, the solvent was evaporated. Unreacted starting amine was separated from the desired ligand by high vacuum distillation (50°C and 10<sup>-3</sup>) mbar and the residue obtained was dried at 60°C and 10<sup>-3</sup> mbar for 12 h. **HL<sup>2</sup>** was obtained as light yellow oil.



Yield:	5.59g, 60 %
Empirical formula:	C <sub>25</sub> H <sub>54</sub> N <sub>8</sub>
Molecular weight:	466.5 g/mol
<sup>1</sup> H-NMR (CDCl <sub>3</sub> ) δ (ppm):	1.48 (p, <i>J</i> = 7.1 Hz CH <sub>2</sub> (β), 8H), 2.04 (s, CH <sub>3</sub> , 24H), 2.12 (t, <i>J</i> = 7.1 Hz, CH <sub>2</sub> (α), 8H), 2.31 (t, <i>J</i> = 7.1 Hz, CH <sub>2</sub> (γ), 8H), 3.47 (s, pz-CH <sub>2</sub> , 4H), 5.77 (s, pz-CH, 1H)
<sup>13</sup> C-NMR (CDCl <sub>3</sub> ) δ (ppm):	24.6 (CH <sub>2</sub> (β)), 44.8 (CH <sub>3</sub> ), 44.9 (CH <sub>3</sub> ), 50.0 (pz-CH <sub>2</sub> ), 51.2 (CH <sub>2</sub> (α)), 57.1 (CH <sub>2</sub> (γ)), 102.2 (pz-C <sup>4</sup> ), pz-C <sup>3/5</sup> not observed
MS (EI) <i>m/z</i> (%):	466 (20) [C <sub>25</sub> H <sub>54</sub> N <sub>8</sub> ] <sup>+</sup> 380 (5) [C <sub>25</sub> H <sub>54</sub> N <sub>8</sub> – (CH <sub>2</sub> ) <sub>3</sub> N(CH <sub>3</sub> ) <sub>2</sub> ] <sup>+</sup> 281 (40) [C <sub>25</sub> H <sub>54</sub> N <sub>8</sub> – {N(CH <sub>3</sub> )(CH <sub>2</sub> ) <sub>3</sub> N(CH <sub>3</sub> ) <sub>2</sub> } <sub>2</sub> ] <sup>+</sup>
Elemental analysis (%):	for C <sub>25</sub> H <sub>54</sub> N <sub>8</sub> ·2H <sub>2</sub> O calcd.: C 59.72, H 11.63, N 22.29 found: C 60.27, H 11.76, N 22.91

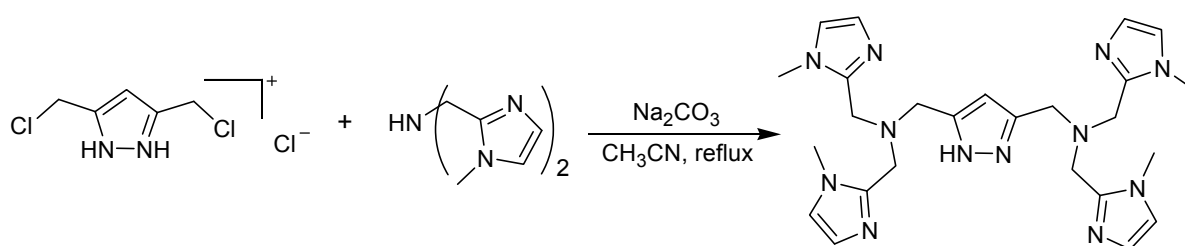
**ligand HL<sup>3</sup>:**



*N,N*-bis[(6-methyl-pyridin-2-yl)methyl]amine (5.33 g, 20 mmol) and 3,5-bis(chloromethyl)pyrazole hydrochloride (2.01 g, 10 mmol) were dissolved in 500 mL of MeCN and Na<sub>2</sub>CO<sub>3</sub> (12.5 g, 0.12 mol, pre-dried at 100-120°C and 10<sup>-3</sup> mbar) was added to this solution. The reaction mixture was refluxed for 24 h while stirring. After filtration, the solvent was evaporated and the residue was dried at 60°C and 10<sup>-5</sup> mbar for 12 h. **HL<sup>3</sup>** was obtained as a white solid.

Yield:	3.9g, 72 %
Empirical formula:	C <sub>33</sub> H <sub>38</sub> N <sub>8</sub>
Molecular weight:	546.3 g/mol
Melting point:	110-112°C
<sup>1</sup> H-NMR (CD <sub>3</sub> OD) δ (ppm):	2.45 (s, CH <sub>3</sub> , 12H), 3.72 (s, pz-CH <sub>2</sub> , 4H; NCH <sub>2</sub> , 8H), 6.31 (s, pz-CH, 1H), 7.07 (d, <i>J</i> = 7.6 Hz, py-CH, 4H), 7.40 (d, <i>J</i> = 7.7 Hz, py-CH, 4H), 7.62 (t, <i>J</i> = 7.7 Hz, py-CH, 4H)
<sup>13</sup> C-NMR (CD <sub>3</sub> OD) δ (ppm):	23.7 (CH <sub>3</sub> ), 60.69 (CH <sub>2</sub> ), 106.1 (pz-C <sup>4</sup> ), 121.5 (py-C), 123.2 (py-C), 138.80 (py-C), 158.67 (py-C), 157.76 (py-C), pz-C <sup>3/5</sup> not observed
MS (EI) <i>m/z</i> (%):	546 (10) [C <sub>33</sub> H <sub>38</sub> N <sub>8</sub> ] <sup>+</sup> 440 (100) [C <sub>33</sub> H <sub>38</sub> N <sub>8</sub> – (CH <sub>2</sub> )C <sub>5</sub> H <sub>3</sub> N(CH <sub>3</sub> )] <sup>+</sup>
Elemental analysis (%):	for C <sub>33</sub> H <sub>38</sub> N <sub>8</sub> ·H <sub>2</sub> O calcd.: C 70.19, H 7.14, N 19.84 found: C 70.03, H 7.12, N 19.56

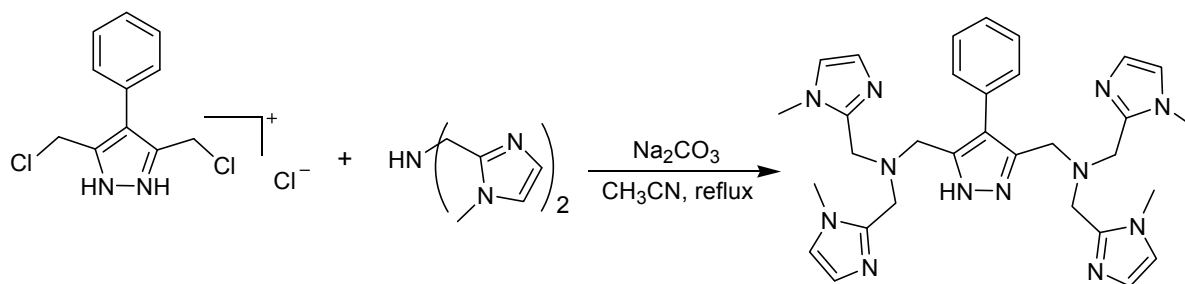
**ligand HL<sup>4</sup>:**



*N,N*-Bis[2-(1-methylimidazolyl)methyl]amine (20.50 g, 100 mmol) and 3,5-bis(chloromethyl)pyrazole hydrochloride (10.25 g, 50 mmol) were dissolved in 700 mL of MeCN and Na<sub>2</sub>CO<sub>3</sub> (53 g, 0.50 mol, pre-dried at 100-120°C and 10<sup>-3</sup> mbar) was added to this solution. The reaction mixture was refluxed for 24 h while stirring. After filtration, the solvent was evaporated and the residue was dried at 60°C and 10<sup>-3</sup> mbar for 12 h. **HL<sup>4</sup>** was obtained as a light yellow solid.

Yield:	20.80 g, 83 %
Empirical formula:	C <sub>25</sub> H <sub>34</sub> N <sub>12</sub>
Molecular weight:	502.3 g/mol
Melting point:	78-80°C
<sup>1</sup> H-NMR (CDCl <sub>3</sub> ) δ (ppm):	3.45 (s, CH <sub>3</sub> , 12H), 3.57 (s, pzCH <sub>2</sub> , 4H), 3.62 (s, NCH <sub>2</sub> , 8H), 6.14 (s, pz-CH, 1H), 6.79 (d, <i>J</i> = 1 Hz, im-CH, 4H), 6.91 (d, <i>J</i> = 1 Hz, im-CH, 4H)
<sup>13</sup> C-NMR (CDCl <sub>3</sub> ) δ (ppm):	32.4 (CH <sub>3</sub> ), 48.6 (CH <sub>2</sub> ), 49.0 (CH <sub>2</sub> ), 106.7 (pz-C <sup>4</sup> ), 121.4 (im-C), 127.0 (im-C), 145.0 (im-C <sup>2</sup> ), pz-C <sup>3/5</sup> not observed
MS (EI) <i>m/z</i> (%):	502 (5) [C <sub>25</sub> H <sub>34</sub> N <sub>12</sub> ] <sup>+</sup> 407 (100) [C <sub>25</sub> H <sub>34</sub> N <sub>12</sub> – (CH <sub>2</sub> )C <sub>3</sub> H <sub>2</sub> N <sub>2</sub> (CH <sub>3</sub> )] <sup>+</sup>
Elemental analysis (%):	for C <sub>25</sub> H <sub>34</sub> N <sub>12</sub> ·H <sub>2</sub> O calcd.: C 57.67, H 6.58, N 32.28 found: C 57.88, H 6.81, N 32.78

**ligand HL<sup>5</sup>:**



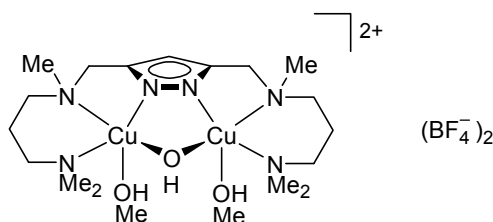
3,5-Bis(chloromethyl)-4-phenylpyrazole hydrochloride (1.80 g, 6 mmol) and bis[2-(1-methylimidazolyl)methyl]amine (2.46 g, 12 mmol) were dissolved in 100 mL of MeCN and Na<sub>2</sub>CO<sub>3</sub> (6.36 g, 60 mmol, pre-dried at 100-120°C and 10<sup>-3</sup> mbar) was added to this solution. The reaction mixture was refluxed for 48 h while stirring. After filtration, the solvent was evaporated and the residue was dried at 60°C and 10<sup>-3</sup> mbar for 12 h. **HL<sup>5</sup>** was obtained as a light yellow solid.

Yield:	1.76 g, 51 %
Empirical formula:	C <sub>31</sub> H <sub>38</sub> N <sub>12</sub>
Molecular weight:	578.7 g/mol
Melting point:	41-45°C
<sup>1</sup> H-NMR (CDCl <sub>3</sub> ) δ (ppm):	3.20 (s, CH <sub>3</sub> , 12H), 3.58 (s, NCH <sub>2</sub> , 8H), 3.79 (s, pz-CH <sub>2</sub> , 4H), 6.69 (d, <i>J</i> = 1 Hz, im-CH, 4H), 6.871 (d, <i>J</i> = 1 Hz, im-CH, 4H), 7.0 (m, Ar-CH, 2H), 7.16 (m, Ar-CH, 3H)
<sup>13</sup> C-NMR (CDCl <sub>3</sub> ) δ (ppm):	32.2 (CH <sub>3</sub> ), 48.3 (CH <sub>2</sub> ), 49.0 (CH <sub>2</sub> ), 120.2 (pz-C <sup>4</sup> ), 121.4 (im- C), 126.0 (Ar-CH), 127.0 (im-C), 128.4 (Ar-CH), 128.8 (Ar-CH), 133.3 (Ar-CH), 145.0 (im-C <sup>2</sup> ), Ar-C <sup>6</sup> not observed, pz-C <sup>3/5</sup> not observed
MS (EI) <i>m/z</i> (%):	578 (5) [C <sub>31</sub> H <sub>38</sub> N <sub>12</sub> ] <sup>+</sup> 483 (30) [C <sub>31</sub> H <sub>38</sub> N <sub>12</sub> – (CH <sub>2</sub> )C <sub>3</sub> H <sub>2</sub> N <sub>2</sub> (CH <sub>3</sub> )] <sup>+</sup>
Elemental analysis (%):	for C <sub>31</sub> H <sub>38</sub> N <sub>12</sub> ·3H <sub>2</sub> O calcd.: C 58.84, H 7.01, N 26.56 found: C 58.70, H 7.00, N 26.40



### 14.3 Synthesis of complexes

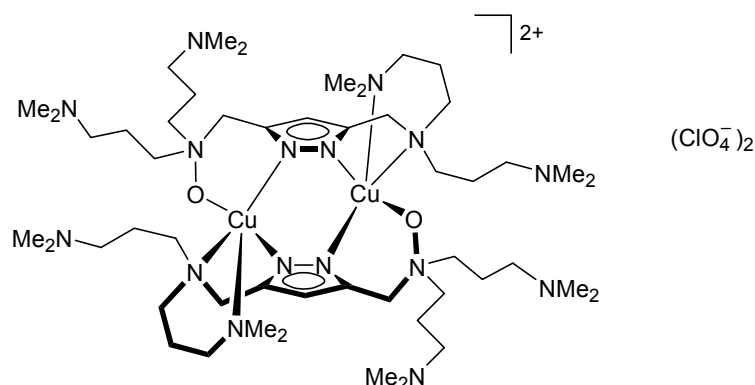
#### Preparation of $[\text{Cu}_2\text{L}^1(\mu\text{-OH})(\text{MeOH})_2](\text{BF}_4)_2$ (**1**)



A solution of **HL**<sup>1</sup> (0.08 g, 0.25 mmol) in methanol (20 mL) was treated with KO<sup>*t*</sup>Bu (0.06 g, 0.50 mmol) and stirred for 10 min at room temperature. Cu(BF<sub>4</sub>)<sub>2</sub>·4H<sub>2</sub>O (0.15 g, 0.50 mmol) was then added and the green solution was stirred for 2 h. After evaporation of the solvent, the crude product was redissolved in 5 ml of MeOH and slow diffusion of Et<sub>2</sub>O into this solution led to the formation of blue-green crystals of **1**.

Yield:	0.12 g, 68 %
Empirical formula:	C <sub>19</sub> H <sub>44</sub> Cu <sub>2</sub> N <sub>6</sub> O <sub>3</sub> B <sub>2</sub> F <sub>8</sub>
Molecular weight:	705.3 g/mol
IR (KBr) $\nu$ (cm <sup>-1</sup> ):	3494 (w), 1632 (m), 1466 (m), 1320 (w), 1082 (vs), 824 (w), 522 (w)
MS (FAB, glycerin) $m/z$ (%):	449(100) [Cu <sub>2</sub> L <sup>1</sup> ] <sup>+</sup> , 468 (50) [Cu <sub>2</sub> L <sup>1</sup> (OH)+2H] <sup>+</sup>
Elemental analysis (%):	for C <sub>18</sub> H <sub>40</sub> Cu <sub>2</sub> N <sub>6</sub> O <sub>2</sub> B <sub>2</sub> F <sub>8</sub> calcd.: C 32.11, H 5.99, N 12.48 found: C 29.67, H 5.58, N 11.86
UV/vis (MeCN) $\lambda$ (nm) [ $\epsilon$ ] (L mol <sup>-1</sup> cm <sup>-1</sup> ):	628 (282)

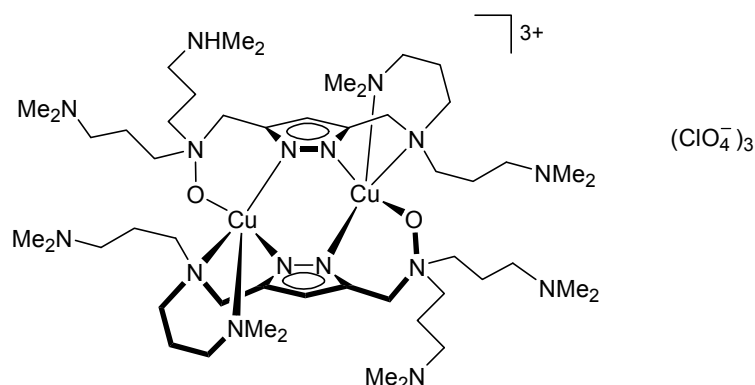
### Preparation of $[\text{Cu}_2(\text{L}^2\text{O})_2](\text{ClO}_4)_2$ (**3**)



A solution of **HL**<sup>2</sup> (0.12 g, 0.25 mmol) in methanol (20 mL) was treated with KO<sup>t</sup>Bu (0.06 g, 0.50 mmol) and stirred for 10 min at room temperature. Cu(ClO<sub>4</sub>)<sub>2</sub>·6H<sub>2</sub>O (0.18 g, 0.50 mmol) was then added and the green mixture was stirred for 2 h. After evaporation of the solvent *in vacuo*, the crude product was redissolved in 10 ml of EtOH and slow diffusion of petroleum ether (PE 40-60) into this solution led to the formation of blue-green crystals of **3**·0.47H<sub>2</sub>O.

Yield:	5 mg, 3.0 %
Empirical formula:	C <sub>50</sub> H <sub>106</sub> Cu <sub>2</sub> N <sub>16</sub> O <sub>10</sub> Cl <sub>2</sub> ·0.47H <sub>2</sub> O
Molecular weight:	1297.9 g/mol
IR (KBr) $\nu$ (cm <sup>-1</sup> ):	3429 (m), 2958 (w), 1635 (w), 1467 (m), 1257 (w), 1152 (w), 1090 (vs), 801 (m), 625 (m), 503 (w)
MS (ESI, MeOH) $m/z$ (%):	1189 (95) $[\text{Cu}_2\text{L}^2\text{O}_2(\text{ClO}_4)-2\text{H}]^+$ , 1125 (100) $[\text{Cu}_2\text{L}^2\text{O}_2(\text{MeOH})]^+$

# Preparation of $[\text{Cu}_2\text{H}(\text{L}^2\text{O})_2](\text{ClO}_4)_3$ (**3a**)



A solution of **HL**<sup>2</sup> (0.12 g, 0.25 mmol) in methanol (20 mL) was treated with KO<sup>t</sup>Bu (0.06 g, 0.50 mmol) and stirred for 10 min at room temperature. Cu(ClO<sub>4</sub>)<sub>2</sub>·6H<sub>2</sub>O (0.18 g, 0.50 mmol) was then added and the green solution was stirred for 2 h. After evaporation of solvent, the crude product was redissolved in 10 ml of MeOH and slow diffusion of Et<sub>2</sub>O into this solution led to the formation of blue-green crystals of **3a**·3MeOH.

Yield: 4 mg, 2.2 %

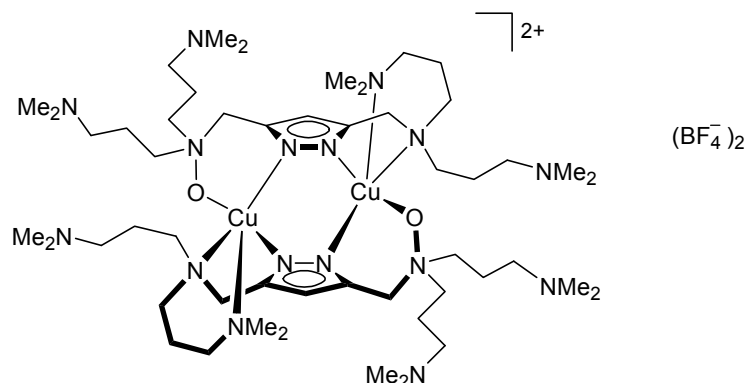
Empirical formula: C<sub>50</sub>H<sub>107</sub>Cu<sub>2</sub>N<sub>16</sub>O<sub>15</sub>Cl<sub>3</sub>·3MeOH

Molecular weight: 1486.0 g/mol

IR (KBr)  $\nu$  (cm<sup>-1</sup>): 3410 (w), 2963 (w), 1259 (s), 1094 (vs), 1025 (s), 802 (s), 625 (w), 503 (w)

MS (ESI, MeOH)  $m/z$  (%): 1389 (15)  $[\text{Cu}_2\text{L}^2_2\text{O}_2(\text{ClO}_4)_3-2\text{H}]^+$ , 1289 (55)  $[\text{Cu}_2\text{L}^2_2\text{O}_2(\text{ClO}_4)_2-2\text{H}]^+$ , 1189 (100)  $[\text{Cu}_2\text{L}^2_2\text{O}_2(\text{ClO}_4)-2\text{H}]^+$

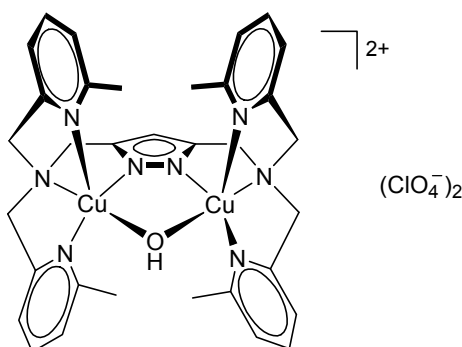
### Preparation of $[\text{Cu}_2(\text{L}^2\text{O})_2](\text{BF}_4)_2$ (**3b**)



A solution of **HL**<sup>2</sup> (0.12 g, 0.25 mmol) in methanol (20 mL) was treated with KO<sup>t</sup>Bu (0.06 g, 0.50 mmol) and stirred for 10 min at room temperature. Cu(BF<sub>4</sub>)<sub>2</sub>·4H<sub>2</sub>O (0.13 g, 0.50 mmol) was then added and the green solution was stirred for 2 h. After evaporation of the solvent *in vacuo*, the crude product was dissolved in 10 ml of CH<sub>2</sub>Cl<sub>2</sub> and slow diffusion of Et<sub>2</sub>O into this solution led to the formation of blue-green crystals of **3b**.

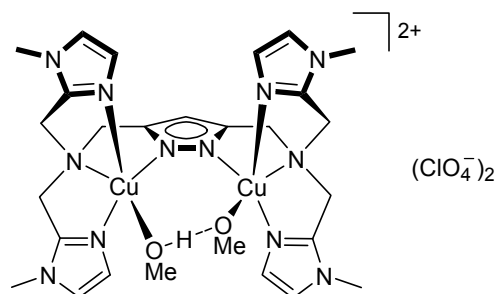
Yield:	3.5 mg, 1.9 %
Empirical formula:	C <sub>50</sub> H <sub>106</sub> Cu <sub>2</sub> N <sub>16</sub> O <sub>2</sub> B <sub>2</sub> F <sub>8</sub>
Molecular weight:	1264.2 g/mol
IR (KBr) $\nu$ (cm <sup>-1</sup> ):	3434 (m), 2961 (w), 2820 (w), 2767 (w), 1634 (w), 1464 (m), 1257 (m), 1156 (w), 1082 (vs), 801 (s)
MS (ESI, MeCN) $m/z$ (%):	1177 (5) [Cu <sub>2</sub> L <sup>2</sup> O <sub>2</sub> (BF <sub>4</sub> ) <sup>+</sup> ]

**Preparation of  $[\text{Cu}_2\text{L}^3(\mu\text{-OH})](\text{ClO}_4)_2$  (**4**)**



A solution of **HL**<sup>3</sup> (0.14 g, 0.25 mmol) in MeCN/MeOH (20 mL; 1:1 v/v) was treated with KOtBu (0.06 g, 0.50 mmol) and stirred for 10 min at room temperature. Cu(ClO<sub>4</sub>)<sub>2</sub>·6H<sub>2</sub>O (0.18 g, 0.50 mmol) was then added and the green solution was stirred for 2 h. After evaporation of the solvent, the crude product was redissolved in 5 ml of MeCN/CH<sub>2</sub>Cl<sub>2</sub> and slow diffusion of Et<sub>2</sub>O into this solution led to the formation of green crystals of **4** (*insufficient quality for a high-resolution X-ray crystallographic analysis*).

Yield:	0.28 g, 63 %
Empirical formula:	C <sub>33</sub> H <sub>37</sub> Cu <sub>2</sub> N <sub>8</sub> O <sub>9</sub> Cl <sub>2</sub>
Molecular weight:	887.7 g/mol
IR (KBr) $\nu$ (cm <sup>-1</sup> ):	1577 (s), 1440 (m), 1369 (w), 1261 (w), 1090 (vs), 1009 (w), 959 (w), 882 (w), 786 (m), 623 (s)
MS (ESI, MeCN) $m/z$ (%):	829 (20) $[\text{Cu}_2\text{L}^3(\text{OH})(\text{MeCN})\text{ClO}_4]^+$
Elemental analysis (%):	for C <sub>33</sub> H <sub>37</sub> Cu <sub>2</sub> N <sub>8</sub> O <sub>9</sub> Cl <sub>2</sub> calcd.: C 44.65, H 4.20, N 12.62 found: C 44.35, H 4.25, N 11.79
UV/vis (MeCN) $\lambda$ (nm) $[\epsilon]$ (L mol <sup>-1</sup> cm <sup>-1</sup> ):	816 (291)

**Preparation of  $[\text{Cu}_2\text{L}^4(\text{OMe})(\text{MeOH})](\text{ClO}_4)_2$  (**5a**)**


A solution of **HL**<sup>4</sup> (2.63 g, 5.24 mmol) in methanol (100 mL) was treated with *KOtBu* (0.58 g, 5.24 mmol) and stirred for 10 min at room temperature.  $\text{Cu}(\text{NO}_3)_2 \cdot 3\text{H}_2\text{O}$  (2.51 g, 10.48 mmol) was then added and stirring of the green solution was continued for 2 h. After addition of  $\text{H}_2\text{O}$  (900 mL), the mixture was purified by ion-exchange chromatography on a SP-Sephadex C25 column. The main blue fraction was collected by washing the column with a 0.4 M aqueous solution of  $\text{NaNO}_3$ . The solvent was evaporated on a rotary evaporator and the residue extracted three times with MeCN to remove  $\text{NaNO}_3$  by filtration. The combined MeCN phases were evaporated to dryness and the residue re-dissolved in water. A 0.2 M NaOH solution was then slowly added until the solution reached pH 9, concomitant with a colour change from blue to deep green. Addition of excess  $\text{NaClO}_4$  yielded a green precipitate, which was separated by filtration and dried. Slow diffusion of  $\text{Et}_2\text{O}$  into a solution of the crude product in MeCN/MeOH (2:1) led to the formation of green crystals of **5a**·MeCN.

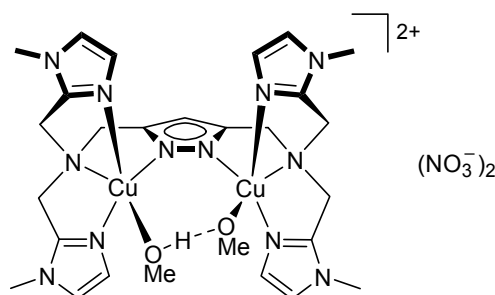
Yield:	2.92 g, 60 %
Empirical formula:	$\text{C}_{27}\text{H}_{40}\text{Cu}_2\text{N}_{12}\text{O}_{10}\text{Cl}_2 \cdot \text{MeCN}$
Molecular weight:	931.7 g/mol
IR (KBr) $\nu$ ( $\text{cm}^{-1}$ ):	3458 (s), 3132 (w), 1555 (m), 1509 (w), 1454 (w), 1381 (w), 1286 (w), 1086 (vs), 953 (w), 871 (w), 665 (w), 626 (m)
MS (FAB, glycerin) $m/z$ (%):	726 (10) $[\text{Cu}_2\text{L}^4(\text{ClO}_4)]^+$ , 627 (100) $[\text{Cu}_2\text{L}^4]^+$
Elemental analysis (%):	for $\text{C}_{27}\text{H}_{40}\text{Cu}_2\text{N}_{12}\text{O}_{10}\text{Cl}_2 \cdot \text{MeCN}$ calcd.: C 34.80, H 4.29, N 18.04 found: C 34.82, H 4.27, N 18.96

UV/vis (MeCN/MeOH)  $\lambda$  (nm)

$[\epsilon]$  (L mol<sup>-1</sup> cm<sup>-1</sup>): 730sh (135) 962 (269)

Diffuse reflectance: 952

### Preparation of [Cu<sub>2</sub>L<sup>4</sup>(OMe)(MeOH)](NO<sub>3</sub>)<sub>2</sub> (**5b**)



A solution of **HL**<sup>4</sup> (0.10 g, 0.20 mmol) in methanol (50 mL) was treated with two equivalents of KO<sup>t</sup>Bu (0.04 g, 0.40 mmol) and the solution was stirred for 10 min. Cu(NO<sub>3</sub>)<sub>2</sub>·3H<sub>2</sub>O (0.09 g, 0.40 mmol) was then added and stirring of the resulting green solution was continued for 2 h at room temperature. After evaporation of all volatile material, the remaining green solid was dissolved in a mixture of MeCN/MeOH (2:1). Slow diffusion of Et<sub>2</sub>O into this solution led to the formation of green crystals of **5b**·2MeOH.

Yield: 0.10 g, 57 %

Empirical formula: C<sub>27</sub>H<sub>40</sub>Cu<sub>2</sub>N<sub>14</sub>O<sub>8</sub>·2MeOH

Molecular weight: 879.9 g/mol

IR (KBr)  $\nu$  (cm<sup>-1</sup>): 3429 (s), 2943 (w), 1508 (m), 1355 (vs), 1283 (w), 1160 (w), 1095 (w), 1036 (w), 951 (w), 874 (w), 759 (w)

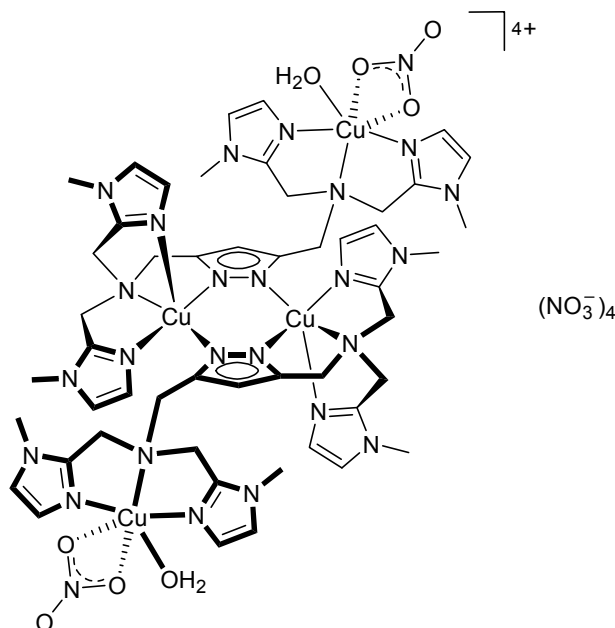
MS (FAB, glycerine)  $m/z$  (%): 689 (10) [Cu<sub>2</sub>L<sup>4</sup>(NO<sub>3</sub>)]<sup>+</sup>, 627 (100) [Cu<sub>2</sub>L<sup>4</sup>]<sup>+</sup>

Elemental analysis (%): for C<sub>27</sub>H<sub>40</sub>Cu<sub>2</sub>N<sub>14</sub>O<sub>8</sub>·2MeOH  
calcd.: C 39.59, H 5.50, N 22.29  
found: C 39.76, H 5.35, N 22.73

UV/vis (MeCN/MeOH)  $\lambda$  (nm)

$[\epsilon]$  (L mol<sup>-1</sup> cm<sup>-1</sup>): 726sh (124), 962 (278)

### Preparation of $[\{\text{Cu}_2\text{L}^4(\text{NO}_3)(\text{H}_2\text{O})\}_2](\text{NO}_3)_4$ (**6**)



A solution of **HL**<sup>4</sup> (2.63 g, 5.24 mmol) in methanol (100 mL) was treated with KO<sup>*t*</sup>Bu (0.58 g, 5.24 mmol) and stirred for 10 min at room temperature. Cu(NO<sub>3</sub>)<sub>2</sub>·3H<sub>2</sub>O (2.51 g, 10.48 mmol) was then added and stirring of the green solution was continued for 2 h. After addition of H<sub>2</sub>O (900 mL), the mixture was purified by ion-exchange chromatography on a SP-Sephadex C25 column. The main blue fraction was collected by washing the column with an aqueous 0.4 M NaNO<sub>3</sub> solution. The solvent was evaporated and the residue extracted three times with MeCN to remove NaNO<sub>3</sub> by filtration. The crude product was then redissolved in water and from this aqueous solution green-blue crystals of **6**·5H<sub>2</sub>O were obtained.

Yield: 3.44 g, 75 %

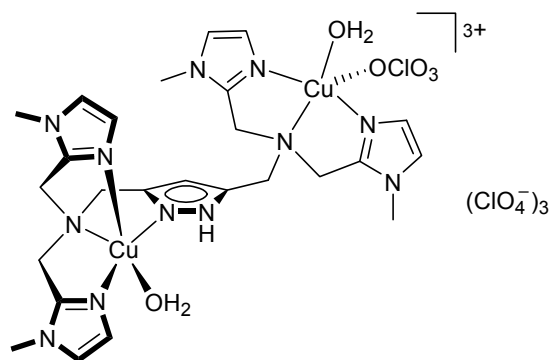
Empirical formula: C<sub>50</sub>H<sub>80</sub>Cu<sub>4</sub>N<sub>30</sub>O<sub>25</sub>·5H<sub>2</sub>O

Molecular weight: 1755.6 g/mol



IR (KBr) $\nu$ (cm <sup>-1</sup> ):	3420 (m), 3125 (w), 1624 (w), 1509 (m), 1352 (vs), 1167 (w), 1093 (w), 1011 (w), 951 (w), 872 (w), 831 (w), 754 (m)
MS (FAB, 3-NBA) $m/z$ (%):	689 (50) [Cu <sub>2</sub> L <sup>4</sup> (NO <sub>3</sub> )] <sup>+</sup> , 627 (100) [Cu <sub>2</sub> L <sup>4</sup> ] <sup>+</sup>
Elemental analysis (%):	for C <sub>50</sub> H <sub>80</sub> Cu <sub>4</sub> N <sub>30</sub> O <sub>25</sub> ·5H <sub>2</sub> O calcd.: C 34.21, H 4.59, N 23.94 found: C 34.76, H 4.50, N 23.73
UV/vis (MeCN/MeOH) $\lambda$ (nm)	
[ $\epsilon$ ] (L mol <sup>-1</sup> cm <sup>-1</sup> ):	689 (281), 923 (272)
Diffuse reflectance:	705, 918

### Preparation of [Cu<sub>2</sub>HL<sup>4</sup>(H<sub>2</sub>O)<sub>2</sub>(ClO<sub>4</sub>)](ClO<sub>4</sub>)<sub>3</sub> (7)



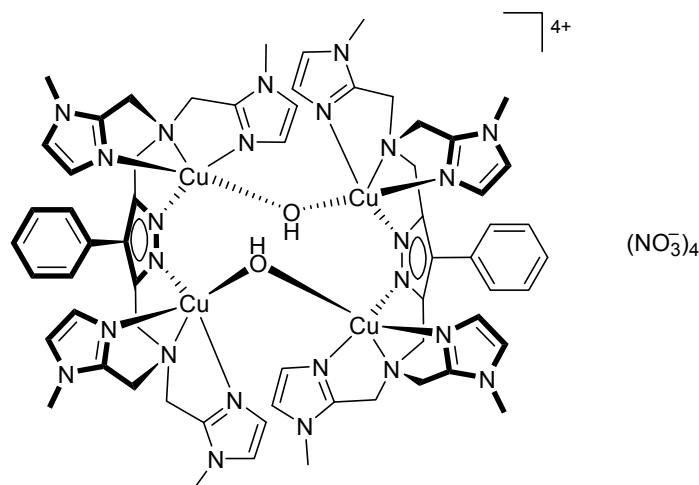
Aqueous HClO<sub>4</sub> (5-10 % (w)) was slowly added to a solution of **6** (0.17 g, 0.10 mmol) in water (10 mL) until the pH 4 was reached. After addition of methanol (5 mL) the solution was left standing for 2 days, during which time slow evaporation of the solvent led to the formation of blue crystals of **7**·2H<sub>2</sub>O.

Yield:	0.18 g, 86 %
Empirical formula:	C <sub>25</sub> H <sub>38</sub> Cu <sub>2</sub> N <sub>12</sub> O <sub>18</sub> Cl <sub>4</sub> ·2H <sub>2</sub> O
Molecular weight:	1099.6 g/mol
IR (KBr) $\nu$ (cm <sup>-1</sup> ):	3460 (w), 1628 (w), 1555 (w), 1509 (w), 1381 (w), 1088 (vs), 626 (m)
MS (FAB, 3-NBA) $m/z$ (%):	825 (50) [Cu <sub>2</sub> L <sup>4</sup> (ClO <sub>4</sub> ) <sub>2</sub> ] <sup>+</sup> , 726 (55) [Cu <sub>2</sub> L <sup>4</sup> (ClO <sub>4</sub> )] <sup>+</sup> , 627 (75) [Cu <sub>2</sub> L <sup>4</sup> ] <sup>+</sup>

Elemental analysis (%): for  $C_{25}H_{38}Cu_2N_{12}O_{18}Cl_4 \cdot 2H_2O$   
 calcd.: C 27.28, H 3.82, N 15.27  
 found: C 27.77, H 3.96, N 15.23

UV/vis (MeCN/MeOH)  $\lambda$   
 (nm)  $[\epsilon]$  ( $L \text{ mol}^{-1} \text{ cm}^{-1}$ ): 677 (96)  
 Diffuse reflectance: 689

### Preparation of $[Cu_2L^5]_2(\mu-OH)_2(NO_3)_4$ (**8**)



A solution of **HL**<sup>5</sup> (0.12 g, 0.20 mmol) in MeCN/MeOH (10 mL; 1:1 v/v) was treated with two equivalents of KO<sup>t</sup>Bu (0.04 g, 0.40 mmol) and stirred for 10 min. Cu(NO<sub>3</sub>)<sub>2</sub>·3H<sub>2</sub>O (0.09 g, 0.40 mmol) was then added and stirring of the resulting green solution was continued for 2 h at room temperature. After evaporation of all volatiles, the remaining green solid was dissolved in a mixture of CH<sub>3</sub>CN/CH<sub>3</sub>OH (2:1 v/v). Slow diffusion of Et<sub>2</sub>O into this solution led to the formation of green crystals of **8**·0.5MeCN.

Yield: 0.1 g, 58 %

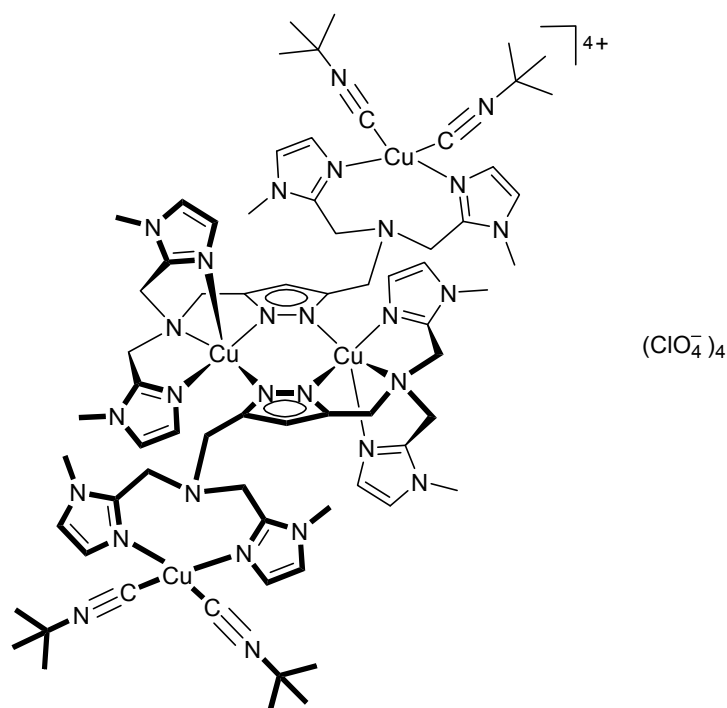
Empirical formula: C<sub>62</sub>H<sub>76</sub>Cu<sub>4</sub>N<sub>28</sub>O<sub>14</sub>·0.5MeCN

Molecular weight: 1712.2 g/mol

IR (KBr)  $\nu$  ( $cm^{-1}$ ): 3420 (m), 1596 (w), 1509 (w), 1383 (vs), 1163 (w), 1090 (w),

	1012 (w), 944 (w), 828 (w), 656 (w)
MS (FAB, glycerin) $m/z$ (%):	827 (4) $[\text{Cu}_2\text{L}^5(\text{NO}_3)_2]^+$ , 766 (2.5) $[\text{Cu}_2\text{L}^5(\text{NO}_3)]^+$ , 703 (4.5) $[\text{Cu}_2\text{L}^5]^+$
UV/vis (MeCN/MeOH) $\lambda$ (nm)	
$[\epsilon]$ ( $\text{L mol}^{-1} \text{ cm}^{-1}$ ):	726sh (135), 995 (280)

### Preparation of $[\text{L}^4\{(\text{Me}_3\text{CNC})_2\text{Cu}^{\text{I}}\}\text{Cu}^{\text{II}}]_2(\text{ClO}_4)_4$ (**9**)

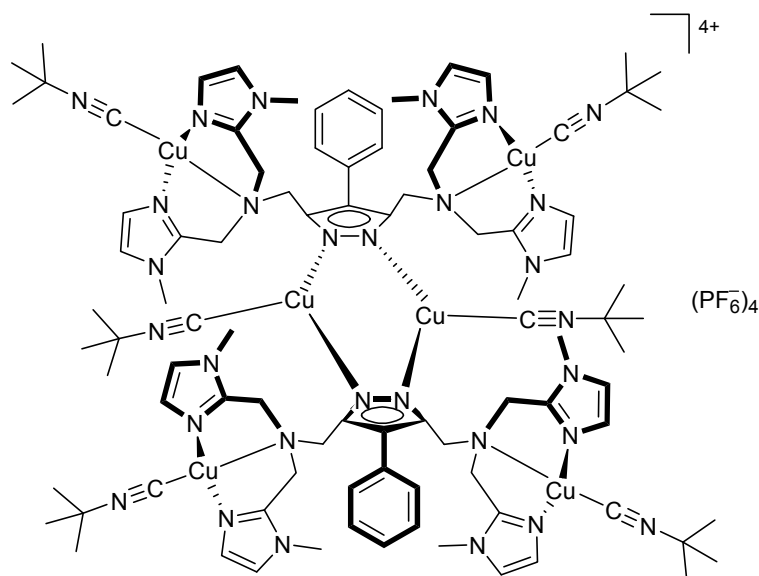


Under strict anaerobic conditions, complex **5a** (0.04 g, 0.05 mmol) was dissolved in MeCN/CH<sub>2</sub>Cl<sub>2</sub> (5 mL; ratio 2:3). The solution was stirred for 10 min and then TMP (0.03 g, 0.25 mmol) was added, which led to an immediate colour change of the reaction mixture from green to deep red. After 48 h of storage in an N<sub>2</sub>-filled glove box, the colour of the solution had changed to yellow-green and a green precipitate had formed. The solution was filtered and the green residue was dried under anaerobic conditions. The dry powder/solid was dissolved in 3 mL of MeCN and 2 equivalents (0.1 mmol, 0.012 mL) of *tert*-butyl isocyanide per copper ion was added, anticipating the complete reduction of initial complex **5a** to the

desired Cu(I)Cu(II) complex. Slow diffusion of Et<sub>2</sub>O into the resulting intensely green coloured solution led to the formation of light-green crystals of **9·7MeCN**.

Yield:	0.045 g, 80 %
Empirical formula:	C <sub>70</sub> H <sub>102</sub> Cu <sub>4</sub> N <sub>28</sub> O <sub>16</sub> Cl <sub>4</sub> ·7MeCN
Molecular weight:	2275.5 g/mol
IR (KBr) $\nu$ (cm <sup>-1</sup> ):	3420 (s), 2173 (s), 2151 (s), 1628 (w), 1504 (m), 1449 (w), 1379 (w), 1285 (w), 1090 (vs), 952 (w), 757 (w), 625 (m)
UV/vis (MeCN) $\lambda$ (nm) [ $\epsilon$ ] (L mol <sup>-1</sup> cm <sup>-1</sup> ):	695sh (119) 948 (383)

#### Preparation of [L<sup>5</sup>{(*t*BuNC)Cu}<sub>3</sub>]<sub>2</sub>(PF<sub>6</sub>)<sub>4</sub> (**10**)

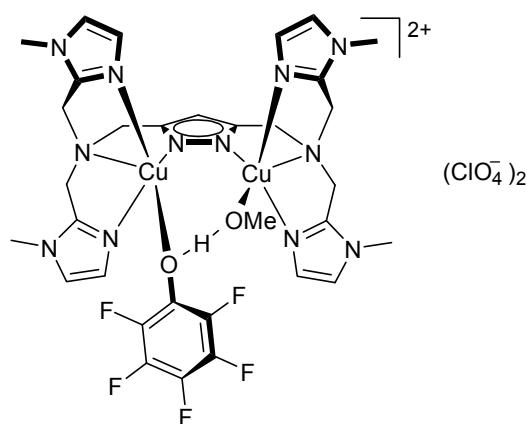


Under strict anaerobic conditions, a solution of **HL**<sup>5</sup> (0.12 g, 0.20 mmol) in MeCN (10 mL) was treated with one equivalent of KO<sup>*t*</sup>Bu (0.02 g, 0.20 mmol) and stirred for 2 h. Cu(MeCN)<sub>4</sub>(PF<sub>6</sub>) (0.15 g, 0.40 mmol) was then added and stirring of the resulting light-yellow solution was continued for 2 h at room temperature. Subsequently, one equivalent (0.40 mmol, 0.048 mL) of *tert*-butyl isocyanide (*t*BuNC) (1:1 ratio to Cu) was added and

stirring was continued for 30 min. Slow diffusion of Et<sub>2</sub>O into this solution led to the formation of colourless crystals of **10**.

Yield:	0.13 g, 68 %
Empirical formula:	C <sub>92</sub> H <sub>128</sub> Cu <sub>6</sub> N <sub>30</sub> P <sub>4</sub> F <sub>24</sub>
Molecular weight:	2615.6 g/mol
IR (KBr) $\nu$ (cm <sup>-1</sup> ):	2985 (w), 2164 (vs), 1541 (w), 1504 (m), 1448 (w), 1371 (m), 1284 (m), 1202 (m), 1084 (s), 842 (vs), 758 (m), 558 (m)
<sup>1</sup> H-NMR (CD <sub>3</sub> CN) $\delta$ (ppm):	1.44 (s, <i>t</i> Bu, 27H), 3.38 (s, CH <sub>3</sub> , 12H), 3.55 (s, NCH <sub>2</sub> , 8H), 3.86 (s, pzCH <sub>2</sub> , 4H), 6.94 (m, im-CH, 8H), 7.32 (m, Ar-CH, 5H)

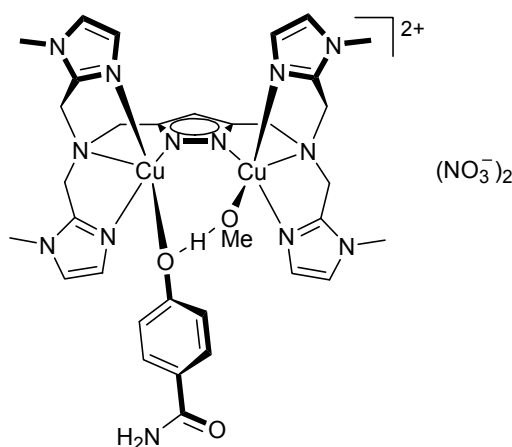
#### Preparation of [Cu<sub>2</sub>L<sup>4</sup>(OC<sub>6</sub>F<sub>5</sub>)(MeOH)](ClO<sub>4</sub>)<sub>2</sub> (**11**)



To a solution of **HL**<sup>4</sup> (0.10 g, 0.20 mmol) in methanol (50 mL) was added KO<sup>*t*</sup>Bu (0.04 g, 0.40 mmol) and the solution was stirred for 10 min. Cu(ClO<sub>4</sub>)<sub>2</sub>·6H<sub>2</sub>O (0.15 g, 0.40 mmol) was then added and the green solution was stirred at room temperature for 2 h; a small amount of green precipitate formed during this time. Subsequently, pentafluorophenol (C<sub>6</sub>H<sub>5</sub>OH) (0.36 g, 2.00 mmol) was added to the green mixture, concomitant with an immediate colour-change of the reaction from green to yellow-green. After additional stirring for 2 h, the solution was filtered and layered with Et<sub>2</sub>O, yielding yellow-green crystals of **11**·MeOH overnight.

Yield:	0.12 g, 56 %
Empirical formula:	C <sub>32</sub> H <sub>37</sub> Cu <sub>2</sub> N <sub>12</sub> O <sub>10</sub> F <sub>5</sub> Cl <sub>2</sub> ·MeOH
Molecular weight:	1074.7 g/mol
IR (KBr) $\nu$ (cm <sup>-1</sup> ):	3401 (w), 1504 (vs), 1282 (w), 1101 (vs), 995 (m), 877 (w), 760 (m), 625 (m)
MS (FAB, 3-NBA) $m/z$ (%):	1009 (15) [Cu <sub>2</sub> L <sup>4</sup> (C <sub>6</sub> F <sub>5</sub> O)(ClO <sub>4</sub> ) <sub>2</sub> ] <sup>+</sup> , 910 (15) [Cu <sub>2</sub> L <sup>4</sup> (C <sub>6</sub> F <sub>5</sub> O)(ClO <sub>4</sub> )] <sup>+</sup> , 726 (25) [Cu <sub>2</sub> L <sup>4</sup> (ClO <sub>4</sub> )] <sup>+</sup> , 627 (100) [Cu <sub>2</sub> L <sup>4</sup> ] <sup>+</sup>
UV/vis (MeCN) $\lambda$ (nm) [ $\epsilon$ ] (L mol <sup>-1</sup> cm <sup>-1</sup> ):	397 (1240), 989 (250)

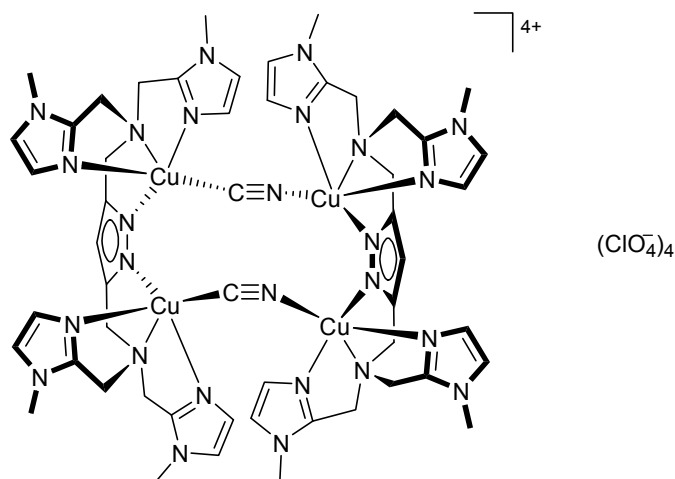
#### Preparation of [CuL<sup>4</sup>(OC<sub>6</sub>H<sub>4</sub>C(O)NH<sub>2</sub>)Cu(MeOH)](NO<sub>3</sub>)<sub>2</sub> (**12**)



To 0.10 g (0.20 mmol) of **HL**<sup>4</sup> in 50 mL methanol, 0.04 g (0.40 mmol) of potassium *tert*-butylate (KO<sup>*t*</sup>Bu) was added. The solution was stirred for 10 min and 0.09 g (0.40 mmol) of Cu(NO<sub>3</sub>)<sub>2</sub>·3H<sub>2</sub>O was then added. The green solution was stirred at room temperature for 2 h and then 0.274 g (2 mmol) of 4-hydroxybenzamide was added as a powder to the green mixture. The colour of the reaction mixture changed from green to yellow-brown. After additional stirring for 2 h, the solution was filtered and layered with Et<sub>2</sub>O, yielding brown crystals of **12**·4MeOH overnight.

Yield:	0.18 g, 87 %
Empirical formula:	C <sub>33</sub> H <sub>43</sub> Cu <sub>2</sub> N <sub>15</sub> O <sub>9</sub> ·4MeOH
Molecular weight:	1049.1 g/mol
IR (KBr) $\nu$ (cm <sup>-1</sup> ):	3410 (w), 1653 (m), 1593 (m), 1505 (s), 1381 (vs), 1282 (s), 1163 (w), 1092 (w), 1031 (w), 1001 (w), 949 (w), 852 (w), 758 (m), 666 (w)
MS (ESI, MeCN) $m/z$ (%):	825 (5) [Cu <sub>2</sub> L <sup>4</sup> (OC <sub>6</sub> H <sub>4</sub> C(O)NH <sub>2</sub> )NO <sub>3</sub> ] <sup>+</sup> , 751 (8) [Cu <sub>2</sub> L <sup>4</sup> (NO <sub>3</sub> ) <sub>2</sub> ] <sup>+</sup> , 689 (10) [Cu <sub>2</sub> L <sup>4</sup> (NO <sub>3</sub> )] <sup>+</sup> , 627 (9) [Cu <sub>2</sub> L <sup>4</sup> ] <sup>+</sup>
Elemental analysis (%):	for C <sub>33</sub> H <sub>43</sub> Cu <sub>2</sub> N <sub>15</sub> O <sub>9</sub> ·2MeOH calcd.: C 42.68, H 5.22, N 21.33 found: C 38.71, H 4.80, N 21.27
UV/vis (MeCN) $\lambda$ (nm) [ $\epsilon$ ] (L mol <sup>-1</sup> cm <sup>-1</sup> ):	446 (1210), 983 (226)

#### Preparation of [{Cu<sub>2</sub>L<sup>4</sup>}( $\mu$ -CN)<sub>2</sub>](ClO<sub>4</sub>)<sub>4</sub> (**13**)

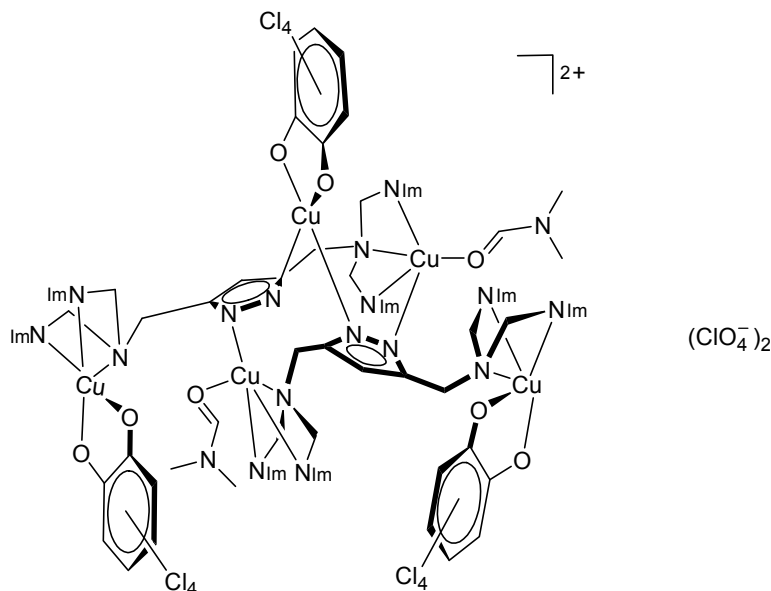


To a 47 mM solution of complex **5a** in MeCN (3 mL), a 47 mM solution of HOCF<sub>3</sub>BP in MeCN was added in a stepwise manner with the aim to perform a Job experiment. Addition of the substrate led to the usual formation of a red coloured copper-phenolate species, but this proved to be only a short-lived complex, as further unexpected colour change to deep green

occurred within 2 h after Job experiment was finished. Slow diffusion of Et<sub>2</sub>O into the green mixture of HO CF<sub>3</sub>BP and **5a** induced the formation of dark green crystals of **13**·4MeCN.

Yield:	0.14 g, 50 %
Empirical formula:	C <sub>52</sub> H <sub>66</sub> Cu <sub>4</sub> N <sub>26</sub> O <sub>16</sub> Cl <sub>4</sub> ·4MeCN
Molecular weight:	1871.4 g/mol
IR (KBr) $\nu$ (cm <sup>-1</sup> ):	3420 (s), 3123 (w), 2927 (w), 2174 (w), 2017 (w), 1628 (w), 1553 (m), 1509 (s), 1451 (w), 1356 (w), 1284 (w), 1089 (vs), 949 (w), 871 (w), 758 (m), 625 (s), 449 (w)
MS (FAB, 3-NBA) $m/z$ (%):	1508 (5) [Cu <sub>4</sub> L <sup>4</sup> <sub>2</sub> (CN) <sub>2</sub> (ClO <sub>4</sub> ) <sub>2</sub> ] <sup>+</sup> , 754 (15) [Cu <sub>2</sub> L <sup>4</sup> (CN)(ClO <sub>4</sub> )] <sup>+</sup> , 728 (25) [Cu <sub>2</sub> L <sup>4</sup> (ClO <sub>4</sub> )] <sup>+</sup> , 627 (100) [Cu <sub>2</sub> L <sup>4</sup> ] <sup>+</sup>
UV/vis (MeCN) $\lambda$ (nm) [ $\epsilon$ ] (L mol <sup>-1</sup> cm <sup>-1</sup> ):	671 (276), 879 (306)

#### Preparation of [Cu<sub>5</sub>L<sup>4</sup><sub>2</sub>(C<sub>6</sub>Cl<sub>4</sub>O<sub>2</sub>)<sub>3</sub>(DMF)<sub>2</sub>](ClO<sub>4</sub>)<sub>2</sub> (**14**)

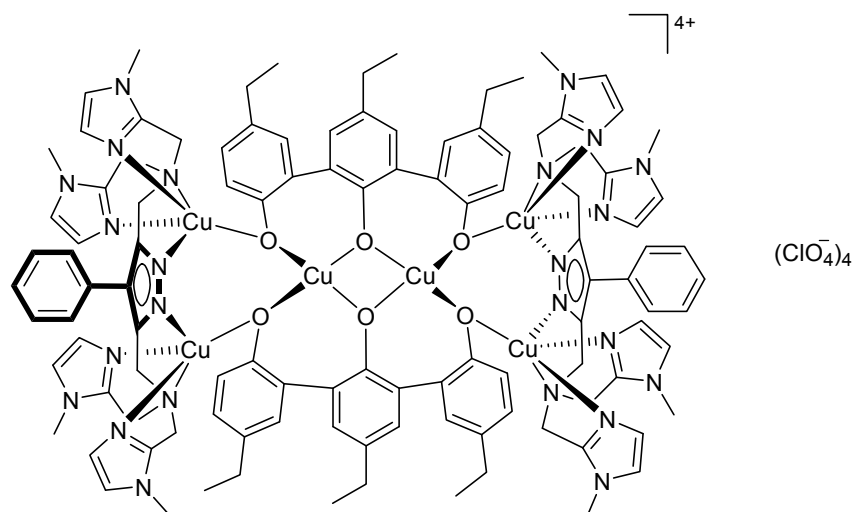


To a solution of **HL**<sup>4</sup> (0.10 g, 0.20 mmol) in methanol (50 mL) were added two equivalents of KO<sup>t</sup>Bu (0.04 g, 0.40 mmol) and subsequently, after 10 min of stirring, two equivalents of Cu(ClO<sub>4</sub>)<sub>2</sub>·6H<sub>2</sub>O (0.14 g, 0.40 mmol). The reaction was completed by addition of one



equivalent of tetrachlorocatechol (TCC) (0.05 g, 0.20 mmol), which was pretreated with one equivalent of KO<sup>t</sup>Bu (0.02 g, 0.20 mmol) to deprotonate one of the OH-groups. The colour of the reaction mixture changed from green to dark-brown. After the solvent was evaporated, the crude residue was dissolved in a MeCN/DMF mixture from which single crystals of complex **14** were obtained by slow diffusion of Et<sub>2</sub>O.

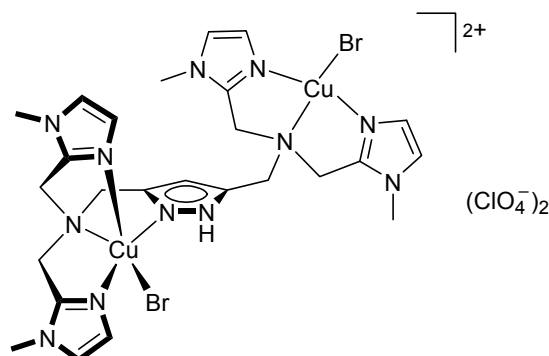
Yield:	0.18 g, 75 %
Empirical formula:	C <sub>74</sub> H <sub>80</sub> Cu <sub>5</sub> N <sub>26</sub> O <sub>16</sub> Cl <sub>14</sub>
Molecular weight:	2403.6 g/mol
IR (KBr) $\nu$ (cm <sup>-1</sup> ):	3411 (m), 3129 (w), 1630 (w), 1542 (w), 1509 (m), 1452 (s), 1372 (w), 1287 (w), 1255 (m), 1089 (vs), 966 (w), 886 (w), 796 (w), 749 (m), 623 (s)
MS (ESI, MeCN) $m/z$ (%):	1183 (10) [Cu <sub>3</sub> L <sup>4</sup> (TCC) <sub>2</sub> ] <sup>+</sup> , 937(60) [Cu <sub>2</sub> L <sup>4</sup> (TCC)(MeOH) <sub>2</sub> ] <sup>+</sup> , 872 (75) [Cu <sub>2</sub> L <sup>4</sup> (TCC)] <sup>+</sup> , 627 (100) [Cu <sub>2</sub> L <sup>4</sup> ] <sup>+</sup>
Elemental analysis (%):	for C <sub>74</sub> H <sub>80</sub> Cu <sub>5</sub> N <sub>26</sub> O <sub>16</sub> Cl <sub>14</sub> ·6H <sub>2</sub> O calcd.: C 35.39, H 3.69, N 14.50 found: C 34.28, H 3.70, N 14.92
UV/vis (MeCN) $\lambda$ (nm) [ $\epsilon$ ] (L mol <sup>-1</sup> cm <sup>-1</sup> ):	702 (282), 917 (303)

**Preparation of  $[\text{Cu}_4\text{L}^5_2\{\text{Cu}_2((\text{C}_8\text{H}_8\text{O})_3)_2\}](\text{ClO}_4)_4$  (**15**)**


A solution of **HL**<sup>5</sup> (0.12 g, 0.20 mmol) in 10 mL methanol was treated with two equivalents of KO<sup>t</sup>Bu (0.04 g, 0.40 mmol) and the solution stirred for 10 min. Cu(ClO<sub>4</sub>)<sub>2</sub>·6H<sub>2</sub>O (0.15 g, 0.40 mmol) was then added and stirring of the resulting green mixture continued for 2 h at room temperature. After evaporation of all volatile material the remaining green solid was dissolved in MeCN and insoluble by-product (KClO<sub>4</sub>) was filtered off. To the again redissolved pure powder of complex ten equivalents of C<sub>8</sub>H<sub>9</sub>OH were added with following addition of one equivalent of KO<sup>t</sup>Bu. The colour of reaction mixture changed to deep red. Slow diffusion of Et<sub>2</sub>O into this solution led to the formation of black crystals of **15**.

Yield:	0.011 g, 6.5 %
Empirical formula:	C <sub>110</sub> H <sub>122</sub> Cu <sub>6</sub> N <sub>24</sub> O <sub>22</sub> Cl <sub>4</sub>
Molecular weight:	2647.5 g/mol
IR (KBr) $\nu$ (cm <sup>-1</sup> ):	3414 (w), 3229 (w), 3126 (w), 2942 (w), 1625 (m), 1555 (m), 1506 (s), 1439 (m), 1375 (w), 1287 (w), 1112 (vs), 1088 (vs), 987 (w), 955 (w), 845 (w), 757 (m), 625 (s)
MS (ESI-HR, MeCN)	calcd.: 1224.22790
$m/z$ (%):	found: 1224.23 $[\text{Cu}_4\text{L}^5_2\{\text{Cu}_2((\text{C}_8\text{H}_8\text{O})_3)_2\}](\text{ClO}_4)_2]^{2+}$
UV/vis (MeCN) $\lambda$ (nm) [ $\epsilon$ ] (L mol <sup>-1</sup> cm <sup>-1</sup> ):	732, 972*
Diffuse reflectance:	427, 633, 1039

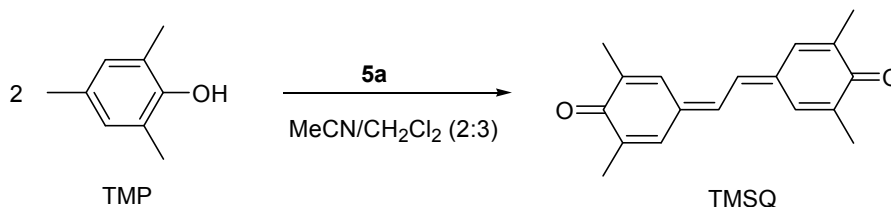
\*  $\epsilon$  is not given: big errors in calculations because of the very diluted solution of **15**

**Preparation of  $[\text{HL}^4\{\text{CuBr}\}_2](\text{ClO}_4)_2$  (**17**)**


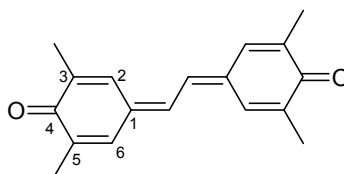
Complex **5a** (0.05 g, 0.05 mmol) was dissolved in MeCN (10 mL). The green solution was stirred for 10 min and then 4-bromo-2,6-dimethylphenol (DMBrP) (0.1 g, 0.5 mmol) was added. An immediate colour change of the reaction mixture from green to deep-red was observed concomitant with another colour change to deep green within 10 min. The solution was left standing for one day, during which time slow evaporation of the solvent led to the formation of blue crystals of **17**·MeCN.

Yield:	0.04 g, 71 %
Empirical formula:	$\text{C}_{25}\text{H}_{34}\text{Cu}_2\text{N}_{12}\text{O}_8\text{Br}_2\text{Cl}_2 \cdot \text{MeCN}$
Molecular weight:	1029.5 g/mol
IR (KBr) $\nu$ ( $\text{cm}^{-1}$ ):	3414 (w), 3125 (w), 2940 (w), 1624 (w), 1555 (m), 1506 (s), 1450 (m), 1375 (w), 1287 (w), 1105 (vs), 985 (m), 955 (m), 845 (m), 757 (s), 625 (s)
MS (FAB, 3-NBA) $m/z$ (%):	807 (25) $[\text{Cu}_2\text{L}^4\text{Br}_2(\text{ClO}_4)]^+$ , 789 (35) $[\text{Cu}_2\text{L}^4\text{Br}_2]^+$ , 708 (100) $[\text{Cu}_2\text{L}^4\text{Br}]^+$
Elemental analysis (%):	for $\text{C}_{25}\text{H}_{34}\text{Cu}_2\text{N}_{12}\text{O}_8\text{Br}_2\text{Cl}_2$ calcd.: C 30.38, H 3.47, N 17.00 found: C 30.45, H 3.66, N 16.90
UV/vis (DMF) $\lambda$ (nm) $[\epsilon]$ ( $\text{L mol}^{-1} \text{cm}^{-1}$ ):	689 (145)

#### 14.4 Synthesis of 3,3',5,5'-tetramethylstilbene-4,4'-quinone (TMSQ)



Complex **5a** (0.05 g, 0.05 mmol) was dissolved in MeCN/CH<sub>2</sub>Cl<sub>2</sub> (10 mL; ratio 2:3). The green solution was stirred for 10 min and then 2,4,6-trimethylphenol (TMP) (0.03 g, 0.25 mmol) was added. An immediate colour change of the reaction mixture from green to deep-red was observed. The solution was left standing without stirring and after 16 h red crystals of the desired product TMSQ could be isolated.

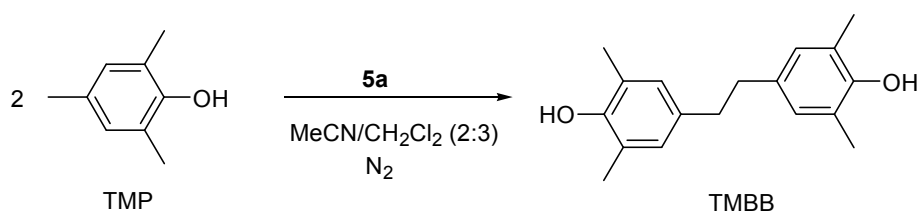


Yield:	0.02 g, 66%
Empirical formula:	C <sub>18</sub> H <sub>18</sub> O <sub>2</sub>
Molecular weight:	266.0 g/mol
<sup>1</sup> H-NMR (CDCl <sub>3</sub> ) δ (ppm):	2.05 (d, <i>J</i> = 1.3 Hz, 6H, CH <sub>3</sub> ), 2.09 (d, <i>J</i> = 1.3 Hz, 6H, CH <sub>3</sub> ), 7.01 (s, 2H, C <sup>2</sup> H), 7.19 (s, 2H, C <sup>6</sup> H), 7.51 (s, 2H, CH)
<sup>13</sup> C-NMR (CDCl <sub>3</sub> ) δ (ppm):	16.5 (CH <sub>3</sub> ), 17.1 (CH <sub>3</sub> ), 128.5, 133.6, 136.9, 137.8, 138.2, 138.5, 187.4 (C=O)
MS (EI) <i>m/z</i> (%):	268 (35) [C <sub>18</sub> H <sub>18</sub> O <sub>2</sub> +2H] <sup>+</sup> , 266 (100) [C <sub>18</sub> H <sub>18</sub> O <sub>2</sub> ] <sup>+</sup> , 251 (38) [C <sub>18</sub> H <sub>18</sub> O+H] <sup>+</sup> , 236 (15) [C <sub>18</sub> H <sub>18</sub> +H] <sup>+</sup>
IR (KBr) ν (cm <sup>-1</sup> ):	1637 (w), 1596 (vs), 1504 (w), 1435 (w), 1371 (w), 1094 (w), 1027 (m), 941 (m)
UV/vis (CH <sub>2</sub> Cl <sub>2</sub> ) λ (nm) [ε]	

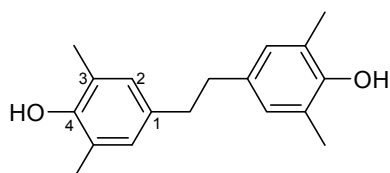
(L mol<sup>-1</sup> cm<sup>-1</sup>): 440 (96000)

Elemental analysis (%): for C<sub>18</sub>H<sub>18</sub>O<sub>2</sub>  
 calcd.: C 81.17, H 6.81  
 found: C 81.05, H 6.78

#### 14.5 Synthesis of 4,4'-dihydroxy-3,3',5,5'-tetramethylbibenzyl (TMBB)



Under strict anaerobic conditions, complex **5a** (0.04 g, 0.05 mmol) was dissolved in MeCN/CH<sub>2</sub>Cl<sub>2</sub> (10 mL; ratio 2:3). The solution was stirred for 10 min and then TMP (0.03 g, 0.25 mmol) was added, which led to an immediate colour change of the reaction mixture from green to deep red. After 48 h of stirring in an N<sub>2</sub>-filled glove box, the colour of the solution had changed to yellow-green. Organic products were then separated from Cu-containing species by chromatography on SiO<sub>2</sub>, using CH<sub>2</sub>Cl<sub>2</sub>/MeOH (9.5:0.5) as eluent. The mixture of organic products was separated by HPLC chromatography (La Flash) with CH<sub>2</sub>Cl<sub>2</sub>/MeOH (9.5:0.5) as an eluent. Only TMP and TMBB were found to be present in the mixture after reaction. Solvent of the fraction containing only TMBB after separation by HPLC was evaporated and TMBB was isolated as a white powder.



Yield: 0.007 g, 100%

## Experimental section

---

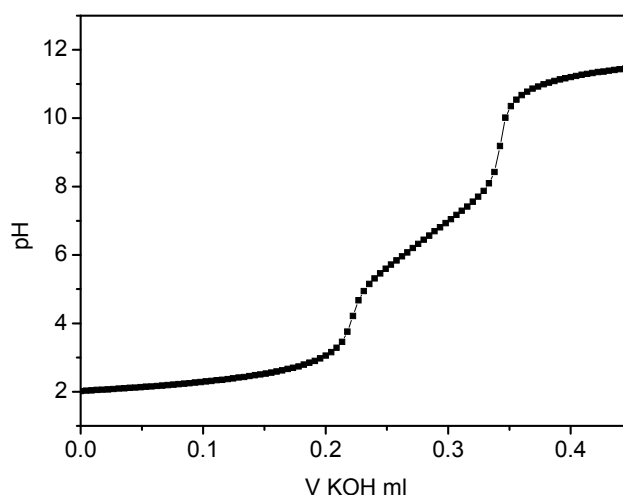
Empirical formula:	$\text{C}_{18}\text{H}_{22}\text{O}_2$
Molecular weight:	270.0 g/mol
$^1\text{H}$ -NMR ( $\text{CDCl}_3$ ) $\delta$ (ppm):	2.21 (s, 12H, $\text{CH}_3$ ), 2.70 (s, 4H, $\text{CH}_2$ ), 6.81 (s, 4H, CH)
$^{13}\text{C}$ -NMR ( $\text{CDCl}_3$ ) $\delta$ (ppm):	15.88 ( $\text{CH}_3$ ), 37.66 ( $\text{CH}_2$ ), 122.7 ( $\text{C}^3$ ), 128.4 ( $\text{C}^2\text{H}$ ), 133.6 ( $\text{C}^1$ ), 150.5 ( $\text{C}^4$ )
MS (EI) $m/z$ (%):	270 (20) [ $\text{C}_{18}\text{H}_{22}\text{O}_2$ ] $^+$ , 135 (100) [ $\text{C}_9\text{H}_{11}\text{O}$ ] $^+$

## 14.6 Potentiometric titrations

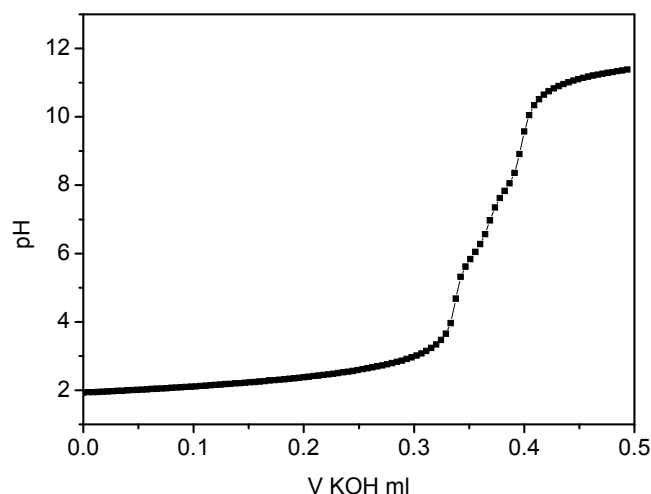
The pH potentiometric titrations were conducted at  $25.0 \pm 0.1$  °C at an ionic strength of 0.2 M (KCl) using a Radiometer PHM 84 pH-meter equipped with a Metrohm 6.0234.100 combined electrode and a Metrohm dosimat 715. Calibration of the electrode and pH-meter was performed using a buffer of potassium biphthalate at pH 4.008. Concentrations of the stock solutions (HCl 0.2004 M and KOH 0.1972 M) were checked and a  $pK_W$  of 13.784 and an Irving factor of 0.079 were obtained following Gran's method.<sup>180</sup> Concentrations of the ligand stock solutions were also determined by Gran's method. The metal ion stock solution was prepared from  $\text{CuCl}_2 \cdot 2\text{H}_2\text{O}$  (Reanal) dissolved in doubly distilled water. The concentration of the metal ion stock solution was determined gravimetrically via precipitation with quinolin-8-olate.

pH-metric titrations were performed in the pH range 2.0 – 10.5 or until precipitation, on samples of 4.00 mL, at an ionic strength of 0.2 M (KCl) and at  $25 \pm 0.1$  °C. Purified, strictly oxygen-free argon was continuously bubbled through the samples during the titrations. The ligand concentrations were varied in the range  $1 \cdot 10^{-3}$  –  $2 \cdot 10^{-3}$  M and metal to ligand ratios were 1:1, 1.5:1 and 2:1.

The pH-metric results were utilised to establish the stoichiometry of species and to calculate the stability constants. Calculations were performed with the computer programs SUPERQUAD and PSEQUAD,<sup>181</sup> while the speciation curves were created with the help of the MEDUSA program.<sup>182</sup>



**Figure 94.** Titration curve of  $\text{HL}^4$ :  $C_{\text{HL}}^4 = 1.5 \cdot 10^{-3}$  M,  $C_{\text{KOH}} = 0.1972$  M.



**Figure 95.** Titration curve of  $\text{HL}^4$  with 2 eq.  $\text{Cu}^{2+}$ :  $C_{\text{HL}}^4 = 1.5 \cdot 10^{-3} \text{ M}$ ,  $C_{\text{KOH}} = 0.1972 \text{ M}$ .

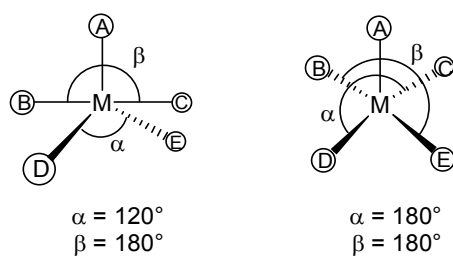
## 14.7 X-ray crystallography

X-ray data were collected on a STOE IPDS II diffractometer (graphite monochromated Mo-K $\alpha$  radiation,  $\lambda = 0.71073 \text{ \AA}$ ) by use of  $\omega$  scans at  $-140 \text{ }^\circ\text{C}$  (Table 4). The structures were solved by direct methods and refined on  $F^2$  using all reflections with SHELX-97.<sup>183</sup> Most of the non-hydrogen atoms were refined anisotropically. Unless otherwise noted, hydrogen atoms were placed in calculated positions and assigned to an isotropic displacement parameter of  $0.08 \text{ \AA}^2$ . Face-indexed absorption corrections were performed numerically with the program X-RED.<sup>184</sup> X-ray data for complex **15** were collected on a Bruker three-circle diffractometer with a graphite monochromator equipped with a SMART 6000 area detector (Cu-K $\alpha$  radiation,  $\lambda = 1.54184 \text{ \AA}$ ). The crystal was cooled to 100K with an Oxford Cryosystem. All calculations were carried out using SHELX software.

### *Calculation of the $\tau$ parameter:*

In a five-co-ordinate system ideally square pyramidal geometry is associated with  $\alpha = \beta = 180^\circ$ , for A as the axial ligand ( $\beta$  is the greater of the basal angles, BMC, Figure 96). For perfectly trigonal bipyramidal geometry,  $\alpha$  becomes  $120^\circ$  and BMC the principal axis. In the great majority of real square pyramidal systems M is displaced out of the BCDE plane toward A, so that these  $C_{4v}$  geometries usually have  $\alpha = \beta < 180^\circ$ , and can be characterised by the value of  $(\beta - \alpha)$ , which is  $0^\circ$  for a  $C_{4v}$ , and  $60^\circ$  for a  $D_{3h}$  co-ordination polyhedron.





**Figure 96.** Schematic representation of the  $\tau$ .

The geometric parameter  $\tau$  is defined as  $\tau = (\beta - \alpha)/60$  and is applicable to five-co-ordinate structures as an index of the degree of trigonality, within the structural continuum between trigonal bipyramidal and rectangular pyramidal. For a perfectly tetragonal geometry  $\tau$  is equal to zero, while it becomes one for a perfectly trigonal bipyramidal geometry.

## 14.8 Crystal data and refinement details

	1	3
formula	C <sub>19</sub> H <sub>44</sub> Cu <sub>2</sub> N <sub>6</sub> O <sub>3</sub> B <sub>2</sub> F <sub>8</sub>	C <sub>50</sub> H <sub>106</sub> Cu <sub>2</sub> N <sub>16</sub> Cl <sub>2</sub> O <sub>10</sub> ·0.47H <sub>2</sub> O
M <sub>r</sub>	705.3	1297.9
crystal size [mm <sup>3</sup> ]	0.32 × 0.28 × 0.26	0.22 × 0.12 × 0.11
crystal system	Monoclinic	Triclinic
space group	<i>P</i> 2 <sub>1</sub>	<i>P</i> −1
<i>a</i> [Å]	7.8856(5)	12.3331(10)
<i>b</i> [Å]	12.2814(9)	12.5231(10)
<i>c</i> [Å]	15.6430(8)	12.6562(10)
$\alpha$ [°]	90	62.598(6)
$\beta$ [°]	99.926(4)	72.108(6)
$\gamma$ [°]	90	88.043(7)
<i>V</i> [Å <sup>3</sup> ]	1492.29(16)	1638.1(2)
<i>Z</i>	2	1
$\rho_{\text{calcd.}}$ [g cm <sup>−3</sup> ]	1.570	1.316
<i>F</i> (000)	728	695
$\mu$ [mm <sup>−1</sup> ]	1.507	0.794
<i>hkl</i> range	±9, −13 to 14, ±18	−14 to 13, ±14, ±14
$\theta$ range [°]	2.12 – 24.79	1.85 – 24.79
measured refl.	16692	14859
unique refl. [ <i>R</i> <sub>int</sub> ]	4691 [0.0484]	5604 [0.0524]
observed refl. ( <i>I</i> > 2σ( <i>I</i> ))	3865	4174
ref. param. / restraints	373 / 2	415 / 3
goodness-of-fit	1.013	1.003
<i>R</i> 1, <i>wR</i> 2 ( <i>I</i> > 2σ( <i>I</i> ))	0.0543, 0.1374	0.0444, 0.0965
<i>R</i> 1, <i>wR</i> 2 (all data)	0.0665, 0.1448	0.0678, 0.1037
resid. el. dens. [e Å <sup>−3</sup> ]	0.840 / −0.473	0.297 / −0.542

	<b>3a</b>	<b>3b</b>
formula	C <sub>50</sub> H <sub>107</sub> Cu <sub>2</sub> N <sub>16</sub> Cl <sub>3</sub> O <sub>15</sub> ·3MeOH	C <sub>50</sub> H <sub>106</sub> Cu <sub>2</sub> N <sub>16</sub> O <sub>2</sub> B <sub>2</sub> F <sub>8</sub>
M <sub>r</sub>	1486.1	1264.2
crystal size [mm <sup>3</sup> ]	0.24 × 0.20 × 0.19	0.23 × 0.16 × 0.12
crystal system	Monoclinic	Triclinic
space group	<i>Pn</i>	<i>P</i> -1
<i>a</i> [Å]	14.9526(14)	12.3153(10)
<i>b</i> [Å]	13.5704(8)	12.3594(11)
<i>c</i> [Å]	17.9599(16)	12.6747(10)
$\alpha$ [°]	90	72.306(6)
$\beta$ [°]	94.254(7)	62.997(6)
$\gamma$ [°]	90	88.085(7)
<i>V</i> [Å <sup>3</sup> ]	3634.3(5)	1625.1(2)
<i>Z</i>	2	1
$\rho_{\text{calcd.}}$ [g cm <sup>-3</sup> ]	1.358	1.292
<i>F</i> (000)	1588	674
$\mu$ [mm <sup>-1</sup> ]	0.767	0.726
<i>hkl</i> range	±17, -14 to 15, -21 to 18	±14, ±14, ±14
$\theta$ range [°]	1.50 – 24.78	1.74 – 24.77
measured refl.	17359	17951
unique refl. [ <i>R</i> <sub>int</sub> ]	11052 [0.0745]	5537 [0.0561]
observed refl. ( <i>I</i> > 2σ( <i>I</i> ))	7168	4106
ref. param. / restraints	810 / 190	362 / 52
goodness-of-fit	1.017	1.032
<i>R</i> 1, <i>wR</i> 2 ( <i>I</i> > 2σ( <i>I</i> ))	0.0782, 0.1685	0.0686, 0.1779
<i>R</i> 1, <i>wR</i> 2 (all data)	0.1270, 0.1953	0.0967, 0.1943
resid. el. dens. [e Å <sup>-3</sup> ]	0.696 / -0.463	1.521 / -0.628

	<b>5a</b>	<b>5b</b>
formula	C <sub>27</sub> H <sub>40</sub> Cu <sub>2</sub> N <sub>12</sub> Cl <sub>2</sub> O <sub>10</sub> ·MeCN	C <sub>27</sub> H <sub>40</sub> Cu <sub>2</sub> N <sub>14</sub> O <sub>8</sub> ·2MeOH
M <sub>r</sub>	931.7	879.9
crystal size [mm <sup>3</sup> ]	0.46 × 0.24 × 0.21	0.40 × 0.23 × 0.12
crystal system	Monoclinic	Triclinic
space group	<i>Cc</i>	<i>P</i> -1
<i>a</i> [Å]	18.1991(9)	11.1984(4)
<i>b</i> [Å]	16.9395(6)	14.9118(6)
<i>c</i> [Å]	13.6063(8)	24.3582(9)
$\alpha$ [°]	90	101.663(3)
$\beta$ [°]	112.350(4)	99.134(3)
$\gamma$ [°]	90	100.299(3)
<i>V</i> [Å <sup>3</sup> ]	3879.5(3)	3838.4(3)
<i>Z</i>	4	4
$\rho_{\text{calcd.}}$ [g cm <sup>-3</sup> ]	1.595	1.523
<i>F</i> (000)	1920	1832
$\mu$ [mm <sup>-1</sup> ]	1.305	1.180
<i>hkl</i> range	±21, ±19, -16 to 15	±13, -15 to 17, ±28
$\theta$ range [°]	1.71 – 24.81	1.43 – 24.79
measured refl.	29113	57759
unique refl. [ <i>R</i> <sub>int</sub> ]	6527 [0.0651]	13096 [0.0591]
observed refl. ( <i>I</i> > 2 $\sigma$ ( <i>I</i> ))	6123	9972
ref. param. / restraints	553 / 4	1010 / 36
goodness-of-fit	1.001	1.017
<i>R</i> 1, <i>wR</i> 2 ( <i>I</i> > 2 $\sigma$ ( <i>I</i> ))	0.0287, 0.0674	0.0520, 0.1262
<i>R</i> 1, <i>wR</i> 2 (all data)	0.0314, 0.0682	0.0743, 0.1367
resid. el. dens. [e Å <sup>-3</sup> ]	0.351 / -0.275	1.439 / -0.743

	<b>6</b>	<b>7</b>
Formula	$C_{50}H_{80}Cu_4N_{30}O_{25} \cdot 5H_2O$	$C_{25}H_{38}Cl_4Cu_2N_{12}O_{18} \cdot 2H_2O$
$M_r$	1755.6	1099.6
crystal size [mm <sup>3</sup> ]	$0.50 \times 0.26 \times 0.21$	$0.50 \times 0.08 \times 0.07$
crystal system	Triclinic	Orthorhombic
space group	$P\bar{1}$	$Pbca$
$a$ [Å]	9.5728(6)	18.1999(8)
$b$ [Å]	13.1348(8)	17.0313(5)
$c$ [Å]	14.5660(9)	26.7503(9)
$\alpha$ [°]	94.003(5)	90
$\beta$ [°]	106.635(5)	90
$\gamma$ [°]	93.850(5)	90
$V$ [Å <sup>3</sup> ]	1743.26(19)	8291.7(5)
$Z$	1	8
$\rho_{\text{calcd.}}$ [g cm <sup>-3</sup> ]	1.672	1.762
$F(000)$	906	4496
$\mu$ [mm <sup>-1</sup> ]	1.305	1.377
$hkl$ range	$\pm 11, \pm 15, -15$ to 17	$\pm 21, -17$ to 20, $-31$ to 27
$\theta$ range [°]	1.56 – 24.74	1.81 – 24.89
measured refl.	27830	78080
unique refl. [ $R_{\text{int}}$ ]	5954 [0.0554]	7173 [0.1116]
observed refl. ( $I > 2\sigma(I)$ )	5232	4914
ref. param. / restraints	563 / 38	627 / 58
goodness-of-fit	1.040	1.005
$R1, wR2$ ( $I > 2\sigma(I)$ )	0.0312, 0.0836	0.0481, 0.1100
$R1, wR2$ (all data)	0.0364, 0.0860	0.0806, 0.1211
resid. el. dens. [e Å <sup>-3</sup> ]	0.439 / –0.533	0.828 / –0.490

	<b>8</b>	<b>9</b>
Formula	C <sub>62</sub> H <sub>76</sub> Cu <sub>4</sub> N <sub>28</sub> O <sub>14</sub> ·0.5MeCN	C <sub>70</sub> H <sub>102</sub> Cu <sub>4</sub> N <sub>28</sub> Cl <sub>4</sub> O <sub>16</sub> ·7MeCN
M <sub>r</sub>	1712.2	2275.5
crystal size [mm <sup>3</sup> ]	0.49 × 0.33 × 0.21	0.30 × 0.24 × 0.19
crystal system	Triclinic	Triclinic
space group	<i>P</i> -1	<i>P</i> -1
<i>a</i> [Å]	15.5078(5)	10.8800(7)
<i>b</i> [Å]	15.9822(6)	14.0868(9)
<i>c</i> [Å]	19.2030(7)	18.5825(12)
$\alpha$ [°]	109.753(3)	100.300(5)
$\beta$ [°]	95.324(3)	102.835(5)
$\gamma$ [°]	92.625(3)	96.127(5)
<i>V</i> [Å <sup>3</sup> ]	4444.9(3)	2700.1(3)
<i>Z</i>	2	1
$\rho_{\text{calcd.}}$ [g cm <sup>-3</sup> ]	1.279	1.473
<i>F</i> (000)	1766	1244
$\mu$ [mm <sup>-1</sup> ]	1.013	0.955
<i>hkl</i> range	±18, ±18, ±22	±12, ±16, ±21
$\theta$ range [°]	1.32 – 24.82	1.68 – 24.76
measured refl.	120620	27741
unique refl. [ <i>R</i> <sub>int</sub> ]	15215 [0.0626]	9163 [0.0517]
observed refl. ( <i>I</i> > 2 $\sigma$ ( <i>I</i> ))	11535	6981
ref. param. / restraints	978 / 86	617 / 0
goodness-of-fit	1.057	1.031
<i>R</i> 1, <i>wR</i> 2 ( <i>I</i> > 2 $\sigma$ ( <i>I</i> ))	0.0579, 0.1684	0.0546, 0.1469
<i>R</i> 1, <i>wR</i> 2 (all data)	0.0744, 0.1773	0.0739, 0.1559
resid. el. dens. [e Å <sup>-3</sup> ]	1.136 / -0.870	0.594 / -1.399

	<b>11</b>	<b>12</b>
Formula	C <sub>32</sub> H <sub>437</sub> Cl <sub>2</sub> Cu <sub>2</sub> F <sub>5</sub> N <sub>12</sub> O <sub>10</sub> ·MeOH	C <sub>33</sub> H <sub>43</sub> Cu <sub>2</sub> N <sub>15</sub> O <sub>9</sub> ·4MeOH
M <sub>r</sub>	1074.7	1049.1
crystal size [mm <sup>3</sup> ]	0.22 × 0.17 × 0.13	0.50 × 0.11 × 0.07
crystal system	Triclinic	Orthorhombic
space group	<i>P</i> -1	<i>Pbca</i>
<i>a</i> [Å]	11.5528(11)	14.7719(5)
<i>b</i> [Å]	13.1929(14)	23.6254(8)
<i>c</i> [Å]	14.9182(14)	27.7160(14)
$\alpha$ [°]	93.767(8)	90
$\beta$ [°]	100.704(8)	90
$\gamma$ [°]	93.458(8)	90
<i>V</i> [Å <sup>3</sup> ]	2223.3(4)	9672.7(7)
<i>Z</i>	2	8
$\rho_{\text{calcd.}}$ [g cm <sup>-3</sup> ]	1.605	1.441
<i>F</i> (000)	1096	4384
$\mu$ [mm <sup>-1</sup> ]	1.167	0.954
<i>hkl</i> range	-11 to 13, $\pm 15$ , $\pm 17$	-15 to 17, $\pm 27$ , $\pm 32$
$\theta$ range [°]	1.55 – 24.77	1.47 – 24.77
measured refl.	21952	70349
unique refl. [ <i>R</i> <sub>int</sub> ]	7560 [0.0973]	8244 [0.0999]
observed refl. ( <i>I</i> > 2 $\sigma$ ( <i>I</i> ))	4877	6307
ref. param. / restraints	607 / 62	619 / 72
goodness-of-fit	1.007	1.113
<i>R</i> 1, <i>wR</i> 2 ( <i>I</i> > 2 $\sigma$ ( <i>I</i> ))	0.0696, 0.1776	0.1110, 0.2784
<i>R</i> 1, <i>wR</i> 2 (all data)	0.1100, 0.2023	0.1353, 0.2919
resid. el. dens. [e Å <sup>-3</sup> ]	0.933 / -0.652	1.768 / -1.677

Experimental section

	<b>13</b>	<b>14</b>
formula	$C_{60}H_{78}Cu_4N_{30}Cl_4O_{16}$	$C_{74}H_{80}Cu_5N_{26}Cl_{14}O_{16}$
$M_r$	1871.4	2403.6
crystal size [mm <sup>3</sup> ]	$0.50 \times 0.37 \times 0.25$	$0.21 \times 0.18 \times 0.15$
crystal system	Triclinic	Monoclinic
space group	$P\bar{1}$	$C2/c$
$a$ [Å]	14.9304(6)	13.5632(7)
$b$ [Å]	15.3395(6)	31.5050(15)
$c$ [Å]	19.4766(8)	30.5438(17)
$\alpha$ [°]	96.812(3)	90
$\beta$ [°]	90.133(3)	96.195(4)
$\gamma$ [°]	113.409(3)	90
$V$ [Å <sup>3</sup> ]	4058.6(3)	12975.4(12)
$Z$	2	4
$\rho_{calcd.}$ [g cm <sup>-3</sup> ]	1.531	1.230
$F(000)$	1920	4868
$\mu$ [mm <sup>-1</sup> ]	1.246	1.151
$hkl$ range	$\pm 19, \pm 19, \pm 25$	$-11$ to $15, \pm 37, -36$ to $35$
$\theta$ range [°]	$1.49 - 27.41$	$1.29 - 24.84$
measured refl.	80546	37794
unique refl. [ $R_{int}$ ]	18316 [0.0456]	10803 [0.0671]
observed refl. ( $I > 2\sigma(I)$ )	13711	6149
ref. param. / restraints	1089 / 155	615 / 0
goodness-of-fit	1.018	1.001
$R1, wR2$ ( $I > 2\sigma(I)$ )	0.0437, 0.1203	0.0592, 0.1398
$R1, wR2$ (all data)	0.0612, 0.1272	0.0976, 0.1511
resid. el. dens. [e Å <sup>-3</sup> ]	1.205 / -0.672	0.483 / -0.643



	<b>17</b>
formula	C <sub>25</sub> H <sub>34</sub> Cu <sub>2</sub> N <sub>12</sub> Br <sub>2</sub> Cl <sub>2</sub> O <sub>8</sub> ·MeCN
M <sub>r</sub>	1029.5
crystal size [mm <sup>3</sup> ]	0.50 × 0.11 × 0.07
crystal system	Monoclinic
space group	<i>P</i> 2 <sub>1</sub> / <i>n</i>
<i>a</i> [Å]	21.9846(12)
<i>b</i> [Å]	7.8001(2)
<i>c</i> [Å]	24.1070(17)
$\alpha$ [°]	90
$\beta$ [°]	115.222(5)
$\gamma$ [°]	90
<i>V</i> [Å <sup>3</sup> ]	3739.8(3)
<i>Z</i>	4
$\rho_{\text{calcd.}}$ [g cm <sup>-3</sup> ]	1.828
<i>F</i> (000)	2064
$\mu$ [mm <sup>-1</sup> ]	3.483
<i>hkl</i> range	±25, -9 to 18, ±28
$\theta$ range [°]	1.65 – 24.79
measured refl.	49669
unique refl. [ <i>R</i> <sub>int</sub> ]	6390 [0.0957]
observed refl. ( <i>I</i> > 2σ( <i>I</i> ))	4082
ref. param. / restraints	483 / 119
goodness-of-fit	1.039
<i>R</i> 1, <i>wR</i> 2 ( <i>I</i> > 2σ( <i>I</i> ))	0.0671, 0.1567
<i>R</i> 1, <i>wR</i> 2 (all data)	0.1096, 0.1760
resid. el. dens. [e Å <sup>-3</sup> ]	1.510 / -1.369

## 15 Literature

- <sup>1</sup> Klausener A., Jentsch J.D. In: Cornils B, Herrmann WA (eds) *Applied Homogeneous Catalysis with Organometallic Compounds*, VCH, Weinheim 1, 169, **1996**.
- <sup>2</sup> (a) Kaim W., Rall J. *Angew. Chem. Int. Ed.* **1996**, 35, 43; (b) Malmström B.G., Leckner J. *Curr. Opin. Chem. Biol.* **1998**, 2, 286; (c) Pascaly M., Jolk I., Krebs B. *Chemie in unsere Zeit* **1999**, 33, 334.
- <sup>3</sup> Carey F.A., Sundberg R.J. *Organische Chemie*, VCH, Weinheim, 1, **1995**.
- <sup>4</sup> Streitwieser A., Heathcock C.H., Kosower E.M. *Organische Chemie*, VCH, 2, Weinheim **1994**.
- <sup>5</sup> (a) Smidt J., Hafner W., Jira R., Sedlmeier J., Rüttinger R. Consortium für Elektrochemische Industrie DE 1 049 845, **1959**, (b) Jira R., Blau W., Grimm D. *Hydrocarbon Processing* 55, 97, **1975**.
- <sup>6</sup> Jira R. In: Cornils R, Herrmann WA (eds) *Applied Homogeneous Catalysis with Organometallic Compounds*, VCH, Weinheim **1996**, 374., *ibid* **2002** 1, 386.
- <sup>7</sup> (a) Naworski J.S., Velez E.S. In: Leach B.A. (ed) *Applied Industrial Catalysis*, Academic Press, New York, 239, **1983**; (b) Spector M.L., Heinemann H., Miller K.D. *Ind. Eng. Chem. Process Res. Dev.* 6, **1967**, 327.
- <sup>8</sup> Hathaway B.J. in *Comprehensive Coordination Chemistry*, 5, Pergamon, New York, **1987**.
- <sup>9</sup> Jameson R.F. *Met. Ions Biol. Syst.* **1981**, 12, 1.
- <sup>10</sup> Nigh W.G. *Oxidation in Organic Chemistry*, Part B, Trahanovsky W.S. Ed., Academic, New York, 1, **1973**.
- <sup>11</sup> Koval I. A., Gamez P., Belle C., Selmeczi K., Reedijk J. *Chem. Soc. Rev.* **2006**, 35, 814.
- <sup>12</sup> (a) Steinhagen H., Helmchen G. *Angew. Chem. Int. Ed.* **1996**, 35, 2339; (b) Fenton D.E., Okawa H. *Chem. Ber./Recueil* **1997**, 130, 433; (c) Van den Beuken E.K., Feringa B.L. *Tetrahedron* **1998**, 54, 12985; (d) Bosnich B. *Inorg. Chem.* **1999**, 38, 2554; (e) Belle C., Pierre J.-L. *Eur. J. Inorg. Chem.* **2003**, 4137.
- <sup>13</sup> Klingele J., Dechert S., Meyer F. *Coord. Chem. Rev.* submitted.
- <sup>14</sup> Schenck T.G., Downes J.M., Milne C.R.C., Mackenzie P.B., Boucher H., Whelan J., Bosnich B. *Inorg. Chem.* **1985**, 24, 2334.
- <sup>15</sup> (a) Meyer F., Beyreuther S., Heinze K., Zsolnai L. *Chem. Ber./Recueil* **1997**, 130, 605; (b) Meyer F., Heinze K., Nuber B., Zsolnai L. *J. Chem. Soc., Dalton Trans.* **1998**,

- 207-213; (c) Konrad M., Meyer F., Heinze K., Zsolnai, L. *J. Chem. Soc., Dalton Trans.* **1998**, 199; (d) Buchler S., Meyer F., Jacobi A., Kircher P., Zsolnai L. *Z. Naturforsch. B* **1999**, 54, 1295; (e) Konrad M., Wuthe S., Meyer F., Kaifer E. *Eur. J. Inorg. Chem.* **2001**, 2233; (f) Buchler S., Meyer F., Kaifer E., Pritzkow H. *Inorg. Chim. Acta* **2002**, 337, 371; (g) Röder J.C., Meyer F., Kaifer E., Pritzkow H. *Eur. J. Inorg. Chem.* **2004**, 1646; (h) Ackermann J., Meyer F., Pritzkow H. *Inorg. Chim. Acta* **2004**, 357, 3703-3711.
- <sup>16</sup> Siegfried L., Kaden T.A., Meyer, F., Kircher P., Pritzkow H. *J. Chem. Soc., Dalton Trans.* **2001**, 2310.
- <sup>17</sup> (a) Kamiyusuki T., Okawa H., Matsumoto N., Kida S. *J. Chem. Soc., Dalton Trans.* **1990**, 195; (b) Mernari B., Abraham F., Lagrenée M., Drillon M., Legoli P. *J. Chem. Soc., Dalton Trans.* **1993**, 1707; (c) Weller H., Siegfried L., Neuburger M., Zehnder M., Kaden T.A. *Helv. Chim. Acta* **1997**, 80, 2315; (d) Kaden T.A. *Coord. Chem. Rev.* **1999**, 190-192, 371; (e) Tanaka S., Dubs C., Inagaki A., Akita M. *Organometallics* **2005**, 24, 163; (f) Miranda C., Escarti F., Lamarque L., Garcia-Espana E., Navarro P., Latorre J., Lloret F., Jimenez H.R., Yunta M.J.R. *Eur. J. Inorg. Chem.* **2005**, 189; (g) Zinn P.J., Powell D.R., Day V.W., Hendrich M.P., Sorrell T.N., Borovik A.S. *Inorg. Chem.* **2006**, 45, 3484.
- <sup>18</sup> Kaim W., Schwederski B. *Bioanorganische Chemie*, Teubner Studienbücher, Stuttgart, **1991**.
- <sup>19</sup> Voet D., Voet J.G., Pratt C.W. *Lehrbuch der Biochemie*, Wiley-VCH, Weinheim, **2002**.
- <sup>20</sup> Gerdemann C., Eicken C., Krebs B. *Acc. Chem. Res.* **2002**, 35, 183.
- <sup>21</sup> Gaykema W.P.J., Hol W.G.J., Vereijken J.M., Soeter N.M., Bak H.J., Beintema J.J. *Nature* **1984**, 309, 23.
- <sup>22</sup> Magnus K.A., Thon-Tat H., Carpenter J.E. *Chem. Rev.* **1994**, 94, 727.
- <sup>23</sup> Cuff M.E., Miller K.I., van Holde K.E., Hendrickson W.A. *J. Mol. Biol.* **1998**, 278, 855.
- <sup>24</sup> Magnus K.A., Hazes B., Thon-Tat H., Bonaventura C., Bonaventura J., Hol W.G.J. *Proteins : Structure, Function and Genetics* **1994**, 19, 302.
- <sup>25</sup> (a) Ito N., Phillips S.E.V., Stevens C., Ogel Z.B, McPherson M.J., Keen J.N., Yadav K.D.S., Knowles P.F. *Nature* **1991**, 350, 87; (b) Ito N., Phillips S.E.V., Yadav K.D.S., Knowles P.F.J. *Mol Biol.* **1994**, 238, 794.
- <sup>26</sup> Klinman J.P. *Chem. Rev.* **1996**, 96, 2541.

- 27 (a) Eisensmith R.C., Woo S.L.C. *Mol. Biol. Med.* **1991**, 8, 3; (b) Fitzpatrick P.F. *Biochemistry* **2003**, 42, 14083.
- 28 (a) Tainer J.A., Getzoff E.D., Beem K.M., Richardson J.S., Richardson D.C. *J. Mol. Biol.* **1982**, 160, 181; (b) Tainer J.A., Getzoff E.D., Richardson J.S., Richardson D.C. *Nature* **1983**, 306, 284.
- 29 Solomon E.I., Baldwin M.J., Lowery M.D. *Chem. Rev.* **1992**, 92, 521.
- 30 (a) Volbeda A., Hol W.G.J. *J. Mol. Biol.* **1989**, 206, 531; (b) Volbeda A., Hol W.G.J. *J. Mol. Biol.* **1989**, 209, 249.
- 31 Matoba Y., Kumagai T., Yamamoto A., Yoshitsu H., Sugiyama M. *J. Biol. Chem.* **2006**, 31, 8981.
- 32 Klabunde T., Eicken C., Sacchettini J.C., Krebs B. *Nat. Struct. Biol.* **1998**, 5, 1084.
- 33 (a) Eicken C., Krebs B., Sacchettini J.C. *Curr. Opin. Struct. Biol.* **1999**, 9, 677; (b) Gerdemann C., Eicken C., Krebs B. *Acc. Chem. Res.* **2002**, 183.
- 34 Siegbahn P.E.M. *J. Biol. Inorg. Chem.* **2004**, 9, 577.
- 35 Decker H., Schweikardt T., Tuczek F. *Angew. Chem. Int. Ed.* **2006**, 45, 4546.
- 36 (a) Decker H., Dillinger R., Tuczek F. *Angew. Chem. Int. Ed.* **2000**, 39, 1591; (b) Siegbahn P.E.M. *J. Biol. Inorg. Chem.* **2003**, 8, 567; (c) Granata A., Monzani E., Bubacco L., Casella L. *Chem. Eur. J.* **2006**, 12, 2504; (d) Cramer C.J., Wloch M., Piecuch P., Puzzarini C., Gagliardi L. *J. Phys. Chem. A.* **2006**, 110, 1991.
- 37 (a) Bertrand T., Jolivald C., Briozzo P., Caminade E., Joly N., Madzak C., Mougin C. *Biochemistry* **2002**, 41, 7325; (b) Piontec K., Antorini M., Choinowski T. *J. Biol. Chem.* **2002**, 277, 37663; (c) Claus H. *Micron* **2004**, 35, 93.
- 38 Hakulinen N., Kiiskinen L.L., Kruus K., Saloheimo M., Paananen A., Koivula A., Rouvinen J. *Nat. Struct. Biol.* **2002**, 9, 601.
- 39 Messerschmidt A., Rossi A., Ladenstein R., Huber R., Bolognesi M., Gatti G., Machesini A., Petruzzelli R., Finazzi-Agró A. *J. Mol. Biol.* **1989**, 206, 513.
- 40 Wang Y., DuBois J., Hedman B., Hodgson K., Stack T. *Science* **1998**, 279, 537.
- 41 Chaudhuri P., Hess M., Weyhermüller T., Wieghardt K. *Angew. Chem. Int. Ed.* **1999**, 38, 1095.
- 42 Karlin K.D., Hayes J.C., Gultneh Y., Cruse R.W., McKown J.W., Hutchinson J.P., Zubieta J. *J. Am. Chem. Soc.* **1984**, 106, 2121.
- 43 Karlin K.D., Kaderli S., Zuberbühler A.D. *Acc. Chem. Res.* **1997**, 30, 139.
- 44 Santagostini L., Gullotti M., Monzani E., Casella L., Dillinger R., Tuczek F. *Chem. Eur. J.* **2000**, 6, 519.

- 45 Monzani E., Quinti L., Perotti A., Casella L., Gullotti M., Randaccio L., Geremia S.,  
Nardin G., Faleschini P., Tabbi G. *Inorg. Chem.* **1998**, 37, 553.
- 46 Monzani E., Battaini G., Perotti A., Casella L., Gullotti M., Santagostini L., Randaccio  
L., Geremia S., Nardin G., Zanello P., Opromolla G. *Inorg. Chem.* **1999**, 38, 5359.
- 47 Casella L., Monzani E., Gullotti M., Cavagnino D., Cerina G., Santagostini L., Ugo R.  
*Inorg. Chem.* **1996**, 35, 7516.
- 48 Karlin K.D., Zubieta J. *Copper Coordination Chemistry: Biochemical and Inorganic  
Perspectives*, Adenine, New York, **1983**.
- 49 Karlin K.D., Hayes J.C., Juen S., Hutchinson J.P., Zubieta J. *Inorg. Chem.* **1982**, 21,  
4106.
- 50 Kleywegt G.J., Wiesmeijer W.G.R., van Dreil G.J., Driessen W.L., Reedijk J.,  
Noordik J.H. *J. Chem. Soc., Dalton Trans.* **1985**, 2177.
- 51 Karlin K.D., Dahlstrom P.L., Hayes J.C., Simon R.A., Zubieta J. *Cryst. Struct.  
Commun.* **1982**, 11, 907.
- 52 Sorrell T.N., Jameson D.L. *Inorg. Chem.* **1982**, 21, 1014.
- 53 Berreau L.M. *Eur. J. Inorg. Chem.* **2006**, 273.
- 54 (a) Schindler S. *Eur. J. Inorg. Chem.* **2000**, 2311; (b) Würtele C., Gaoutchenova E.,  
Harms K., Holthausen M.C., Sundermeyer J., Schindler S. *Angew. Chem. Int. Ed.*  
**2006**, 45, 3867.
- 55 (a) Jacobson R.J., Tyeklar Z., Farooq A., Karlin K.D., Liu S., Zubieta J. *J. Am. Chem.  
Soc.* **1988**, 110, 3690; (b) Wei N., Murthy N.N., Tyeklar Z., Karlin K.D. *Inorg. Chem.*  
**1994**, 33, 1177; (c) Schatz M., Becker M., Thaler F., Hampel F., Schindler S.,  
Jacobson R.R., Tyeklar Z., Murthy N.N., Ghosh P., Chen Q., Zubieta J., Karlin K.  
*Inorg. Chem.* **2001**, 40, 2312; (d) Uozumi K., Hayashi Y., Suzuki M., Uehara A.  
*Chem. Lett.* **1993**, 963; (e) Komiyama K., Furutachi H., Nagatomo S., Hashimoto A.,  
Hayashi H., Fujinami S., Suzuki M., Kitagawa T. *Bull. Chem. Soc. Jpn.* **2004**, 77, 59.
- 56 Bol J.E., Driessen W.L., Ho A.Y.N., Maase B., Que L., Reedijk J. *Angew. Chem. Int.  
Ed.* **1997**, 36, 998.
- 57 Bode R.H., Bol J.E., Driessen W.L., Hulsbergen F.B., Reedijk J., Spek A.L. *Inorg.  
Chem.* **1999**, 38, 1239.
- 58 van der Vlugt J.I., Meyer F. *Top. Organomet. Chem.* **2007**, 22, 191.
- 59 (a) Mirica L.M., Vance M., Rudd D.J., Hedman B., Hodgson K.O., Solomon E.I.,  
Stack T.D.P. *J. Am. Chem. Soc.* **2002**, 124, 9332; (b) Mirica L.M., Rudd D.J., Vance

- M.A., Solomon E.I., Hodgson K.O., Hedman B., Stack T.D.P. *J. Am. Chem. Soc.* **2006**, *128*, 2654.
- 60 Mahadevan V., DuBois J.L., Hedman B., Hodgson K.O., Stack T.D.P. *J. Am. Chem. Soc.* **1999**, *121*, 5583.
- 61 (a) Santagostini L., Gullotti M., Monzani E., Casella L., Dillinger R., Tuczek F. *Chem. Eur. J.* **2000**, *6*, 529; (b) Battaini G, de Carolis M., Monzani E., Tuczek F., Casella L. *Chem. Commun.* **2003**, 726; (c) Palavicini S., Granata A., Monzani E., Casella L. *J. Am. Chem. Soc.* **2005**, *127*, 18031.
- 62 Itoh S., Kumei H., Taki M., Nagatomo S., Kitagawa T., Fukuzumi S. *J. Am. Chem. Soc.* **2001**, *123*, 6708.
- 63 Monzani E., Quinti L., Perotti A., Casella L., Gullotti M., Randaccio L., Geremia S., Nardin G., Faleschini P., Tabbi G. *Inorg. Chem.* **1998**, *37*, 553.
- 64 Mirica L.M., Vance M., Rudd D.J., Hedman B., Hodgson K.O., Solomon E.I., Stack T.D.P. *Science* **2005**, *308*, 1890.
- 65 Mukherjee R. *N. Proc. Indian. Natn. Sci. Acad.* **2004**, *70*, 329.
- 66 Monzani E., Battaini G., Perotti A., Casella L., Gullotti M., Santagostini L., Nardin G., Randaccio L., Geremia S., Zanello P., Opromolla G. *Inorg. Chem.* **1999**, *38*, 5359.
- 67 (a) Selmeczi K., Réglie M., Giorgi M., Speier G. *Coord. Chem. Rev.* **2003**, *245*, 191; (b) Kaizer J., Csonka R., Speier G., Giorgi M., Réglie M. *J. Mol. Catal. A: Chem.* **2005**, *235*, 81.
- 68 Selmeczi K., Réglie M., Speier G., Peintler G. *React. Kinet. Catal. Lett.* **2004**, *81*, 143
- 69 Granata A., Monzani E., Casella L. *J. Biol. Inorg. Chem.* **2004**, *9*, 903.
- 70 Koval I.A., Belle C., Selmeczi K., Philouze C., Saint-Aman E., Schuitema A.M., Gamez P., Pierre J.L., Reedijk J. *J. Biol. Inorg. Chem.* **2005**, *10*, 739.
- 71 Ackermann J., Meyer F., Kaifer E., Pritzkow H. *Chem. Eur. J.* **2002**, *8*, 247.
- 72 Kao C.H., Wei H.H., Liu Y.H., Lee G.H., Wang Y., Lee C.J. *J. Inorg. Biochem.* **2001**, *84*, 171.
- 73 Malachowski M.R. *Inorg. Chim. Acta* **1989**, *162*, 199.
- 74 Ackermann J., Buchler S., Meyer F. *C. R. Chimie* **2006**, *10*, 421.
- 75 (a) Oishi N., Nishida Y., Ida K., Kida S. *Bull. Chem. Soc. Jpn.* **1980**, *53*, 2847; (b) Mukherjee J., Mukherjee R. *Inorg. Chim. Acta* **2002**, *337*, 429.
- 76 Kao C.H., Wei H.H., Liu Y.H., Lee G.H., Wang Y., Lee C.J. *J. Inorg. Biochem.* **2001**, *84*, 171.

- 77 (a) Torelli S., Belle C., Gautier-Luneau I., Pierre J.L., Saint-Aman E., Latour J.M., Le Pape L., Luneau D. *Inorg. Chem.* **2000**, *39*, 3526; (b) Belle C., Beguin C., Gautier-Luneau I., Hamman S., Philouze C., Pierre J.L., Thomas F., Torelli S., Saint-Aman E., Bonin M. *Inorg. Chem.* **2002**, *41*, 479.
- 78 (a) Reim J., Krebs B. *J. Chem. Soc., Dalton. Trans.* **1997**, 3793; (b) Anekwe J., Hammerschmidt A., Rompel A., Krebs B. *Z. anorg. allg. Chem.* **2006**, *632*, 1057.
- 79 Merkel M., Möller N., Piacenza M., Grimme S., Rompel A., Krebs B. *Chem. Eur. J.* **2005**, *11*, 1201.
- 80 Thirumavalavan M., Akilan P., Kandaswamy M., Chinnakali K., Senthil Kumar G., Fun H.K. *Inorg. Chem.* **2003**, *42*, 3308.
- 81 (a) Meyer F., Heinze K., Nuber B., Zsolnai L. *J. Chem. Soc., Dalton Trans.* **1998**, 207; (b) Meyer F., Rutsch P. *Chem. Commun.* **1998**, 1037.
- 82 Baesjou P.J., Driessen W.L., Challa G., Reedijk J. *J. Mol. Catal. A: Chem.* **1996**, *110*, 195.
- 83 (a) Hay A.S. *J. Polym. Sci., Part A: Polym. Chem.* **1998**, *36*, 505; (b) Gamez P., Simons C., Steensma R., Driessen W.L., Challa G., Reedijk J. *Eur. Polym. J.* **2001**, *37*, 1293; (c) Gamez P., Simons C., Aromi G., Driessen W.L., Challa G., Reedijk J. *Appl. Catal. A* **2001**, *214*, 187.
- 84 Gamez P., van Dijk J.A.P.P., Driessen W.L., Challa G., Reedijk J. *Adv. Synth. Catal.* **2002**, *344*, 890.
- 85 Saito K., Tago T., Masuyama T., Nishide H. *Angew. Chem. Int. Ed.* **2004**, *43*, 730.
- 86 Ullmann R. F. *Chem. Ber.* **1904**, *37*, 853.
- 87 Saawyer J.S., Schmittling E.A., Palkowitz J.A., Smith W.J. *J. Org. Chem.* **1998**, *63*, 6338.
- 88 Gupta R., Mukherjee R. *Tetrahedron Lett.* **2000**, *41*, 7763.
- 89 Kodera M., Shimakoshi H., Tachi Y., Katayama K., Kano K. *Chem. Lett.* **1998**, *27*, 441.
- 90 (a) Schuchardt U., Cardoso D., Sercheli R., Pereira R., da Cruz R.S., Guerreiro M.C., Mandelli D., Spinacé E.V. and Pires E.L. *Appl. Catal. A* **2001**, *211*, 1; (b) Sheldon R.A. and Kochi J.K. in *Metal-Catalyzed Oxidations of Organic Compounds*, Academic Press, New York, **1981**.
- 91 (a) Shimokawa C., Yokota S., Tachi Y., Nishiwaki N., Ariga M., Itoh S. *Inorg. Chem.* **2003**, *42*, 8395; (b) Shimokawa C., Teraoka J., Tachi Y., Itoh S. *J. Inorg. Biochem.* **2006**, *100*, 1118.

- 92 Lieberman R.L., Rosenzweig A.C. *Nature* **2005**, 434, 177.
- 93 (a) Murahashi S.I., Oda Y., Naota T., Komiya N. *J. Chem. Soc., Chem. Commun.* **1993**, 139; (b) Komiya N., Naota T., Murahashi S.I. *Tetrahedron Lett.* **1996**, 37, 1633.
- 94 (a) Kirillov A.M., Kopylovich M.N., Kirillova M.V., Haukka M., Guedes da Silva M.F.C., Pombeiro A.J.L. *Angew. Chem. Int. Ed.* **2005**, 44, 4345; (b) Kirillov A.M., Kopylovich M.N., Kirillova M.V., Karabach E.Y.; Haukka M., Guedes da Silva M.F.C., Pombeiro A.J.L. *Adv. Synth. Catal.* **2006**, 348, 159.
- 95 Costas M., Llobet A. *J. Mol. Cat. A: Chem.* **1999**, 142, 113.
- 96 (a) Takehira K., Shimizu M., Watanabe Y., Orita H., Hayakawa T. *Tetrahedron Lett.* **1990**, 31, 2607; (b) Shimizu M., Watanabe Y., Orita H., Hayakawa T., Takehira K. *Tetrahedron Lett.* **1991**, 32, 2053; (c) Shimizu M., Watanabe Y., Orita H., Hayakawa T. *Bull. Chem. Soc. Jpn.* **1993**, 66, 251.
- 97 van den Heuvel R.H.H., Fraaije M.W., Ferrer M., Mattevi A., van Berkel W.J.H. *Proc. Natl. Acad. Sci. USA* **2000**, 97, 9455.
- 98 Boldron C., Gamez P., Tooke D.M., Spek A.L., Reedijk J. *Angew. Chem. Int. Ed.* **2005**, 44, 3585.
- 99 Boldron C., Özalp-Yaman S., Gamez P., Tooke D.M., Spek A.L., Reedijk J. *Dalton Trans.* **2005**, 21, 3535.
- 100 Schenck T.G., Downes J.M., Milne C.R.C., MacKenzie P.B., Boucher H., Whelan J., Bosnich B. *Inorg. Chem.* **1985**, 24, 2334.
- 101 Bradshaw J.S., Nielsen R.B., Tse P., Arena G., Wilson B.E., Dalley N.K., Lamb J.D., Christensen J.C., Izatt R.M. *J. Heterocycl. Chem.* **1986**, 23, 361.
- 102 Röder J.C., Meyer F., Pritzkow H. *Organometallics* **2001**, 20, 811.
- 103 (a) Nagao H., Komeda N., Mukaida M., Suzuki M., Tanaka K. *Inorg. Chem.* **1996**, 35, 6809; (b) Oberhausen K.J., Richardson, J.F., Buchanan R.M., Pierce W. *Polyhedron* **1989**, 8, 659; (c) Rodriguez M.C., Morgenstern-Badarau I., Cesario M., Guilhem J., Keita B., Nadjo L. *Inorg. Chem.* **1996**, 35, 7804.
- 104 (a) Myhre P.C., Maxey C.T., Bebout D.C., Swedberg S.H., Petersen B.L. *J. Org. Chem.* **1990**, 55, 3417; (b) first fully developed in the group of Prof. F. Meyer by Anna Sachse.
- 105 Buchner E., van der Heide C. *Berichte d.D.chem.Gesellschaft* **1901**, 31.
- 106 Addison A.W., Rao T.N., Reedijk J., Van Rijn J., Verschoor G.C. *J. Chem. Soc., Dalton Trans.* **1984**, 1349.
- 107 unpublished results by Ackermann J., Gamez P., Reedijk J., Meyer F.



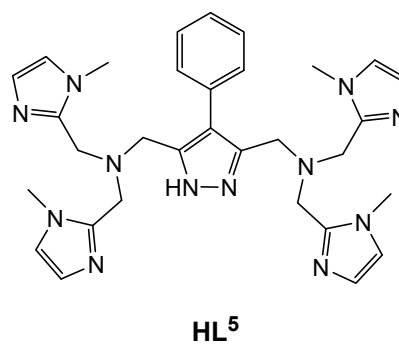
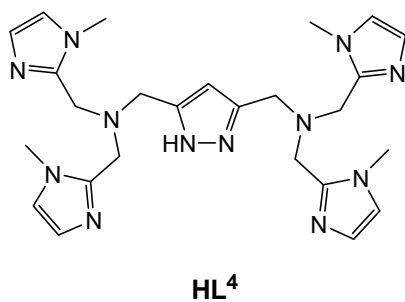
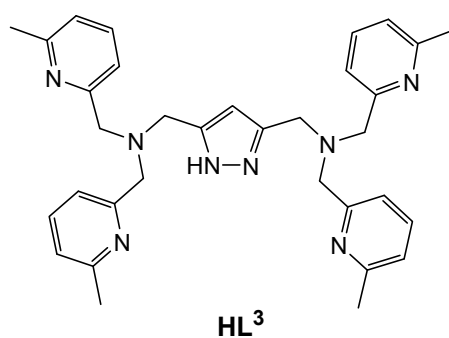
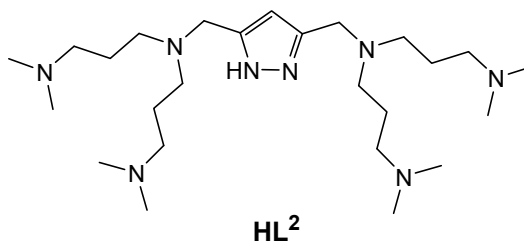
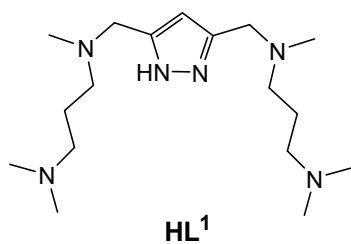
- 108 Ackermann J. Dissertation, Georg-August University Göttingen, **2003**.
- 109 Buijs W., Comba P., Corneli D., Pritzkow H. *J. Organomet. Chem.* **2002**, 641, 71.
- 110 Xin Zhang C., Liang H.C., Kim E., Gan O.F., Tyeklár Z., Karlin K.D., Lam K.C.,  
Rheingold A.L., Kaderli S., Zuberbühler A.D. *Chem. Commun.* **2001**, 631.
- 111 Alvarino Gil M. Dissertation, Georg-August University Göttingen, **2006**.
- 112 unpublished results by Nie F.-M.
- 113 Ackermann J., Meyer F., Pritzkow H. *Inorg. Chim. Acta* **2004**, 357, 3703.
- 114 Chiu Y.-H., Canary J.W. *Inorg. Chem.* **2003**, 42, 5107.
- 115 Oberhausen K.J., O'Brien R.J., Richardson J.F., Buchanan R.M. *Inorg. Chim. Acta*  
**1990**, 173, 145.
- 116 Lever A.B.P. *Inorganic Electronic Spectroscopy*, Elsevier, 1984.
- 117 (a) Meyer F., Pritzkow H. *Chem. Commun.* **1998**, 1555; (b) Meyer F., Kaifer E.,  
Kircher P., Heinze K., Pritzkow, H. *Chem. Eur. J.* **1999**, 5, 1617; (c) Meyer F., Hyla-  
Kryspin I., Kaifer E., Kircher P. *Eur. J. Inorg. Chem.* **2000**, 771; (d) Kryatov S.V.,  
Rybak-Akimova E.V., Meyer F., Pritzkow H. *Eur. J. Inorg. Chem.* **2003**, 1581; (e)  
Bauer-Siebenlist B., Meyer F., Farkas E., Vidovic D., Seijo J.A.C., Herbst-Irmer R.,  
Pritzkow H. *Inorg. Chem.* **2004**, 43, 4189; (f) Bauer-Siebenlist B., Meyer F., Farkas  
E., Vidovic D., Dechert S. *Chem. Eur. J.* **2005**, 11, 4349; (g) Bauer-Siebenlist B.,  
Dechert S., Meyer F. *Chem. Eur. J.* **2005**, 11, 5343.
- 118 Kahn O. *Molecular Magnetism*, Wiley-VCH, Publishers Inc., **1993**.
- 119 Simulation of the experimental magnetic data with a full-matrix diagonalisation of  
exchange coupling and Zeeman splitting was performed with the julX program: E.  
Bill, Max-Planck Institute for Bioinorganic Chemistry, Mülheim/Ruhr, Germany.
- 120 (a) Meyer F., Jacobi A., Zsolnai L. *Chem. Ber./Recueil* **1997**, 130, 1441; (b)  
Teichgräber J., Leibel G., Dechert S., Meyer F. *Z. anorg. allg. Chem.* **2005**, 631,  
2613.
- 121 Bayoñ J.C., Esteban P., Net G., Rasmussen P.G., Baker K.N., Hahn C.W., Gumz  
M.M. *Inorg. Chem.* **1991**, 30, 2572.
- 122 Kamiyuki T., Okawa H., Matsumoto N., Kida S. *J. Chem. Soc., Dalton Trans.* **1990**,  
195.
- 123 Matsushima H., Hamada H., Watanabe K., Koikawa M., Tokii T. *J. Chem. Soc.,  
Dalton Trans.* **1999**, 971.
- 124 Ajò D., Bencini A., Mani F. *Inorg. Chem.* **1988**, 27, 2437.

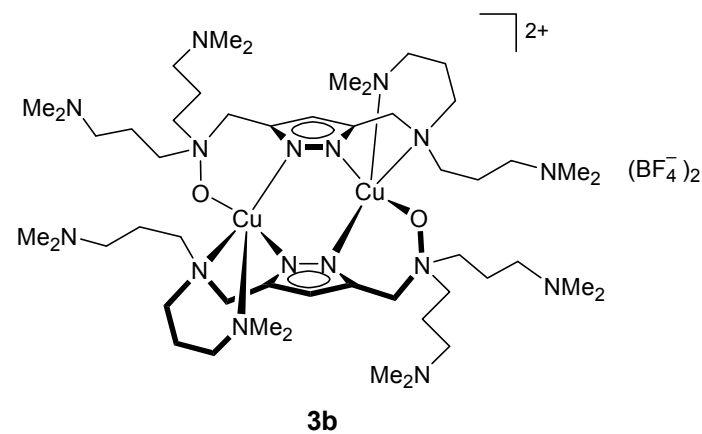
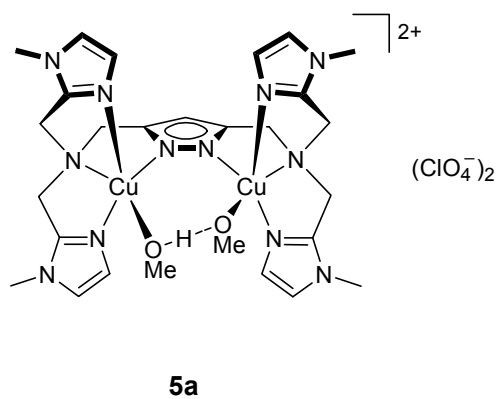
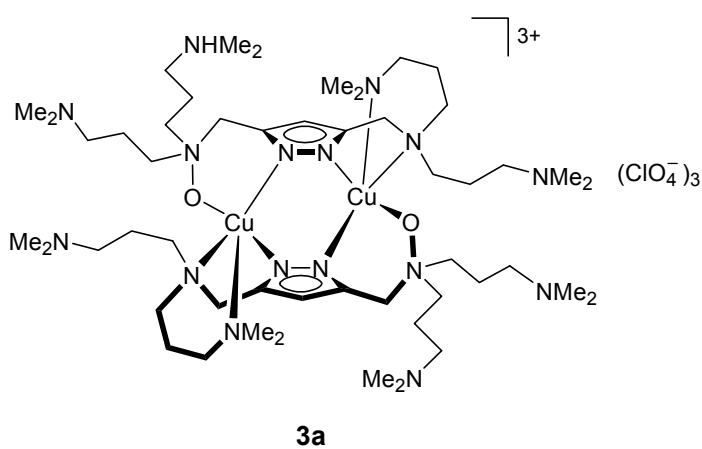
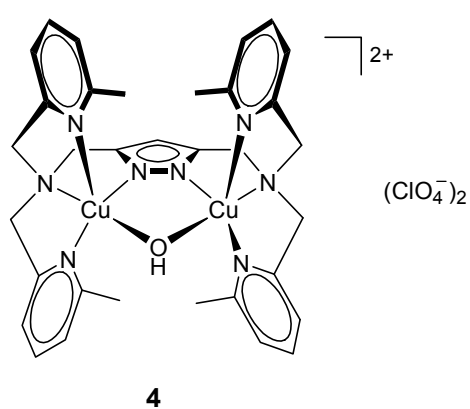
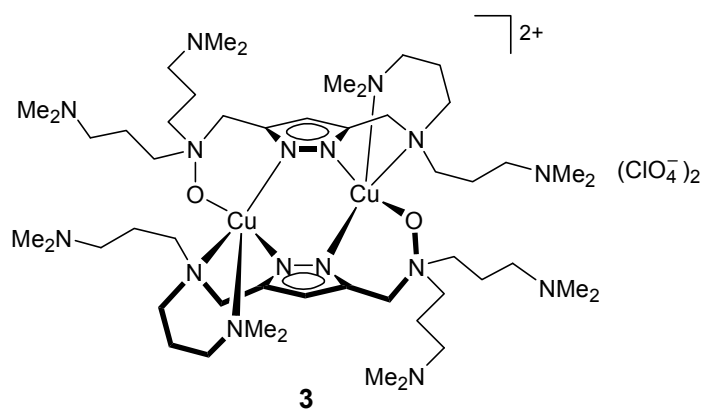
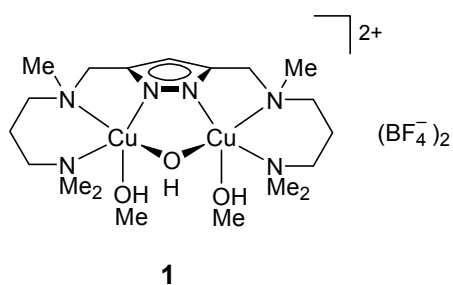
- 125 Hanot V.P., Robert T.D., Kolnaar J., Haasnoot J.P., Reedijk J., Kooijman H., Spek  
A.L. *J. Chem. Soc., Dalton Trans.* **1996**, 4275.
- 126 Boldron C., Aromí G., Challa G., Gamez P., Reedijk J. *Chem. Commun.* **2005**, 5808.
- 127 Balogh V., Fetizon M., Golfier M. *J. Org. Chem.* **1971**, 36, 1339.
- 128 Oyaizu K., Saito K., Tsuchida E. *Chem. Lett.* **2000**, 1318.
- 129 Butte Jr., W.A., Price C.C. *J. Am. Chem. Soc.* **1962**, 84, 3567.
- 130 Jackman L.M., Chen X. *J. Am. Chem. Soc.* **1997**, 119, 8681.
- 131 Harrod J.F. *Can. J. Chem.* **1969**, 47, 637.
- 132 Jazdzewski B.A., Holland P.L., Pink M., Young V.G., Jr. Spencer D.J.E., Tolman  
W.B. *Inorg. Chem.* **2001**, 40, 6097.
- 133 Kitajima N., Koda T., Iwata Y., Morooka Y. *J. Am. Chem. Soc.* **1990**, 112, 8833.
- 134 Baesjou P.J., Driessen W.L., Challa G., Reedijk J. *J. Am. Chem. Soc.* **1997**, 119,  
12590.
- 135 Cosgrove S.L., Waters W.A. *J. Chem. Soc.* **1951**, 388.
- 136 Walling C., Hodgson R.B., Jr. *J. Am. Chem. Soc.* **1958**, 80, 228.
- 137 Auerbach U., Eckert U., Wieghardt K., Nuber B., Weiss J. *Inorg. Chem.* **1990**, 29,  
938.
- 138 Sokolowski A., Leutbecher H., Weyhermüller T., Schnepf R., Bothe E., Bill E.,  
Hildebrandt P., Wieghardt K. *J. Biol. Inorg. Chem.* **1997**, 2, 444.
- 139 Halfen J.A., Jazdzewski B.A., Mahapatra S., Berreau L.M., Wilkinson E.C., Que L.,  
Jr., Tolman W.B. *J. Am. Chem. Soc.* **1997**, 35, 8217.
- 140 Schnepf R., Sokolowski A., Müller J., Bachler V., Wieghardt K., Hildebrandt P. *J.*  
*Am. Chem. Soc.* **1998**, 120, 2352.
- 141 Hockertz J., Steenzen S., Wieghardt K., Hildebrandt P. *J. Am. Chem. Soc.* **1993**, 115,  
11222.
- 142 Müller J., Weyhermüller T., Bill E., Hildebrandt P., Ould-Moussa L., Glaser T.,  
Wieghardt K. *Angew. Chem. Int. Ed.* **1998**, 37, 616.
- 143 Sokolowski A., Müller J., Weyhermüller T., Schnepf R., Hildebrandt P., Hildenbrand  
K., Bothe E., Wieghardt K. *J. Am. Chem. Soc.* **1997**, 119, 8889.
- 144 (a) Sokolowski A., Adam B., Weyhermüller T., Kikuchi A., Hildenbrand K., Schnepf  
R., Hildebrandt P., Bill E., Wieghardt K. *Inorg. Chem.* **1997**, 36, 3702; (b) Snodin  
M.D., Ould-Moussa L., Wallman U., Lecomte S., Bachler V., Bill E., Hummel H.,  
Weyhermüller T., Hildebrandt P., Wieghardt K. *Chem. Eur. J.* **1999**, 5, 2554.
- 145 Mukherjee A., McGlashen M.L., Spiro T.G. *J. Phys. Chem.* **1995**, 99, 4912.

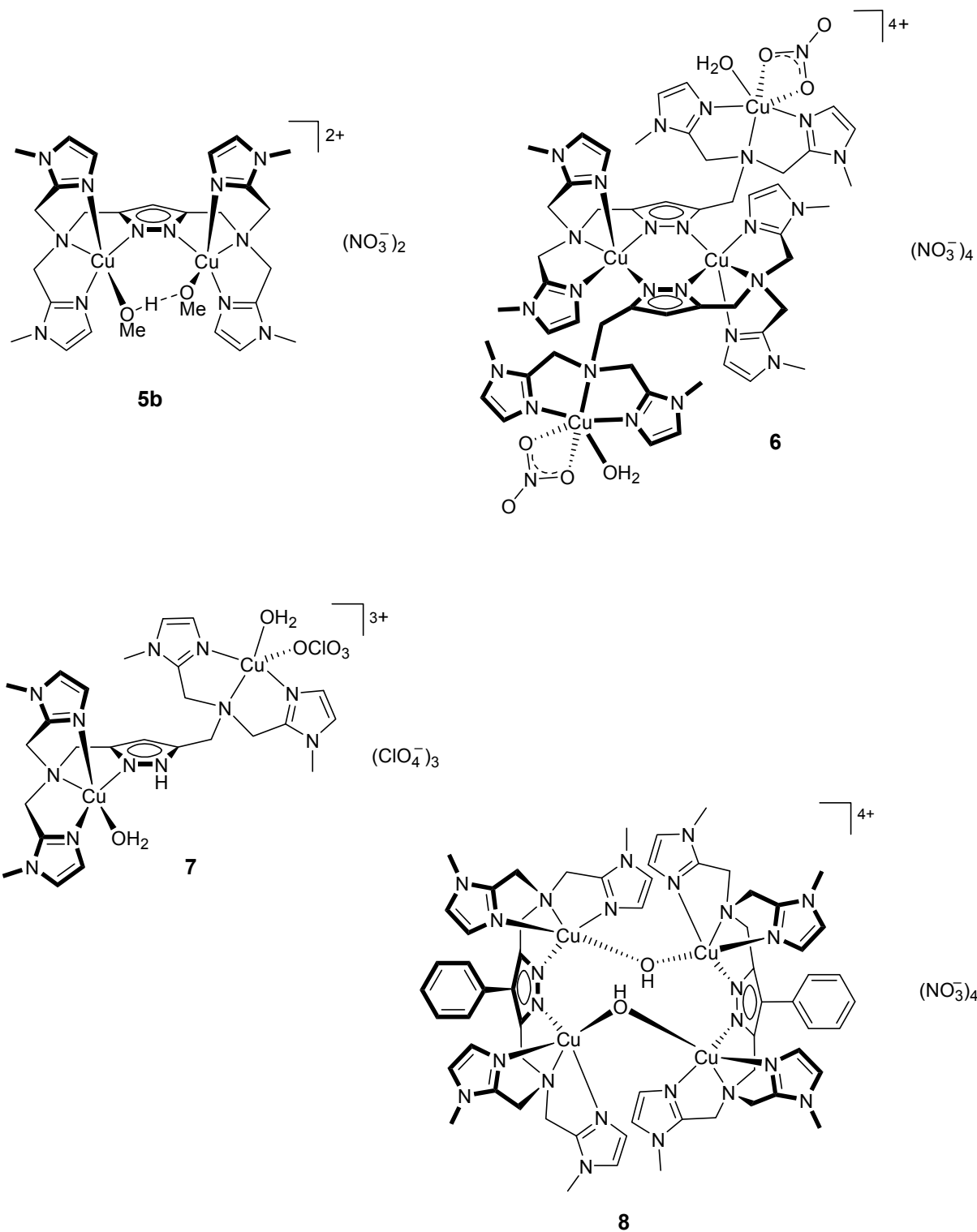
- 146 (a) Tripathi G.N.R., Schuler R.H. *J. Phys. Chem.* **1988**, 92, 5129; (b) Qin Y., Wheeler  
R.A. *J. Am. Chem. Soc.* **1995**, 117, 6083.
- 147 Pyrz J.W., Karlin K.D., Sorrell T.N., Vogel G.C., Que L., Jr. *Inorg. Chem.* **1984**, 23,  
4581.
- 148 Bill E., Müller J., Weyhermüller T., Wieghardt K. *Inorg. Chem.* **1999**, 38, 5795.
- 149 Altwicker E.R. *Chem. Rev.* **1967**, 67, 475.
- 150 Job P. *Ann. Chim.* **1928**, 9, 113.
- 151 Wada A., Honda Y., Yamaguchi S., Nagamoto S., Kitagawa T., Jitsukawa K., Masuda  
H. *Inorg. Chem.* **2004**, 43, 5725.
- 152 Ardizzoia G.A., Angaroni M.A., La Monica G., Masciocchi N., Moret M. *J. Chem.*  
*Soc., Dalton Trans.* **1990**, 2277.
- 153 Ardizzoia G.A., Beccalli E.M., La Monica G., Masciocchi N., Moret M. *Inorg. Chem.*  
**1992**, 31, 2706.
- 154 Ardizzoia G.A., Cenini S., La Monica G., Masciocchi N., Moret M. *Inorg. Chem.*  
**1994**, 33, 1458.
- 155 Dias H.V.R., Lu H.L., Gorden J.D., Jin W. *Inorg. Chem.* **1996**, 35, 2149.
- 156 (a) Knowles P.F., Ito N. In *Perspectives in Bioinorganic Chemistry*; Jai Press:  
London, **1994**, 2, 207; (b) Whittaker J.W., Whittaker M.M. *Pure Appl. Chem.* **1998**,  
70, 903.
- 157 Solomon E.I., Sundaram U.M., Machonkin T.E. *Chem. Rev.* **1996**, 96, 2563.
- 158 (a) Wang Y., DuBois J.L., Hedman B., Hodgson K.O., Stack T.D.P. *Science* **1998**,  
279, 537; (b) Chaudhuri P., Hess M., Flörke U., Wieghardt K. *Angew. Chem., Int. Ed.*  
**1998**, 37, 2217; (c) Chaudhuri P., Hess M., Weyhermüller T., Wieghardt K. *Angew.*  
*Chem., Int. Ed.* **1999**, 38, 1095; (d) Chaudhuri P., Hess M., Müller J., Hildenbrand K.,  
Bill E., Weyhermüller T., Wieghardt K. *J. Am. Chem. Soc.* **1999**, 121, 9599.
- 159 (a) Hay A.S. *J. Polym. Sci., Part A: Polym. Chem.* **1998**, 36, 505; (b) Higashimura H.,  
Kubota M., Shiga A., Fujisawa K., Morooka Y., Uyama H., Kobayashi S.  
*Macromolecules* **2000**, 33, 1986.
- 160 Jazdzewski B.A., Tolman W.B. *Coord. Chem. Rev.* **2000**, 200-202, 633.
- 161 (a) Bullock J.I., Hobson R.J., Povey D.C. *J. Chem. Soc., Dalton Trans.* **1974**, 2037;  
(b) Calderazzo F., Marchetti F., Dell'Amico G., Pelizzi G., Colligiani A. *J. Chem.*  
*Soc., Dalton Trans.* **1980**, 1419; (c) Whittaker M., Chuang Y., Whittaker J. *J. Am.*  
*Chem. Soc.* **1993**, 115, 10029.

- <sup>162</sup> (a) Karlin K.D., Cohen B.I., Hayes J.C., Farooq A, Zubieta J. *Inorg. Chem.* **1987**, *26*, 147; (b) Rajendran U., Viswanathan R., Palaniandavar M., Lakshminarayanan M. *J. Chem. Soc., Dalton. Trans.* **1992**, 3563; (c) Uma R., Viswanathan R., Palaniandavar M., Lakshminarayanan M. *J. Chem. Soc., Dalton Trans.* **1994**, 1219; (d) Adams H., Bailey N.A., Barbarin C.O.R.D., Fenton D.E., He Q.-Y. *J. Chem. Soc., Dalton Trans.* **1995**, 2323; (e) Adams H., Bailey N.A., Campbell I.K., Fenton D.E., He Q.-Y. *J. Chem. Soc., Dalton Trans.* **1996**, 2233; (f) Ito S., Nishino S., Itoh H., Ohba S., Nishida Y. *Polyhedron* **1998**, *17*, 1637.
- <sup>163</sup> (a) Karlin K.D., Cohen B.I. *Inorg. Chim. Acta* **1985**, *107*, L17; (b) Adams H., Bailey N.A., Fenton D.E., He Q., Ohba M., Okawa H. *Inorg. Chim. Acta* **1994**, *215* 1; (c) Itoh S., Takayama S., Arakawa R., Furuta A., Komatsu M., Ishida A., Takamuku S., Fukuzumi S. *Inorg. Chem.* **1997**, *36*, 1407; (d) Itoh S., Taki M., Takayama S., Nagatomo S., Kitagawa T., Sakurada N., Arakawa R., Fukuzumi S. *Angew. Chem. Int. Ed.* **1999**, *38*, 2774.
- <sup>164</sup> Que L., Jr. In *Biological Applications of Raman Spectroscopy*; Wiley: New York, **1988**, 491.
- <sup>165</sup> Pyrz J. W., Roe A. L., Stern L. J., Que L., Jr. *J. Am. Chem. Soc.* **1985**, *107*, 614.
- <sup>166</sup> Li L., Sarjeant A.A.N., Vance M.A., Zakharov L.N., Rheingold A.L., Solomon E.I., Karlin K.D. *J. Am. Chem. Soc.* **2005**, *127*, 15360.
- <sup>167</sup> (a) Lever A.B.P., Ramaswamy B.S., Pickens S.R. *Inorg. Chim. Acta* **1980**, *46*, L59-61; (b) Demmin T.R., Swerdloff M.D., Rogic M.M. *J. Am. Chem. Soc.* **1981**, *103*, 5795; (c) Bolus D., Vigee G.S. *Inorg. Chim. Acta* **1982**, *67*, 19; (d) Speier G.J. *Mol. Catal.* **1986**, *37*, 259; (e) Réglier M., Jorand C., Waegell B. *J. Chem. Soc., Chem. Commun.* **1990**, 1752; (f) Chyn J.-P., Urbach F.L. *Inorg. Chim. Acta* **1991**, *189*, 157; (g) Malachowski M.R., Tomlinson L.J., Davidson M.G., Hall M.J. *J. Coord. Chem.* **1992**, *25*, 171; (h) Rockcliffe D.A., Martell A.E. *J. Mol. Catal. A* **1995**, *99*, 101; (i) Zippel F., Ahlers F., Werner R., Haase W., Nolting H.-F., Krebs B. *Inorg. Chem.* **1996**, *35*, 3409; (j) Chung Y.-H., Wei H.-H., Liu Y.-H., Lee G.-H., Wang Y. *J. Chem. Soc., Dalton Trans.* **1997**, 2825; (k) Manzur J., Garcia A.M., Rivas V., Atria A.M., Valenzuela J., Spodine E. *Polyhedron* **1997**, *16*, 2299.
- <sup>168</sup> Malachowski M.R., Huynh H.B., Tomlinson L.J., Kelly R.S., Jr., Furbie J.W. *J. Chem. Soc., Dalton Trans.* **1995**, 31.

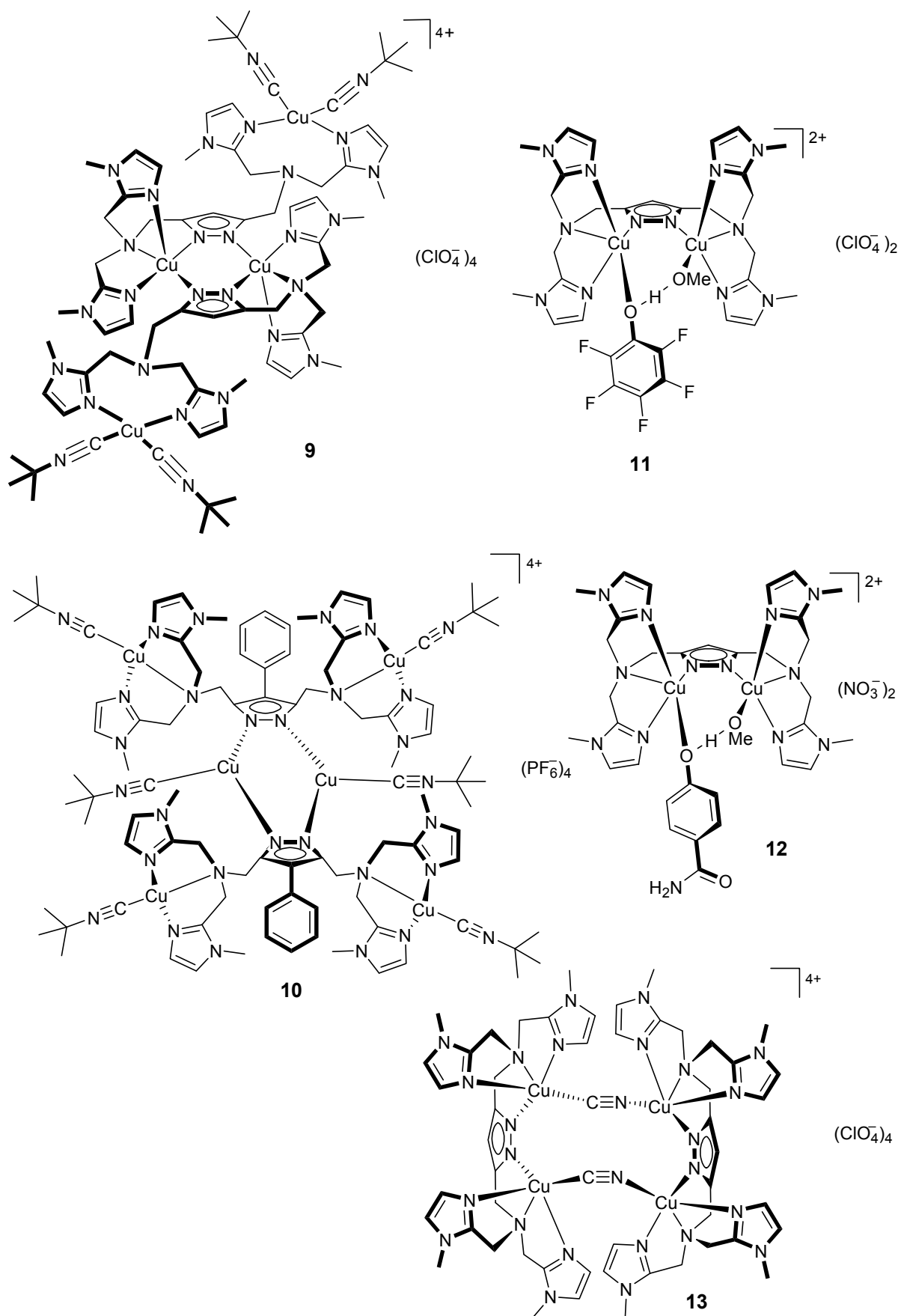
- 169 (a) Casellato U., Tamburini S., Vigato P.A., de Stefani A., Vidali M., Fenton D.E. *Inorg. Chim. Acta* **1983**, 69, 45; (b) Malachowski M.R., Davidson M.G. *Inorg. Chim. Acta* **1989**, 162, 199.
- 170 (a) Karlin K.D., Gultneh Y., Nicholson T., Zubieta J. *Inorg. Chem.* **1985**, 24, 3725; (b) Börzel H., Comba P., Pritzkow H. *Chem. Commun.* **2001**, 97.
- 171 Berreau L.M., Mahapatra S., Halfen J.A., Houser R.P., Young V.G., Tolman W.B. *Angew. Chem. Int. Ed.* **1999**, 38, 207.
- 172 Song Y.-F., van Albada G.A., Tang J., Mutikainen I., Turpeinen U., Massera C., Roubeau O., Costa J.S., Gamez P., Reedijk J. *Inorg. Chem.* **2007**, 46, 4944.
- 173 (a) Sahoo S.K., Liu W., Samuelson L.A., Kumar J., Cholli A.L. *Macromolecules* **2002**, 35, 9990; (b) Asakura K., Honda E., Osanai S. *Chem. Lett.* **1995**, 583.
- 174 Gleason J.G., Holden K.G., Nelson C.F.Y. *US Pat.* **1975**, 3,860,631.
- 175 Gong Y.F., Kato K., Kimoto H. *Bull. Chem. Soc. Jpn.* **2002**, 75, 2637.
- 176 Yan J.M., Zhang Z.J., Yuan D.Q., Xie R.G., Zhao H.M. *Synth. Commun.* **1994**, 24, 47.
- 177 Habata Y., Akabori S. *J. Chem. Soc., Dalton Trans.* **1996**, 3871.
- 178 Itoh T., Nakanishi E., Okayama M., Kubo M. *Macromolecules* **2000**, 33, 269.
- 179 Gamez P., Gupta S., Reedijk J. *C. R. Chimie* **2007**, 10, 295.
- 180 Gran G. *Analyst* **1952**, 77, 661.
- 181 (a) Gans P., Sabatini A., Vacca A. *J. Chem. Soc., Dalton Trans.* **1985**, 1195; (b) Zékány L., Nagypál I. in: D.L. Leggett (Ed.), *Computational Methods for the Determination of Stability Constants*, Plenum Press, New York, **1985**, 291.
- 182 Puigdomenech I. *MEDUSA and Hydra software for chemical equilibrium calculations*, Royal Institute of Technology (KTH), Stockholm, Sweden.
- 183 Sheldrick G.M. SHELXL-97, *Program for Crystal Structure Refinement*, University of Göttingen, Göttingen (Germany), **1997**. Sheldrick, G.M. SHELXS-97, *Program for Crystal Structure Solution*, University of Göttingen, Göttingen (Germany), **1997**.
- 184 STOE & CIE GmbH, X-RED, Darmstadt, **2002**.

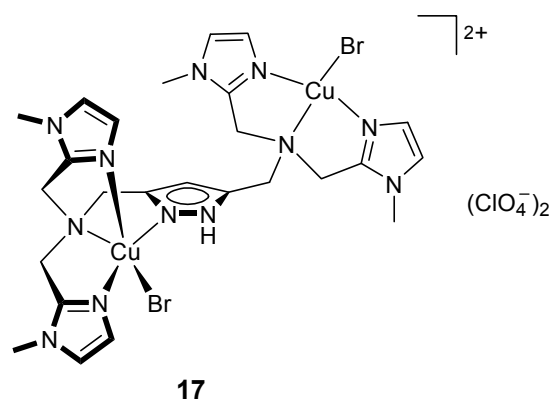
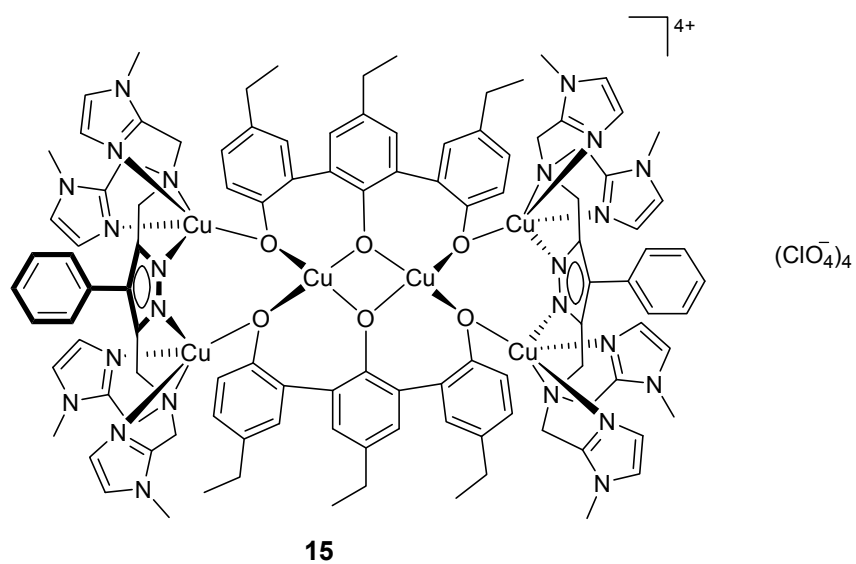
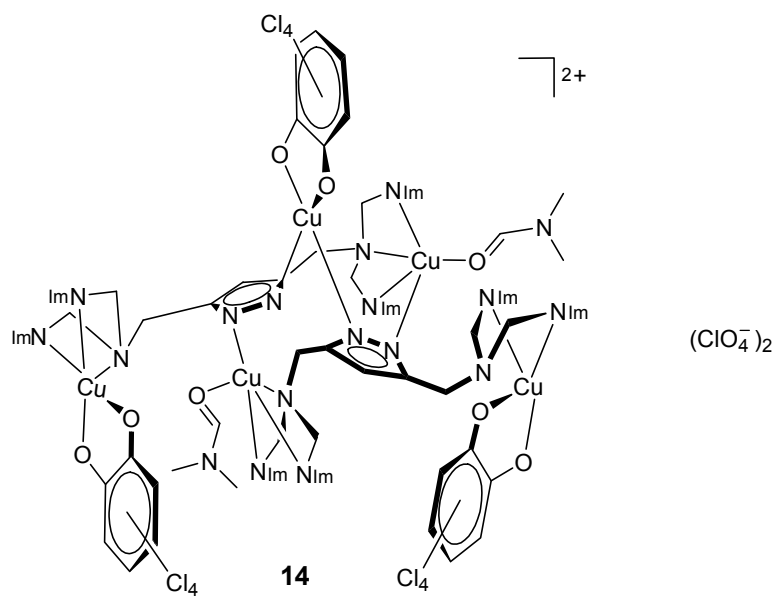












## Acknowledgments

Very strange and exiting, this last part that has to be written, as it is an incredible part of the thesis where only heart and soul are participating and one can not find any formulas or figures, just feelings. You look at the word “Acknowledgments” and your skin is crawling because you are at the end....At the end of something very important and significant for the whole entire life.

“On this basis”, I would like to direct my initial acknowledgment towards my supervisor Prof. Dr. Franc Meyer. I am truly grateful for a great and amazing chemistry-time here in Göttingen. I am thankful for *an-in-time motivation moments* which were so important and gave me the power to move on, even if it was hard and at some point impossible. All these moments gave me a chance to create a “golden bag” full with various chemical experiences and to open the world of science.

I would like to express my special thanks to Petra, who was incredibly kind and helpful in fixing all sorts of things during my whole time here. It was very important to be welcomed with warmth.

The whole working group will remain in my heart. My kind thanks to Rosanna and Jens, who were the first to show me my lab, my near future and the first synthesis of the dicopper(II) complex. And especially thank you for a nice time before the scary presentation in Ladenburg. My sincere thanks to Dr. Maringgele for fruitful discussions during the long evenings in the lab and for spending a lot of time showing me how to work with kilos of ligands. My lab-mates, Stamatia and Maria, are acknowledged for a nice time in lab 208 and for enjoying listening to Sirtaki. Many thanks to Jörg Teichgräber who was all the time around to help in the lab and to observe boiling solvents! I am thankful to all for a nice time (unfortunately, not that often) to hang around in Göttingen and during working trips. Dear Dr. Guido Leibelng is acknowledged for a great help in understanding of german laws and simply for a nice time! For the X-ray analyses I would like to acknowledge Dr. Sebastian Dechert who was very patient and showed endurance with all my “unexpected” structures; also thanks for the Raman measurements. My endless acknowledgments to the ukrainian part of the working group. Серёжа, большое спасибо за поддержку в течении этих четырёх лет. За весёлые чаяпития и шутки, за мудрые советы и дискуссии. За помощь по приезду в Гёттинген во всем. For the great help during a very important part of the thesis I want to thank Dr. Sasha Prykhod'ko. It was a big pleasure to work with you and I think that our team did well. For a nice half-a-year time in the lab, especially during early coming

evenings, useful discussions and simply nice feelings bringing me closer to Kiev I am thankful to Larisa Penkova. To Dr. Michael Stollenz I want to say thanks for a nice time in practicum.

For the EPR measurements as well as for endless help with all administrative paper work I want to acknowledge Dr. Claudia Stückl. The divisions for NMR spectroscopy, mass spectrometry and elemental analysis I would like to acknowledge for their timely support during the research.

Financial support from the DFG (International Research Training Group GRK 1422 "Metal Sites in Biomolecules: Structures, Regulation and Mechanisms") and the Gottlieb Daimler- und Karl Benz-foundation for research fellowships is gratefully acknowledged.

For very productive and interesting seminars within the IRTG I want to thank to all people from the Inorganic Chemistry, Structural Biology, Plant Biology and Organic Chemistry departments, as well as for a nice and funny time during the Workshops in Kassel and Lund. In particular, I am thankful to Cristian Grosse from AK Sheldrick for X-Ray measurements.

For a very heavy job, the corrections of the whole thesis I am grateful to Dr. Jarl Ivar van der Vlugt. I am thankful for veritably useful and helpful discussions concerning the scientific and the real world. For the nice company to hang out with in Göttingen and for a shared passion in playing pool! Dank je wel, Jarl!!!

I am thankful to my friends Lamiae, Mustapha, Mladen and Claudia for a lot of nice moments during these four years: for discussions on politics and culture, for shared human-being feelings coming from abroad, for funny times in the german course. I want to thank to my friend Olga for "cheer up" phone talks! For the light in the darkness, for care, for giving strength to believe in yourself, for a nice time during travelling around and just for being I am thankful to Anna.

Loving thanks to my family: to my dear cousin (sister) here and to all back home. For the endless support and love, for gigantic care on a thousand kilometres distance, which I felt every single day, I want to thank my dear parents.

*The trick is in what one emphasizes. We either make ourselves miserable, or we make ourselves strong. The amount of work is the same.*

*The Wheel of Time*

*Carlos Castaneda*

**Curriculum vitae**

<i>Name</i>	Angelina Prokofieva
<i>Date of birth:</i>	April 2 <sup>th</sup> 1982, Kiev (Ukraine)
<i>Nationality:</i>	Ukrainian
<i>Marital status:</i>	Single
<i>Pre-Academic Education:</i>	Sep 1988 – Jul 1998 High school № 294, Kiev, Ukraine
<i>Academic Career:</i>	Sep 1998 – Jun 2002 Undergraduate Student at the Chemistry Department of the National Taras Shevchenko University, Kiev, Ukraine Sep 2002 – Jun 2003 M.Sc. Student <i>with honor</i> at the Chemistry Department of the National Taras Shevchenko University, Kiev, Ukraine <u>Area:</u> Crystal engineering: coordination polymers of 3d-metals based on bipyrazolyl ligands
<i>Promotion:</i>	Nov 2003 – current Ph.D. Student at the Göttingen University, Institut of Inorganic Chemistry Promotor: Prof.Dr. F.Meyer <u>Area:</u> Modelling of the active site of type 3 copper enzymes, bioinspired catalysis Thesis title: “ <i>Bioinspired oxidation reactions of phenols with dinuclear copper complexes</i> ”
<i>Awards and Prizes:</i>	May 2003 First Prize at the Ukrainian students and post-graduate students conference Sep 2004 – Aug 2006 Predoctoral Research Scholarship (Gottlieb Daimler- und Karl Benz-Stiftung) 25-30 June 2006 Prize for attendance of the 56 <sup>th</sup> Lindau Meeting of Nobel Laureates (18 <sup>th</sup> Meeting dedicated to chemistry), Lindau, Germany Okt 2006 – Nov 2007 Scholarship within the International Research Training Group (Internationales Graduirtenkolleg 1422)

### Scientific publications

A. Prokofieva, A. I. Prikhod'ko, E. A. Enyedy, E. Farkas, W. Maringgele, S. Demeshko, S. Dechert, F. Meyer, Oligonuclear copper complexes of a bioinspired pyrazolate-bridging ligand: synthesis, structures and equilibria in solution, *Inorg.Chem.*, **2007**, 46, 4298.

A. Prokofieva, A. I. Prikhod'ko, S. Dechert, F. Meyer, Selective benzylic C-C coupling catalyzed by a bioinspired dicopper complex, Hot Article, *Chem.Comm.*, **2008**, DOI: 10.1039/b718162k

A. Prokofieva, C. Große, G. M. Sheldrick, F. Meyer, Oxidative *ortho* C-C coupling of 4-ethylphenol catalyzed by a bioinspired dicopper complex – trapping of an oligomeric intermediate, in preparation for *Chem.Comm.*

A. Prokofieva, A. I. Prikhod'ko, S. Schmatz, S. Dechert, M. Bennati, F. Meyer, Oxidative C-C coupling of 2,4,6-trimethylphenol catalyzed by a dicopper complex - mechanistic insights, in preparation for *Chem. Eur. J.*

### Presentations at International Conferences and Workshops

A. Prokofieva, K. Domasevich, “*Coordination polymers of 3d-metals based on N,N'-dimethyl-4,4'-bipyrazolyl*”, 4<sup>th</sup> Ukrainian students and post-graduate students conference, Kiev, Ukraine, 21-23 May, **2003**

A. Prokofieva, A. I. Prikhod'ko, F. Meyer, “*Oxidative phenol coupling by pyrazolate-based dicopper complexes*” 2. Koordinationschemikertreffen, Göttingen, Germany, 19-21 February, **2006**

A. Prokofieva, A. I. Prikhod'ko, F. Meyer, “*Bioinspired oxidation reactions with oligonuclear copper complexes*”, 1<sup>st</sup> workshop of the International Research Training Group, Reinhardswaldschule, Kassel, Germany, 25-27 January, **2007**

### Posters at International Conferences and Workshops

A. Prokofieva, J. Ackermann, S. Dechert, F. Meyer, “*Bioimimetic oxidation reactions with pyrazolate-based dicopper complexes*”, European Biological Inorganic Chemistry Conference (Eurobic7), Garmisch-Partenkirchen, Germany, 29 August-2 September, **2004**

A. Prokofieva, J. Ackermann, S. Dechert, F. Meyer, “*Bioinspired oxidation reactions with pyrazolate-based dicopper complexes*,” Workshop on Biomimetic Metal Oxidative Transformation, Marburg/Giessen, Germany, 29-30 January, **2005**

A. Prokofieva, A. I. Prikhod’ko, S. Dechert, F. Meyer, “*Bioinspired oxidation reactions with oligonuclear copper complexes*,” 2<sup>nd</sup> workshop of the International Research Training Group, Lund, Sweden, 20-22 June, **2007**

A. Prokofieva, A. I. Prikhod’ko, S. Dechert, F. Meyer, “*Bioinspired oxidation reactions with oligonuclear copper complexes*”, 13<sup>th</sup> International Conference on Biological Inorganic Chemistry (ICBIC), Vienna, Austria, 15-20 July, **2007**